



## SUPRAMOLECULAR CHEMISTRY OF BIS-PORPHYRINS

Laura Patricia Hernández Eguía

ISBN: 978-84-694-0308-2  
Dipòsit Legal: T-204-2011

**ADVERTIMENT.** La consulta d'aquesta tesi queda condicionada a l'acceptació de les següents condicions d'ús: La difusió d'aquesta tesi per mitjà del servei TDX ([www.tesisenxarxa.net](http://www.tesisenxarxa.net)) ha estat autoritzada pels titulars dels drets de propietat intel·lectual únicament per a usos privats emmarcats en activitats d'investigació i docència. No s'autoritza la seva reproducció amb finalitats de lucre ni la seva difusió i posada a disposició des d'un lloc aliè al servei TDX. No s'autoritza la presentació del seu contingut en una finestra o marc aliè a TDX (framing). Aquesta reserva de drets afecta tant al resum de presentació de la tesi com als seus continguts. En la utilització o cita de parts de la tesi és obligat indicar el nom de la persona autora.

**ADVERTENCIA.** La consulta de esta tesis queda condicionada a la aceptación de las siguientes condiciones de uso: La difusión de esta tesis por medio del servicio TDR ([www.tesisenred.net](http://www.tesisenred.net)) ha sido autorizada por los titulares de los derechos de propiedad intelectual únicamente para usos privados enmarcados en actividades de investigación y docencia. No se autoriza su reproducción con finalidades de lucro ni su difusión y puesta a disposición desde un sitio ajeno al servicio TDR. No se autoriza la presentación de su contenido en una ventana o marco ajeno a TDR (framing). Esta reserva de derechos afecta tanto al resumen de presentación de la tesis como a sus contenidos. En la utilización o cita de partes de la tesis es obligado indicar el nombre de la persona autora.

**WARNING.** On having consulted this thesis you're accepting the following use conditions: Spreading this thesis by the TDX ([www.tesisenxarxa.net](http://www.tesisenxarxa.net)) service has been authorized by the titular of the intellectual property rights only for private uses placed in investigation and teaching activities. Reproduction with lucrative aims is not authorized neither its spreading and availability from a site foreign to the TDX service. Introducing its content in a window or frame foreign to the TDX service is not authorized (framing). This rights affect to the presentation summary of the thesis as well as to its contents. In the using or citation of parts of the thesis it's obliged to indicate the name of the author.

UNIVERSITAT ROVIRA I VIRGILI  
SUPRAMOLECULAR CHEMISTRY OF BIS-PORPHYRINS  
Laura Patricia Hernández Eguía  
ISBN:978-84-694-0308-2/DL:T-204-2011

UNIVERSITAT ROVIRA I VIRGILI  
SUPRAMOLECULAR CHEMISTRY OF BIS-PORPHYRINS  
Laura Patricia Hernández Eguía  
ISBN:978-84-694-0308-2/DL:T-204-2011

*Laura P. Hernández Eguía*

# Supramolecular Chemistry of Bis-porphyrins

PhD Thesis

Supervised by Prof. Pablo Ballester Balaguer

Institut Català d'Investigació Química (ICIQ)



UNIVERSITAT ROVIRA I VIRGILI

Tarragona  
2010

UNIVERSITAT ROVIRA I VIRGILI  
SUPRAMOLECULAR CHEMISTRY OF BIS-PORPHYRINS  
Laura Patricia Hernández Eguía  
ISBN:978-84-694-0308-2/DL:T-204-2011



UNIVERSITAT ROVIRA I VIRGILI

Av. Països Catalans, 16  
43007 Tarragona  
Tel. 977 920 218  
Fax. 977 920 225

Prof. Pablo Ballester Balaguer, Group Leader of the Institute of Chemical Research of Catalonia (ICIQ) and Research Professor of the Catalan Institution for Research and Advanced Studies (ICREA),

CERTIFIES, that the present research work entitled "Supramolecular Chemistry of bis-porphyrins" that Laura P. Hernández Eguía presents to obtain the PhD degree in Chemistry, has been carried out under my supervision in the ICIQ and and fulfils all the requirements to be awarded with the "Doctor Europaeus" Mention.

Tarragona, 25 October 2010

PhD Thesis supervisor

Prof. Pablo Ballester Balaguer

UNIVERSITAT ROVIRA I VIRGILI  
SUPRAMOLECULAR CHEMISTRY OF BIS-PORPHYRINS  
Laura Patricia Hernández Eguía  
ISBN:978-84-694-0308-2/DL:T-204-2011

***“Quien quiera enseñarnos la verdad que no nos la diga. Que nos sitúe de tal modo  
que la podamos descubrir nosotros mismos”***

José Ortega y Gasset

UNIVERSITAT ROVIRA I VIRGILI  
SUPRAMOLECULAR CHEMISTRY OF BIS-PORPHYRINS  
Laura Patricia Hernández Eguía  
ISBN:978-84-694-0308-2/DL:T-204-2011

En este momento en el que esta etapa de 4 años llega a su fin me doy cuenta de que se ha hecho corto el trayecto, pero, en cambio, son muchas las personas que han hecho posible que hoy me encuentre escribiendo estas palabras.

En primer lugar estas letras de agradecimiento son para mi director de tesis. Gracias Pau, por tu confianza y tus consejos, por situarme de un modo que me ha permitido conseguir lo que me propuse hace unos años y por las maravillosas oportunidades de las que he podido disfrutar dentro de tu grupo de investigación.

A este grupo de investigación, también le debo mucho. A todos sus miembros desde el inicio: Ana y M<sup>a</sup> Ángeles (mis mamás del laboratorio), muchas gracias por todo, desde el primer día hasta siempre...; Toni, Guzmán, Ana C., Bego, Almu y Muñoz (Vitrin), muchas gracias por vuestras risas, chistes, juegos, rosquilletas que han amenizado muchos "ratos". Y a los que estáis ahora por aquí: Marcos & Eddy, Olga y Mónica, por la serenidad, tan necesaria, que aportáis, Inma et al., (maestra de la papiroflexia), Virginia (mi heredera, en muchos aspectos...) y Moira (la mejor profe de italiano, "siempre fuera de contexto"), muchas gracias por toda vuestra ayuda y por haber conseguido formar un grupo tan divertido, como si de un juego se tratara... Por supuesto no me olvido de Rubén de Parla, David, Carmela y Tony. Gracias a todos, chic@s. Bea, a ti, gracias por todo lo que haces por nosotros.

He tenido también la gran suerte de hacer muchos amigos por aquí. Alba, te has convertido en alguien muy especial, ya lo sabes: "Kop-kun-Kaa". Núria, sabes que te agradezco todo lo que has hecho por mí, que ha sido mucho. Roberto y Cecilia, porque tanto uno como otro hacéis que no exista el estado de "calma" y, Helmut, el alemano más exótico. Los que estáis en Holanda: Elisa, mi compañera de bolitas (fullerenos) y boleros... David Max, gracias por lo bien que me has hecho sentir siempre, por tus detalles y por todo lo que te preocupas por mí.

Un grupo muy especial también y digno de mención es el de la "cocina de la planta baja". Gracias a todos (Kerman, Albert, mi pequeña Gloria, Simona, Sergio, Jandro, Yvette, Marta, Ángel, David...) porque la hora de la comida siempre ha sido un momento de desconexión muy necesario en el día a día. No me olvidaré de las discusiones filosóficas que han tenido lugar ahí. Jordi, a ti agradecerte el recibir tus frases, casi diarias, y tu confianza en mi (sabes que me puedes dejar a Nais cuando quieras...).

Tengo que agradecer a alguien muy importante en los dos últimos años para que mucho de este trabajo saliera adelante y lo más importante, me diera fuerza, ánimo y muchas ideas. ¡Muchas gracias Eduardo! Espero que todo te vaya muy bien y sigas, al menos, igual que hasta ahora.

Gracias a todo el soporte técnico del ICIQ, por resolver dudas, tratar de hacer el trabajo más fácil y toda la paciencia que nos demuestran: Kerman, Gabriel, Enrique, Simona, Sergio, Gisela, Mariona, Eduardo, Marta, Jordi, Fernando, Noemí y Alba. A todo el equipo de informática por todo el trabajo que hacen y la dedicación que ponen en ello para que todo funcione correctamente. Antón, a ti también te recuerdo, ¿eh? Y a las personas del ICIQ que siempre están dispuestas a regalar una sonrisa: María Fernández y Diana, los chicos de logística y el personal de mantenimiento.

Durante i tre mesi trascorsi a Bologna ho avuto la possibilità di imparare molte cose, grazie soprattutto all'aiuto de la Prof. Lucia Flamigni e alla pazienza e gentilezza di Barbara Ventura. Ve ne sono molto riconoscente. Così come ringrazio tutti i colleghi del CNR per l'accoglienza che mi hanno riservato. Infine, un grazie particolare va alle ragazze più belle di tutta Bologna: Paola, Michela, Antonella, Lucia e Federica.... siete meravigliose.

A los que estáis ahora mismo a mi alrededor en esta sala de escritura de tesis, Mihai, Vero y Carolina. Bueno, hemos compartido muchos momentos de desesperación y también de risas y cantos que han hecho que estar aquí escribiendo haya sido una experiencia inolvidable. Os deseo lo mejor.

Mis amigos más viejos, los vigüeses: Laura, Ana, María, Rosalía, Roi y Fernando. Aunque nos hayamos visto poco durante estos años, siempre os tengo presentes y sé que esto no cambiará nunca. Gracias por todo vuestro apoyo. Sois los mejores. José, tú no eres vigüés, eres de un poco más lejos, pero sabes que opino lo mismo y que te agradezco muchísimo tu ayuda y la de tus hermanos.

Seguro que no hubiera llegado hasta aquí sin la ayuda de mi familia. Me siento la persona más afortunada por tener esta familia. Abuelo, puede que la rama investigadora me venga de ti, ¿no crees? Aunque seguro que tan organizada como tú no llegaré a ser nunca. Casi te pido que me numeres las moléculas como tú numeras a las personas en tus álbumes de fotos. Sí, a las moléculas o "enanos" como tú los llamas. La botita con los enanitos ha sido mi amuleto durante estos años y ahora puedes ver aquí como los he ido encontrando, aunque haya costado lo suyo. Muchas gracias por todo tu interés en mi

trabajo, y tus sabias palabras. Yiya, ojalá pueda heredar tu dulzura, tu vitalidad y tu forma de mantenerte siempre bien; siempre, estando contigo o escuchándote por teléfono has conseguido relajarme. A mis padres, estoy segura de que no les puedo agradecer ni con palabras ni con gestos todo lo que han hecho siempre por mí y todo su apoyo incondicional. Sois los mejores. Eso sí, mamá, gracias por haber comido tantas “cosas ricas”. Álex, hermanito, no pierdas nunca tu fuerza para conseguir lo que quieres. A Marta, Susana y Cruz, gracias por todo lo que me habéis transmitido, de un modo u otro.

Y todo tiene un fin, no sé todavía si por suerte o por desgracia. Ha costado llegar hasta aquí, pero ahora, desde lo alto, puedo ver que ha valido la pena. Si hablo de alturas, vías y caminos es para agradecer a Jaime toda su ayuda, paciencia, consejos y cariño durante el recorrido hacia ésta y muchas otras cimas...

Laura

El trabajo recogido en esta memoria ha sido posible gracias a la concesión por parte del Ministerio de Educación y Ciencia de una Beca Predoctoral de Formación de Profesorado Universitario (FPU: AP2006-02914) y a la financiación del Institut Català d'Investigació Química (ICIQ). Además, se ha desarrollado dentro del marco de los proyectos CTQ2005-08989-C01-C02/BQU y CTQ2008-00222/BQU del MICINN, INTECAT (CSD2006-003) perteneciente al Programa Consolider Ingenio 2010 y al DURSI (2009SGR6868) de la Generalitat de Catalunya.



UNIVERSITAT ROVIRA I VIRGILI



Consolider Ingenio 2010  
CSD2006-003  
Diseño de Consolider  
para una Química Sostenible:  
una Aproximación Integrada



UNIVERSITAT ROVIRA I VIRGILI  
SUPRAMOLECULAR CHEMISTRY OF BIS-PORPHYRINS  
Laura Patricia Hernández Eguía  
ISBN:978-84-694-0308-2/DL:T-204-2011

UNIVERSITAT ROVIRA I VIRGILI  
SUPRAMOLECULAR CHEMISTRY OF BIS-PORPHYRINS  
Laura Patricia Hernández Eguía  
ISBN:978-84-694-0308-2/DL:T-204-2011

*A mis padres, y a los suyos.*

UNIVERSITAT ROVIRA I VIRGILI  
SUPRAMOLECULAR CHEMISTRY OF BIS-PORPHYRINS  
Laura Patricia Hernández Eguía  
ISBN:978-84-694-0308-2/DL:T-204-2011

## TABLE OF CONTENTS

|  |            |
|--|------------|
| <b>RESUMEN</b>   | <b>19</b>  |
| <b>ABBREVIATIONS AND ACRONYMS</b>  | <b>23</b>  |
| <b>GENERAL INTRODUCTION</b>  | <b>25</b>  |
| 1. INTRODUCTION .....  | 27         |
| 2. SUPRAMOLECULAR PORPHYRIN-FULLERENE CHEMISTRY .....  | 29         |
| 2.1 <i>Monoporphyrins and fullerenes</i> .....   | 30         |
| 2.2 <i>Bis-porphyrins and fullerenes</i> .....   | 44         |
| 3. SUPRAMOLECULAR CHEMISTRY OF ZN-PORPHYRINS WITH NITROGENATED LIGANDS. .56                    |            |
| 3.1 <i>Zn-porphyrin monomers binding amines</i> .....  | 57         |
| 3.2 <i>Porphyrin dimers binding amines</i> .....   | 62         |
| 4. OBJECTIVES .....  | 69         |
| <b>CHAPTER 1</b>   | <b>71</b>  |
| 1. INTRODUCTION .....  | 73         |
| 2. RESULTS AND DISCUSSION .....  | 75         |
| 2.1 <i>UV-visible titration experiment at micromolar concentrations</i> .....                  | 78         |
| 2.2 <i><sup>1</sup>H NMR titration experiment at millimolar concentrations</i> .....           | 80         |
| 2.3 <i>Synthesis</i> .....   | 83         |
| 3. CONCLUSIONS .....   | 94         |
| 4. EXPERIMENTAL SECTION .....  | 95         |
| 4.1 <i>General information and instrumentation</i> .....                                       | 95         |
| 4.2 <i>Binding studies</i> .....   | 96         |
| a. <i><sup>1</sup>H NMR titrations</i> .....   | 96         |
| b. <i>UV-visible titrations</i> .....  | 96         |
| 4.3 <i>Synthesis</i> .....   | 97         |
| <b>CHAPTER 2</b>   | <b>103</b> |
| 1. INTRODUCTION .....  | 105        |
| 2. RESULTS AND DISCUSSION .....  | 107        |
| 2.3 <i>Synthesis of the bis-porphyrin macrocycle Zn<sub>2</sub>-12</i> .....                   | 107        |
| 2.4 <i>Synthesis of bis-porphyrin tweezers receptors using the Hay coupling reaction</i> ..... | 119        |
| 2.5 <i>Synthesis of bis-porphyrin macrocycles using the Hay coupling reaction</i> .....        | 125        |
| 3. CONCLUSIONS .....   | 138        |
| 4. EXPERIMENTAL SECTION .....  | 138        |
| 4.1 <i>General information and instrumentation</i> .....                                       | 138        |
| 4.2 <i>Synthesis</i> .....   | 139        |

|   |            |
|---|------------|
| <b>CHAPTER 3</b>  | <b>147</b> |
| 1. INTRODUCTION .....   | 149        |
| 2. RESULTS AND DISCUSSION .....   | 150        |
| 2.1 <i>Bis-porphyrin tweezers: mono- and ditopic amines</i> .....   | 150        |
| a. <i>UV-visible titrations</i> .....   | 153        |
| b. <i><sup>1</sup>H NMR titrations</i> .....  | 165        |
| 2.2 <i>Binding studies of bis-porphyrin macrocycles with ditopic amines</i> .....   | 171        |
| a. <i>UV-visible titrations</i> .....   | 171        |
| b. <i><sup>1</sup>H NMR titrations</i> .....  | 175        |
| <i>We also carried out titrations in CDCl<sub>3</sub> at millimolar concentrations using <sup>1</sup>H NMR spectroscopy at room temperature in order to gain additional information on the structure of the inclusion 1:1 complexes. ....</i> |            |
| 3. CONCLUSIONS .....  | 178        |
| 4. EXPERIMENTAL SECTION .....   | 178        |
| 4.1 <i>General information and instrumentation</i> .....  | 178        |
| 4.2 <i>Binding studies</i> .....  | 180        |
| a. <i>UV-visible titrations</i> .....   | 180        |
| b. <i><sup>1</sup>H NMR titrations</i> .....  | 180        |
| <b>CHAPTER 4</b>  | <b>181</b> |
| 1. INTRODUCTION .....   | 183        |
| 2. RESULTS AND DISCUSSION .....   | 187        |
| 2.1 <i>Binding studies of the cyclic bis-porphyrin receptors with C<sub>60</sub> and C<sub>70</sub>: Photophysical characterization of the solution assemblies.</i> .....   | 187        |
| 2.2 <i>Binding studies with C<sub>60</sub> and C<sub>70</sub></i> .....   | 191        |
| a. <i>UV-visible and fluorescence titrations</i> .....  | 191        |
| b. <i><sup>1</sup>H NMR titrations</i> .....  | 195        |
| 2.3 <i>Preliminary photophysical studies of the systems cyclic bis-porphyrin/fullerene</i> .....  | 201        |
| 2.4 <i>Binding with the endohedral fullerene Sc<sub>3</sub>N@C<sub>80</sub>: solution and solid state</i> .....   | 204        |
| 3. CONCLUSIONS .....  | 213        |
| 4. EXPERIMENTAL SECTION .....   | 214        |
| 4.1 <i>General information and instrumentation</i> .....  | 214        |
| 2.1 <i>Binding studies</i> .....  | 215        |
| a. <i><sup>1</sup>H NMR titrations</i> .....  | 215        |
| b. <i>UV-visible and fluorescence titrations</i> .....  | 215        |
| <b>CHAPTER 5</b>  | <b>217</b> |
| 1. INTRODUCTION .....   | 219        |
| 2. RESULTS AND DISCUSSION .....   | 224        |
| 2.1 <i>Synthesis and purification</i> .....   | 224        |
| 2.2 <i>Coordination studies</i> .....   | 227        |
| 3. CONCLUSIONS .....  | 238        |
| 4. EXPERIMENTAL SECTION .....   | 239        |
| 4.1 <i>General information and instrumentation</i> .....  | 239        |

|     |                                     |     |
|-----|-------------------------------------|-----|
| 4.2 | <i>Binding studies</i> .....        | 241 |
| a.  | <sup>1</sup> H NMR titrations ..... | 241 |
| b.  | UV-visible titrations .....         | 241 |
| c.  | Circular dichroism titrations ..... | 241 |
| 4.3 | <i>Synthesis</i> .....              | 242 |

UNIVERSITAT ROVIRA I VIRGILI  
SUPRAMOLECULAR CHEMISTRY OF BIS-PORPHYRINS  
Laura Patricia Hernández Eguía  
ISBN:978-84-694-0308-2/DL:T-204-2011

## Resumen

En este trabajo de tesis doctoral se desarrollan básicamente dos aspectos. El primero, es la síntesis de receptores bis-porfínicos metalados con zinc, tanto acíclicos como cíclicos, y con diferente grado de saturación de las cadenas carbonadas (Figura 1), y el segundo, trata sobre los estudios de complejación llevados a cabo con ligandos de diferente tipo y propiedades: aminas y fullerenos. Los primeros se unen mediante enlaces de coordinación metal-nitrógeno, mientras que los segundos se basan en interacciones  $\pi-\pi$  entre el anillo aromático de la porfirina y la estructura con un marcado carácter aromático de los fullerenos.

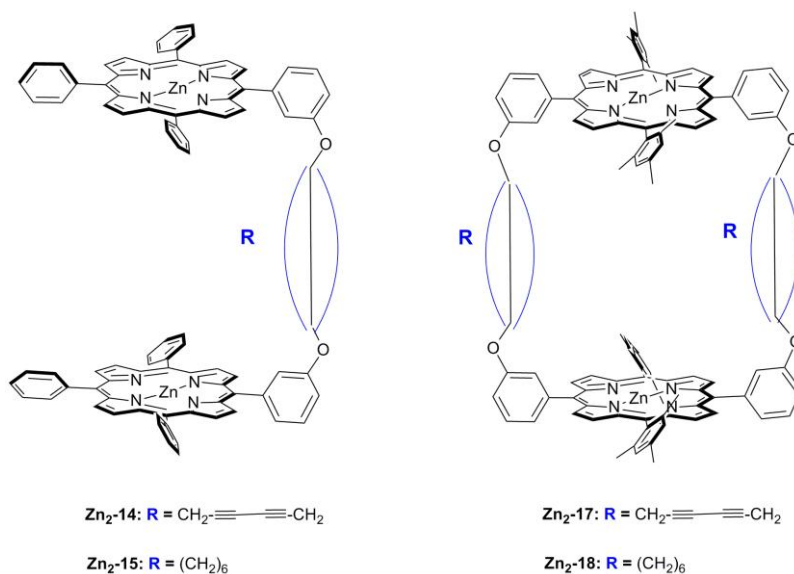
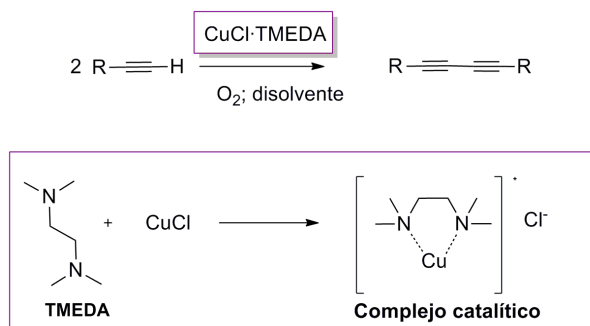


**Figura 1.** Estructuras de las dos bis-porfirinas de zinc acíclicas, **Zn<sub>2</sub>-14** y **Zn<sub>2</sub>-15** y de los macrociclos bis-porfínicos, **Zn<sub>2</sub>-17** y **Zn<sub>2</sub>-18**. Cada pareja de receptores se compone de uno con la cadena o cadenas insaturadas y otro con ellas completamente reducidas.

En la introducción general de esta memoria se hace una amplia revisión sobre los trabajos de investigación llevados a cabo, principalmente en los últimos 15 años, en el ámbito de los complejos supramoleculares entre mono- y bis-porfirinas con fullerenos y aminas destacando las propiedades más relevantes para el entendimiento de lo que en esta tesis se tratará.

En los dos primeros capítulos se describe la síntesis de los dos tipos de receptores haciendo un uso exhaustivo de “moléculas-plantilla” para facilitar la unión covalente tal y como queremos que tenga lugar. Los dos tipos de reacciones de acoplamiento descritos son la metátesis de olefinas con catalizadores de Grubbs (capítulo 1) y el acoplamiento oxidativo de triples enlaces de Hay (capítulo 2), siendo la última la estudiada en mayor detalle y con mejores resultados (Esquema 1).



**Esquema 1.** Dos acetilenos terminales dan lugar a uniones diacetilénicas bajo las condiciones de acoplamiento de Hay. El complejo catalítico se compone de Cu(I) con dos enlaces de coordinación con el TMEDA, de esta forma es soluble en la mayoría de disolventes orgánicos.

Esto se ha debido a un problema con la pureza en las monoporfirinas de partida, que presentaba una mezcla de los isómeros *cis* y *trans* en relación con las cadenas olefinicas o propargílicas, del que fuimos conscientes cuando ya trabajábamos con acoplamientos de triples enlaces para crear los receptores bis-porfirínicos. El objetivo fue el conseguir un isómero *trans* puro de la monoporfirina dipropargilada, y se consiguió al cambiar el sustituyente fenílico en *meso* por un trimetilfenilo.

En los capítulos 3 y 4 se exponen los resultados derivados de la complejación con aminas, monotópicas (quinuclidina y piridina) y ditópicas (DABCO y 4,4'-bipiridina) y fullerenos ( $\text{C}_{60}$ ,  $\text{C}_{70}$  y  $\text{Sc}_3\text{N}@C_{80}$ , un fullereno endohédrico proporcionado por el grupo del Prof. L. Echegoyen) respectivamente (Figura 2). Nuestro interés reside en estudiar cómo el tipo de cadena, con triples enlaces o completamente hidrogenada, de unión entre los dos anillos de porfirina, influye en las propiedades de unión con

los dos tipos de familia de ligandos, así como evaluar el efecto del macrociclo en la estabilidad de los complejos. Los correspondientes estudios se llevan a cabo mediante diferentes técnicas espectroscópicas: RMN de  $^1\text{H}$ , UV-visible y fluorescencia, donde el análisis matemático de los datos nos permite caracterizar termodinámicamente los procesos de coordinación en los que los receptores porfirínicos están implicados.

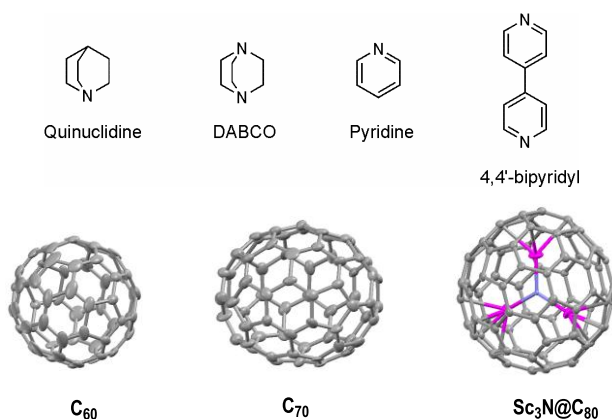


**Figura 2.** Estructuras de los dos conjuntos de ligandos con los que se han llevado a cabo estudios de complejación con los sistemas bis-porfirínicos.

Además de estos estudios que tienen lugar en disolución, hemos sido capaces de determinar diferentes geometrías de complejación para los fullerenos con los receptores bis-porfirínicos cíclicos en estado sólido, ya que el crecimiento de cristales apropiados para su medida por rayos-X fue posible. Además, y como en los objetivos iniciales de esta tesis doctoral queríamos diseñar ensamblajes funcionales, algunos estudios fotofísicos preliminares con los complejos supramoleculares formados entre los dímeros cíclicos porfirínicos y los fullerenos, C<sub>60</sub> y C<sub>70</sub>, se han llevado a cabo en colaboración con Prof. Lucia Flamigni y Dra. Barbara Ventura en el ISOF-CNR, en Bologna. En concreto, usando complejos bis-porfirina:fullereno, estudiamos los procesos de transferencia electrónica inducida fotoquímicamente como punto de partida en el desarrollo de aplicaciones de conversión de luz en energía. Estudios más avanzados de los aquí descritos están llevándose a cabo en estos momentos en el grupo de Bologna (capítulo 4).

Por último, en el capítulo 5, se exponen los resultados que hemos obtenido al derivar uno de los ciclopéptidos del grupo de investigación del Prof. J.R. Granja con

una o dos porfirinas de zinc y emplear el ensamblaje supramolecular tipo “sándwich” entre bis-porfirinas y aminas ditópicas para controlar la mezcla regioisomérica que tiene lugar en el proceso de autoensamblaje entre los ciclopeptidos al formar dímeros (Figura 3).

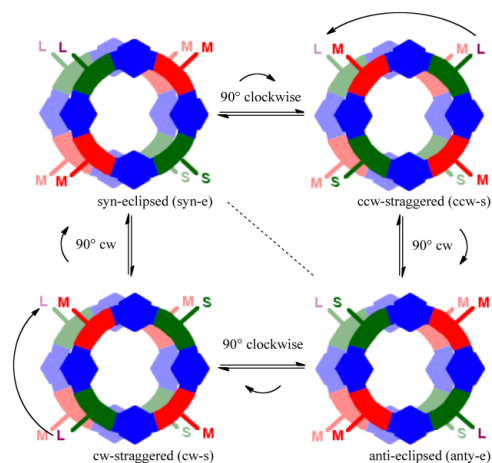


**Figura 3.** Representación esquemática de los cuatro dimeros no equivalentes que se forman en disolución cuando el DABCO no está presente en el sistema.

El objetivo de este trabajo es mostrar la relación que hay entre estructura y función cuando los ciclopeptidos se funcionalizan con unidades de porfirina que son capaces de formar complejos tipo sándwich con ligandos ditópicos, en este caso DABCO. Los estudios se han realizado basándonos principalmente en técnicas espectrofotométricas: UV-visible y dicroísmo circular. También, y como discute a lo largo de toda la tesis, la unión del DABCO entre dos unidades de porfirina se sigue fácilmente por RMN de  $^1\text{H}$  al dar una señal característica a -5ppm. En este capítulo se reflejan los resultados que han sido recientemente aceptados para publicación: Hernández-Eguía, Laura P.; Brea, R. J.; Castedo, L.; Ballester, P.; Granja, J. “Regioisomeric Control induced by DABCO Coordination to Rotatable Self-Assembled Bis- and Tetra-porphyrin  $\alpha,\gamma$ -Cyclic Octapeptide Dimers (DABCO = 1,4-Diazabicyclo[2.2.2]octane).” Chem. Eur. J. (2010).

## Abbreviations and Acronyms

Additionally to the recommendations of “Guidelines for authors” in *J. Org. Chem.*, other abbreviations and acronyms have been used:

|                     |   |
|---------------------|---|
| $\alpha$            | cooperativity coefficient                   |
| $\gamma$ -Ach       | 3-aminocyclohexanecarboxylic acid           |
| AcO                 | acetate                                     |
| Bipy                | 4,4'-bipyridyl                              |
| CP                  | cyclopeptide                                |
| CPK                 | Corey-Pauling-Koltun space-filling model    |
| DIC                 | N,N'-diisopropylcarbodiimide                |
| DPYP                | 5,15-bis(4-pyridyl)-10,20-diphenylporphyrin |
| DCM                 | dichloromethane                             |
| DOSY                | Diffusion-Ordered-Spectroscopy              |
| EM                  | effective molarity                          |
| $\phi$              | quantum yield                               |
| GPC                 | gel permeation chromatography               |
| H <sub>2</sub> TpyP | <i>meso</i> -tetra-(4-pyridyl)porphyrin     |
| NIR                 | near infrared                               |
| TPP                 | tetraphenylporphyrin                        |
| Phe                 | phenylalanine                               |
| Ser                 | serine                                      |
| $\tau$              | excited state lifetime                      |
| TOL                 | toluene                                     |
| UV-visible          | ultraviolet-visible                         |

UNIVERSITAT ROVIRA I VIRGILI  
SUPRAMOLECULAR CHEMISTRY OF BIS-PORPHYRINS  
Laura Patricia Hernández Eguía  
ISBN:978-84-694-0308-2/DL:T-204-2011

## GENERAL INTRODUCTION

***“Supramolecular systems induced by coordination of mono- and bis-porphyrins with fullerenes and nitrogen ligand molecules”***

UNIVERSITAT ROVIRA I VIRGILI  
SUPRAMOLECULAR CHEMISTRY OF BIS-PORPHYRINS  
Laura Patricia Hernández Eguía  
ISBN:978-84-694-0308-2/DL:T-204-2011

## 1. Introduction

Non-covalent forces are key to maintain molecules together in supramolecular chemistry; likewise the covalent bond is the essence of the link between atoms in molecules. Non-covalent interactions are always weaker than covalent bonds though they can have different strengths, from weak to very strong, i.e. metal coordination, donor-acceptor, electrostatic van der Waals interactions, hydrogen bonding, etc.

When synthetic molecules behave in the same way than their biological counterparts in Nature, that means they self-assemble and self-organize<sup>1,2</sup> into molecular systems, we are confronted with supramolecular chemistry.

As much of the inspiration and origins of supramolecular chemistry comes from the chemistry found in living biological systems, many studies have been focused on developing artificial photosynthetic systems to achieve light-to-energy conversion, similarly to the natural photosynthetic system that converts solar energy into chemical energy very efficiently and is regarded as one of the most elaborate nanobiological machines.<sup>3,4,5</sup>

One of the main challenges in the field of supramolecular chemistry is the translation of molecular structure into function. In fact, synthetic multiporphyrin assemblies have been extensively investigated in materials science and nanotechnology and, in particular, its application to light-induced functions has attracted a great deal of interest.

Porphyrins are one of the most common and versatile chromophores. These molecular components introduce photochemical and redox properties to the overall assembled architectures in which they participate. The structure of a porphyrin consists basically of four pyrrole units connected through their  $\alpha$ -carbon atoms by  $sp^2$  hybridized carbon atoms, termed the "meso-carbons". They are aromatic and a highly conjugated system, therefore they are deeply colored. In fact, the origin of its name derives from the greek word for "purple": πορφύρα (porphyra). But porphyrins also

---

<sup>1</sup> Lehn, J. M. *Pure Appl. Chem.* **1994**, 66, 1961-1966.

<sup>2</sup> Lehn, J. M. *Reports on Progress in Physics* **2004**, 67, 249-265.

<sup>3</sup> Takahashi, R.; Kobuke, Y. *J. Am. Chem. Soc.* **2003**, 125, 2372-2373.

<sup>4</sup> Peng, X. B.; Aratani, N.; Takagi, A.; Matsumoto, T.; Kawai, T.; Hwang, I. W.; Ahn, T. K.; Kim, D.; Osuka, A. *J. Am. Chem. Soc.* **2004**, 126, 4468-4469.

<sup>5</sup> Kim, D.; Osuka, A. *Acc. Chem. Res.* **2004**, 37, 735-745.

are red in blood (heme) and green in leaves (chlorophyll). They can be functionalized at the *meso*- and  $\beta$ -positions (Figure 1). The porphyrins units can incorporate a metal atom through a chemical reaction usually termed as metallation, and the coordination chemistry of the metal centre can be used to introduce additional components and features to the overall assembly.

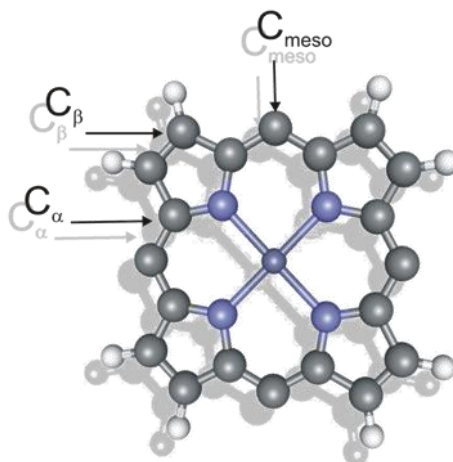


**Figure 1.** Molecular structure of a porphyrin. The three types of carbons in the porphyrinic ring are highlighted (*meso*,  $\alpha$  and  $\beta$ -carbons).

Porphyrins offer a variety of desirable features such as a rigid and planar geometry, high stability, intense electronic absorption, strong fluorescence emission, and a small HOMO-LUMO energy gap. For all this motivation supramolecular architectures containing porphyrins and metalloporphyrins are particularly attractive.

To synthesize supramolecular systems it is necessary to reach a “compromise” between the use of non-covalent and covalent bonds. The purely covalent approximation implies a high synthetic effort. Furthermore, the construction of cyclic covalent structures using covalent chemistry is highly limited by kinetic control. The desired macrocyclic or oligocyclic structures are obtained in direct competition with other polymeric and undesired cyclic species in which the starting material is kinetically trapped. The non-covalent approximation is a good alternative which makes spontaneous the formation of a cyclic assembly of multiple components under

reversible conditions, so the supramolecular structure is constructed in a very selective way. However, the main problem of the supramolecular approach is the low thermodynamic stability of the non-covalent interaction when compared to the covalent bond.

This general introduction is divided in two sections. The first one describes assembly processes of porphyrins and metalloporphyrins induced by complexation with fullerenes. The second section is dedicated to the supramolecular chemistry of metalloporphyrins induced by coordination with mono and ditopic nitrogenated ligands. We mainly focus in non-covalent structures and we describe in some detail their thermodynamic stability features and their application in photophysical studies. The selected examples span the last 15 years.

## 2. Supramolecular porphyrin-fullerene chemistry

Fullerenes, are charming and valuable spherical molecules with low reduction potentials and strong electron acceptor properties, specifically they can accept up to six electrons.<sup>6,7,8,9,10</sup> The molecular recognition process between fullerenes and porphyrins was recognized in a very unintentional way, prompting the birth of a new supramolecular recognition element.<sup>11</sup>

The use in supramolecular chemistry of porphyrins and fullerenes is appreciated not only for the affinity that exists between the flat tetrapyrrole ring and the curved surface of the fullerene,<sup>12,13</sup> but also for the capability that the porphyrin-fullerene assemblies possess to photoinduce charge-separated species mimicking the natural photosynthesis processes.<sup>14,15</sup> In fact, porphyrins are the most commonly used

<sup>6</sup> Martin, N.; Sanchez, L.; Illescas, B.; Perez, I. *Chem. Rev.* **1998**, *98*, 2527-2547.

<sup>7</sup> Imahori, H.; Sakata, Y. *Eur. J. Org. Chem.* **1999**, 2445-2457.

<sup>8</sup> Guldi, D. M. *Chem. Commun.* **2000**, 321-327.

<sup>9</sup> Hirsch, A.; Editor *Fullerenes and Related Structures*, **1999**.

<sup>10</sup> Perez, E. M.; Martin, N. *Pure Appl. Chem.* **2010**, *82*, 523-533.

<sup>11</sup> Diederich, F.; Gomez-Lopez, M. *Chem. Soc. Rev.* **1999**, *28*, 263-277.

<sup>12</sup> Sun, D.; Tham, F. S.; Reed, C. A.; Boyd, P. D. W. *Proc. Natl. Acad. Sci. U. S. A.* **2002**, *99*, 5088-5092.

<sup>13</sup> Boyd, P. D. W.; Reed, C. A. *Acc. Chem. Res.* **2005**, *38*, 235-242.

<sup>14</sup> Gust, D.; Moore, T. A.; Moore, A. L. *Acc. Chem. Res.* **2001**, *34*, 40-48.

building blocks in artificial photosynthetic systems as sensitizers and electron donors and one of the best binding units used in fullerene receptors.

## 2.1 Monoporphyrins and fullerenes

The proximity between a porphyrin and a fullerene was advanced by Hoffman in 1995<sup>16</sup> when they obtained, looking for charge transfer molecular crystals, the crystal structure of a porphyrazine, octakis(dimethylamino)porphyrazine, **1**, with C<sub>60</sub> packing in a three-dimensional network where each C<sub>60</sub> is sandwiched between two porphyrazines (Figure 2).

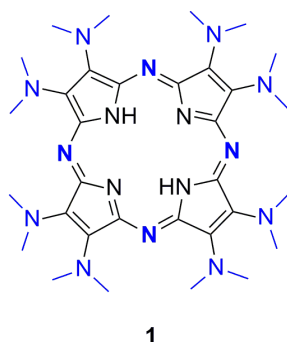


Figure 2. Molecular structure of porphyrazine **1**.

With these crystals grown from toluene solution, they determined a distance from the center of the porphyrazine to the centroid of the fullerene of 6.3 Å and they established the existence of van der Waals contact between them.

In 1997 Boyd & Reed<sup>17</sup> investigated if monosubstituted fullerides (C<sub>60</sub><sup>1-</sup>) retained much of its parent C<sub>60</sub> character. They prepared a pyrrolidine-linked tetraphenylporphyrin/C<sub>60</sub> dyad **2** and found that in the solid state, **2**, packs forming self-assembled dimers. An interesting feature of the solid structure is the

<sup>15</sup> Wasielewski, M. R. *J. Org. Chem.* **2006**, *71*, 5051-5066.

<sup>16</sup> Eichhorn, D. M.; Yang, S. L.; Jarrell, W.; Baumann, T. F.; Beall, L. S.; White, A. J. P.; Williams, D. J.; Barrett, A. G. M.; Hoffman, B. M. *J. Chem. Soc., Chem. Commun.* **1995**, 1703-1704.

<sup>17</sup> Sun, Y. P.; Drovetskaya, T.; Bolskar, R. D.; Bau, R.; Boyd, P. D. W.; Reed, C. A. *J. Org. Chem.* **1997**, *62*, 3642-3649.

intermolecular packing relationship of C<sub>60</sub> to the porphyrin unit. There are two distinct crystallographic contacts: intra-dimer and inter-dimer (Figure 3). In both cases, however, the distance between the closest C<sub>60</sub> carbon atom to the mean plane of the 16-atom inner core of the porphyrin ring is very short: 2.78 Å (inter-dimer) and 2.79 Å (intra-dimer). These distances are clearly shorter than the separation observed in the solid state for graphite inter-layer (3.35 Å), interfacial porphyrin-porphyrin (> 3.2 Å), C<sub>60</sub> to C<sub>60</sub> (> 3.2 Å) and C<sub>60</sub> form arene ring (3.0 – 3.5 Å). This observation suggested that the π-π interaction between C<sub>60</sub> and the porphyrin unit is substantially augmented probably due to strong donor-acceptor interactions (Figure 3). In contrast to the usual view of C<sub>60</sub> as an acceptor, the sense of this donor-acceptor relationship might be with C<sub>60</sub> acting as donor and the porphyrin unit being the acceptor. If this was the case, one could expect that the more electron rich bonds of the fullerene (6:6 junctures) should preferentially interact with the porphyrin unit. The X-ray crystal structure bore out this expectation, at least in one of the two interaction geometries.

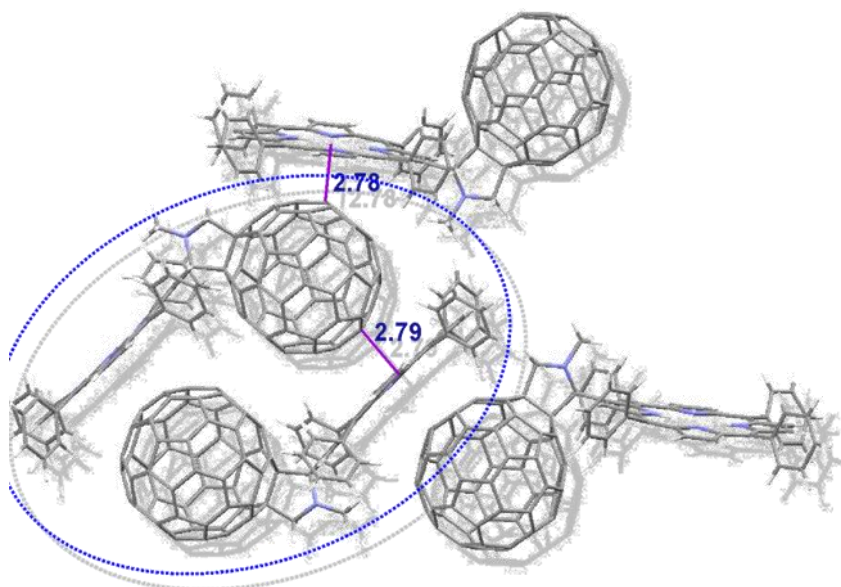


**Figure 3.** Drawing of the packing of the X-ray crystal structure of **2**. C<sub>60</sub> is covalently linked to a tetraaryl monoporphyrin. The blue ellipsoidal circle is rounded one of the self-assembled dimers. The inter-dimer and intra-dimer distances between the closest C<sub>60</sub> atom to the inner core of the porphyrin plane are indicated.

Further studies were carried out involving not only buckminsterfullerene  $C_{60}$  but also  $C_{70}$ . The attractive interaction involving fullerenes and porphyrins derived from the close fullerene/porphyrin distance observed in the crystal structure of **2** could have been a result of the crystal packing because the fullerene and the porphyrin are covalently attached. In 1999 Boyd & Reed showed that the association of  $C_{60}/C_{70}$  and tetraphenylporphyrins (TPPs) is also found in untethered cocrystallates and that this type of interaction also exists in solution.<sup>18</sup> The TPPs used in the study possess aliphatic substituents and favorable “solvation” CH- $\pi$  interactions of these residues with  $C_{60}$  and  $C_{70}$  were observed in the solid structures. This seems to be the next most important interactions in these systems after  $\pi$ - $\pi$  interactions, and is consistent with the relative solubility of  $C_{60}$  in arenes versus alkenes.<sup>19</sup> Another important finding of this study is the greater porphyrin-fullerene contact area observed for the 1:1  $C_{70}$  TPP clusters with respect to  $C_{60}$ , as long as the interaction geometry is side-on rather than end-on (Figure 4).

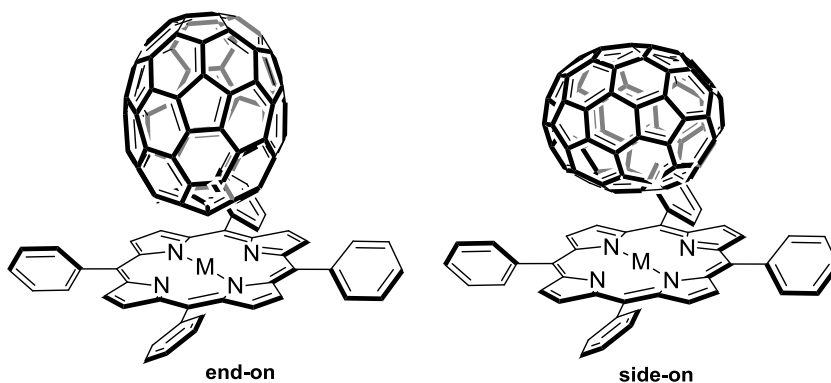


**Figure 4.** Schematic representation of the two possible geometries, end-on and side-on, when  $C_{70}$  is interacting with the porphyrin surface of the tetraphenylporphyrin (TPP).

Photoinduced electron transfer processes between  $C_{60}/C_{70}$  and zinc tetraphenylporphyrin in polar solvents were investigated, using nanosecond laser

<sup>18</sup> Boyd, P. D. W.; Hodgson, M. C.; Rickard, C. E. F.; Oliver, A. G.; Chaker, L.; Brothers, P. J.; Bolskar, R. D.; Tham, F. S.; Reed, C. A. *J. Am. Chem. Soc.* **1999**, *121*, 10487-10495.

<sup>19</sup> Ruoff, R. S.; Tse, D. S.; Malhotra, R.; Lorents, D. C. *J. Phys. Chem.* **1993**, *97*, 3379-3383.

photolysis examining the near-IR region, in 1998 by Ito et al.<sup>20</sup> The authors describe an electron transfer process that occur when one of the two partners, the fullerene or the Zn-porphyrin, is photoexcited and encounter the other in solution. It is a bimolecular process controlled by diffusion and it is possible if the concentration of the two species is high (they work around  $10^{-4}$  M). In fact, the electron transfer they observe occurs upon collision of one photoexcited partner with the other. The ion radicals must be detected to assure that the system involves electron transfer. The transient absorption bands for highly conjugated molecules such as C<sub>60</sub>/C<sub>70</sub> are supposed to appear in the near-IR region of the spectrum. When the C<sub>60</sub>/C<sub>70</sub> chromophore was predominantly photoexcited, electron transfer took place from the ZnTPP ground state to the lower energy triplet excited state of the fullerene, <sup>3</sup>C<sub>60</sub><sup>\*</sup>/<sup>3</sup>C<sub>70</sub><sup>\*</sup>, yielding the corresponding fulleride (C<sub>60</sub><sup>-</sup>/C<sub>70</sub><sup>-</sup>). On the contrary, when the species predominantly excited was the ZnTPP unit, it is the triplet state <sup>3</sup>ZnTPP<sup>\*</sup> that donates the electron to the ground state of the fullerene producing the corresponding anion radical C<sub>60</sub><sup>-</sup>/C<sub>70</sub><sup>-</sup>. The efficiency of the electron transfer via photoexcitation to the triplet state of the fullerene is higher than the route involving the ZnTPP triplet state.

In 1999 Diederich et al.<sup>21</sup> reported the binding of ZnTPP with a methanofullerene derivative bearing a pyridyl moiety, **3**. The photophysical properties of the assembly were studied and compared to the analogous fullerene mono-malonate without the pyridyl group, **4**, which did not show any sign of complexation with the ZnTPP at  $\mu$ M concentration (Figure 5).

<sup>20</sup> Nojiri, T.; Watanabe, A.; Ito, O. *J. Phys. Chem. A* **1998**, *102*, 5215-5219.

<sup>21</sup> Armaroli, N.; Diederich, F.; Echegoyen, L.; Habicher, T.; Flamigni, L.; Marconi, G.; Nierengarten, J. F. *New J. Chem.* **1999**, *23*, 77-83.

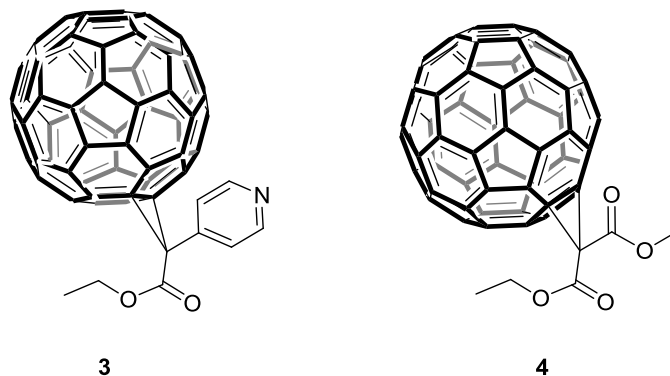


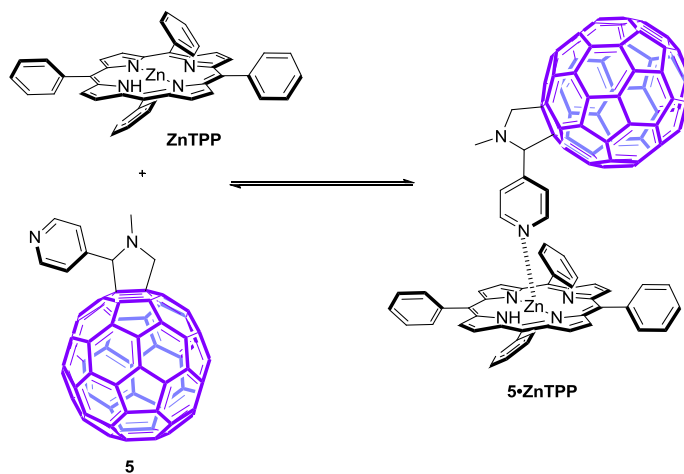
**Figure 5.** Structures of pyridyl-substituted methanofullerene derivative, **3**, and its analogous fullerene mono-malonate adduct **4**.

The association constant value determined for the 1:1 complex, **3**•ZnTPP, using <sup>1</sup>H NMR titrations in C<sub>6</sub>D<sub>6</sub> solution was  $K_a = 3.6 \times 10^3 \text{ M}^{-1}$ . This value is in good agreement with the one derived from luminiscence experiment in toluene,  $K_a = 3 \times 10^3 \text{ M}^{-1}$ . The addition of large amounts of **3** to the solution of ZnTPP produced a 50 % diminution of the porphyrin fluorescence. Moreover, the absorption spectrum of the mixture showed a 10 nm red-shift in the Soret band with respect the free ZnTPP. A similar red-shift is characteristic for axial binding of pyridine ligands to zinc porphyrins. This was the first non-covalent assembly, using coordination chemistry, reported in solution between a fullerene and a porphyrin. The complex formation is induced by the coordination of the pyridyl moiety to the Zn ion. All attempts to find experimental evidence on the mechanism of the photoinduced process (electron or energy transfer) was unsuccessful. This fluorescence quenching was finally associated with a fast photoinduced energy transfer to the fullerene unit. Nevertheless, this statement is simply based on reported preference of electron transfer to occur in toluene when the porphyrin and the fullerene moieties are facing each other, while energy transfer happens when the components are located at longer distances.<sup>22</sup> Additional prove favoring this hypothesis was derived from the known fast energy transfer mechanism reported through non-covalent bonds.<sup>23</sup>

<sup>22</sup> Kuciauskas, D.; Lin, S.; Seely, G. R.; Moore, A. L.; Moore, T. A.; Gust, D.; Drovetskaya, T.; Reed, C. A.; Boyd, P. D. W. *J. Phys. Chem.* **1996**, *100*, 15926-15932.

<sup>23</sup> Armaroli, N.; Barigelletti, F.; Calogero, G.; Flamigni, L.; White, C. M.; Ward, M. D. *Chem. Commun.* **1997**, 2181-2182.

Almost at the same time, Guldi et al.<sup>24</sup> published that ZnTPP can also be assembled with a somewhat related C<sub>60</sub> derivative, **5**, also having a pyridine residue yielding the corresponding axially coordinated pyridine-metal complex (Scheme 1). UV-visible spectrophotometric titrations carried out in non coordinating solvent like dichloromethane (DCM) or toluene (TOL) revealed that the incremental addition, of **5** to the solution of ZnTPP induced a red-shift in the two Q bands (DCM, 548→559 nm; 588→598 nm) and a narrowing effect in the Soret band. Both effects are characteristic for the formation of axially coordinated pyridine-Zn-porphyrin complexes.<sup>25,26,27</sup> In solutions of coordinating solvents like THF or benzonitrile, it was not possible to derive a dependence of the spectral changes with concentration due to solvent competition. The ZnTPP•**5** 1:1 complex formed in non-coordinated solvents features a NIR-fingerprint absorption band at 1100 nm which was assigned to the photoinduced charge-separated radical pair.



**Scheme 1.** Complexation equilibrium for the coordination process of ZnTPP with the C<sub>60</sub> pyridyl derivative **5**. The 1:1 complex is formed through an axial coordination between the pyridine nitrogen and Zn atom.

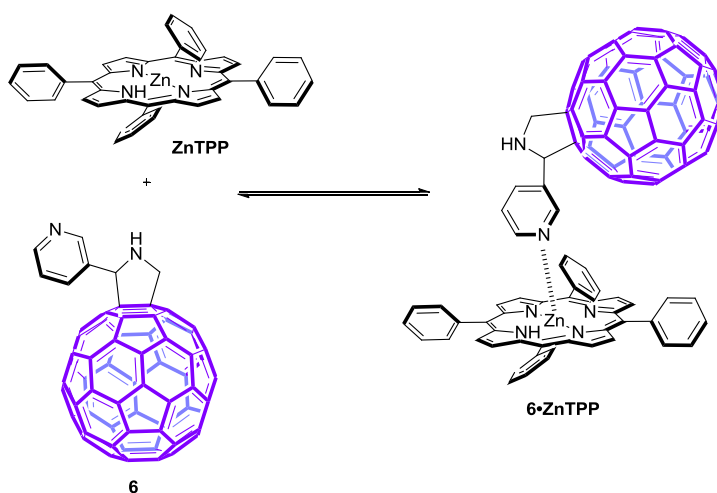
<sup>24</sup> Da Ros, T.; Prato, M.; Guldi, D.; Alessio, E.; Ruzzi, M.; Pasimeni, L. *Chem. Commun.* **1999**, 635-636.

<sup>25</sup> Fujisawa, J.; Ishii, K.; Ohba, Y.; Yamauchi, S.; Fuhs, M.; Mobius, K. *J. Phys. Chem. A* **1997**, *101*, 5869-5876.

<sup>26</sup> Hunter, C. A.; Hyde, R. K. *Angew. Chem., Int. Ed. Engl.* **1996**, *35*, 1936-1939.

<sup>27</sup> Hunter, C. A.; Shannon, R. J. *Chem. Commun.* **1996**, 1361-1362.

A similar structure lacking the methyl substituent in the pyrrolidine nitrogen and with the covalent attachment of the pyridyl residue in the *meta* position instead of the *para* position of the aromatic ring was also described (Scheme 2).<sup>28</sup> The 1:1 coordination complex of the electron acceptor derivative, **6**, with ZnTPP in 1,2-dichlorobenzene showed the spectral features that are characteristic of penta-coordinated 1:1 zinc porphyrins axially bound to nitrogenated ligands, such are red-shifted Soret and Q bands and the presence of isosbestic points in the UV-visible titration experiment. The formation of the coordination complex was also probed using <sup>1</sup>H NMR titrations. An association constant value of  $K_a = 7.3 \times 10^3 \text{ M}^{-1}$  was determined.



**Scheme 2.** Complexation equilibrium for the coordination process of ZnTPP with the C<sub>60</sub> pyridyl derivative **6**. The 1:1 complex is formed through an axial coordination between the pyridine nitrogen and Zn atom.

In the previous examples we described that the interaction involved in complex formation is the pyridyl-metal axial coordination bond. Thus, the non-covalent porphyrin-fullerene dyads are constructed without the direct implication of  $\pi$ - $\pi$  interactions.

<sup>28</sup> D'Souza, F.; Deviprasad, G. R.; Rahman, M. S.; Choi, J. P. *Inorg. Chem.* **1999**, *38*, 2157-2160.

The generality of the supramolecular recognition element between the flat tetrapyrrole and the curved surface of the fullerenes appeared not only in the solid state with tetraphenylporphyrins as mentioned above but also became evident in the interaction of  $\beta$ -octaethylmetalporphyrins and fullerenes ( $C_{60}$ ,  $C_{60}O$ ,  $C_{70}$  and  $C_{120}O$ ). Olmstead, Balch et al. solved the solid state structures of eight complexes of fullerenes with the  $\beta$ -pyrrole substituted octaethyl metallo porphyrins by X-Ray diffraction analysis of single crystals grown from benzene solutions.<sup>29</sup>

In 2001 Lyubovskaya et al.<sup>30</sup> described a series of new solid-state complexes of tetraphenylporphyrins [M(tpp)] ( $M=H_2$ , Mn, Co, Cu, Zn and FeCl) with  $C_{60}$  and  $C_{70}$ . For example, they obtained two crystal structures of  $H_2TPP$  and  $C_{60}$  in which the only difference resides in the number of solvent molecules present in the unit cell. This subtle difference originates two distinct packing motifs: a honeycomb-like with continuous channels in the case of the unit cell composed of  $H_2TPP \cdot 2C_{60} \cdot 3C_6H_6$  (Figure 6) and graphite-like layers for  $H_2TPP \cdot 2C_{60} \cdot 4C_6H_6$  (Figure 7).

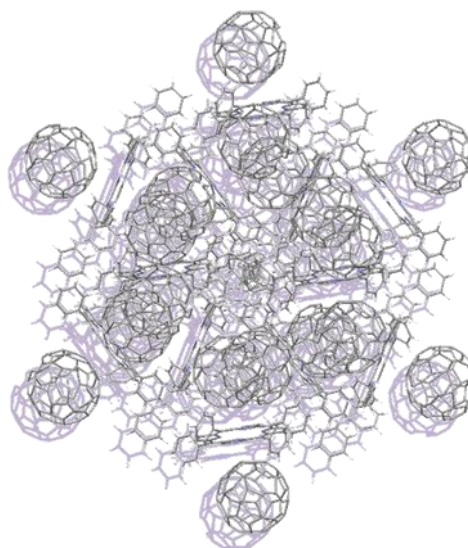


**Figure 6.** Honeycomb-like packing motif in the X-ray crystal structure of  $H_2TPP \cdot 2C_{60} \cdot 3C_6H_6$ . Each tetraphenylporphyrin is sandwiched between two molecules of  $C_{60}$  and they are forming continuous channels.

<sup>29</sup> Olmstead, M. M.; Costa, D. A.; Maitra, K.; Noll, B. C.; Phillips, S. L.; Van Calcar, P. M.; Balch, A. L. *J. Am. Chem. Soc.* **1999**, *121*, 7090-7097.

<sup>30</sup> Konarev, D. V.; Neretin, I. S.; Slovokhotov, Y. L.; Yudanov, E. I.; Drichko, N. V.; Shul'ga, Y. M.; Tarasov, B. P.; Gumanov, L. L.; Batsanov, A. S.; Howard, J. A. K.; Lyubovskaya, R. N. *Chem.--Eur. J.* **2001**, *7*, 2605-2616.

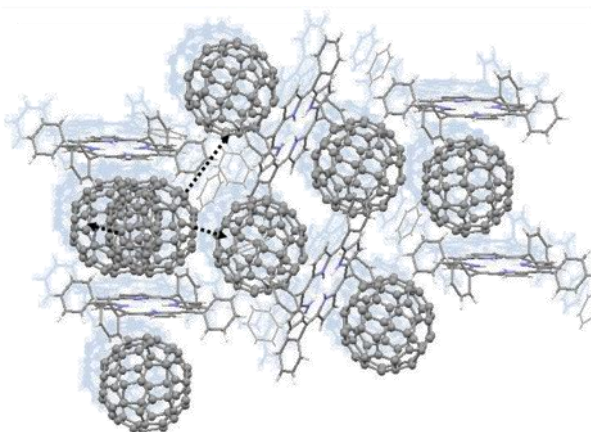


**Figure 7.** Graphite-like layers in the packing of the X-ray crystal structure for  $\text{H}_2\text{TPP}\cdot 2\text{C}_{60}\cdot 4\text{C}_6\text{H}_6$ . The  $\text{C}_{60}$  molecules which appear sandwiched between tetraphenylporphyrin units belonging to different layers. Three direct interactions with other  $\text{C}_{60}$  molecules are established from each  $\text{C}_{60}$  (highlighted with the arrows).

The understanding of the structures found in the crystal packing helped to further the porphyrin-fullerene interaction with the aim of performing chromatographic separations of fullerenes using anchored tetraphenyl porphyrins in silica gel stationary phases. In this work IR, ESR, UV-visible and X-ray photoelectron spectroscopies were combined in the characterization of the systems. The obtained results indicated that charge transfer was not taken place in the ground state. Probably, the photoexcitation of the systems induced the charge transfer. It was also stated that the metalloporphyrins MTPP formed thermodynamically more stable complexes with  $\text{C}_{70}$  than with  $\text{C}_{60}$ . This observation probably arises from the greater tendency of  $\text{C}_{70}$  to be involved in  $d-\pi$  interactions between the metal and the fullerene. However, the possible increase in the contact area between  $\text{C}_{70}$  and MTPP could also be an important factor in the complex stabilization.

In 2002 two different solid-state porphyrin-fullerene frameworks were reported by Boyd and Reed<sup>31</sup> in which the fundamental pillar was the free base *meso*-tetra-(4-pyridyl)porphyrin:  $\text{H}_2\text{TpyP}$ . One of them consists of a two-dimensional sheet structure of  $\text{H}_2\text{TpyP}$  coordinated to  $\text{Pb}^{2+}$  cations and  $\text{C}_{60}$  molecules sandwiched between two

<sup>31</sup> Sun, D.; Tham, F. S.; Reed, C. A.; Boyd, P. D. W. *Proc. Natl. Acad. Sci. U. S. A.* **2002**, *99*, 5088-5092.

adjacent layers. When  $C_{60}$  is sandwiched between the layers the interlayer separation is 12.1 Å. In the absence of  $C_{60}$  the interlayer distance is 5.5 Å. The overall skeleton of the structure resembles a zeolite and presents potential applications in catalysis, separations or sensing (Figures 8 and 9). The other solid-state structure is formed by a one-dimensional ribbon of porphyrins ligated with  $Hg^{2+}$  cations and intercalating  $C_{70}$  molecules in a side-on orientation maximizing van der Waals interactions (Figures 10 and 11).

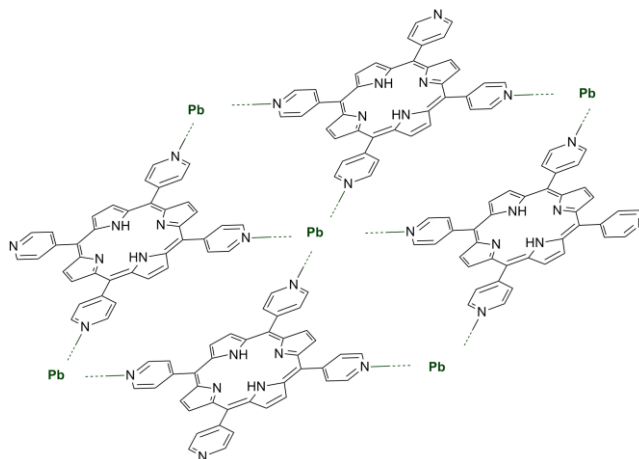


**Figure 8.** Schematic two-dimensional sheet structure of H<sub>2</sub>TpyP coordinated to Pb<sup>2+</sup> cations.

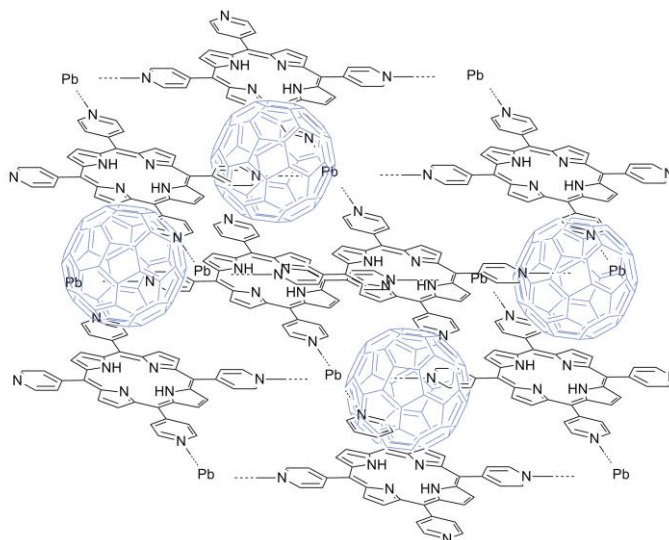


**Figure 9.** Schematic representation of the two layers of the crystal packing of H<sub>2</sub>TpyP coordinated to Pb<sup>2+</sup> cations and C<sub>60</sub> molecules sandwiched between two adjacent layers. Interlayer separation of 12.1 Å.

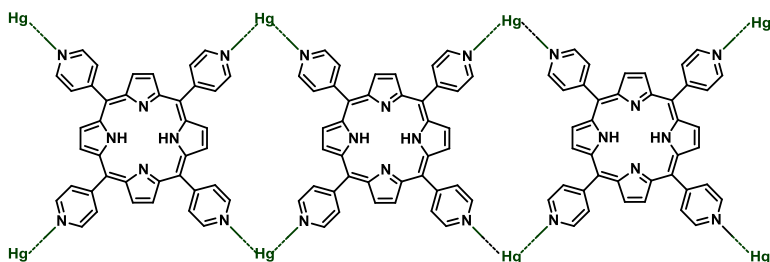


Figure 10. Schematic drawing of  $H_2TpyP$  ligated with  $Hg^{2+}$  cations.

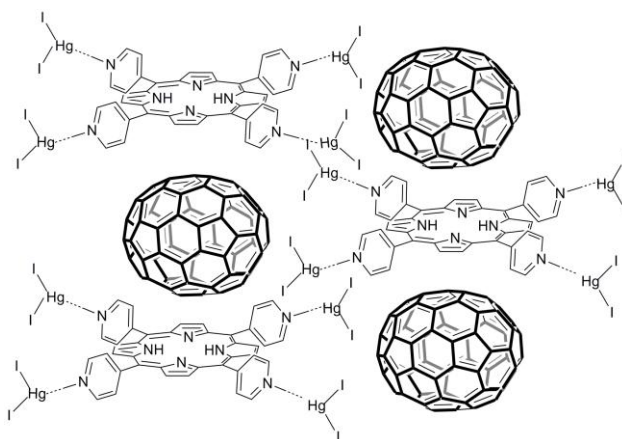


Figure 11.  $C_{70}$  is accommodated in a side-on orientation, having its fivefold axis parallel to the porphyrin plane, between two layers of ribbons located at  $12.5 \text{ \AA}$  from each other. The motif here is an intercalated ribbon.

The introduction of additional binding sites in order to increase the affinity of fullerene-porphyrin supramolecular complexes formed through  $\pi$ - $\pi$  interactions is a reasonable idea. Thus, Solladié and Nierengarten<sup>32,33</sup> added a crown ether unit to the porphyrin unit, **7**, and an ammonium function to the  $C_{60}$  component, **8**. The resulting 1:1 complex, **8•7**, containing the above-mentioned modifications is shown in Figure 12 as an equilibrium between the open and closed forms **8•7o**  $\leftrightarrow$  **8•7c**. The association constant value for the 1:1 assembly was calculated using fluorescence titrations as  $K_a = 3.8 \times 10^5 \text{ M}^{-1}$  and it is two orders of magnitude bigger than the value for the

<sup>32</sup> Solladié, N.; Walther, M. E.; Gross, M.; Duarte, T. M. F.; Bourgogne, C.; Nierengarten, J. F. *Chem. Commun.* **2003**, 2412-2413.

<sup>33</sup> Nierengarten, J. F.; Solladié, N. *J. Porphyrins Phthalocyanines* **2005**, *9*, 760-768.

ammonium-crown ether interaction ( $K_a = 3.5 \times 10^3 \text{ M}^{-1}$ ).<sup>34</sup> This increment in the association constant value states the importance of the intramolecular stacking between the fullerene and the porphyrin moieties. The complexity of the aggregates that can be constructed using this methodology was increased by attaching a second crown ether binding site to the porphyrin unit. In doing so, thermodynamically stable 2:1 complexes ( $\text{C}_{60}$ :porphyrin) were also assembled. These more complex structures were studied by  $^1\text{H}$  NMR and luminiscence techniques in  $\text{CDCl}_3$  and  $\text{CH}_2\text{Cl}_2$  respectively, and the stable assembled 2:1 complexes were also supported by electrospray mass spectrometry. However, they didn't report any association constant. Later, they studied the assembly of very similar compounds, with the exception that the porphyrin unit was not present, that gave rise to 2:1 conjugates, and the association constants were calculated. Positive cooperativity was present in this system, since  $K_2/K_1 \approx 4$  (0.25 is the value expected for a statistical model with two identical binding sites).<sup>35</sup> Taking this result into account one could state that for the previous case (2:1 complexes including porphyrins) the stability of the system was based on a positive cooperativity induce by coordination of the first binding site into the second one.

<sup>34</sup> Gutierrez-Nava, M.; Nierengarten, H.; Masson, P.; Van Dorsselaer, A.; Nierengarten, J. F. *Tetrahedron Lett.* **2003**, *44*, 3043-3046.

<sup>35</sup> Nierengarten, J. F.; Hahn, U.; Duarte, T. M. F.; Cardinali, F.; Solladie, N.; Walther, M. E.; Van Dorsselaer, A.; Herschbach, H.; Leize, E.; Albrecht-Gary, A. M.; Trabolsi, A.; Elhabiri, M. *C. R. Chim.* **2006**, *9*, 1022-1030.

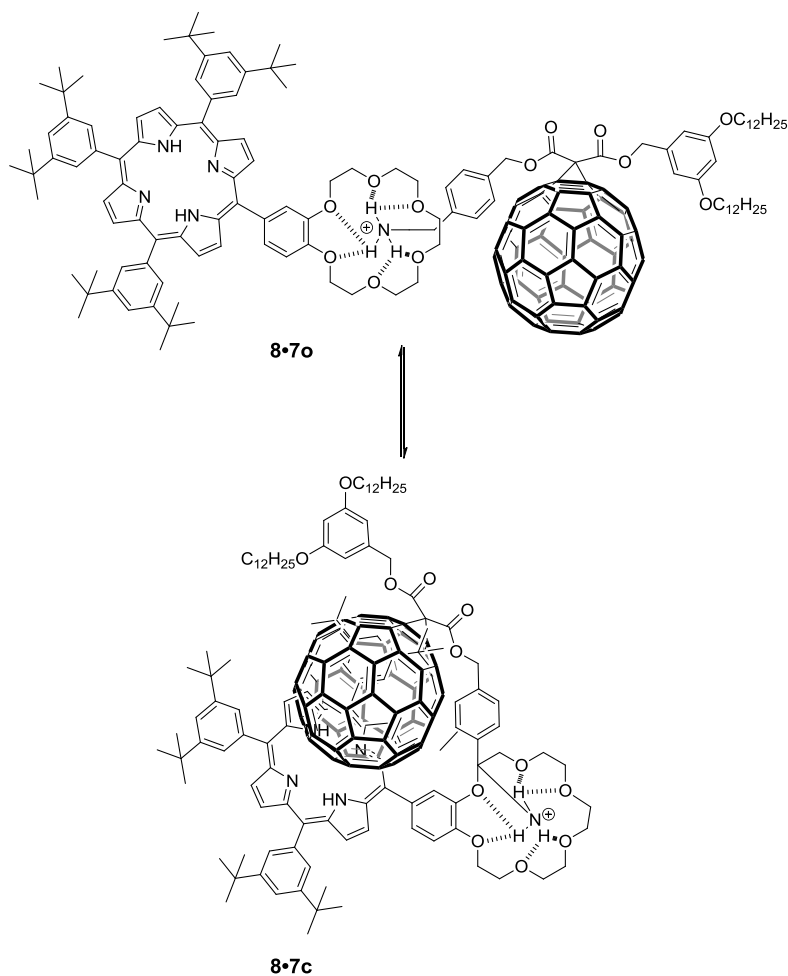


**Figure 12.** Schematic representation of the open conformer, **8•7o**, and the closed one, **8•7c**. The former is in fast exchange while the latter is in slow exchange with uncomplexed **7** and **8** on the NMR time-scale.

Bhattacharya et al.<sup>36</sup> carried out spectroscopic studies in toluene solution and *ab initio* calculations of two tetraaryl porphyrins, **9** and **10** (Figure 13), complexed with C<sub>60</sub> and C<sub>70</sub>.

<sup>36</sup> Bhattacharya, S.; Shimawaki, T.; Peng, X. B.; Ashokkumar, A.; Aonuma, S.; Kimura, T.; Komatsu, N. *Chem. Phys. Lett.* **2006**, *430*, 435-442.

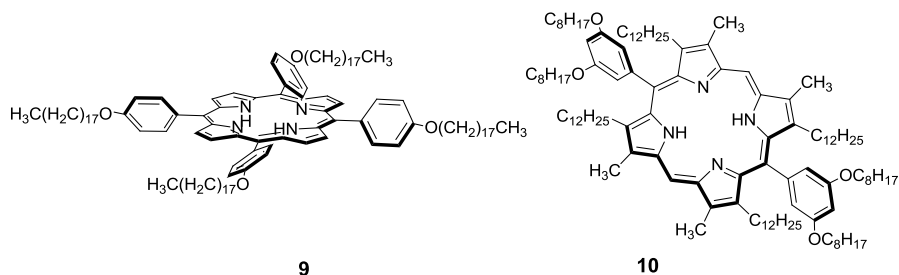


**Figure 13.** Structures of the the two tetraaryl porphyrins, **9** and **10**.

The values of the binding constants were determined using a Stern-Volmer plot derived from the data obtained in the steady-state emission titration experiments:

$$\frac{F_0}{F} = 1 + K[\text{fullerene}]$$

The calculated association constants value are  $K_a \sim 1.6 \times 10^4 \text{ M}^{-1}$  for the complexes with  $C_{70}$ . Most likely, the egg-shaped structure of  $C_{70}$  compared to the spherical shape of  $C_{60}$  is responsible to an increase in the contact area in the complex that translates in an increase of 8.5 fold in the binding affinity of  $C_{70}$ . Moreover, this selectivity ratio can be substantially increased by the inclusion of long chain n-alkyl group to the tetraaryl porphyrin unit.<sup>37</sup>

More recently, the supramolecular systems formed by the interaction of TPPs with fullerenes have found applications in material science. In this case, DFT calculations have been used to explain the relative orientation of ZnTPP and  $C_{70}$  deposited onto a surface under high vacuum. The obtained results give support to the idea that the charge transfer between the two components does not take place in ground state but only in the photoinduced excited state.<sup>38</sup>

<sup>37</sup> Bhattacharya, S.; Chattopadhyay, S.; Nayak, S. K.; Bhattacharya, S. (Banerjee), M. *Spectrochim. Acta, Part A* **2007**, *68*, 427-431.

<sup>38</sup> Vilmercati, P.; Castellarin-Cudia, C.; Gebauer, R.; Ghosh, P.; Lizzit, S.; Petaccia, L.; Cepek, C.; Larciprete, R.; Verdini, A.; Floreano, L.; Morgante, A.; Goldoni, A. *J. Am. Chem. Soc.* **2009**, *131*, 644-652.

## 2.2 Bis-porphyrins and fullerenes

The self-generated attraction of fullerenes to porphyrins promotes the assembly of supramolecular architectures with interesting properties for charge transfer applications. As discussed above, a single porphyrin-fullerene interaction produces a 1:1 complex with a stability constant value in the order of  $10^3$ - $10^4$  M<sup>-1</sup>. This value is too small to produce the quantitative assembly of the porphyrin-fullerene complexes at the micromolar concentrations required for the photophysical studies. Porphyrin dimers bind fullerenes with higher association constant values due to the multivalency effect.<sup>39</sup>

Taking into account the knowledge gained from the studies with monoporphyrin systems, several classes of bis-porphyrin architectures have been designed and synthesized for the inclusion and encapsulation of fullerenes in order to minimize the reorganization required for the binding. In the following section we present a brief account on several of these systems using examples appeared in recent literature. We classified the described systems in two categories: acyclic and cyclic bis-porphyrins hosts.

### 2.2.1. Acyclic bis-porphyrins as hosts

Boyd and Reed communicated the synthesis of two similar supramolecular jaw-like bis-porphyrins, **11a** and **11b** (Figure 14), only differing in the *meso* phenyl substituents. In both of them the link between the two porphyrin units is mediated by coordination to an organometallic palladium complex, *trans*-Pd(DMSO)<sub>2</sub>Cl<sub>2</sub>. The coordination bond is established between the *meso*-pyridyl substituent of the asymmetric A<sub>3</sub>B porphyrin unit and the Pd(II) center.<sup>40</sup>

---

<sup>39</sup> Mulder, A.; Huskens, J.; Reinhoudt, D. N. *Org. Biomol. Chem.* **2004**, *2*, 3409-3424.

<sup>40</sup> Sun, D. Y.; Tham, F. S.; Reed, C. A.; Chaker, L.; Burgess, M.; Boyd, P. D. W. *J. Am. Chem. Soc.* **2000**, *122*, 10704-10705.

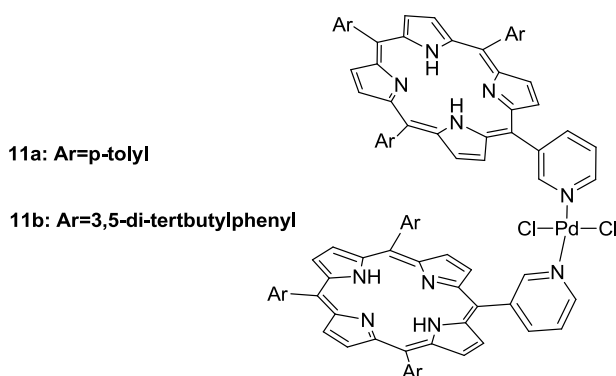


**Figure 14.** Structures of the two new jaw-like bis-porphyrins **11a** and **11b**.

The authors stated that the “chelate” effect, a particular example of multivalency, must be an important factor in achieving a very high thermodynamic stabilization in the 1:1 complex. The complexation processes of these hosts with  $C_{60}$  and  $C_{70}$  were studied by means of  $^1H$  NMR,  $^{13}C$  NMR, UV-visible and fluorescence titrations. The preferred binding for  $C_{70}$  in front of  $C_{60}$  was also noticed. However, only the association constant value for the interaction between  $C_{60}$  and **11b** was reported by  $^{13}C$  NMR titrations ( $K_a = 5.2 \times 10^3 M^{-1}$ ).

In relation to the structural characterization of the complexes, the use of mass spectrometry with matrix assisted laser desorption ionization (MALDI) produced positive molecular ions that correspond to the mass of the 1:1 complexes. In addition, the use of single crystal X-ray diffraction analysis allowed to solve the solid state structure of the sandwich complex of porphyrin dimer **11b**, with  $C_{60}$  sandwiched between the two porphyrin units. The use of an stoichiometric excess of  $Pd(Cl)_2(DMSO)_2$  with respect to the the porphyrin derivative induced a partial metallation of the sandwich complex,  $Pd_{1.5}11b \cdot C_{60}$ , for which a Pd- $C_{60}$  shorter distance of 2.86 Å was determined (Figure 15).

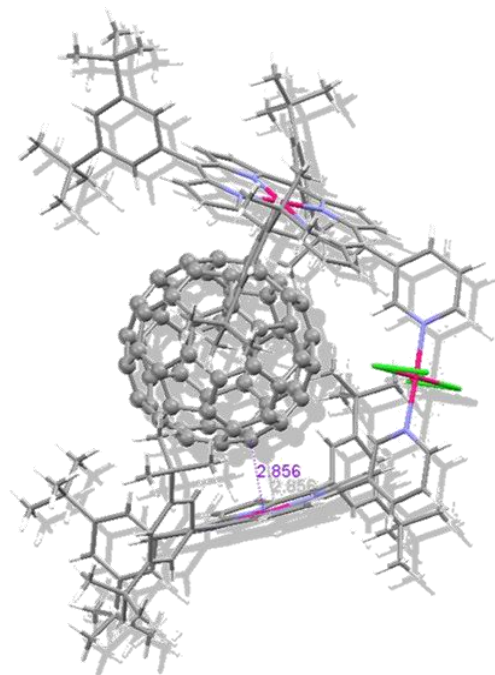


**Figure 15.** X-ray crystal structure of the partial palladium metallated bis-porphyrin **11b** with  $C_{60}$  ( $Pd_{1.5}11b \cdot C_{60}$ ). Pd---C( $C_{60}$ ) distance: 2.856 Å.

One year later, the same authors published the design and synthesis of other three new jaws porphyrins that are depicted in Figure 16.<sup>41</sup>

Within the receptor series, **12c** showed a higher binding affinity for  $C_{60}$ . This host adopts a less strained structure on complex formation. The structure of **12c** is somewhat preorganized for fullerene binding. The results that pointed out to a higher stability constants for the  $C_{60} \cdot 12c$  derived from MALDI mass spectrometry and  $^1H$  NMR titrations. Several metals were introduced in the porphyrin units of **12c** and the corresponding association constants of the resulting 1:1 complexes with  $C_{60}$  were determined by  $^{13}C$  NMR titrations. The affinity of  $M_2 \cdot 12c$  for  $C_{60}$  increases in the following order:  $Fe^{2+} < Pd^{2+} < Zn^{2+} < Mn^{2+} < Co^{2+} < Cu^{2+} < 2H$ . The reason for a higher binding constant of  $C_{60}$  and the free base of **12c** was ascribed to a favorable

<sup>41</sup> Sun, D. Y.; Tham, F. S.; Reed, C. A.; Chaker, L.; Boyd, P. D. W. *J. Am. Chem. Soc.* **2002**, *124*, 6604-6612.

electrostatic attraction between the electronegative 6:6 ring-juncture bond of the fullerene and the NH centers of the porphyrin which are electron poor.

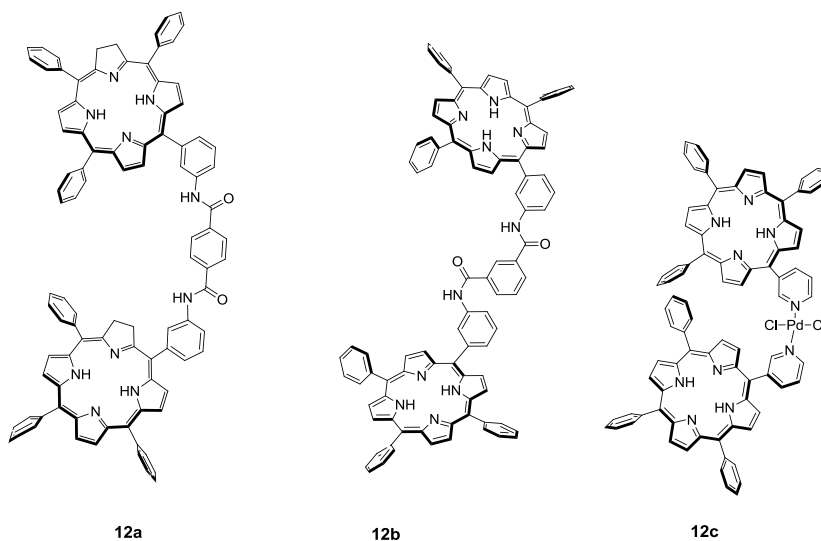


**Figure 16.** Molecular structures of the three porphyrin hosts **12** introduced by Boyd et al.

An interesting work related to the binding of fullerenes and bis-porphyrins displaying an allosteric effect was published by Ayabe et al.<sup>42</sup> in 2002. The zinc bis-porphyrin **13** can only bind C<sub>60</sub> by forming a sandwich complex when the dimer is in the “switch on” function, that is in the *syn*-conformation. The addition of a Pd(II) salt triggers a conformational change by coordination to the pyridyl residues and induces that **13** adopts the required *syn*-conformation (Figure 17).

<sup>42</sup> Ayabe, M.; Ikeda, A.; Shinkai, S.; Sakamoto, S.; Yamaguchi, K. *Chem. Commun.* **2002**, 1032-1033.

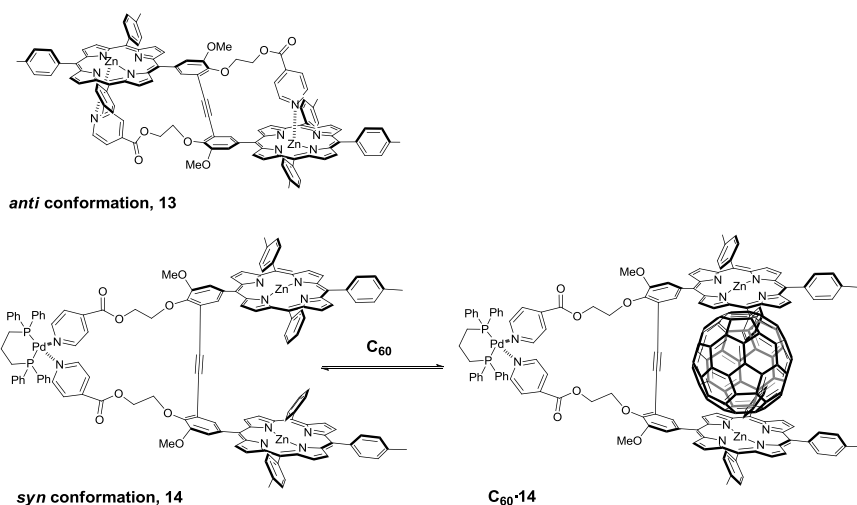


**Figure 17.** Anti conformation of bis-porphyrin **13**. The Pd(II) complex of **13** induces the porphyrin units to adopt a *syn* conformation. Bis-porphyrin **14** forms a sandwich complex with C<sub>60</sub>.

The structure of the 1:1 complex  $C_{60}\cdot\mathbf{14}$  was characterized using cold electrospray ionization (ESI) mass spectrometry and <sup>1</sup>H NMR experiments. The <sup>1</sup>H NMR spectrum of the *anti*-conformation **13** shows that the signals corresponding to the  $\alpha$ - and  $\beta$ -protons of the pyridyl groups are high field shifted due to the strong shielding effect of the porphyrin rings. The pyridyl residues are involved in an axial coordination bond through a N---Zn<sup>2+</sup> interaction. When **13** adopts the *syn*-conformation **14** by the addition of the palladium complex, the pyridyl protons move downfield, due to the formation of new coordination bonds between the N atom and the Pd(II) centers.

The association constant value for the  $C_{70}\cdot\mathbf{14}$  complex was calculated to be  $3.7 \times 10^4 \text{ M}^{-1}$  using UV-visible absorption spectroscopy. Using the same titration methodology the analogous complex with C<sub>60</sub>,  $C_{60}\cdot\mathbf{14}$ , displayed a diminution of one order of magnitude ( $5.1 \times 10^3 \text{ M}^{-1}$ ) in its stability constant. More recently, Aida et al. described a complex derived from an acyclic bis-porphyrin that self-assembles into a

porphyrin nanotube including C<sub>60</sub> and C<sub>70</sub>. This type of architecture can be considered as the first example of a supramolecular *peapod* (Figure 18).<sup>43</sup>

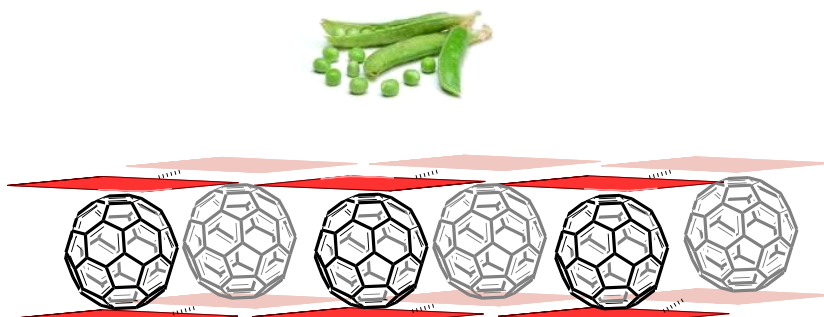


**Figure 18.** Schematic representation of a peapod, where fullerenes seem to be the beans inside.

Li et al. reported<sup>44</sup> the complexation properties of two porphyrin tweezers **15** and **16** (Figure 19) with C<sub>60</sub>, C<sub>70</sub> and a series of C<sub>60</sub> derivatives, **17**, **18** and **19** (Figure 20). The binding was probed using <sup>1</sup>H and <sup>13</sup>C NMR spectroscopy as well as fluorescent, UV-vis and CD spectroscopy (chiral induction is observed for the tweezers when they complex **19**, bearing a chiral phenylalanine). The titration experiments were performed in chloroform and toluene. C<sub>60</sub> is sparingly and appreciable soluble in chloroalkanes (like chloroform) and toluene respectively.<sup>19</sup> This fact implies that the fullerene must be well solvated on toluene, hampering the complexation with a porphyrin, and therefore, the association constant should be lower in toluene than in chloroform.

<sup>43</sup> Yamaguchi, T.; Ishii, N.; Tashiro, K.; Aida, T. *J. Am. Chem. Soc.* **2003**, *125*, 13934-13935.

<sup>44</sup> Wu, Z. Q.; Shao, X. B.; Li, C.; Hou, J. L.; Wang, K.; Jiang, X. K.; Li, Z. T. *J. Am. Chem. Soc.* **2005**, *127*, 17460-17468.

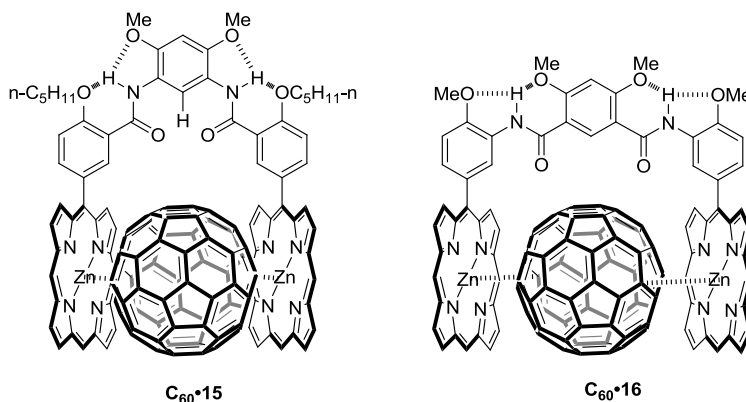


**Figure 19.** Molecular structures of molecular tweezers, **15** and **16**, with preorganized conformations stabilized by intramolecular hydrogen bonding. It is shown how C<sub>60</sub> fits better the cavity with the tweezer **15** than with **16**.

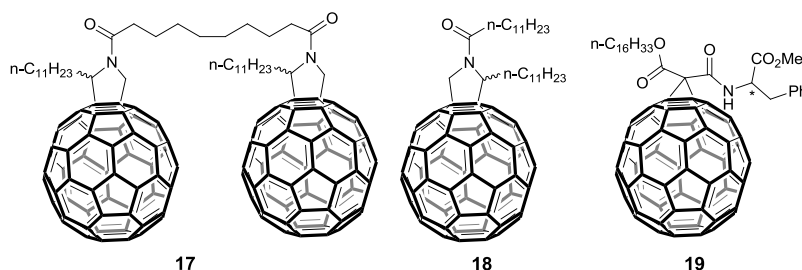


**Figure 20.** Structures of the three C<sub>60</sub> fullerene derivatives **17**, **18** and **19**.

The results obtained in this study (Table 1) serve to highlight the importance of the preorganization achieved by the use of intramolecular hydrogen bonding to control the conformation of the free receptors. In fact, the addition of just 10% (v/v) of methanol to the chloroform solutions produced a reduction in the association constant values of more than one order of magnitude. Most likely, the preorganization of the receptor's conformation that is based on the intramolecular hydrogen bonding is partially disrupted by the addition of a competitive polar solvent like methanol and a net reduction of the binding affinity for the fullerene is observed. It is necessary to stress again the good affinity of the porphyrin dimers towards the egg-shaped C<sub>70</sub>. The association constants are one order of magnitude higher with C<sub>70</sub> ( $1.1 \times 10^6 \text{ M}^{-1}$ ), if we compared with the spherical C<sub>60</sub> ( $1 \times 10^5 \text{ M}^{-1}$ ), in the case of tweezer **15**. Regarding to tweezer **16**, the stability constant with C<sub>70</sub> is almost two orders of

magnitud bigger, surely due to the expansion of the tweezer cavity. Table 1 summarises the association constant values calculated by Li et al. for receptors **15** and **16** with a series of fullerenes. The analysis of data allowed us to drawn several conclusions. Tweezer **15** binds  $C_{60}$  with a constant of  $1 \times 10^5 M^{-1}$ ; it recognizes the fullerene dimer **17**, with an association constant value which is almost one order of magnitude higher,  $7.6 \times 10^5 M^{-1}$ . Most likely, this enhancement of complex stability is due to the supplementary aromatic interaction of the second  $C_{60}$  unit with the porphyrin (Figure 21). Fullerene derivatives **18** and **19** feature stability constants values of approximately one order of magnitude lower than  $C_{60}$ . Probably, the reduced affinity is due to some steric of the substituents the fullerenes with the bis-porphyrin receptor. For the second tweezer, **16**, the trend is the same, but lower association constant values are described because the cavity is too big to accommodate  $C_{60}$  and their derivatives.

**Table 1.** Association constant values for the porphyrin-fullerene complexes determined by UV-visible titrations. ( $K_a (M^{-1})$ ).

|           | $C_{60}$              | $C_{70}$              | <b>17</b>                                      | <b>18</b>                                      | <b>19</b>             |
|-----------|-----------------------|-----------------------|--|--|-----------------------|
| <b>15</b> | $1 \times 10^5 (T)$   | $1.1 \times 10^6 (T)$ | $7.6 \times 10^5 (T)$<br>$4.7 \times 10^4 (C)$ | $6 \times 10^4 (T)$<br>$1.6 \times 10^4 (C)$   | $3.2 \times 10^3 (C)$ |
| <b>16</b> | $2.7 \times 10^4 (T)$ | $9.8 \times 10^5 (T)$ | $1.8 \times 10^5 (T)$<br>$4.1 \times 10^4 (C)$ | $1.2 \times 10^4 (T)$<br>$7.9 \times 10^3 (C)$ | $1.5 \times 10^3 (C)$ |

(T): toluene; (C): chloroform

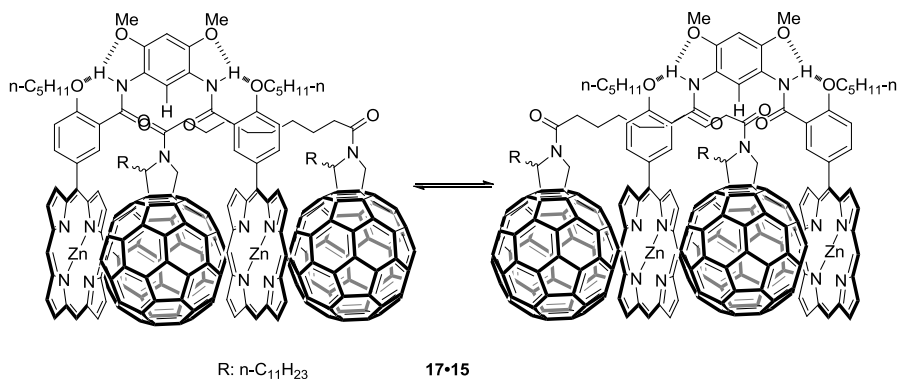


**Figure 21.** Dynamic exchange process (rapid on the  $^1H$  NMR time scale) for complex **17•15**.

## 2.2.2. Cyclic bis-porphyrins hosts

The first cyclic bis-porphyrin host for the inclusion of fullerenes was reported by Aida and co-workers in 1999.<sup>45</sup> Bis-porphyrin **Zn<sub>2</sub>-21** was obtained after catalytic hydrogenation of the rigid diacetylenic spacers present in bis-porphyrin **H<sub>2</sub>-20** followed by metalation with Zn(AcO)<sub>2</sub> (Figure 22). The bis-acetylenic host **Zn<sub>2</sub>-20** does not show any sign of complexation with C<sub>60</sub> in terms of spectral changes in the UV-visible spectrum. However and to the best of our knowledge, **Zn<sub>2</sub>-21** binds C<sub>60</sub> in organic solvents (i.e. benzene) with the higher affinity constant value reported ( $K_a=6.7 \times 10^5 \text{ M}^{-1}$ ) so far for a Zn-bis-porphyrin host.

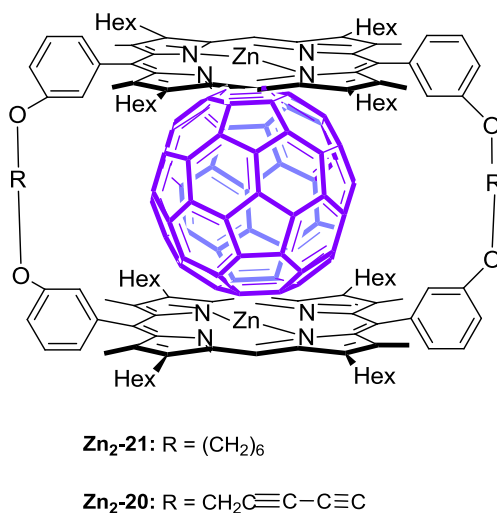


**Figure 22.** Molecular structures of cyclic bis-porphyrin **Zn<sub>2</sub>-20** and **Zn<sub>2</sub>-21** hosts designed for including fullerenes C<sub>60</sub> and C<sub>70</sub>.

In 2001, the same authors published two other studies<sup>46,47</sup> focusing on the effect of the central metal, in the porphyrin rings of the macrocycle **M<sub>2</sub>-21**, in the complexation abilities of the hosts with C<sub>60</sub> and C<sub>70</sub> as guests. Using different spectroscopic techniques as well as cyclic voltammetry experiments they found a remarkable affinity

<sup>45</sup> Tashiro, K.; Aida, T.; Zheng, J.-Y.; Kinbara, K.; Saigo, K.; Sakamoto, S.; Yamaguchi, K. *J. Am. Chem. Soc.* **1999**, *121*, 9477-9478.

<sup>46</sup> Zheng, J. Y.; Tashiro, K.; Hirabayashi, Y.; Kinbara, K.; Saigo, K.; Aida, T.; Sakamoto, S.; Yamaguchi, K. *Angew. Chem., Int. Ed.* **2001**, *40*, 1858-1861.

<sup>47</sup> Tashiro, K.; Aida, T. *J. Inclusion Phenom. Macrocyclic Chem.* **2001**, *41*, 215-217.

of the fullerenes for the bis-porphyrins containing metal ions of group 9, Co(III) and Rh(III). The group 10 and 11 metal ions, Cu(II), Ni(II) and Ag(I), when inserted into the porphyrin units of **M<sub>2</sub>-21** produced cyclic receptors displaying lower binding affinities for the two fullerenes. The trend observed in the binding affinities as a function of the metal inserted in the porphyrin unit of **M<sub>2</sub>-21** is independent of the fullerene used. It is worth noting that also in this case the stability constants for C<sub>70</sub> are one order of magnitude greater than for C<sub>60</sub>. The main reason put forward by the authors to explain this result relies on the shape difference between C<sub>70</sub> and C<sub>60</sub> also commented above (ellipsoidal vs spherical). C<sub>70</sub> has an ellipsoidal egg-shape and contains five nonchemically equivalent carbon atoms that can be observed as different <sup>13</sup>C NMR signals. Three signals belong to the equatorial part of C<sub>70</sub> and two to the poles (Figure 23). When complexed with bis-porphyrin **M<sub>2</sub>-21** all carbon signals of C<sub>70</sub> experience upfield shifts. The experienced chemical shift changes are greater for the equatorial carbon atoms. Therefore, it is concluded that C<sub>70</sub> is complexed in a “side-on” conformation, by the bis-porphyrin cyclic host **M<sub>2</sub>-21** in order to maximize π–π interactions.

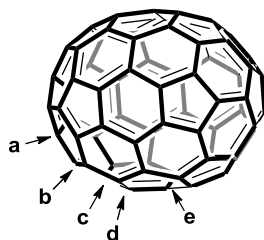


**Figure 23.** Molecular structure of the ellipsoidal egg-shape structure of C<sub>70</sub>. The five non-equivalent carbon atoms are marked.

In 2005 Sanders et al.<sup>48</sup> communicated the isolation of a notably stretchable cyclic dimer of porphyrins, **22**, which is a virtuous receptor for C<sub>60</sub> along with diamines (see below in 3.2). In this work they did not derive an association binding constant value for the macrocycle **22** with C<sub>60</sub>, mainly because the isothermal titration experiments were performed in CHCl<sub>3</sub> solution and the resulting inclusion complex with C<sub>60</sub> presented a low solubility in this solvent. They also monitored the binding of C<sub>60</sub> with

<sup>48</sup> Kieran, A. L.; Pascu, S. I.; Jarrosson, T.; Sanders, J. K. M. *Chem. Commun.* **2005**, 1276-1278.

**22** using  $^1\text{H}$  NMR spectroscopy in  $\text{CS}_2:\text{CDCl}_3$  9:1 by incremental addition of the fullerene to the solution of the host. Due to the simplification of the signals in the aromatic region of the porphyrin dimer upon  $\text{C}_{60}$  complexation and to the emergence of a single and sharp *meso*-H, the authors stated that the complexation of  $\text{C}_{60}$  by **22** increased the rigidity of the host. The free host was present in solution as a mixture of several conformations. Crystals of the  $\text{C}_{60}\cdot\mathbf{22}$  complex were grown by hexane addition to an equimolar concentrated solution in  $\text{CDCl}_3:\text{CS}_2$  1:9 (Figure 24). In the solid state, the tilt angle between the porphyrin planes of the complex is  $11^\circ$ , a much smaller value than the one reported by Boyd et al. for **8b** with  $\text{C}_{60}$  ( $42^\circ$ ).

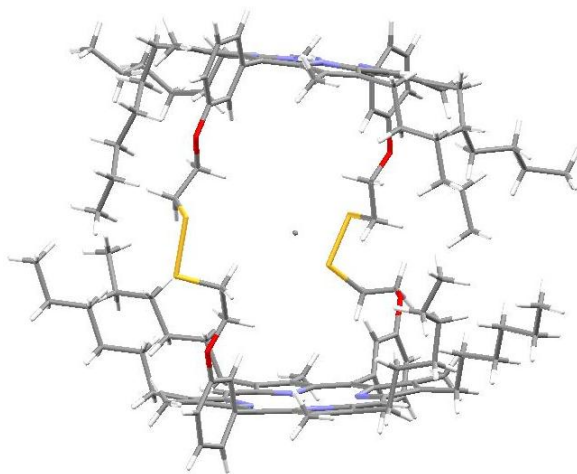


**Figure 24.** Solid state structure of receptor **22**. It is assumed that  $\text{C}_{60}$  is located inside the cavity, but it was difficult to determine its exact position due to disorder.

A nickel(II) metalated cyclic porphyrin dimer, **23**, with two butadiyne linkers was synthesized by Tani et al. in 2007 (Figure 25).<sup>49</sup> The aim of this work was the construction of a tubular assembly using the *trans-meso* pyridyl groups of the dimer to induce a self-assembly process by interaction with a hydrogen-bonding donor or a metal ion. Surprisingly, when crystals of the Ni(II)-dimer **23** were obtained, the crystal packing suggested a nanotube motif, along the crystallographic *b* direction. However, the nanotube was not formed by the presence of a hydrogen-bonding donor or a

<sup>49</sup> Nobukuni, H.; Shimazaki, Y.; Tani, F.; Naruta, Y. *Angew. Chem., Int. Ed.* **2007**, *46*, 8975-8978.

metal ion, but by self-assembly of **23** through non-covalent interactions between adjacent cyclic dimers. Each dimer experience four CH $\cdots$ N interactions and two  $\pi$ - $\pi$  interactions with adjacent molecules. The two CH $\cdots$ N interactions are established between  $\beta$ -pyrrolic protons and the nitrogen of the pyridyl groups (one of the C-N distance is shorter than the other). The additional  $\pi$ - $\pi$  interaction takes place between the *meso*-pyridyl groups (see figure 26).

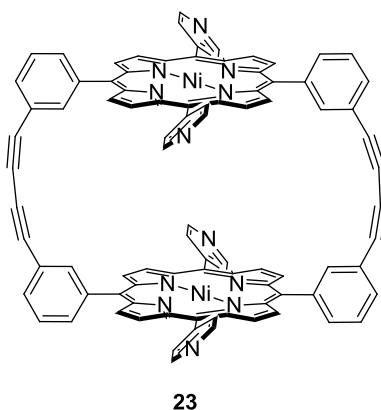


**Figure 25.** Molecular structure of the cyclic Ni(II)-porphyrin dimer, **23**.

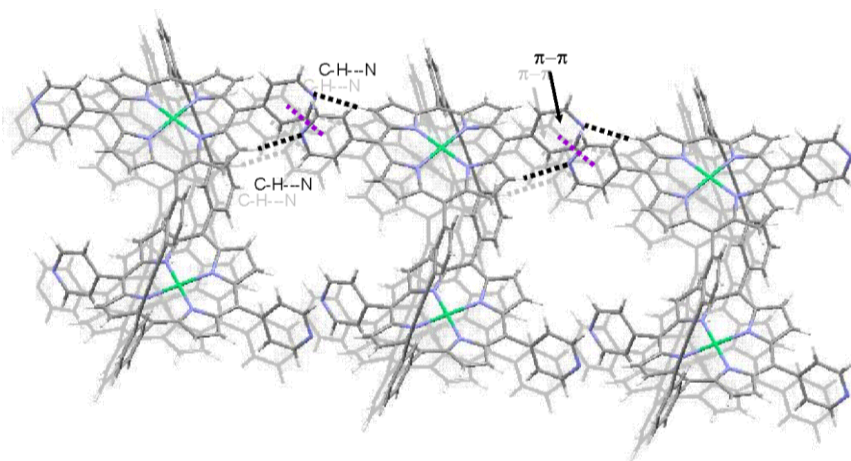


**Figure 26.** Two types of non-covalent interactions between the cyclic Ni(II)-porphyrin dimers, found in the packing of the crystal structure.

Bis-porphyrin **23** presents a proper cavity size to include C<sub>60</sub>. In solution, the inclusion properties of **23** were probed using UV-visible titration in CHCl<sub>3</sub>:Toluene mixture. A simple titration experiment allowed to derive an association constant value of  $K_a = 2 \times 10^5 \text{ M}^{-1}$  for the 1:1 complex. The 1:1 stoichiometry of the complex in solution was confirmed by ESI-MS analysis of a 1:1 mixture of **23** and C<sub>60</sub> revealing the presence of a molecular peak of an ion that corresponds to the expected molecular weight. Moreover, a <sup>13</sup>C NMR spectrum of the 1:1 mixture of **23** and <sup>13</sup>C-enriched C<sub>60</sub> exhibited upfield shifts in the carbon signal of C<sub>60</sub>, indicating its inclusion in the cavity of the dimer. In addition, the inclusion complex was also detected in the solid state by growing single crystals in the presence of one equivalent of C<sub>60</sub>. An analogous tubular assembly than in the case of free **23** is formed. The fullerenes are aligned inside the channel generated by **23** (the distance between the centers of the fullerene is 14.5 Å). The solid state structure constitutes an example of supramolecular peapod. In this case, since the cavity of **23** is smaller than in the cyclic dimer **M<sub>2</sub>-21**, the fullerene is not located above the center of the porphyrin units.

### 3. Supramolecular chemistry of Zn-porphyrins with nitrogenated ligands.

Assemblies based on the well-known coordination bond that is established between the metal center of a Zn-porphyrin and a nitrogen atom of a ligand will be the focus of this section. Zinc porphyrins are one of the most frequently used components in dynamic supramolecular systems.<sup>50</sup> The zinc porphyrin/nitrogen complex displays a so-called 'labile bond', and is generally considered to be kinetically labile and difficult to isolate. Although each coordination interaction is thermodynamically weak and dynamic, the sum of several interactions provides thermodynamically stable structures of multi-porphyrin aggregates. The arrangement of non-covalent oligoporphyrin architectures is an important challenge to

---

<sup>50</sup> Satake, A.; Kobuke, Y. *Tetrahedron* **2005**, *61*, 13-41.

mimic the bacterial photosynthetic systems<sup>51,52,53,54,55</sup> and to derive functions from these molecular materials.<sup>56</sup>

The construction of porphyrin oligomers through self-assembly of monomers can occur by using ligands possessing several coordination sites. The most common ligands for this purpose and the most studied ones are ditopic amines, and among them, 1,4-diazabicyclo [2.2.2] octane (DABCO) and 4,4'-bipyridine (Bipy). Not only the assembly of porphyrin monomers, but also the behavior of acyclic and cyclic bis-porphyrins with ditopic amines have been extensively examined. However, it is adequate to understand first the thermodynamic characterization of a simple zinc monoporphyrin binding to monotopic and ditopic amine ligands in order to appreciate the assembly behavior of dimeric porphyrins towards nitrogenated ligands.

First, we describe the thermodynamic characterization of the zinc metal-nitrogen interaction regarding to zinc monoporphyrins. Next, several examples involving acyclic and cyclic dimers of zinc porphyrins and their binding with amine ligands will be described.

### 3.1 Zn-porphyrin monomers binding amines

A monomeric porphyrin and a monotopic amine ligand give a simple 1:1 complex through axial coordination to the metal binding site in the porphyrin core with a binding constant,  $K$ . This binding constant is known as the microscopic binding constant,  $K_m$ , for the interaction between the nitrogen of the amine ligand and the metal inside the porphyrin. When a ditopic ligand is used, the macroscopic association constant for the 1:1 complex with a monoporphyrin can be related to the microscopic value of the model system using the following equation  $K_1 = 2K_m$ . The statistical factor of 2 emerges when considering that the ligand has two different

<sup>51</sup> Haycock, R. A.; Hunter, C. A.; James, D. A.; Michelsen, U.; Sutton, L. R. *Org. Lett.* **2000**, *2*, 2435-2438.

<sup>52</sup> Haycock, R. A.; Yartsev, A.; Michelsen, U.; Sundstrom, V.; Hunter, C. A. *Angew. Chem., Int. Ed.* **2000**, *39*, 3616-3619.

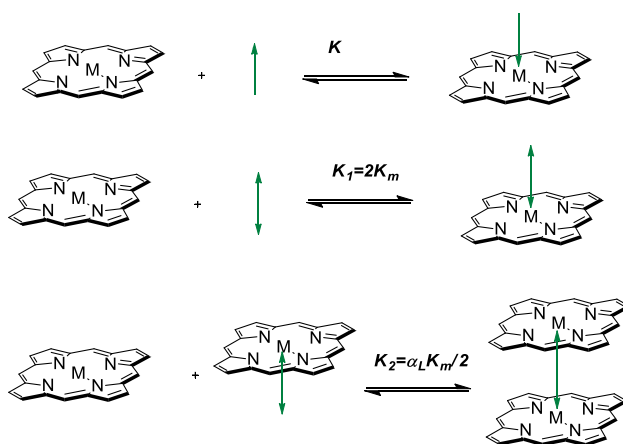
<sup>53</sup> Kuroda, Y.; Sugou, K.; Sasaki, K. *J. Am. Chem. Soc.* **2000**, *122*, 7833-7834.

<sup>54</sup> Takahashi, R.; Kobuke, Y. *J. Am. Chem. Soc.* **2003**, *125*, 2372-2373.

<sup>55</sup> Shoji, O.; Okada, S.; Satake, A.; Kobuke, Y. *J. Am. Chem. Soc.* **2005**, *127*, 2201-2210.

<sup>56</sup> Anderson, H. L. *Chem. Commun.* **1999**, 2323-2330.

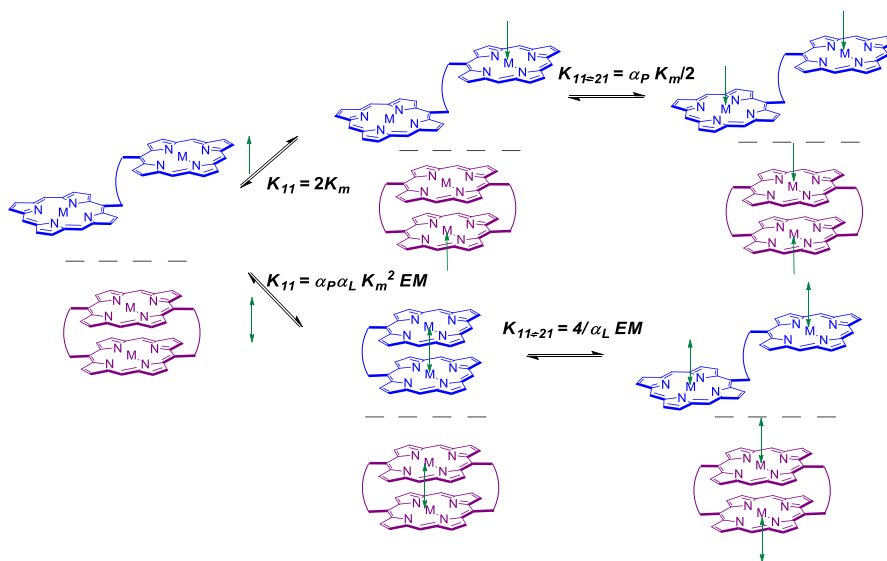
binding sites to interact with the Zn-porphyrin. In this case, an additional porphyrin monomer can also bind the other nitrogen in the ligand, and the equilibrium constant for the second binding event forming a 1:2 complex can be statistically estimated as  $K_2 = \alpha_L K_m / 2$  (Figure 27). Since there are two ways to disrupt the 1:2 complex but only one possibility to form the complex from the 1:1 aggregate the statistical correction implies a division by a factor of 2. The parameter  $\alpha_L$  is included to quantify the cooperativity between the two binding sites of the ligand. Thus,  $K_1$  and  $K_2$  are related by the relationship  $4K_2 = \alpha_L K_1$ . When  $\alpha_L = 1$ , then  $4K_2 = K_1$  and there is no cooperativity. Both sites act completely independent; if  $4K_2 > K_1$  a positive cooperativity is present in the system ( $\alpha_L > 1$ ) and when  $4K_2 < K_1$  the cooperativity is said to be negative ( $\alpha_L < 1$ ). A positive cooperativity implies that the second binding is enhanced, while when the cooperativity is negative the second binding is rather inhibited by the first interaction.<sup>57</sup>



**Figure 27.** Simplified representations of the equilibria involved in the binding of a metallo-porphyrin with a mono- and a ditopic ligand.

If we increase the complexity of the system, adding another unit of porphyrin and forming bis-porphyrin tweezers or cyclic bis-porphyrins. The binding equilibria that take place in solution are illustrated in Figure 28.

<sup>57</sup> Anderson, H. L.; Hunter, C. A.; Meah, M. N.; Sanders, J. K. M. *J. Am. Chem. Soc.* **1990**, *112*, 5780-5789.

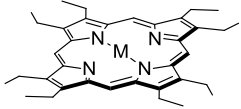
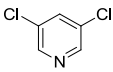
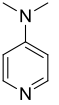


**Figure 28.** Simplified representations of the equilibria involved in the binding of a metallo-bis-porphyrin, open dimer as a tweezer in blue and cyclic dimer in violet colour, with a mono- and a ditopic ligand.  $\alpha_L$  is the cooperativity factor of the ligand.

In 1993 Summers and Stolzenberg<sup>58</sup> reported the stability constants and thermodynamic data for the coordination of piperidine, pyridine, and substituted pyridines to zinc (II) complexes of octaethylporphyrin (OEP), **24**, among others, in toluene solution at 25°C. Under the conditions of the study, only 1:1 complexes are formed. Except for the 2-substituted pyridines, where the steric repulsion between the  $\alpha$ -substituent to the N atom and the porphyrin plane not allow a good fitting of the ligand. As tabulated in table 2, the association constants increase with the increase of the  $pK_a$  values of the protonated form of the ligand. In this table are summarised the  $pK_a$  values and the association constants of **24** with the pyridine derivatives obtained from UV-visible titrations.

<sup>58</sup> Summers, J. S.; Stolzenberg, A. M. *J. Am. Chem. Soc.* **1993**, *115*, 10559-10567.

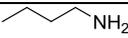
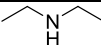
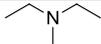
**Table 2.** Association constants, determined by UV-visible titrations, of zinc octaethylporphyrin, **24**, with pyridine derivatives. The  $pK_a$  values of the pyridine ligands are also reported.

| Porphyrin  | Ligand   | $pK_a$ | $K (M^{-1})$       |
|--|--|--------|--------------------|
| <br><b>24</b> | <br><b>3,5-Cl<sub>2</sub>Py</b>   | 0.67   | $1.26 \times 10^2$ |
|  | <br><b>4-CNPy</b>                 | 1.90   | $1.02 \times 10^3$ |
|  | <br><b>Pyridine</b>               | 5.17   | $2.34 \times 10^3$ |
|  | <br><b>2-MePy</b>                 | 5.96   | $6.93 \times 10^1$ |
|  | <br><b>4-MePy</b>                | 6.00   | $4.68 \times 10^3$ |
|  | <br><b>2,4-Me<sub>2</sub>Py</b> | 6.74   | $1.78 \times 10^2$ |
|  | <br><b>4-NMe<sub>2</sub>Py</b>  | 9.71   | $4.57 \times 10^4$ |

Not only pyridine derivatives can bind Zn-porphyrins, also aliphatic amines can be axially coordinated to them (Table 3). In this case, also the  $pK_a$  influences the affinity of the binding (the larger the  $pK_a$ , the greater the association constant). The steric effect is quite more significant than the basicity for the determination of the

association constant. Other conclusion that can be drawn from table 3 include that secondary and tertiary amines have lower association constants than the primary ones, and cyclic amines present also larger binding constants than the acyclic ones because the repulsion between the porphyrin plane and the substituents is lower.

**Table 3.** Association constants, determined from the UV-visible titrations, of zinc-tetraphenylporphyrin, **24**, with aliphatic amines. The pK<sub>a</sub> values of the amine ligands are also reported.

| Porphyrin | Ligand   | pK <sub>a</sub> | K (M <sup>-1</sup> ) <sup>a</sup> |
|-----------|--|-----------------|-----------------------------------|
| ZnTPP     | <br>n-BuNH <sub>2</sub> | 10.64           | 1.26 x 10 <sup>2</sup>            |
|           | <br>Et <sub>2</sub> NH  | 10.8            | 1.02 x 10 <sup>3</sup>            |
|           | <br>Azetidine           | 11.29           | 2.34 x 10 <sup>3</sup>            |
|           | <br>piperidine          | 11.1            | 4.68 x 10 <sup>3</sup>            |
|           | <br>Et <sub>3</sub> N | 10.72           | 1.78 x 10 <sup>2</sup>            |
|           | <br>DABCO             | 8.60, 2.90      | 4.57 x 10 <sup>4</sup>            |
|           | <br>Quinuclidine      | 10.95           | 3.56 x 10 <sup>4</sup>            |

<sup>a</sup>All these association binding constants were determined by UV-visible titrations at a micromolar concentration (10<sup>-6</sup> M) of the zinc porphyrin monomer. When a complex is formed, the Soret band, which is the most intense band of absorption of the electronic spectrum of a porphyrin and is located more or less between 400-430 nm of the visible spectrum, experiments a bathochromic shift.

### 3.2 Porphyrin dimers binding amines

Solladié et al. reported in 2001<sup>59</sup> and 2004<sup>60</sup> the synthesis of two rigid cofacial bis-porphyrinic tweezers, **25** with a mono-anthracenic spacer and **26** with a tris-anthracenic one respectively (Figure 29). Both anthracenic spacers can collect light selectively and transfer it to the Zn-porphyrins. The electronic coupling between the two porphyrins in the tweezers takes place when a guest diamine molecule is inserted in the cavity generating 1:1 host-guest co-facial complexes.

Tweezer **25** with the fixed mono-anthracenic spacer enhances the stability of the 1:1 complexes formed with small bidentate bases, pyrazine and DABCO, by three orders of magnitude with respect to a reference monoporphyrin: Zn-5,10,15,20-tetra(3,5-di-*tert*-butylphenyl)porphyrin and it must be due to the multivalency of the zinc bis-porphyrin. The association constants of the two 1:1 pyrazine•**25** and DABCO•**25** host-guest complexes were determined by means of UV-visible titrations in CH<sub>2</sub>Cl<sub>2</sub> as  $K_a = 4 \times 10^5 \text{ M}^{-1}$  and  $K_a = 1 \times 10^7 \text{ M}^{-1}$  respectively.

Tweezer **26** with the tris-anthracenic spacer allows the fitting of the cavity size to accommodate guests of different lengths because the acetylenic axis can rotate. For this host, the insertion of three different ditopic guests, pyrazine, DABCO and 4,4'-bipyridine, was studied using UV-visible titrations in CH<sub>2</sub>Cl<sub>2</sub>. Pyrazine and DABCO bind tweezer **26** with association constants that are two orders of magnitude lower than for tweezer **25** ( $K_a = 8 \times 10^3 \text{ M}^{-1}$  (pyrazine) and  $K_a = 4 \times 10^5 \text{ M}^{-1}$  (DABCO)). The reason of the decrease in the binding affinities could be due to the fact that the host must rotate the porphyrin units around its acetylenic axis to allow the good fit with these small guests and adopt a high energy conformation (Figure 29). Titration with the larger guest 4,4'-bipyridine was also monitored producing an association constant of  $K_a = 4 \times 10^4 \text{ M}^{-1}$ .

<sup>59</sup> Brettar, J.; Gisselbrecht, J. P.; Gross, M.; Solladie, N. *Chem. Commun.* **2001**, 733-734.

<sup>60</sup> Rein, R.; Gross, M.; Solladie, N. *Chem. Commun.* **2004**, 1992-1993.

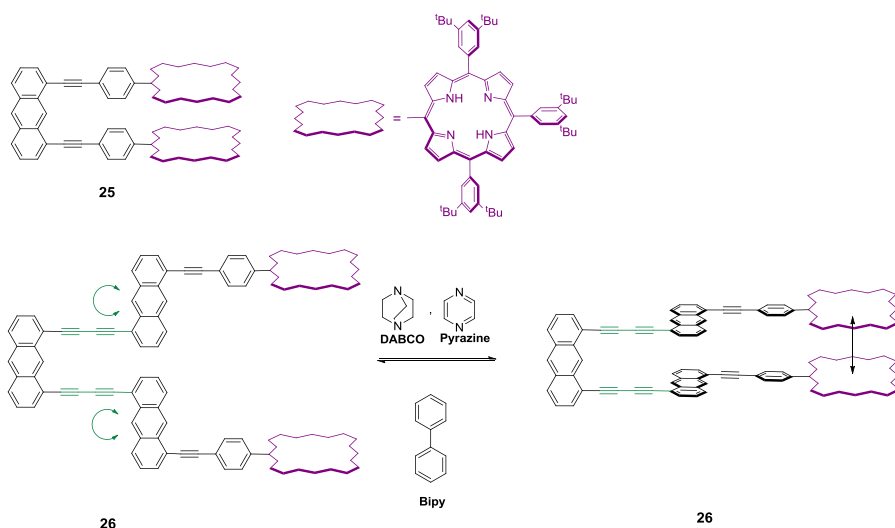


**Figure 29.** Representation of the equilibria involved in the binding of a metallo-monoporphyrin with a mono- and a ditopic ligand.

Sanders et al. in 2003<sup>61</sup> described the selective synthesis of a disulfide-linked cyclic porphyrin dimer when DABCO was used as template.

Starting from the bis-benzylthiol substituted Zn-porphyrin, **27**, addition of DBU, under air and without templates, leads to the cyclization of the monomer. HPLC analysis of the reaction mixture indicates that it is constituted and by three different components: cyclic dimer, **28** (87%), cyclic trimer (11%) and higher oligomers (2%). When 0.5 equivalents of DABCO are added during the reaction the equilibrium is shifted towards the exclusive formation of the cyclic dimer (99%, by analytical HPLC). The cavity of the cyclic dimer has an appropriate size for the inclusion of DABCO. The X-ray crystal structure of the complex, DABCO•**28**, was obtained in CHCl<sub>3</sub> by slow evaporation of MeOH, and the Zn-Zn distance is 7.053 Å (Figure 30). 4,4'-bipyridine is too large to fit the size of this cyclic dimer and when it was used as a template of the reaction, dimer **28** was obtained in small quantity.

<sup>61</sup> Kieran, A. L.; Bond, A. D.; Belenguer, A. M.; Sanders, J. K. M. *Chem. Commun.* **2003**, 2674-2675.

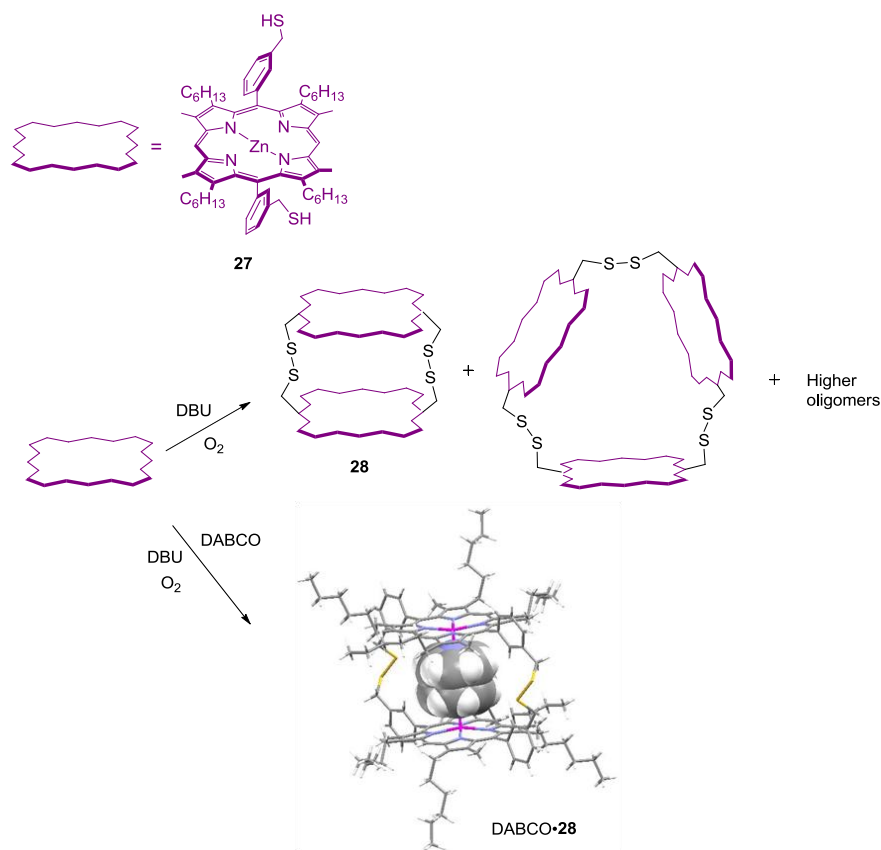


**Figure 30.** Oxidation and cyclization of the bis-benzylthiol substituted Zn-porphyrin, **27**, in absence of template and in presence of DABCO, giving the DABCO•**28** complex (X-ray crystal structure is depicted there).

In 2005<sup>62</sup> Sanders described the synthesis of the more flexible disulfide-linked cyclic porphyrin dimer, **22** (its interaction with C<sub>60</sub> was discussed before in section 2.2.2.).

When the cyclization reaction was performed starting from the monomer **29**, and without the addition of any guest as template, a mixture of products with a ratio 94: 5: 1 corresponding to dimer: trimer: tetramer was obtained. In this case, the ratio of the mixture of products changes to 98: 2, dimer: trimer, when templates of different size,

<sup>62</sup> Kieran, A. L.; Pascu, S. I.; Jarrosson, T.; Sanders, J. K. M. *Chem. Commun.* **2005**, 1276-1278.

DABCO and Bipy, are added. This result suggests a higher flexibility of this macrocycle when compared with **28** (Figure 31).

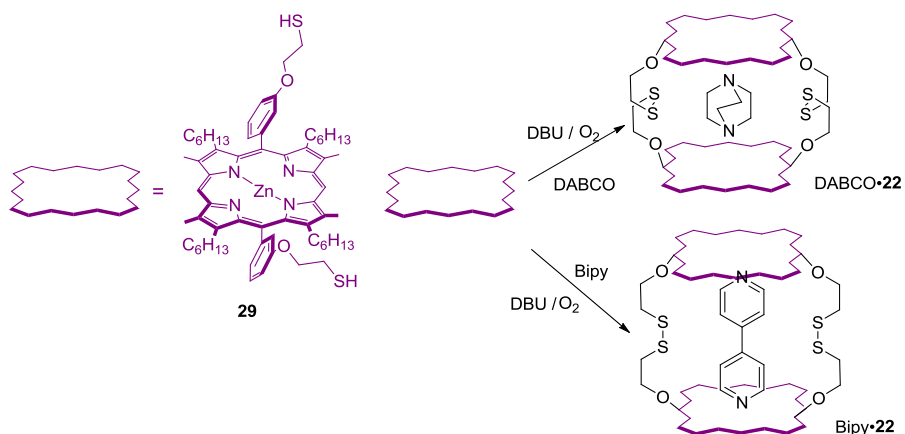


**Figure 31.** Oxidation and cyclization of the Zn-porphyrin monomer **29**. Here are represented the cyclic dimer structures when DABCO and Bipy are added as templates giving DABCO•**22** and Bipy•**22**.

Association binding constants for the cyclic dimer **22** with two ditopic amines of different size were determined by isothermal titration calorimetry (ITC) in  $\text{CHCl}_3$  solution. DABCO displayed an increase of one order of magnitude in the binding constant with respect to Bipy.  $K_a$  (4,4'-bipyridyl) =  $0.5 \times 10^6 \text{ M}^{-1}$  and  $K_a$  (DABCO) =  $7.5 \times 10^6 \text{ M}^{-1}$ . Flexible linkers of different lengths like the ones discussed above can be used to synthesize cyclic bis-porphyrin receptors with different templates.

The same year, Ballester et al.<sup>63</sup> reported dramatic differences in the stoichiometry and the three-dimensional structures of the supramolecular complexes assembled with DABCO and three flexible isomeric and acyclic Zn-bis-porphyrins (**30a**, **30b**, **30c**) differing only in the substitution pattern: **30a**, *ortho*, **30b**, *meta*, **30c**, *para* (Figure 32). Only in one case, the bis-porphyrin **30c**, is involved in the formation of a 2+2 multicomponent assembly with DABCO. The other two bis-porphyrins, **30a** and **30b**, form an intramolecular cofacial 1:1 sandwich complex, limiting their potential use in

<sup>63</sup> Ballester, P.; Costa, A.; Castilla, A. M.; Deya, P. M.; Frontera, A.; Gomila, R. M.; Hunter, C. A. *Chem.--Eur. J.* **2005**, *11*, 2196-2206.

higher multicomponent assemblies. This dissimilar behavior was established when the association constant values determined in the fit of the UV-visible titrations data to two possible binding models were used to simulate and compare with the profiles of destruction of the 1:1 sandwich complexes at millimolar concentrations. The simple fitting of the UV-visible titration data revealed to be not adequate to determine the binding model that was operative in each case.

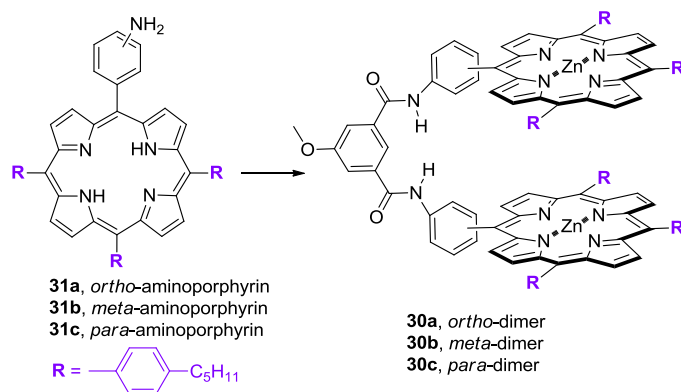


**Figure 32.** Line structures of the three isomeric zinc bis-porphyrins and the corresponding monomeric precursor.

Taking into account the importance of the substitution pattern of the *meso* phenyl group of the bis-porphyrins in the formation of inter- or intramolecular sandwich type complexes with DABCO, in 2006 Ballester et al. selected the *para*-substituted aminoporphyrin monomer **31c** in the design of a self-assembled molecular receptor based on a double-decker porphyrin array.<sup>64</sup> The coupling of the *para* aminoporphyrin **31c** with a benzene-1,3,5-tricarboxamide core afforded a trisporphyrin molecular scaffold, **32**, (Figure 33) which, after metallation, is capable of self-assemble in the presence of certain diamines into an intramolecular sandwich complex with cage-like structure. Thermodynamic studies of the formation process of the molecular cage were carried out. The analysis of the UV-visible data allowed to determine the stability constant of the 3:2 complex as,  $K_{32} = (8 \pm 2) \times 10^{27} \text{ M}^{-4}$ .

<sup>64</sup> Ballester, P.; Oliva, A. I.; Costa, A.; Deya, P. M.; Frontera, A.; Gomila, R. M.; Hunter, C. A. *J. Am. Chem. Soc.* **2006**, *128*, 5560-5569.

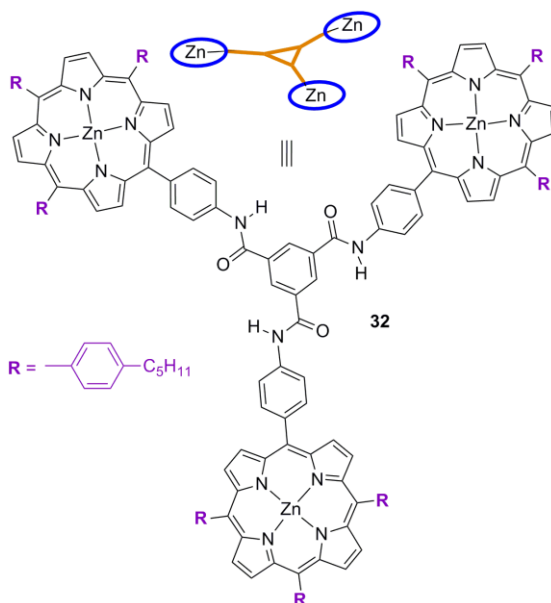


**Figure 33.** Structure of the Zn-trisporphyrin **32**.

By changing the diamine ligand, it should be possible to modify the size of the internal cavity or have access to molecular cages with different properties Ballester, Flamigni et al. reported the spectroscopic and photophysical behavior of a double-decker assembly with 5,15-bis(4-pyridyl)-10,20-diphenylporphyrin (DPYP) as pillars, and compared its spectroscopic properties with those of the assemblies derived from DABCO and Bipy.<sup>65</sup> DPYP is photochemically active while DABCO and Bipy are photochemically “innocent”. The photophysical experiments were carried out taking into account that at spectroscopic concentrations (DPYP)<sub>3</sub>•**32**<sub>2</sub> is presented in solution with both **32** and free base guest DPYP (all strongly absorbing in the spectral region of interest). Even in these conditions, it was possible to observe an efficient photoinduced energy transfer (96%) from the top and bottom part to the side walls of the cage (Figure 34).

<sup>65</sup> Flamigni, L.; Ventura, B.; Oliva, A. I.; Ballester, P. *Chem.--Eur. J.* **2008**, *14*, 4214-4224.

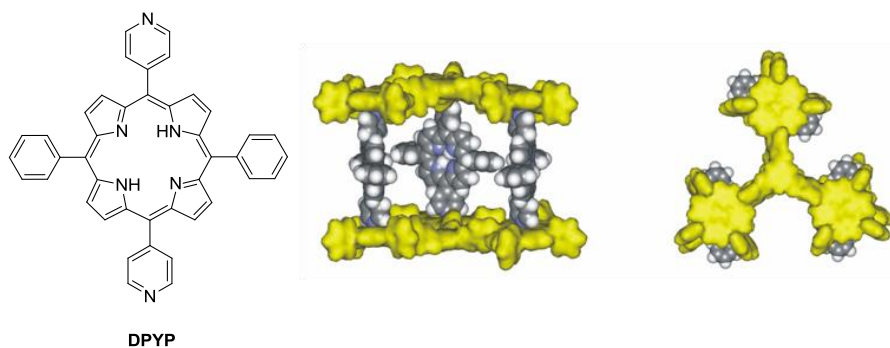


**Figure 34.** Linear drawing of the 5,15-bis(4-pyridyl)-10,20-diphenylporphyrin (DPYP) and side and top view of the molecular mechanics optimized structures (CACHe<sup>66</sup>, MM3) of the trigonal molecular cage formed by coordination of three DPYP as pillars and two Zn-trisporphyrin **32** as bases. DPYP appears as CPK representation whereas **32** is shown with van der Waals surface model

We expect that this introduction provides the reader with the sufficient background for confronting the following chapters of the thesis.

<sup>66</sup> CACHe WorkSystem, version 6.1.12.33; Fujitsu Limited (USA), 2004.

## 4. Objectives

The aims of this work have to do mainly with two different topics: a) the synthesis of bis-porphyrin receptors and b) the study of their complexation properties on binding two families of dissimilar ligands: amines and fullerenes.

The first objective of this work consisted in the design of cyclic bis-porphyrin architectures having an aromatic cavity big enough for the inclusion of selected guests (ditopic amines and fullerenes). The following goal was the synthesis of the designed macrocyclic structures. We also wanted to characterize and determine the binding properties of the prepared receptors in the complexation with mono- and ditopic amines mediated by coordination bonds, as well as in the formation of inclusion complexes with fullerenes driven by  $\pi$ - $\pi$  interactions.

In order to achieve the synthesis of the designed receptors we have made an extensive use of template-assisted covalent synthesis. Our original plan considered the use of templates of different lengths in combination with a great variety of coupling reactions. Due to unexpected results, we have only been able to assay Grubbs metathesis and Hay coupling reactions starting from adequately substituted monoporphyrins as key reactions for the cyclization step. The results we have obtained in the synthetic objective are summarised in Chapters 1 and 2.

We were also interested in evaluating how the number of carbon chains used as spacers of the bis-porphyrin receptors, as well as the degree of saturation of those chains will translate in their binding properties with the two families of selected guest. For this reason, we planned to probe the coordination of the amine ligands and the inclusion of the fullerenes using different spectroscopic techniques. Our expectations were that the mathematical analyses of the data obtained in the binding and titration experiments would allow us to fully characterize thermodynamically the coordination processes in which the receptors were involved. Most likely, the results of these studies will also permit to derive binding stoichiometries and complexation geometries for the complexes formed not only in solution but also in the solid state assuming that suitable single crystals were grown. Chapter 3 and 4 describe our findings in the complexation process with amines and fullerenes respectively. Completely unanticipated in our objectives, however, we have been able to include the study of

the binding of an endohedral fullerene. This compound was kindly provided by the group of Prof. L. Echegoyen.

The initial objectives of this work included the use of the structures we designed in functional assemblies. In this sense, we imagine the use of the of the bis-porphyrin:fullerene complexes for light triggered electron transfer processes with potential applications in light to energy conversion studies. Preliminary photophysical characterization results of these systems are described in chapter 4. Finally, chapter 5 describes the results we have obtained in the application of the sandwich motif "bis-porphyrin-ditopic amine" for controlling the regioisomeric mixture obtained in the self-assembly process of dimers derived from cyclopeptides. This work was undertaken in collaboration with the group of Prof. J. Granja. The objective of the work was to show the relationship that exists between structure and function when cyclopeptides are equipped with external porphyrin binding units capable of forming sandwich complexes with ditopic ligands like DABCO. Time has not permitted the evolution of our initial systems into more elaborated ones in which the sandwich binding motif could be used as external trigger of other photophysical or chemical functions of the assemblies.

## CHAPTER 1

***“Templated-synthesis of cyclic bis-porphyrin receptors using the olefin metathesis reaction”***

UNIVERSITAT ROVIRA I VIRGILI  
SUPRAMOLECULAR CHEMISTRY OF BIS-PORPHYRINS  
Laura Patricia Hernández Eguía  
ISBN:978-84-694-0308-2/DL:T-204-2011

## 1. Introduction

In this chapter, we will discuss our synthetic strategy for the construction of cyclic bis-porphyrin receptors based on the use of zinc metallated porphyrins, adequately functionalized with terminal double bonds as basic molecular component (Figure 1).

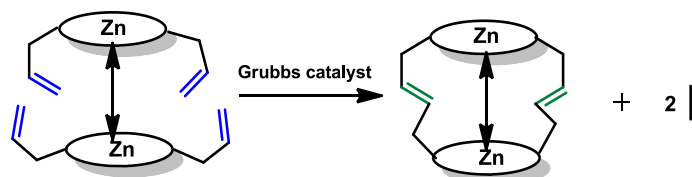
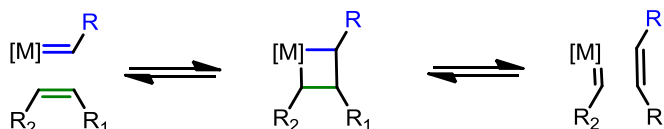


Figure 1. Schematic representation of the process.

The application of the olefin metathesis reaction,<sup>1,2</sup> (Scheme 1) under appropriate conditions, should yield a cyclic dimeric receptor through the formation of covalent bonds between the terminal alkenyl substituents of two different molecular components.



Scheme 1. Olefin metathesis reaction mechanism.

Other two essential components for the reaction are an adequate diamine, i.e. 1,4-diazabicyclo[2.2.2]octane (DABCO), which will be used to template the formation of a supramolecular 2:1 (porphyrin:diamine) sandwich porphyrin complex and a first or second generation Grubbs catalyst to induce the metathesis reaction between the basic porphyrin components (Figure 2).

<sup>1</sup> Trnka, T. M.; Grubbs, R. H. *Acc. Chem. Res.* **2001**, *34*, 18-29.

<sup>2</sup> Scholl, M.; Ding, S.; Lee, C. W.; Grubbs, R. H. *Org. Lett.* **1999**, *1*, 953-956.

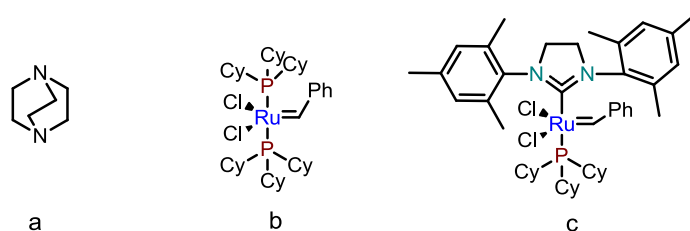


**Figure 2.** Molecular structures of a) 1,4-diazabicyclo[2.2.2]octane (DABCO), b) first generation Grubbs catalyst, c) second generation Grubbs catalyst.

DABCO has been extensively used in combination with zinc porphyrin oligomers to assemble a large number of supramolecular complexes through axial coordination.<sup>3</sup> This zinc porphyrin/DABCO binding system has been widely studied by Sanders, Anderson and our research group.<sup>4,5</sup>

It is well known that concentration plays an important role in the speciation of even very simple self-assembly processes.<sup>6</sup> In the initial experiments we propose to treat a 2:1 mixture of a monoporphyrim substituted either with two or four allyl groups with a diamine (i.e. DABCO) acting as template. Each allyl group is positioned in the *meta*-position of the *meso* phenyl substituents of the porphyrin. The 2:1 stoichiometric mixture of porphyrin and diamine in the appropriate concentration range should lead to the formation of a 2:1 complex with sandwich-like structure. This methodology allows the preparation of molecules having a topology of “molecular cage”.<sup>7</sup> Moreover, the size of the cavity will be controlled by the size of the templating diamine used. In a later step, the template will be removed and the porphyrins demetallated. Moreover, we envisioned that the covalently connected cage thus formed could be used as a molecular unit for the construction of more elaborated tube-like supramolecular aggregates.

<sup>3</sup> Mak, C. C.; Bampos, N.; Sanders, J. K. M. *Angew. Chem., Int. Ed.* **1998**, *37*, 3020-3023.

<sup>4</sup> a) Hunter, C. A.; Meah, M. N.; Sanders, J. K. M. *J. Am. Chem. Soc.* **1990**, *112*, 5773-80. b) Anderson, H. L.; Sanders, J. K. M. *J. Chem. Soc., Chem. Commun.* **1989**, 1714-1715

<sup>5</sup> Ballester, P.; Oliva, A. I.; Costa, A.; Deya, P. M.; Frontera, A.; Gomila, R. M.; Hunter, C. A. *J. Am. Chem. Soc.* **2006**, *128*, 5560-5569.

<sup>6</sup> Ercolani, G. *J. Phys. Chem. B* **2003**, *107*, 5052-5057.

<sup>7</sup> van Gerven, P. C. M.; Elemans, J. A. A. W.; Gerritsen, J. W.; Speller, S.; Nolte, R. J. M.; Rowan, A. E. *Chem. Commun. (Cambridge, U. K.)* **2005**, 3535-3537.

## 2. Results and discussion

Our final aim is the construction of “molecular cages” using supramolecularly assisted covalent chemistry. The two porphyrin units will constitute the “bottom” and the “top” parts of the cage. The molecular structures of the two zinc porphyrins that will be used for the formation of the molecular cages are shown in Figure 3 (see above). Both porphyrins are substituted with allyl groups in *meta* position of the *meso*-phenyl substituents. These allyl residues are necessary for the metathesis reaction that will be used to close covalently the structure of the molecular cage which has to be first preorganized employing a diamine template.

We first needed to fully characterize thermodynamically the system in order to find out the right concentration and stoichiometry that will yield the almost quantitative formation of the templated sandwich complex. The previous formation of the sandwich complex in a quantitative manner is a pre-requisite for the Grubbs metathesis reaction to proceed in good yield by avoiding the formation of polymers. The system Zn-monoporphyrin/DABCO can be studied at two very different concentration levels: millimolar and micromolar. At millimolar concentration the binding is probed using proton nuclear magnetic resonance spectroscopy  $^1\text{H}$  NMR. While, at micromolar concentration, UV-visible spectroscopy is the best technique to follow the complexation process.

In order to quantify a binding interaction, the modification of certain physical property (i.e. chemical shift of a proton signal, absorbance, heat absorbed or emitted, etc) is measured as a result of the complexation phenomenon (titration). Next, from the fit of the obtained experimental data to a selected binding model the corresponding thermodynamic parameters can be derived.

The system studied in this chapter consists on a zinc monoporphyrin having two pentylbenzyl and two *meta*-allyloxybenzyl *meso*- substituents in a *trans*- configuration, **Zn-2a** and DABCO as an example of ditopic diamine. Similar complexation behavior is obtained when the porphyrin used is the tetraallyl substituted derivative, **Zn-1** (Figure 3) We decided to use chloroform as solvent to perform the study since the Zn-N interaction has a high thermodynamic stability in this solvent and chloroform is also an adequate solvent to perform Grubbs metathesis reactions.

The binding system is depicted in Scheme 2, where “P” is the free zinc monoporphyrin, “D” is the free DABCO and “PD” and “P<sub>2</sub>D” are the 1:1 and 2:1 complexes respectively. Several aspects should be taken into account in order to extract the microscopic binding constant values from the macroscopic or thermodynamic ones,  $K_1$  and  $K_2$ , which are the ones that we can assess experimentally.

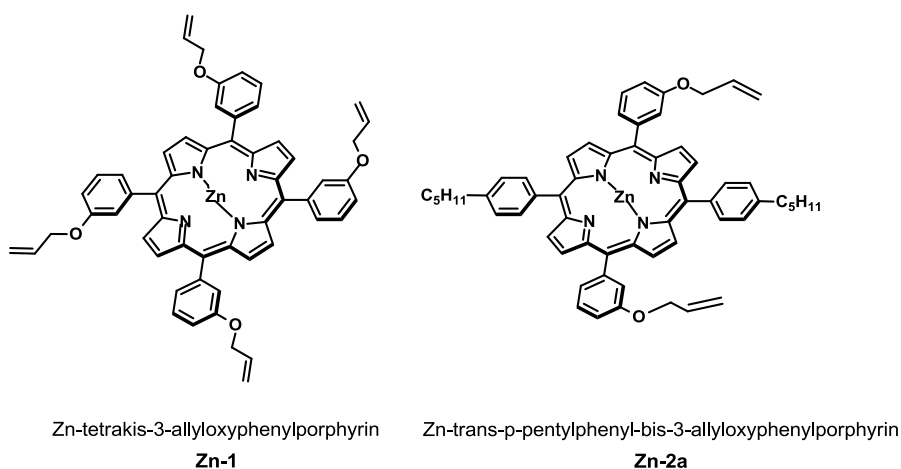
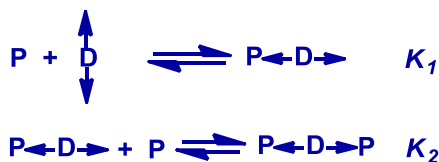


**Figure 3.** Molecular structures of the two zinc porphyrins using in this study, **Zn-1** and **Zn-2a**.



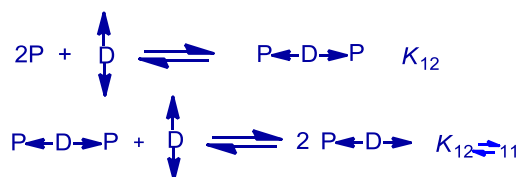
**Scheme 2.** Equilibria involved in the stepwise formation of a sandwich complex between a zinc monoporphyrin (P) and a ditopic ligand (D). The first equilibrium constant is defined as  $K_1$  and the second one by  $K_2$ .

In the first equilibrium, the Zn-porphyrins interact with a ditopic ligand, DABCO, therefore the complex has two ways to form but only one to dissociate and, for this reason, the relationship  $K_1 = 2K_{m1}$  holds. ( $K_{m1}$  represents the microscopic or statistically corrected constant for the stability of the bond Zn-porphyrin-DABCO).

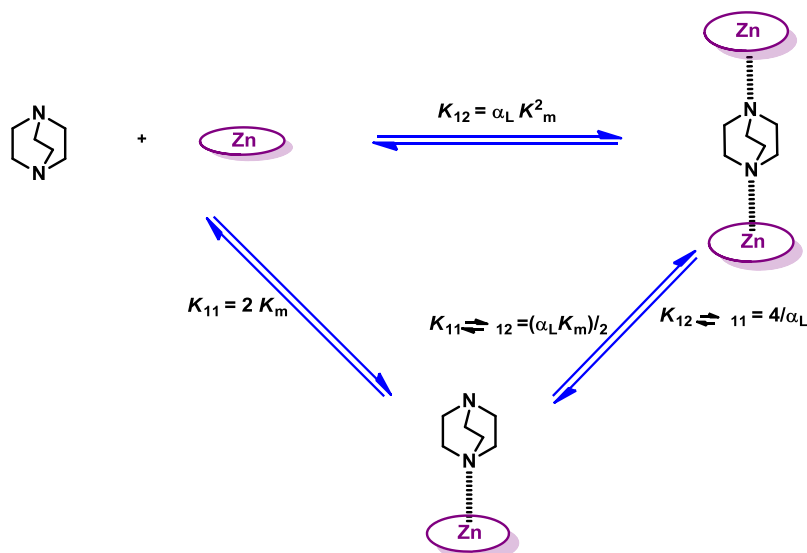
In the case of the second equilibrium, the second porphyrin unit has only one possible way to be bound with the PD complex, however, there are two possibilities to dissociate the  $P_2D$  complex, consequently, the relationship  $K_2 = K_{m2}/2$  is considered ( $K_{m2}$  represents the microscopic stability constant of the second bond Zn-porphyrin-DABCO).

At this point, we also define a new parameter  $\alpha_L = K_{m2}/K_{m1}$  which is the cooperativity coefficient for the binding of the second porphyrin unit to DABCO.

If we now consider the binding system shown in Scheme 3, the thermodynamic stability constants for each equilibrium can be estimated as follows:  $K_{12} = K_1 \cdot K_2 = \alpha_L K_{m1}^2$  and  $K_{12 \leftrightarrow 11} = K_1/K_2 = 4/\alpha_L$ . The latter equilibrium constant  $K_D$  is associated with the destruction of the ternary complex by excess DABCO and can be directly (*vide infra*) determined using  $^1H$  NMR titration. The value calculated  $K_D$  gives a direct way to measure the cooperativity between the two binding sites of DABCO. Scheme 4 depicts the molecular species involved in the thermodynamic cycle.



**Scheme 3.** Overall equilibrium for the formation of the 1:2 complex ( $K_{12}$ ) and the equilibrium corresponding to its destruction due to the addition of excess of DABCO ( $K_{12 \leftrightarrow 11}$ ).



**Scheme 4.** Schematic representation of the species involved in the thermodynamic cycle of binding DABCO to a simple zinc-porphyrin. The overall binding constant  $K_{12}$  and the stepwise constants,  $K_{11}$ ,  $K_{11 \leftrightarrow 12}$ , and  $K_{12 \leftrightarrow 11}$ , are shown as well as their relationship with  $K_m$  (the microscopic binding constant),  $\alpha_L$  (the ligand cooperativity factor), and the statistical correction factors.

## 2.1 UV-visible titration experiment at micromolar concentrations

Titration carried out using UV-visible spectroscopy are specially indicated when the free host, zinc porphyrin in our case, or the free guest, DABCO, absorbs light in wavelengths that are very different from one another.

The coordination of DABCO to the zinc porphyrin was first studied using UV-visible titration in chloroform, under dilute conditions (porphyrin concentrations  $\approx 10^{-6}$  M).

The metallated porphyrin monomer **Zn-1** presents an absorption Soret band at 420 nm and two Q bands at 546 and 587 nm.<sup>8</sup>

The binding of DABCO to the porphyrin results in a shift of the maximum of the Soret band from 420 to 430 nm due to the exclusive formation of axial coordinated complexes

<sup>8</sup> Ballester, P.; Costa, A.; Castilla, A. M.; Deya, P. M.; Frontera, A.; Gomila, R. M.; Hunter, C. A. *Chem.--Eur. J.* **2005**, *11*, 2196-2206.

having a 1:1 stoichiometry, **Zn-1**·DABCO. During the titration experiment we observed the presence of an isosbestic point, which is indicative of the existence of an equilibrium involving only two species (Figure 4).

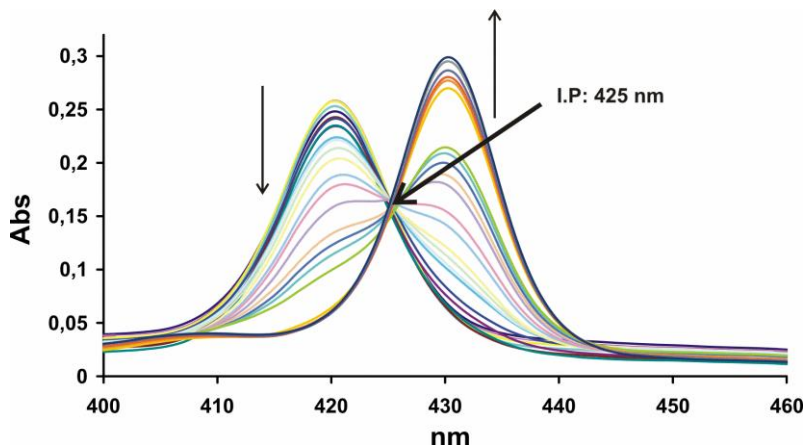


**Figure 4.** UV-visible titration data for the zinc-porphyrin **Zn-1** with DABCO in chloroform. The Soret band shift from 420 to 430 nm is depicted.  $[DABCO] = 0-4.4 \times 10^{-3}$  M,  $[Zn-1] = 1.0 \times 10^{-6}$  M.

The literature indicates that a shift of the Soret band of approximately 10-14 nm is typical for the formation of 1:1 complexes DABCO·Zn-porphyrin. It is known that the complexation of two zinc porphyrins with DABCO yields a co-facial sandwich complex that induces a shift of only 5 nm to the Soret band due to exciton coupling between the chromophores.<sup>9</sup> Since in our case we observed a shift of 10 nm we decided to fit the titration data to a simple binding model considering the exclusive formation of a 1:1 complex. Figure 5 shows the data obtained at two selected wavelengths fitted to the theoretical binding curves.

The fitting procedure allowed us to calculate an association constant value of  $K_{11} = 4.5 \times 10^4$  M<sup>-1</sup> for the 1:1 complex.

<sup>9</sup> Hunter, C. A.; Sanders, J. K. M.; Stone, A. J. *Chem. Phys.* **1989**, *133*, 395-404.

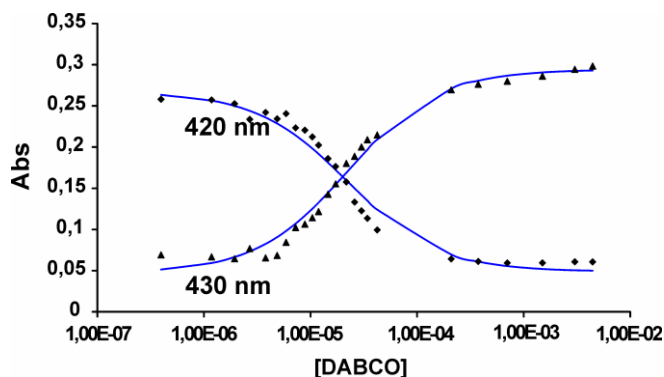


**Figure 5.** UV-visible titration data (change in absorbance at two wavelengths, 420 and 430 nm) for the binding of the zinc-porphyrin **Zn-1** with DABCO in chloroform fitted to the theoretical binding curves for a simple 1:1 binding model.

## 2.2 $^1\text{H}$ NMR titration experiment at millimolar concentrations

Next, the binding process of **Zn-1** with DABCO was probed using  $^1\text{H}$  NMR spectroscopy. We decided to maintain the porphyrin concentration constant throughout the titration experiment in order to diminish any dilution dependent process. In this way the observed proton chemical shift changes can be exclusively related to the complexation process with DABCO (Figure 6).

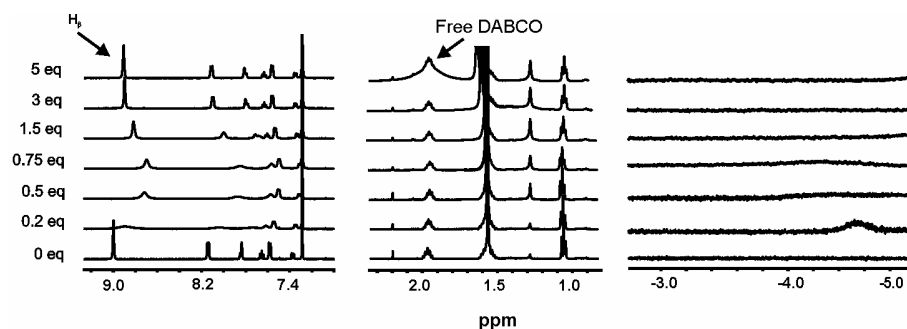


**Figure 6.** Three regions of  $^1\text{H}$  NMR spectra recorded during the titration of **Zn-1** with DABCO in deuterated chloroform. The change in the shifts of  $\beta$ -pyrrolic protons and aromatic protons of the *meso*-phenyl groups are easily detected. The number of equivalents added is indicated.

The binding process was characterized thermodynamically by fitting the observed change of the chemical shift of the  $\beta$ -pyrrol protons to a binding model that includes the formation of 1:1 and 2:1 stoichiometries by means of the SPECFIT software.<sup>10</sup> Figure 7 shows the experimental binding points fitted to the theoretical binding curve for the above mentioned binding model. We have fitted the experimental data assuming that three species contribute to the change in chemical shift: free porphyrin, 1:1 complex and 2:1 complex. The association constant for the 1:1 complex was determined in the UV-visible titration and was maintained constant during the fitting procedure. The only variables that have been optimized during the fitting are the stability constant of the 2:1 complex and the chemical shift value of the  $\beta$ -pyrrolic protons in all the species. We calculated a value of  $K_{21} = 1.2 \times 10^{10} \text{ M}^{-2}$  for the sandwich complex which allows us to derive a cooperativity factor  $\alpha = 0.6$ , indicating that there is small negative cooperativity in the formation of the sandwich complex.

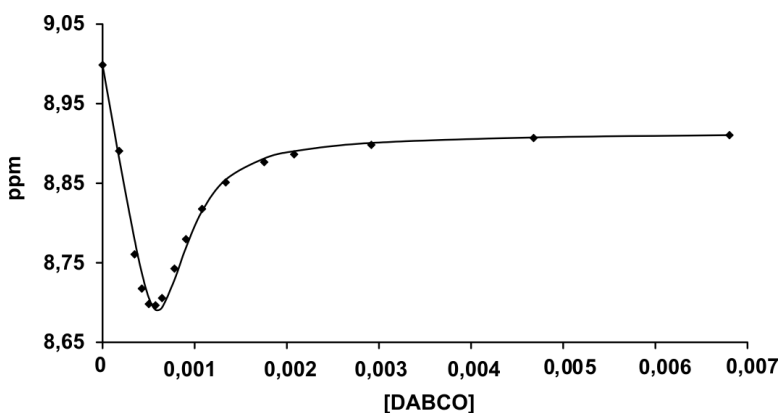


**Figure 7.** Experimental binding points fitted to the theoretical binding curve of the **Zn-1/DABCO**  $^1\text{H}$  NMR titration.

During the  $^1\text{H}$  NMR titration we can detect the formation of the 1:1 and 1:2 complexes. The chemical shift of the methylene protons of the complexed DABCO is diagnostic of the stoichiometry. Thus, the ternary complex  $(\text{Zn-1})_2 \cdot \text{DABCO}$  is characterized by a signal that

<sup>10</sup> SPECFIT, version 3.0; Spectra Software Associates, Marlborough, MA (USA), 2007 a) Gampp, H.; Maeder, M.; Meyer, C. J.; Zuberbuhler, A. D. *Talanta* **1985**, *32*, 95-101 b) Gampp, H.; Maeder, M.; Meyer, C. J.; Zuberbuhler, A. D. *Talanta* **1986**, *33*, 943-951.

resonates at approximately  $\delta = -5$  ppm corresponding to the six-methylene protons of the DABCO sandwiched between two porphyrin units. Whereas a DABCO signal at  $\delta = -3$  ppm is indicative of the binary complex DABCO•**Zn-1** and can be assigned to the three methylene groups in the  $\alpha$ -position with respect to the nitrogen bound to the zinc porphyrin.<sup>11,5,8</sup> In the latter case and working at room temperature the signal of the DABCO protons at  $\delta = -3$  ppm is broad due to the existence of a chemical exchange with free DABCO. The methylene protons of the free DABCO appear at  $\delta = 2.8$  ppm. As the concentration of DABCO is increased, the DABCO proton signal shifts towards 2.8 ppm and grows, this is due to the existence of the mentioned chemical exchange between free and bound DABCO being fast in the NMR timescale (see Figure 6).

Once we have determined all the stability constants it was possible, using the SPECFIT software, to simulate the speciation profiles of the titrations carried out using the full binding model and at two different concentrations: micromolar and millimolar.

As shown in figure 8, when the concentration of **Zn-1** is  $1.0 \times 10^{-6}$  M, only two species are present at a detectable concentration during the titration experiment. The species are the 1:1 complex and the free **Zn-1**. The 2:1 complex is in very low concentration and can be discarded. In figure 9, however we can see that for a concentration of  $10^{-3}$  M of **Zn-1** the 2:1 complex is present at a considerable concentration. In fact, at this concentration, when 0.5 equivalents of DABCO are added the 2:1 complex is almost the exclusive species in solution. Since free DABCO could damage the Grubbs catalyst we should work at a concentration of porphyrin and in a stoichiometric ratio of DABCO to favor the almost exclusive formation of the 2:1 complex while at the same time keeping the concentration of free DABCO as low as possible. When working at millimolar concentration of **Zn-1**, after the addition of more than 0.5 equivalents of DABCO the species present in solution are the 2:1 and the 1:1 complexes, moreover the free DABCO concentration begins to become important. We conclude that the best conditions to achieve the almost exclusive formation of the 2:1 complex are: a) working at millimolar concentration of porphyrin and b) addition of 0.5 equivalents of DABCO.

---

<sup>11</sup> Hunter, C. A.; Meah, M. N.; Sanders, J. K. M. *J. Am. Chem. Soc.* **1990**, *112*, 5773-80.

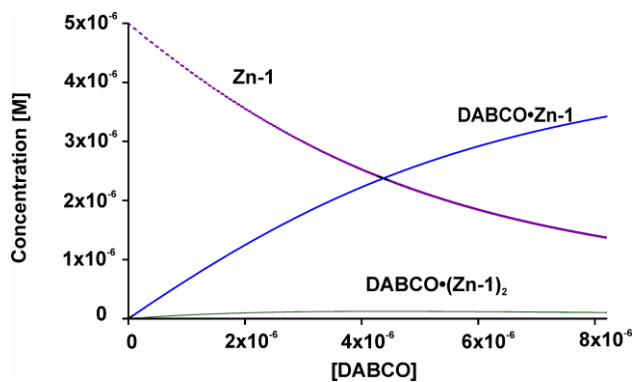


**Figure 8.** Simulated speciation profiles for the species present during a titration of the zinc porphyrin with DABCO at a micromolar concentration of the porphyrin.

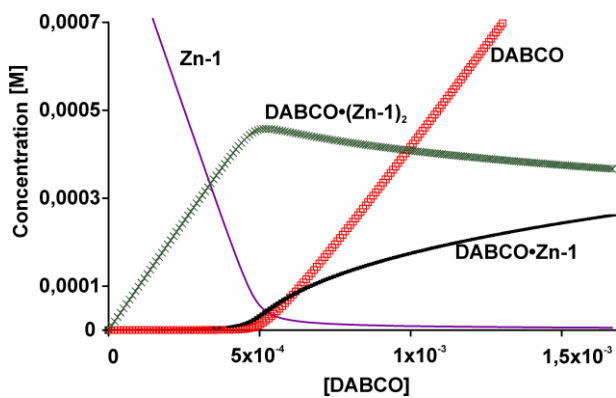
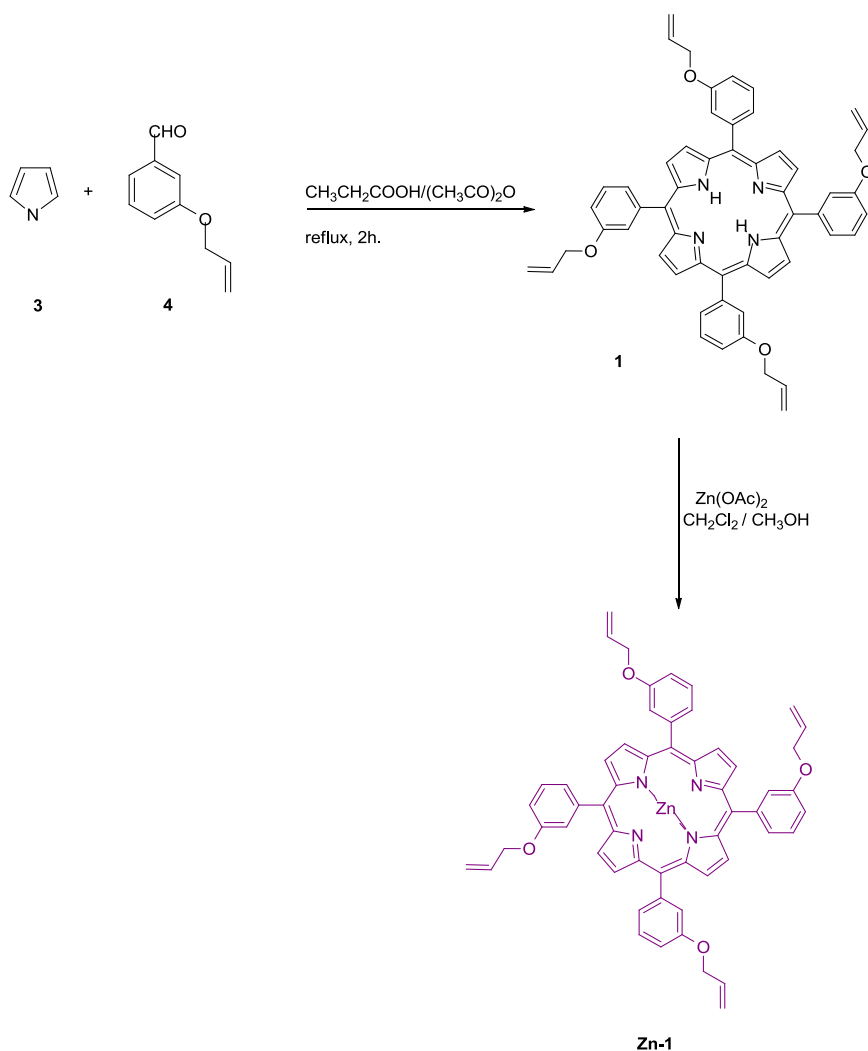


**Figure 9.** Simulated speciation profiles for the species present during a titration of the zinc porphyrin with DABCO at a millimolar concentration of the porphyrin.

## 2.3 Synthesis

The synthesis of the porphyrin **Zn-1** decorated with four allylic substituents is shown in Scheme 5.



**Scheme 5.** Synthesis of the Zn-tetrakis-3-allyloxyphenylporphyrin, **Zn-1**.

The reaction in acidic conditions of pyrrol **3** with 3-allyloxybenzaldehyde **4** in a 1:1 stoichiometric ratio allowed the preparation and isolation of the free base porphyrin **1**. The experimental methodology used for the synthesis of the porphyrins implies the use of refluxing propionic acid during 2h.<sup>12</sup>

<sup>12</sup> Odobel, E. Blart, M. Lagree, M. Villieras, H. Boujtita, N. El Murr, S. Caramori and C. Alberto Bignozzi, *J. Mater. Chem.*, **2003**, 13, 502-510.

The synthesis of an analogous porphyrin having four allylic substituents in the *para* position has already been described using the same method.<sup>13</sup> The tetraallyl porphyrin **1** was isolated as a pure compound after careful column chromatography of the reaction crude. We isolated **1** in an overall reaction yield of approximately 19%. The allylated aldehyde **4** which was used in the preparation of **1** was also synthesized following a described experimental procedure.<sup>14</sup>

The metallation of **1** was achieved by simple treatment of the free base with Zn(OAc)<sub>2</sub> in a solvent mixture CH<sub>2</sub>Cl<sub>2</sub>/CH<sub>3</sub>OH (3:1). The metallated porphyrin **Zn-1** was isolated after column chromatography of the reaction crude using neutral alumina as stationary phase and chloroform as eluent in 81% of yield.

We have already discussed above that when 0.5 equivalents of DABCO are present in a millimolar solution of the porphyrin **Zn-1** the 2:1 sandwich complex is formed almost quantitatively. Therefore, we decided to use DABCO as template to assay the “intramolecular” olefin metathesis reaction on the sandwich complex. The olefin metathesis reaction will covalently connect the two porphyrin units of the sandwich complex, for this reason the reaction can be considered as intramolecular, and will yield a covalent molecular cage. Molecular modelling studies<sup>15</sup> show that the allylic chains placed in the *meta*- position of the *meso*-phenyl groups and connected through an ether linkage had the appropriate number of carbons to be involved in the intramolecular olefin metathesis reaction between two adjacent porphyrins when they are separated by a DABCO molecule. The use of longer diamines as templates, i.e. bispyridyl will require an increase in the number of carbon atoms (Figure 10).

<sup>13</sup> Lindsey, J. S.; Schreiman, I. C.; Hsu, H. C.; Kearney, P. C.; Marguerettaz, A. M. *J. Org. Chem.* **1987**, *52*, 827-36.

<sup>14</sup> Mmutlane, E. M.; Michael, J. P.; Green, I. R.; de Koning, C. B. *Org. Biomol. Chem.* **2004**, *2*, 2461-2470.

<sup>15</sup> *CAChe WorkSystem*, version 6.1.12.33; Fujitsu Limited (USA), **2004**.

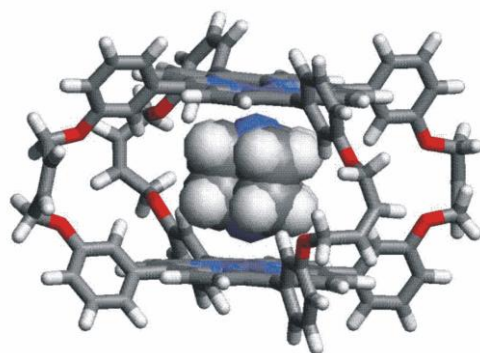
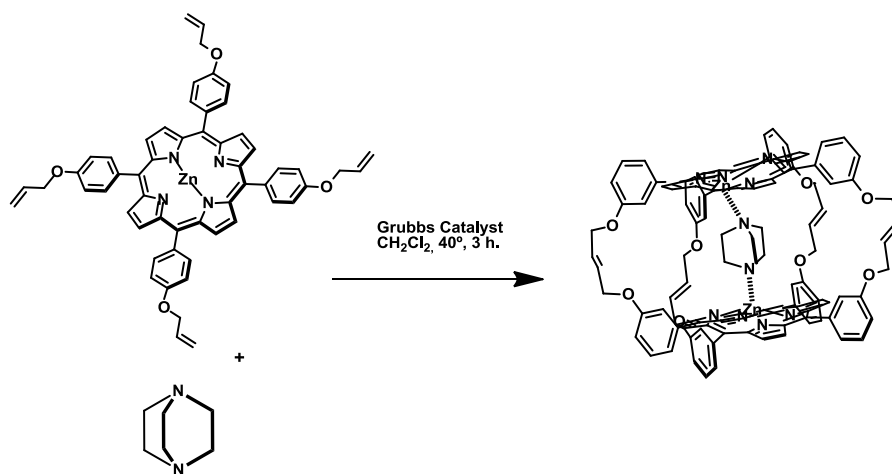


**Figure 10.** CACHE minimized structure of the molecular cage formed in the metathesis reaction of two **Zn-1** bonded to DABCO.

Once porphyrin **Zn-1** was in our hands we decided to study the olefin metathesis reaction (Scheme 6) in the absence and in the presence of the template diamine DABCO.



**Scheme 6.** Experimental conditions to carry out the olefin metathesis reaction.

The reaction was carried out at 1 mM concentration of **Zn-1** using chloroform as solvent and by the sequential addition of 0.5 equivalents of DABCO and 0.4 equivalents of the second generation Grubbs catalyst. After heating the reaction mixture at 40 °C during 3 h the solvent was eliminated and the reaction crude was purified by column chromatography on neutral alumina using chloroform as eluent. We were able to isolate 30 mg of a purple

solid. The  $^1\text{H}$  NMR spectrum of the isolated solid is very complicated and we don't get valuable information. Another possible reaction of the terminal olefins in the presence of the Grubbs catalyst is the isomerization of the double bond to a disubstituted olefin. Furthermore, and as it will be explained in the following chapter, it could have taken place some intramolecular coupling reactions between the two double bonds of allylic chains positioned in *cis*. When the same reaction was carried out without the presence of the template (DABCO) we only recovered the starting material and polymeric products.

In order to gain some insight in the composition of the purple solid isolated from the templated metathesis reaction a MALDI-TOF mass spectrum was performed (Figure 11). The peak with higher intensity corresponds to an ion with molecular weight ( $m/z$  1692.5) that can be assigned to the fully closed molecular cage, that is, the four allyl groups have experienced the metathesis reaction. However, we can also observe other peaks corresponding to molecular ions that have experienced partial metathesis reaction. Thus, the peak at  $m/z$  1720.5 can be assigned to a molecular cage in which only three allyl groups have reacted and consequently the difference in mass with the fully closed cage is two methylenes (28 amu). Likewise, the peak at  $m/z$  1706.5 can be assigned to the molecular ion of a cage that is only covalently linked through two connections. The mass difference of this compound with respect to the fully closed cage corresponds to four methylenes (56 amu).

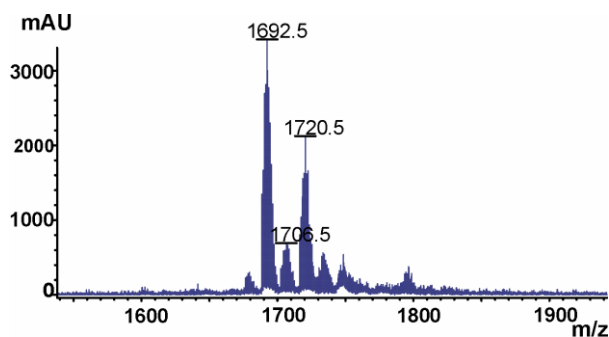


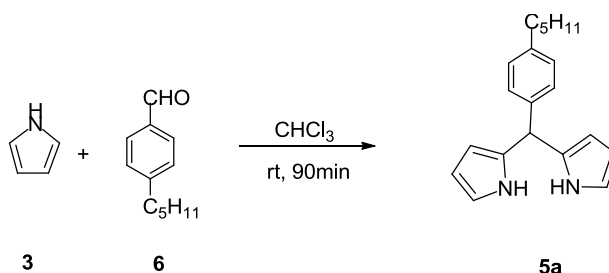
**Figure 11.** MALDI-TOF mass spectrum of the metathesis reaction with **Zn-1**. The closed molecular cage is represented by the peak with  $m/z$  1692.5.

It is worth mentioning that all the molecular ions that were detected correspond to molecular cages that do not include one DABCO molecule in their interior. This

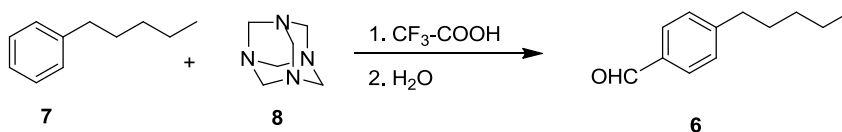
observation is in complete agreement with the reported<sup>8</sup> difficulties of detection of amine complexes of Zn-porphyrins using mass spectrometry.

Due to the hypothesized partial reaction of the allyl groups observed for the tetra-substituted porphyrin we decided to synthesize a new porphyrin decorated with only two allyl groups. We hope that the simplification of the reacting functionality will increase the percentage of the fully reacted product.

We prepared the disubstituted porphyrin **Zn-2a** starting from the dipyrromethane **5a** and the aldehyde. Consequently, we prepared the dipyrromethane precursor **5a** by dropwise addition of an excess of pyrrol **3** (100 equivalents) to a chloroform solution of *p*-pentylbenzaldehyde **6** (Scheme 7). Compound **5** was isolated in 43 % yield as white crystals by recrystallization from ethanol:water. The *p*-pentylbenzaldehyde **6** was also prepared (Scheme 8).



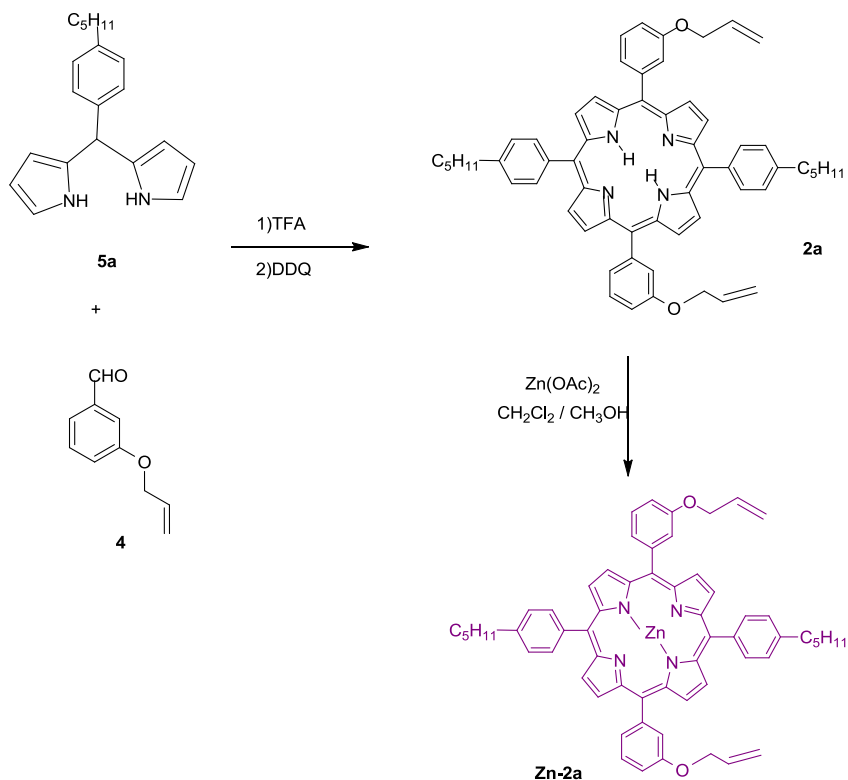
**Scheme 7.** Preparation of the dipyrromethane precursor **5a**.



**Scheme 8.** Synthesis of *p*-pentylbenzaldehyde **6**, a precursor to carry out the synthesis of the dipyrromethane **5a**.

The synthesis of the di-substituted allyl porphyrin **Zn-2a** was carried-out by reacting one equivalent of 5-((4-pentyl)-phenyl)-dipyrromethane **5a** with one equivalent of 3-(allyloxy)benzaldehyde **4** using CH<sub>2</sub>Cl<sub>2</sub> as solvent and in the presence of trifluoroacetic acid (TFA). Dicyanodichloroquinone (DDQ) was added at the end of the reaction time to

assure the full oxidation of the porphyrinogen to the corresponding porphyrin skeleton **2a** (Scheme 9).<sup>16</sup> A fraction containing porphyrin<sup>17</sup> **2a** (*vide infra*) was isolated as a purple solid in a yield of 10% after column chromatography of the reaction crude.



**Scheme 9.** Representation of the synthesis of Zn-2a.

The purification of the fraction containing porphyrin **2a** is a tedious process, due to the fact that five different porphyrin structures are present in the reaction mixture. Even starting from the dipyrromethane precursor, undesired porphyrins are produced due to a scrambling of aldehydes. Dipyrromethane **5a** partially reverts to its starting components, aldehyde and pyrrole, under the reaction conditions of acid catalysis. The <sup>1</sup>H NMR spectrum of the third fraction isolated during the purification of porphyrin **2a** shows a set of

<sup>16</sup> Lindsey, J. S.; Schreiman, I. C.; Hsu, H. C.; Kearney, P. C.; Marguerettaz, A. M. *J. Org. Chem.* **1987**, *52*, 827-36.

<sup>17</sup> In the next chapter the preparation of a related porphyrin having alkynyl substituents afforded a mixture of *cis* and *trans* isomers which was undetectable from the spectroscopic characterization of the isolated product.

proton signals having the multiplicity and chemical shift values expected for the structure of the di-substituted porphyrin **2a**. Finally, the metallation of the fraction containing di-substituted porphyrin **2a** was performed using the same procedure already described for **Zn-1**.

One of the goals of the present work was to implement the use of gel permeation chromatography (GPC) in our research group as an efficient technique for the purification of porphyrin compounds. Until now we have used this technique simply as an analytical tool. Figure 12, shows several examples of GPC chromatograms and illustrates the high resolution power of the GPC technique for the compounds under study.

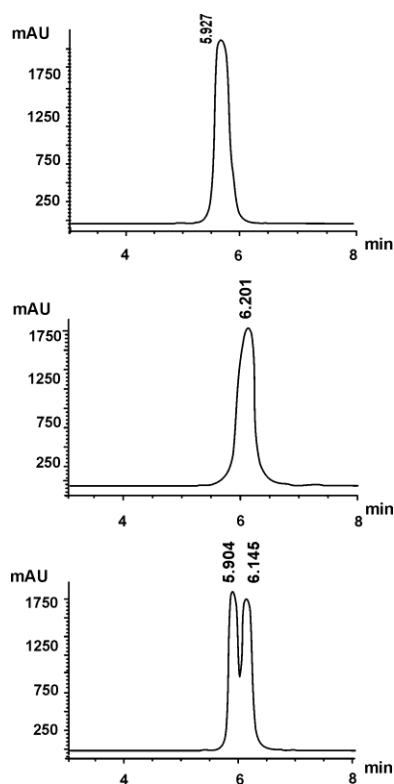


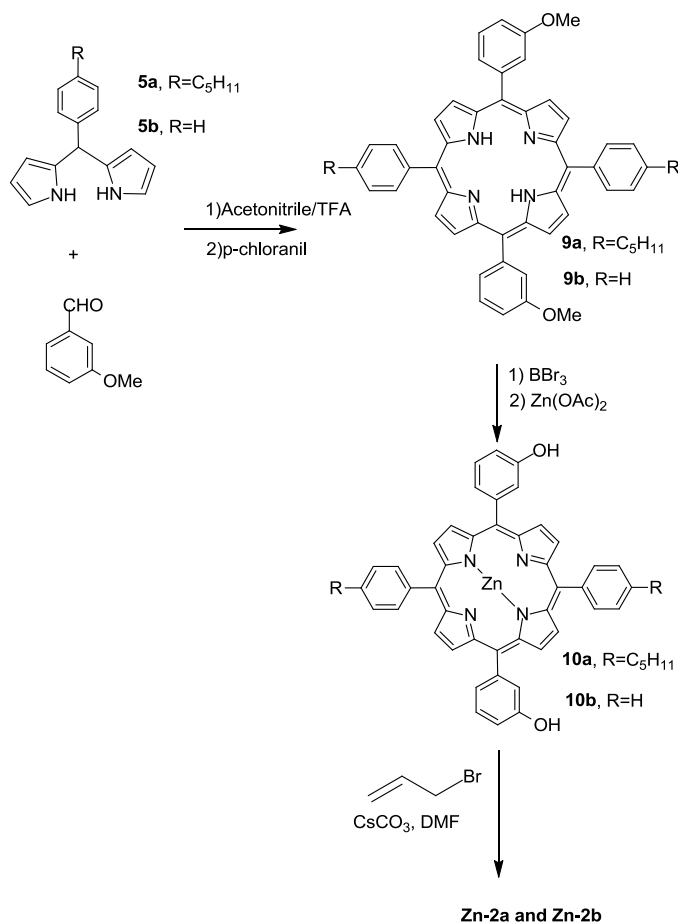
**Figure 12.** GPC chromatograms using  $\text{CH}_2\text{Cl}_2$  as eluent and a flow ratio of 1.5 ml/min. Top: injection of the fraction containing unmetallated porphyrin **2a**. Middle: injection of the reaction crude containing metallated porphyrin **Zn-2a**. Retention time is 6.2 minutes. Bottom: GPC chromatogram of a mixture of metallated and demetallated fractions.

When porphyrin **Zn-2a** was available we repeated the metathesis reaction using this new material and applying the same reaction conditions assayed for **Zn-1**. The obtained reaction crude was analyzed by mass spectrometry (MALDI-TOF technique). The mass spectrum shows that the peak of higher intensity is  $m/z = 1805.1$ . This is the expected value for the covalent cage in which the two porphyrin units are connected through two carbon chains and no DABCO is bound in its cavity. We conclude that the metathesis reaction of the two porphyrins has taken place. But for sure we have also some polymers in the mixture. In fact, the analysis of the reaction crude using the dichloromethane analytical GPC column reveals broad and not well-defined peaks.

The described preparation of the di-allyl-substituted porphyrin **2a** yields the compound in very low percentage. Consequently, we decided to try the preparation of **2a** using a methodology reported by Tashiro et al.<sup>18</sup> for the synthesis of a similar compound. The authors report a yield of 73 % for the synthesis of an analogue porphyrin.

---

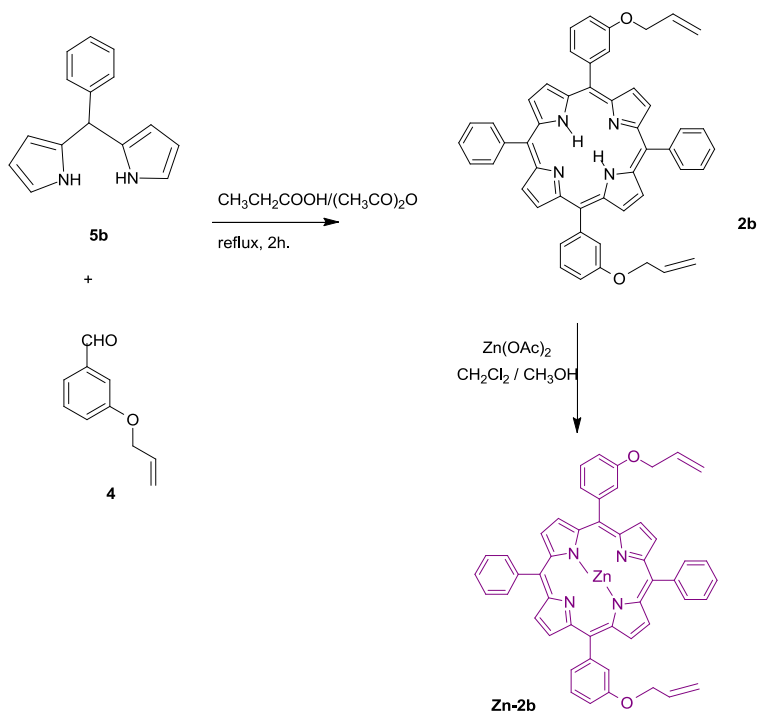
<sup>18</sup> Tashiro, K.; Aida, T.; Zheng, J.-Y.; Kinbara, K.; Saigo, K.; Sakamoto, S.; Yamaguchi, K. *J. Am. Chem. Soc.* **1999**, *121*, 9477-9478.



**Scheme 10.** Synthesis of **Zn-2a** based on the procedure reported by Tashiro.

We tried the synthesis of **9a** using the reported conditions. In our hands, however, we could isolate porphyrin **9a** in just a 10% yield (Scheme 10). It is worth to note that Tashiro used a dipyrromethane derivative not containing the pentyl *meso* substituent. The preparation of dipyrromethane **5a** described before produces the compound in reasonable yield but not in a high degree of purity. We were interested in preparing a *trans*-bis-allyloxyporphyrin using a dipyrromethane not containing the pentyl groups in the *meso*-phenyl ring, **5b**. We wanted to use this compound under the same reaction conditions used in the synthesis of porphyrin **1**. **5b** was synthesized following a described procedure,<sup>19</sup> in aqueous medium.

<sup>19</sup> Rohand, T.; Dolusic, E.; Ngo, T. H.; Maes, W.; Dehaen, W. *Arkivoc* **2007**, 307-324.



**Scheme 11.** Representation of the synthesis of **Zn-2b**, using the same dipyrromethane as in the reported reference.<sup>18</sup>

A fraction containing porphyrin **2b** was isolated in 12% of yield after column chromatography of the crude obtained by reacting **5b** and **4** in propionic acid. **2b** was metallated with  $\text{Zn}(\text{OAc})_2$  affording **Zn-2b** in almost quantitative yield. The subsequent step was the Grubbs metathesis, but unfortunately we were not able to perform an acceptable purification of the reaction crude to obtain a clean porphyrinic macrocycle. Again, from the  $^1\text{H}$  NMR spectrum it was difficult to determine the number and type of species that were present. MALDI mass spectrometry indicated the presence of species with higher molecular weight. We resorted to GPC analysis, this time we performed the analysis of the crude using toluene as eluent and we could obtain a better resolution than with dichloromethane (figure 13). It seems that apart from products with high molecular weights some starting material still remains in the crude.

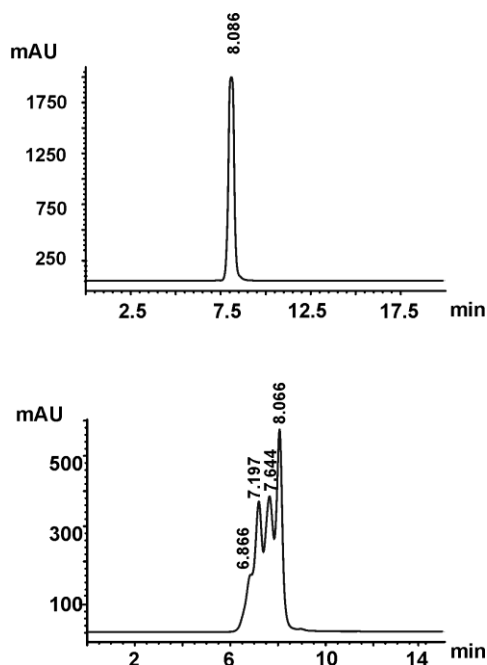


**Figure 13.** GPC chromatograms using toluene as eluent with a flow rate of 1 ml/min. Top: the peak assigned to the Zn-porphyrin, **Zn-2b**, as the starting material for the Grubbs metathesis, has a retention time of 8.1 minutes. Bottom: GPC trace of the metathesis reaction crude.

### 3. Conclusions

In this first chapter we describe our attempts in the synthesis of two zinc porphyrins that can be used for the construction of molecular nanocages. A diamine has been used to template the formation of a 2:1 sandwich complex. The olefin metathesis reaction using Grubbs catalysts was employed to connect covalently the base and the top components of the 2:1 assembly. Moreover, in order to find the best relation of concentrations of the porphyrin and the template to yield the 2:1 sandwich complex almost quantitatively, we have performed UV-visible and  $^1\text{H}$  NMR titrations. We have characterized thermodynamically the self-assembly process of a diamine with a zinc porphyrin. A simple zinc porphyrin at micromolar concentrations forms a 1:1 complex exclusively, whereas at

millimolar concentrations and when 0.5 equivalents of DABCO are added, a 2:1 sandwich complex is formed.

The allylated porphyrins **Zn-1** and **Zn-2a** are obtained in very low yields. But **Zn-2a**, as it will be explained in the next chapter, was probably produced as a mixture of two porphyrins, specifically, two isomers, the *cis* and the *trans*. The former has the allylic chains in the phenyl groups of positions 5 and 10, whereas in the latter the allylic chains are in positions 5 and 15. The metathesis reaction performed with **Zn-1** in the presence of 0.5 equivalents of DABCO affords the desired molecular cage with four covalent connections together with other cages that have reacted partially or intramolecularly. The fraction containing porphyrin **Zn-2a** with two allyl substituents yields the desired cage as the major component of the reaction mixture.

A simplified porphyrin **Zn-2b** was synthesized using propionic acid. The yield was slightly increased in these conditions. However, the analysis of the reaction crudes of the Grubbs metathesis reaction showed although the cyclic bis-porphyrin was present, they were composed by a complex mixture of products.

Having reached this point, we became interested in using propargyl substituents instead of alkenyl groups in order to obtain cyclic dimers by oxidative dimerization of the triple bond. Our hope was that this reaction would produce cleaner reaction crudes. It is worthy of note that later on we became aware that the complexity of the reaction crude derived from the Grubbs metathesis was probably due to the use of an started material composed by a mixture of two isomeric porphyrins.

## 4. Experimental section

### 4.1 General information and instrumentation

All commercial reagents, unless otherwise noted, were reagent grade and used without further purification. Solvents were of HPLC grade quality, obtained commercially and used without further purification. Anhydrous solvents were obtained from a solvent purification system SPS-400-6 from Innovative Technologies, Inc. Pyrrole was freshly distilled under vacuum just prior to use. <sup>1</sup>H NMR spectra were recorded on Bruker Avance 400 (400.1

MHz for  $^1\text{H}$  NMR and 100.6 MHz for  $^{13}\text{C}$ ) and Bruker Avance 500 (500.1 MHz for  $^1\text{H}$  NMR and 125.6 MHz for  $^{13}\text{C}$ ) NMR spectrometers. UV-visible spectra were measured on a UV-Vis spectrophotometer Shimadzu UV-2401PC. High resolution mass spectra were obtained using a Bruker Autoflex MALDI-TOF Mass Spectrometer. Analytical gel permeation chromatography (GPC) was carried out on PLgel 3  $\mu\text{m}$  MIXED E (300 x 7.5 mm) in dichloromethane, and on Styragel® HR1 Toluene (7.8 x 300 mm) Waters column with 100% toluene. Flash column chromatography was performed with Silica gel Scharlab60.

## 4.2 Binding studies

### a. $^1\text{H}$ NMR titrations

We prepared a standard solution of Zn-porphyrin **Zn-1** (1 mM) and using this solution as solvent we prepared a DABCO solution (10 mM) that will be used for the titration experiments. In this way the incremental addition of DABCO to the initial porphyrin solution will not dilute the porphyrin concentration;  $^1\text{H}$  NMR titration was carried out by acquiring a spectrum of an aliquot (500  $\mu\text{L}$ ) of the porphyrin (host) stock solution in  $\text{CDCl}_3$  at a concentration around 1mM, and adding increasing aliquots of the DABCO solution (guest), also in  $\text{CDCl}_3$ , and at a concentration approximately 10 mM. After each addition, a new  $^1\text{H}$  NMR spectrum was acquired.

### b. UV-visible titrations

The UV-visible titration was carried out by running a spectrum of the host solution of **Zn-1** in  $\text{CHCl}_3$  at 1  $\mu\text{M}$  and adding incremental aliquots of a DABCO solution from 0 to  $4 \times 10^{-3}$  M. To avoid the dilution of the host solution the titrating guest solution was prepared using the solution of the host as the solvent. After each addition of guest a new UV-visible spectrum was obtained. The set of data obtained from the UV-visible spectrophotometric titration (25 points from 0 equivalents to 4000 equivalents) were analyzed by fitting the whole series of spectra at 1 nm interval for the UV-visible titration using the software

SPECFIT 3.0, which uses a global system with expanded factor analysis and Marquardt least-squares minimization to obtain globally optimized parameters.

### 4.3 Synthesis

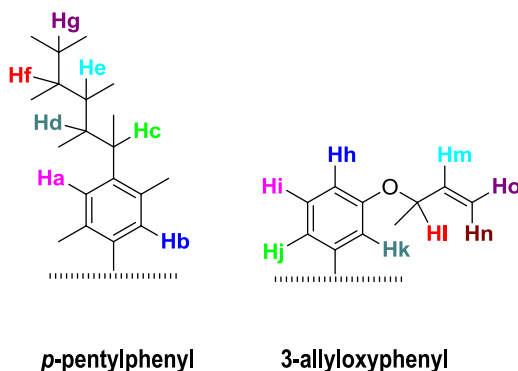


**Figure 14.** The line structures of *p*-pentylphenyl and 3-allyloxyphenyl substituents are drawn with their different types of protons, as a tool for the assignment of the <sup>1</sup>H NMR spectra.

#### Synthesis of 5,10,15,20-tetrakis-3-allyloxyphenyl-porphyrin, 1:

A mixture of 3.6 g (22.36 mmol, 1equivalent) of 3-allyloxybenzaldehyde, **4**, was added to 100 mL of stirring propionic acid (b.p: 140 °C), and the resulting solution was brought to reflux. A solution of 1.5 mL (22.36 mmol, 1equivalent) of distilled pyrrole in propionic acid (3 mL) was added and the mixture was refluxed for 2 h and allowed to cool and stand during the night.

In the flask there was a black liquid. The propionic acid was evaporated and the product was neutralized with bicarbonate, next, the organic fraction was taken. The porphyrin was purified by column chromatography with silica and using CH<sub>2</sub>Cl<sub>2</sub> as eluent. A second small column was needed using CH<sub>2</sub>Cl<sub>2</sub>/hexane 8/2 as eluent. The product was not pure yet, two more columns were prepared (CH<sub>2</sub>Cl<sub>2</sub>/hexane 6/4; CH<sub>2</sub>Cl<sub>2</sub>/hexane 7/3). The final product was obtained in a 18.55% yield.

<sup>1</sup>H NMR (400 MHz, CDCl<sub>3</sub>, 25°C) δ(ppm) 8.90 (s, 8H), 7.83 (d, 4H, *J* = 8.0Hz, **Hh**), 7.82 (s, 4H, **Hk**), 7.66 (t, 4H, *J* = 8.0Hz, **Hi**), 7.38 (d, 4H, *J* = 8.0Hz, **Hj**), 6.17 (ddt, 4H, *J* = 15.9Hz, *J* = 9.3Hz, *J* = 5.3Hz, **Hm**), 5.52 (d, 4H, *J* = 15.9Hz, **Hz**), 5.36 (d, 4H, *J* = 9.3Hz, **Ho**), 4.76 (d, 8H, *J* = 5.3Hz, **Hi**), -2.79 (s, 2H).

### Isolation of the fraction containing 5,15-bis (3-allyloxyphenyl)-10,20-bis(*p*-pentylphenyl)-porphyrin, **2a**:

5-((4-pentyl)phenyl)-dipyromethane, **5a**, (3.61 g, 12.33 mmol) and 3-allyloxybenzaldehyde, **4**, (2 g, 12.33 mmol) were dissolved in CH<sub>2</sub>Cl<sub>2</sub> (600 mL) in a two neck flask protected from light. To the resulting solution TFA (4.25 ml, 36.99 mmol) was added and the reaction was stirred at room temperature. After 30 min, Et<sub>3</sub>N (3.75 ml, 36.99 mmol) was added. DDQ (4.20 g, 18.49 mmol) was added as a solution in THF and the reaction mixture was stirred for 1 h. The crude mixture was filtered through a silica pad, CH<sub>2</sub>Cl<sub>2</sub>/THF, 8:2. After evaporation, the crude product was dissolved in CH<sub>2</sub>Cl<sub>2</sub> and chromatographed (silica, CH<sub>2</sub>Cl<sub>2</sub> then CH<sub>2</sub>Cl<sub>2</sub>/THF, 9:1, then 8:2). 0.25 g was obtained (9.35% of yield).

<sup>1</sup>H NMR (400 MHz, CDCl<sub>3</sub>, 25°C) δ(ppm) 8.89 (s, 8H), 8.13 (d, 4H, *J* = 7.5Hz, **Hb**), 7.84 (d, 2H, *J* = 7.9Hz, **Hh**), 7.83 (s, 2H, **Hk**), 7.65 (t, 2H, *J* = 7.9Hz, **Hi**), 7.58 (d, 4H, *J* = 7.5Hz, **Ha**), 7.37 (d, 2H, *J* = 7.9Hz, **Hj**), 6.17 (ddt, 2H, *J* = 16.3Hz, 10.5Hz, *J* = 4.8Hz, **Hm**), 5.51 (d, 2H, *J* = 16.33Hz, **hn**), 5.35 (d, 2H, *J* = 10.56Hz, **Ho**), 4.75 (d, 4H, *J* = 4.8Hz, **Hi**), 2.97 (t, 4H, *J* = 7.5Hz, **Hc**), 1.94 (tt, 4H, *J* = 7.5Hz and *J* = 7.5Hz, **Hd**), 1.55 (m, 8H, **He** and **Hf**), 1.05 (t, 6H, *J* = 6.8Hz, **Hg**), -2.76 (s, 2H).

### Synthesis of Zn-1:

A solution of 0.87 g of tetrakis-3-allyloxyphenylporphyrin, **1**, (1.04 mmol, 1 equivalent) and 3.01 g (10.04 mmol, 10 equivalents) of Zn(OAc)<sub>2</sub> in 150 mL of CH<sub>2</sub>Cl<sub>2</sub>/CH<sub>3</sub>OH 3:1 in a 250 mL flask was stirred for one hour while was protected of the light exposition. Then, the solvent was evaporated and the solid residue was purified by chromatography with neutral Aluminium oxide (activity I) and CH<sub>2</sub>Cl<sub>2</sub>/THF (99:1) as eluent (81.8% yield).

<sup>1</sup>H NMR (400 MHz, CDCl<sub>3</sub>, 25°C) δ(ppm) 9.01 (s, 8H), 7.84 (d, 4H, *J* = 8.0Hz, **Hh**), 7.83 (s, 4H, **Hk**), 7.65 (t, 4H, *J* = 8.0Hz, **Hi**), 7.37 (d, 4H, *J* = 8.0Hz, **Hj**), 6.16 (ddt, 4H, *J* = 17.2Hz, *J* = 10.5Hz, *J* = 5.2Hz, **Hm**), 5.50 (d, 4H, *J* = 17.2Hz, **hn**), 5.34 (d, 4H, *J* = 10.5Hz, **Ho**), 4.74 (d, 8H, *J* = 5.2Hz, **Hi**).

### Synthesis of Zn-2a (Metallation of the fraction containing **2a**):

A solution of 0.221 g of the fraction containing trans-pentyl-DpyP, **2a**, (0.25 mmol, 1 equivalent) and 0.31 g (2.55 mmol, 10 equivalents) of Zn(OAc)<sub>2</sub> in 100 mL of

CH<sub>2</sub>Cl<sub>2</sub>/CH<sub>3</sub>OH 3:1 in a 250 mL flask was stirred for an hour while was protected of the light exposition. Then, the solvent was evaporated and the solid residue was purified by chromatography with neutral Aluminium oxide (activity I) and CH<sub>2</sub>Cl<sub>2</sub> as eluent and 123 mg were obtained (50.23% of yield).

<sup>1</sup>H NMR (400 MHz, CDCl<sub>3</sub>, 25°C) δ(ppm) 9.00 (8H, s), 8.14 (d, 4H, *J* = 7.8Hz, **Hb**), 7.84 (d, 2H, *J* = 7.9Hz, **Hh**), 7.83 (s, 2H, **Hk**), 7.66 (t, 2H, *J* = 7.9Hz, **Hi**), 7.58 (d, 4H, *J* = 7.8Hz, **Ha**), 7.37 (d, 2H, *J* = 7.9Hz, **Hj**), 6.16 (ddt, 2H, *J* = 17.2Hz, *J* = 11.6Hz, *J* = 5.2Hz, **Hm**), 5.51 (d, 2H, *J* = 17.2Hz, **Hn**), 5.35 (d, 2H, *J* = 11.6Hz, **Ho**), 4.75 (d, 4H, *J* = 5.2Hz, **Hi**), 2.98 (t, 4H, *J* = 7.7Hz, **Hc**), 1.97 (tt, 4H, *J* = 7.7Hz and *J* = 7.7Hz, **Hd**), 1.56 (m, 4H, **He** and **Hf**), 1.06 (t, 6H, *J* = 7.0Hz, **Hg**).

#### **Synthesis of 5-((4-pentyl)-phenyl)-dipyrromethane, 5a:**

Pyrrole (85 mL, 1.12 mol) and *p*-pentylbenzaldehyde, **6**, (2.11 g, 11.97 mmol) were added to a 250-mL single-neck round-bottomed flask. The solution was degassed with a stream of argon for 10 min. InCl<sub>3</sub> (0.25 g, 1.13 mmol, 0.1 equivalents) was added, and the mixture was stirred under nitrogen at room temperature for 1.5 h. The mixture turned yellow during the course of the reaction. NaOH (1.4 g, 34 mmol) was added to quench the reaction. Stirring for 45 min afforded a pale yellow mixture. The mixture was filtered using a Büchner funnel. The contents of the flask and the filtered material were washed with a small amount of dichloromethane. The filtrate was concentrated using a rotary evaporator under vacuum; the resulting yellow solid was dissolved in 60 mL of ethanol/water (4:1) and was set aside overnight at room temperature, affording pale yellow crystals. The solid was filtered using a Büchner funnel, washing with water. The resulting yellow solid was dried. 43% of yield was obtained.

<sup>1</sup>H NMR (400 MHz, CDCl<sub>3</sub>, 25°C) δ(ppm) 7.98 (bs, 2H), 7.15 (s, 4H), 6.71 (m, 2H), 6.18 (m, 2H), 5.95 (m, 2H), 5.47 (s, 1H), 2.60 (t, 2H, *J* = 7.8Hz, **Hc**), 1.62 (tt, 2H, *J* = 7.8Hz and *J* = 7.8Hz, **Hd**), 1.35 (m, 4H, **He** and **Hf**), 0.91 (t, 3H, *J* = 7.0Hz, **Hg**).

#### **Synthesis of *p*-pentylbenzaldehyde, 6:**

Equal amounts of pentylbenzene, **7**, (30 g, 1 equivalent) and hexamethylenetetramine, **8**, (28.39g, 1 equivalent) are mixed in 500 ml of trifluoroacetic acid and heated at reflux for 12 h.

Then, products are concentrated by low pressure distillation and added to 500 ml of ice water. After stirring for 15 min, Na<sub>2</sub>CO<sub>3</sub> is added until the mixture's pH becomes basic. Then the products are extracted with ether and washed with water, drying it afterwards. Distillation (130 °C, 1 mmHg) afforded 20 g of pentyl-benzaldehyde (56% of yield). Special care should be taken in the removal of the trifluoroacetic acid due to its corrosivity.

<sup>1</sup>H NMR (400 MHz, CDCl<sub>3</sub>, 25°C) δ(ppm) 9.98 (s, 1H), 7.81 (d, 2H, *J* = 8.2Hz, **Hb**), 7.34 (d, 2H, *J* = 8.2Hz, **Ha**), 2.69 (t, 2H, *J* = 7.6Hz, **Hc**), 1.66 (tt, 2H, *J* = 7.6Hz and *J* = 7.6Hz, **Hd**), 1.35 (m, 4H, **He** and **Hf**), 0.91 (t, 3H, *J* = 7.0Hz, **Hg**); <sup>13</sup>C NMR (400 MHz, CDCl<sub>3</sub>, 25°C) δ(ppm) 191.9 (CO), 150.5(C), 134.4 (C), 129.9 (CH), 129.1 (CH), 36.2 (CH<sub>2</sub>), 31.4 (CH<sub>2</sub>), 30.8 (CH<sub>2</sub>), 22.5 (CH<sub>2</sub>), 14.0 (CH<sub>3</sub>).

#### Synthesis of 5,15-bis(3-methoxyphenyl)-10,20-bis(*p*-pentylphenyl)-porphyrin, 9a:

To an acetonitrile solution (50 ml) of a mixture of the dipyrromethane, **5a**, (0.77 g, 2.63 mmol) and 3-methoxybenzaldehyde (0.31 g, 2.63 mmol) was added an acetonitrile solution (10 ml) of trifluoroacetic acid (76.4 mg, 0.67 mmol), and the mixture was stirred overnight at room temperature under nitrogen. Then, a THF solution (40 ml) of *p*-chloranil (2.19 g, 8.9 mmol) was added, and the mixture was stirred for 5 h under nitrogen. After evaporation of the reaction mixture, the residue was subjected to column chromatography on alumina followed by silica gel with CH<sub>2</sub>Cl<sub>2</sub> as eluent, where the first fraction was collected and subjected to recrystallization from CH<sub>2</sub>Cl<sub>2</sub>/MeOH to leave the product as purple crystals (9.6% of yield).

<sup>1</sup>H NMR (400 MHz, CDCl<sub>3</sub>, 25°C) δ(ppm) 8.89 (s, 8H), 8.13 (d, 4H, *J* = 7.8Hz, **Hb**), 7.82 (m, 4H), 7.66 (t, 2H, *J* = 8Hz), 7.58 (d, 4H, *J* = 7.8Hz, **Ha**), 7.35 (dd, 2H, *J* = 8Hz and *J* = 2.15Hz), 4.00 (s, 6H), 2.97 (t, 4H, *J* = 7.6Hz, **Hc**), 1.95 (tt, 4H, *J* = 7.6Hz and *J* = 7.6Hz, **Hd**), 1.56 (m, 4H, **He** and **Hf**), 1.05 (t, 6H, *J* = 7Hz, **Hg**), -2.76 (s, 2H).

#### Isolation of the fraction containing 5,15-bis(3-allyloxyphenyl)-10,20-bis(phenyl)-porphyrin, 2b:

A solution of 2.14 g (9.62 mmol, 1 equivalent) of 2,2'-(phenylmethylene)bis(1 *H*-pyrrole), **5b**, and 1.56 g (9.62 mmol, 1 equivalent) of 3-allyloxybenzaldehyde, **4**, in 20 ml of propionic acid was refluxed protected from light for 2 h. The propionic acid was removed under reduced pressure. The black residue was dissolved in CH<sub>2</sub>Cl<sub>2</sub>, washed with

bicarbonate until the pH of the solution was basic, and the organic phase was extracted. The product was purified by flash chromatography using silica and eluting with dichloromethane/hexane 6/4. We obtained 0.420 g of **2b** (12% of yield).

$^1\text{H}$  NMR (400 MHz,  $\text{CDCl}_3$ ,  $25^\circ\text{C}$ )  $\delta$ (ppm) 8.91 (d, 4H,  $J = 4.5\text{Hz}$ ), 8.24 (d, 4H,  $J = 4.5\text{Hz}$ ), 8.24 (dd, 4H,  $J = 8.0\text{Hz}$  and  $J = 1.8\text{Hz}$ , **Hh** and **Hj**), 7.80 (m, 10H), 7.66 (td, 2H,  $J = 8.0\text{Hz}$  and  $J = 1.8\text{Hz}$ , **Hk**), 7.37 (dd, 2H,  $J = 8.0\text{Hz}$  and  $J = 1.8\text{Hz}$ , **Hi**), 6.17 (ddt, 2H,  $J = 17.5\text{Hz}$ ,  $J = 9.9\text{Hz}$ ,  $J = 5.3\text{Hz}$ , **Hm**), 5.52 (d, 2H,  $J = 17.5\text{Hz}$ , **Kn**), 5.46 (d, 2H,  $J = 9.9\text{Hz}$ , **Ho**), 4.75 (d, 4H,  $J = 5.3\text{Hz}$ , **Hi**), -2.77 (s, 2H, -NH-). HR-MS (MALDI)  $m/z$  calcd. for  $\text{C}_{50}\text{H}_{38}\text{N}_4\text{O}_2$  ( $M^+$ ) 726.2989, found: 726.2962 (3.7 ppm). Elemental analysis calcd (%) for  $\text{C}_{50}\text{H}_{38}\text{N}_4\text{O}_2$ : C 82.62 H 5.27 N 7.71 O 4.40; found: C 78.85 H 4.93 N 6.99 O 9.22.

#### **Synthesis of Zn-2b (Metallation of the fraction containing 2b):**

A solution of 0.100 g of the fraction containing 5,15-bis(3-allyloxyphenyl)-10,20-bis(phenyl)-porphyrin, **2b** (0.14 mmol, 1 equivalent) and 0.250 g (1.14 mmol, 10 equivalents) of  $\text{Zn}(\text{OAc})_2$  in 100 mL of  $\text{CH}_2\text{Cl}_2/\text{CH}_3\text{OH}$  3:1 in a 250 mL flask was stirred for an hour while was protected of the light exposition. Then, the solvent was evaporated and the solid residue was purified by chromatography with neutral Aluminium oxide (activity I) and  $\text{CH}_2\text{Cl}_2/\text{THF}$  (99:1) as eluent. 105 mg. were obtained (96% of yield).

$^1\text{H}$  NMR (400 MHz,  $\text{CDCl}_3$ ,  $25^\circ\text{C}$ )  $\delta$ (ppm) 9.02 (d, 4H,  $J = 4.5\text{Hz}$ ), 8.97 (d, 4H,  $J = 4.5\text{Hz}$ ), 8.28 (dd, 4H,  $J = 8.0\text{Hz}$  and  $J = 1.8\text{Hz}$ , **Hh** and **Hj**), 7.83 (m, 10H), 7.66 (td, 2H,  $J = 8.0\text{Hz}$  and  $J = 1.8\text{Hz}$ , **Hk**), 7.36 (dd, 2H,  $J = 8.0\text{Hz}$  and  $J = 1.8\text{Hz}$ , **Hi**), 6.19 (ddt, 2H,  $J = 17.2\text{Hz}$ ,  $J = 10.7\text{Hz}$ ,  $J = 5.1\text{Hz}$ , **Hm**), 5.53 (d, 2H,  $J = 17.21\text{Hz}$ , **Kn**), 5.37 (d, 2H,  $J = 10.7\text{Hz}$ , **Ho**), 4.76 (d, 4H,  $J = 5.1\text{Hz}$ , **Hi**).

#### **Synthesis of 2,2'-(phenylmethylene)bis(1 H-pyrrole), 5b:**

To 400 mL of 0.18 M aqueous HCl, in a 1000 mL flask under  $\text{N}_2$ , 16 mL of distilled pyrrole (3 equiv.) were added, followed by the addition of 8 g of benzaldehyde.

The reaction mixture was stirred at room temperature during 4 h. The precipitated semi-solid product was filtered off and washed with water and hexane. The product was recrystallized in ethanol (60% of yield).

$^1\text{H}$  NMR (400 MHz,  $\text{CDCl}_3$ ,  $25^\circ\text{C}$ )  $\delta$ (ppm) 7.99 (bs, 2H), 7.30 (m, 5H), 6.72 (m, 2H), 6.18 (m, 2H), 5.95 (m, 2H), 5.51 (s, 1H).

**General procedure for the synthesis of the “molecular cages” by the olefin metathesis reaction:**

A solution of DABCO 0.33M (38 mg, 1 mL) in  $\text{CH}_2\text{Cl}_2$  was prepared and an aliquot of 100  $\mu\text{L}$  (3.8 mg, 0.03 mmol, 0.5 equivalents.) was added to a solution of the Zn-porphyrin (1 equivalent) in 40 mL of dry  $\text{CH}_2\text{Cl}_2$ . The system was purged with  $\text{N}_2$  for 60 min and the Grubbs catalyst was added (27 mg, 0.027 mmol, 0.4 equivalents in 0.8 mL of dry  $\text{CH}_2\text{Cl}_2$ ). The reaction mixture was stirred at 40°C for 2 h and then more catalyst was added (10 mg, 0.01 mmol, 0.2 equivalents). After one hour at 40°C, the mixture was allowed to cool and then 2 mL of ethyl vinyl ether were added to quench the catalyst. The purification was performed by column chromatography with aluminium oxide ( $\text{CH}_2\text{Cl}_2/\text{THF}$ , 9/1).

## CHAPTER 2

***“Templated synthesis of linear and cyclic bis-porphyrin receptors  
using the Hay coupling process”***

UNIVERSITAT ROVIRA I VIRGILI  
SUPRAMOLECULAR CHEMISTRY OF BIS-PORPHYRINS  
Laura Patricia Hernández Eguía  
ISBN:978-84-694-0308-2/DL:T-204-2011

## 1. Introduction

The introduction of propargyl groups instead of allyl groups in the porphyrin skeleton allows the use of oxidative coupling reaction of triple bonds, or the azide-alkyne Huisgen cycloaddition reaction,<sup>1</sup> recently referred as “click chemistry” by Sharpless,<sup>2</sup> to quickly generate bis-porphyrin macrocycles that can be considered as molecular “cages”.<sup>3</sup>

In recent years, the coupling of terminal alkynes has been considered as an effective procedure for the molecular construction<sup>4,5,6,7,8,9,10,11,12</sup> of butadiene-linked porphyrin oligomers.

The Glaser Coupling is a synthesis of symmetric or cyclic bisacetylenes via coupling of terminal alkynes. It uses a base and copper(I) that is reoxidized by oxygen in the reaction medium. The related Hay coupling has several advantages compared to Glaser Coupling.<sup>13</sup> The copper(I)-TMEDA (*N,N,N',N'*-tetramethylethylenediamine) complex used is soluble in a wide range of organic solvents, so that is more versatile.<sup>14</sup> Compared to Grubbs's metathesis reaction conditions, Hay conditions are less demanding. They are also very mild and many functional groups are tolerated. All these features make alkyne coupling reaction a versatile tool for the construction of covalently linked complex systems.

<sup>1</sup> Huisgen, R. *Proc. Chem. Soc.* **1961**, 357-396.

<sup>2</sup> Kolb, H. C.; Finn, M. G.; Sharpless, K. B. *Angew. Chem., Int. Ed.* **2001**, *40*, 2004-2021.

<sup>3</sup> Tashiro, K.; Aida, T.; Zheng, J. Y.; Kinbara, K.; Saigo, K.; Sakamoto, S.; Yamaguchi, K. *J. Am. Chem. Soc.* **1999**, *121*, 9477-9478.

<sup>4</sup> Anderson, H. L.; Sanders, J. K. M. *J. Chem. Soc., Chem. Commun.* **1989**, 1714-1715.

<sup>5</sup> Anderson, H. L. *Inorg. Chem.* **1994**, *33*, 972-981.

<sup>6</sup> Taylor, P. N.; Huuskonen, J.; Rumbles, G.; Aplin, R. T.; Williams, E.; Anderson, H. L. *Chem. Commun.* **1998**, 909-910.

<sup>7</sup> Li, J. Z.; Ambrose, A.; Yang, S. I.; Diers, J. R.; Seth, J.; Wack, C. R.; Bocian, D. F.; Holten, D.; Lindsey, J. S. *J. Am. Chem. Soc.* **1999**, *121*, 8927-8940.

<sup>8</sup> Wilson, G. S.; Anderson, H. L. *Chem. Commun.* **1999**, 1539-1540.

<sup>9</sup> Rucareanu, S.; Schuwey, A.; Gossauer, A. *J. Am. Chem. Soc.* **2006**, *128*, 3396-3413.

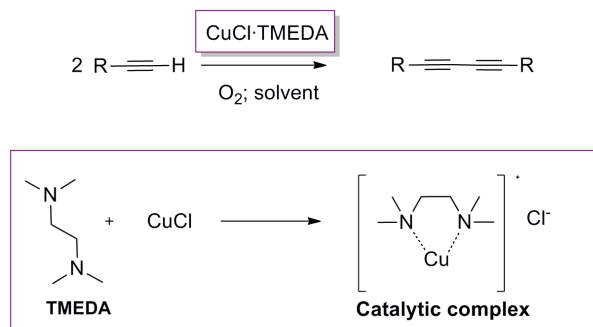
<sup>10</sup> Gottschalk, T.; Jaun, B.; Diederich, F. *Angew. Chem., Int. Ed.* **2007**, *46*, 260-264.

<sup>11</sup> Hoffmann, M.; Wilson, C. J.; Odell, B.; Anderson, H. L. *Angew. Chem., Int. Ed.* **2007**, *46*, 3122-3125.

<sup>12</sup> Zhang, C.; Chen, C. F. *J. Org. Chem.* **2007**, *72*, 9339-9341.

<sup>13</sup> Hay, A. S. *J. Org. Chem.* **1962**, *27*, 3320-3321.

<sup>14</sup> Siemsen, P.; Livingston, R. C.; Diederich, F. *Angew. Chem., Int. Ed.* **2000**, *39*, 2633-2657.



**Scheme 1.** Two terminal acetylenes give rise to diacetylenic unions under the “Hay coupling conditions”. The catalytic complex is composed of Cu (I) with two coordinative bonds to the TMEDA. Thus, it is soluble in most organic solvents.

The oxidative acetylene-acetylene dimerization has often been used in the preparation of open chain linear oligomers<sup>15,16</sup> as well as for ring closing reactions.<sup>17,18,19</sup>

Herein we applied the oxidative conditions of the Hay coupling to a zinc monoporphyrin, **Zn-11**, with two propargyl chain in the *meta* position of the *meso*-phenyl substituent (Scheme 2), to afford a cyclic bis-porphyrin **Zn<sub>2</sub>-12**. In parallel, due to problems experienced in the synthesis and purification of the cyclic dimer **Zn<sub>2</sub>-12** we also tested the Hay coupling zinc monoporphyrin **Zn-13** with only one propargyl chain (Figure 1).

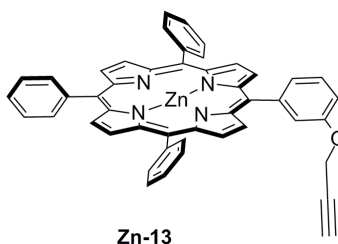


**Figure 1.** Structure of the monopropargylated zinc porphyrin **Zn-13**.

<sup>15</sup> Martin, R. E.; Diederich, F. *Angew. Chem., Int. Ed.* **1999**, *38*, 1350-1377.

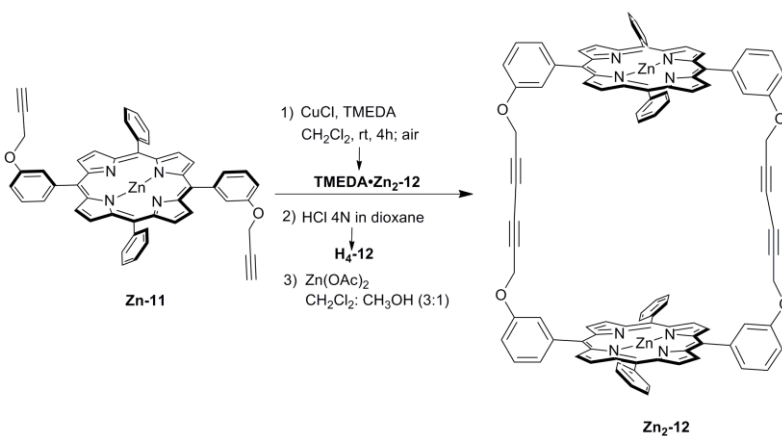
<sup>16</sup> Martin, R. E.; Mader, T.; Diederich, F. *Angew. Chem., Int. Ed.* **1999**, *38*, 817-821.

<sup>17</sup> Tobe, Y.; Nagano, A.; Kawabata, K.; Sonoda, M.; Naemura, K. *Org. Lett.* **2000**, *2*, 3265-3268.

<sup>18</sup> Werz, D. B.; Gleiter, R.; Rominger, F. *J. Org. Chem.* **2004**, *69*, 2945-2952.

<sup>19</sup> Opris, D. M.; Ossenbach, A.; Lentz, D.; Schluter, A. D. *Org. Lett.* **2008**, *10*, 2091-2093.

Fortunately, later on we discovered that the cause of most of the problems experienced in the synthesis of the cyclic dimer **Zn<sub>2</sub>-12** had to do with the purity of the monoporphyrin **Zn-11** used as the starting material. In this chapter we will also explain how we came aware of the presence of a mixture of isomers in the starting material originally used for the synthesis of the cyclic dimer **Zn<sub>2</sub>-12**. The purity problem related to the porphyrin **Zn-11** can also be extrapolated to the monomers used in chapter 1, being the main reason for the difficulties described on the synthesis of the target compounds.



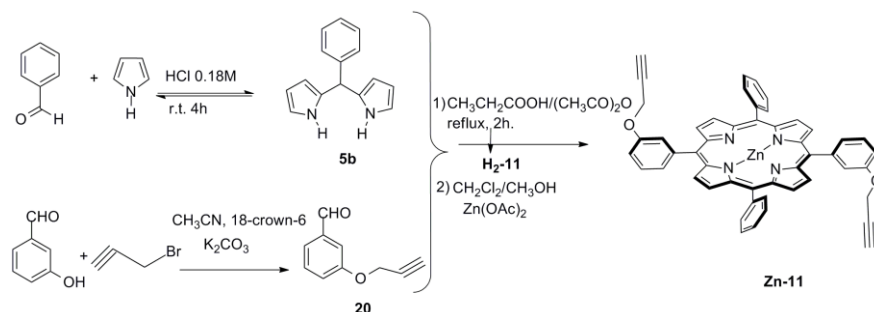
**Scheme 2.** The monomeric diacetylenic zinc porphyrin **Zn-11** dimerizes under the "Hay coupling conditions" to give the cyclic dimer **Zn<sub>2</sub>-12**. After initial removal of the included diamine through demetallation with HCl 4N in dioxane, Zn metals are reintroduced using Zn(OAc)<sub>2</sub>.

## 2. Results and discussion

### 2.3 Synthesis of the bis-porphyrin macrocycle **Zn<sub>2</sub>-12**

For the construction of our cyclic dimer **Zn<sub>2</sub>-12** we designed a zinc monoporphyrin unit, **Zn-11**, bearing four *meso*-aryl substituents: two of them, in *trans*, containing a peripheral functional group (propargyloxy) and two other without substituents. Monoporphyrin **Zn-11** possesses the same skeleton/framework than porphyrin **2b**

described in the previous chapter, differing only in the level of unsaturation of the terminal chains.



Scheme 3. Schematic synthesis of Zn-11.

Trans-substituted *meso*-tetraaryl porphyrins of the ABAB-type, like **H<sub>2</sub>-11**, are readily prepared condensing a 5-arylsubstituted dipyrromethane with an aromatic aldehyde.<sup>20</sup> To ease the synthesis we chose to condense 5-phenyldipyrromethane **5b** (already described in Chapter 1) with 3-propargyloxybenzaldehyde **20** instead of the alternative combination that is reacting benzaldehyde with the dipyrromethane derived from **20**. Next, the fraction isolated as *trans*- **H<sub>2</sub>-11** was metallated with zinc acetate yielding in almost quantitative yield what supposed to be Zn-porphyrin **Zn-11** (Scheme 3). Figure 1 shows the <sup>1</sup>H NMR spectrum of the obtained product as *trans*-**H<sub>2</sub>-11**. (Figure 2).

Next, a methylene chloride solution of the fraction isolated as monoporphyrin **Zn-11** was stirred, open to air, with high molar excess of copper(I) chloride and TMEDA for 4 h to give after usual work-up a dark red solid. The <sup>1</sup>H-NMR analysis of an aliquot of the reaction crude dissolved in  $\text{CHCl}_3-d$  was really complicated and it was very difficult to extract useful information from it (Figure 3a). After initial purification of the reaction crude on a neutral alumina column we proceed to remove the TMEDA that is known to act also as template<sup>21</sup> in the formation of related dimers. In order to obtain the unmetallated free base cyclic dimer **H<sub>4</sub>-12** the above reaction crude was dissolved in dichloromethane and treated with 4N HCl aqueous solution in dioxane until the

<sup>20</sup> Lee, C. H.; Lindsey, J. S. *Tetrahedron* **1994**, *50*, 11427-11440.

<sup>21</sup> Tashiro, K.; Aida, T. *J. Inclusion Phenom. Macrocyclic Chem.* **2001**, *41*, 215-217.

solution became green (indicative of an acid pH). This treatment promoted the demetallation of the porphyrin units of the  $\text{TMEDA}\cdot\text{Zn}_2\text{-12}$  complex and the protonation of the released amine (see Scheme 2).

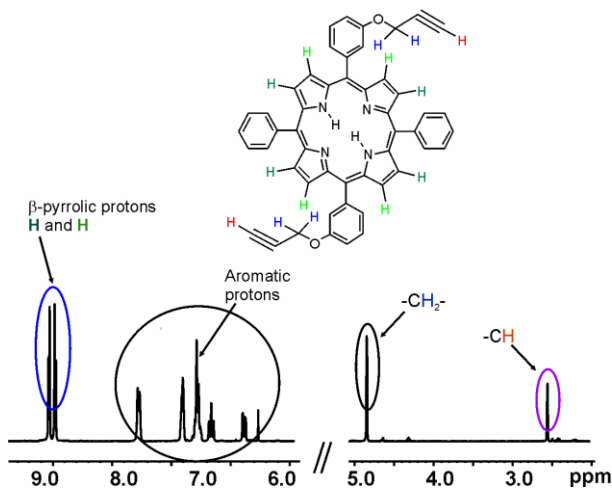


**Figure 2.** <sup>1</sup>H NMR spectrum in CDCl<sub>3</sub> of the fraction isolated as pure *trans*-**H**<sub>2</sub>-**11**. Selected protons are assigned to the corresponding signals.

Subsequently, we washed the organic layer with water in order to eliminate the protonated TMEDA and the metal. The organic layer was basified by washing with a saturated aqueous solution of sodium bicarbonate, dried and evaporated. The metallation of the crude containing the free base macrocycle **H**<sub>4</sub>-**12** was achieved by treatment with Zn(OAc)<sub>2</sub> (20 equiv) in a mixture of dichloromethane and methanol (3:1). The reaction was carried out overnight under nitrogen atmosphere and was protected from light using an aluminium foil. The fraction containing the Zn-metallated porphyrin **Zn**<sub>2</sub>-**12** was isolated in almost quantitative yield after purification on a neutral alumina column chromatography using dichloromethane as the eluent. Figure 3 depicts the <sup>1</sup>H NMR spectra of the porphyrinic fraction obtained after each one of the 4 steps used in the purification process that we described above.

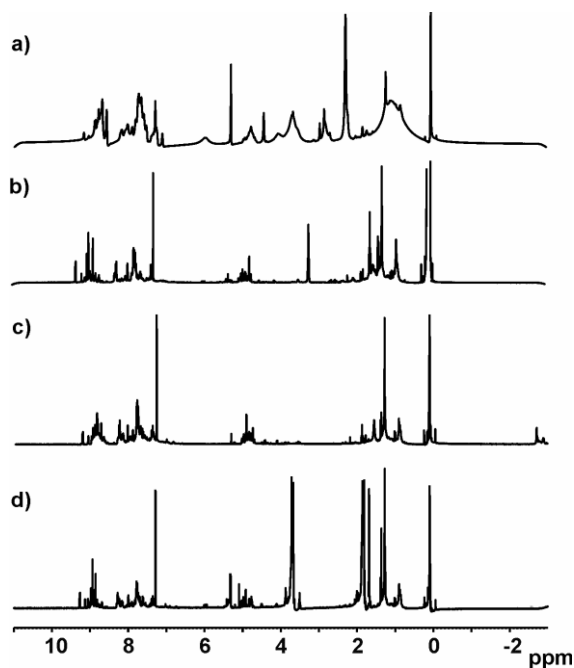


**Figure 3.**  $^1\text{H}$  NMR spectra in  $\text{CDCl}_3$  solution of the porphyrin fraction obtained in each one of the four purification steps of the reaction crude obtained in the Hay coupling reaction of putative **Zn-11**. a) reaction crude; b) after column chromatography on neutral alumina; c) after treatment with 4N HCl.–The NH's- of the free base resonate at  $\delta = -2.7$  ppm; d) after re-metallation with  $\text{Zn}(\text{OAc})_2$ .

The complexity present in the final spectrum (figure 2d) hints to the existence of a mixture of compounds in solution. Thus, we decided to analyze the different fractions obtained in the purification process by GPC (gel permeation chromatography) using toluene as eluent. During the chromatographic analyses the wavelength of the detector was fixed at 420 nm. This is the wavelength for the maximum of the absorbance of the Soret band of the porphyrin ring. The flow was 1 ml/min whereas the concentration of the injected sample was 1 mg/ml. Figure 4 shows two GPC chromatographic traces obtained from the reaction crude of the Hay coupling and the porphyrin fraction after column chromatography on alumina. We concluded that the column purification removed high molecular weight components of the mixture, most likely polymers. Nevertheless, at least two compounds of quite different molecular weight are present in the porphyrin fractions after column purification.

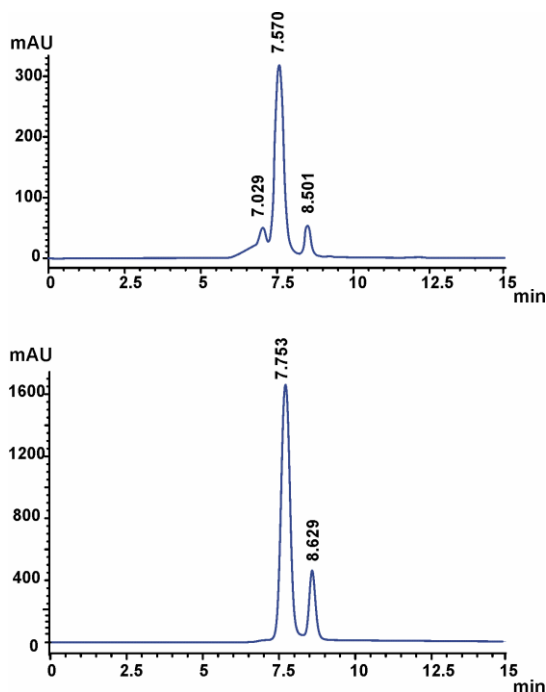


**Figure 4.** GPC chromatographic traces in toluene,  $\lambda=420$  nm. Top: reaction crude of the Hay coupling. Bottom: porphyrin fraction obtained after purification of the crude through an alumina column.

The analysis of the solid used as the starting material, the putative Zn-monoporphyrin **Zn-11**, in the same conditions, is shown in the top chromatographic trace of figure 5. The retention time of the single chromatographic peak obtained was very close to that of the second component of the reaction mixture after alumina purification. Moreover, when the solid used as starting material, putative **Zn-11**, was used to spike a sample of the reaction crude we observed a significant increment of the peak area of the second component of the mixture without detecting splitting of any of the chromatographic peaks (figure 5, bottom). We hypothesized that the second component of the reaction mixture must be unreacted starting material.

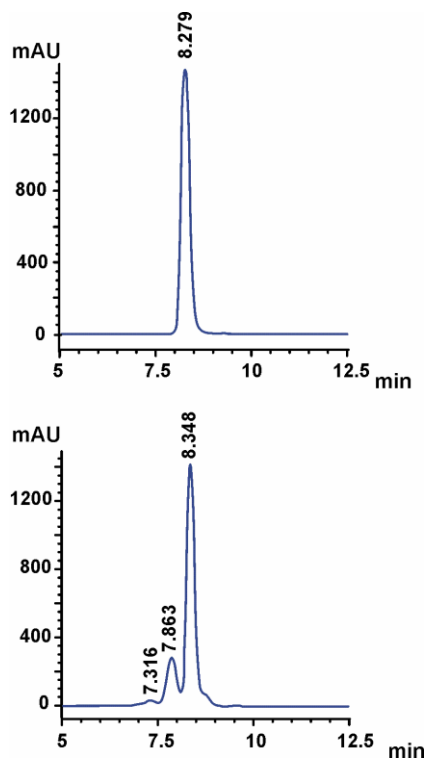


**Figure 5.** GPC chromatograms using toluene as eluent,  $\lambda=420$  nm. Top: starting material used for the Hay Coupling reaction, putative pure **Zn-11**. Bottom: reaction crude obtained from the Hay coupling spiked with the starting material.

For this reason, we tried to avoid the presence of unreacted starting material by changing reaction conditions and pushing the reaction to go to completion. However, all our attempts based on increasing the reaction time, the catalyst amount or both prove to be unsuccessful. A chromatographic peak with the same retention time than the putative **Zn-11** monoporphyrin used as starting material was always present in the analysis of the reaction crudes of the Hay coupling.

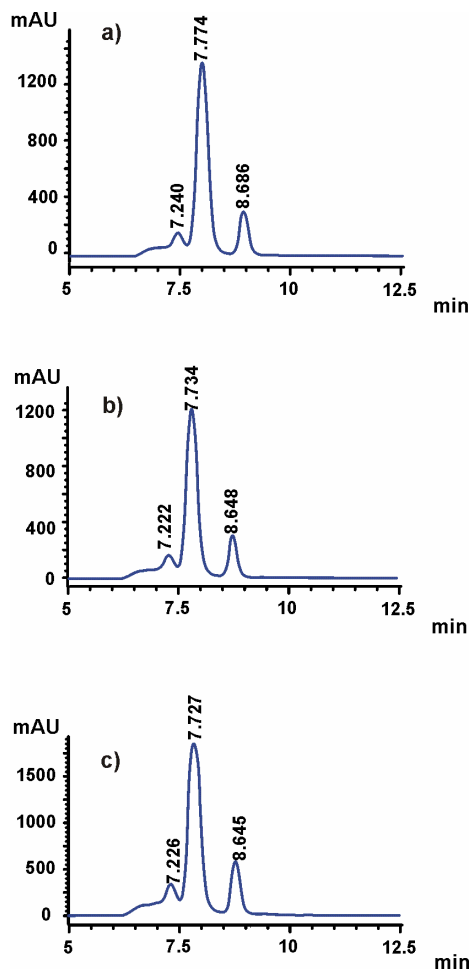


**Figure 6.** Chromatograms of the GPC analysis of the crudes obtained from the Hay Coupling reaction,  $\lambda=420$  nm. Toluene as eluent. a) after 7 hours; b) after 10 hours; c) 24 hours with 50-fold increase in CuCl.

The separation of the two chromatographic peaks observed in the reaction crude of the Hay coupling after purification through alumina column followed by demetallation was achieved by semi-preparative GPC. Both isolated fractions were metallated again with  $\text{Zn}(\text{OAc})_2$  and analyzed by GPC. The GPC analyses revealed a single chromatographic peak for each fraction. Their retention times were almost coincident with those of the two peaks eluting at higher retention time in the chromatogram of the reaction crude (Figure 7).

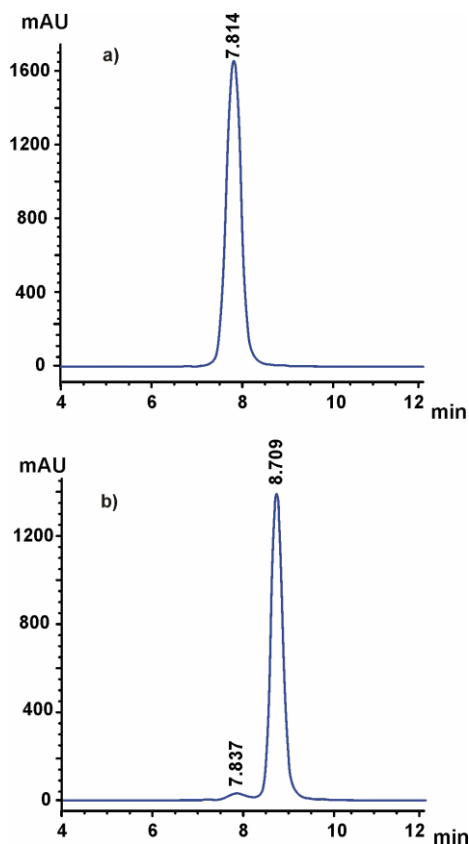


**Figure 7.** GPC chromatograms using toluene as eluent of the fractions isolated from the semi-prep GPC purification,  $\lambda=420$  nm. a) first fraction corresponding to the chromatographic peak with  $t_r$  of 7.81 min; b) second fraction,  $t_r$  8.71 min.

The two fractions corresponding to the two chromatographic peaks were also analyzed using  $^1\text{H}$  NMR spectroscopy. The first peak isolated from the preparative GPC should correspond to the highest molecular weight components of the reaction crude not considering the oligomers that are retained in the alumina column. Our expectations were that this fraction should have contained the cyclic bis-porphyrin **Zn<sub>2</sub>-12** as the major component. However, as shown in Figure 8 the downfield region of the  $^1\text{H}$  NMR spectrum of this fraction is quite complicated suggesting a complex mixture of compounds.

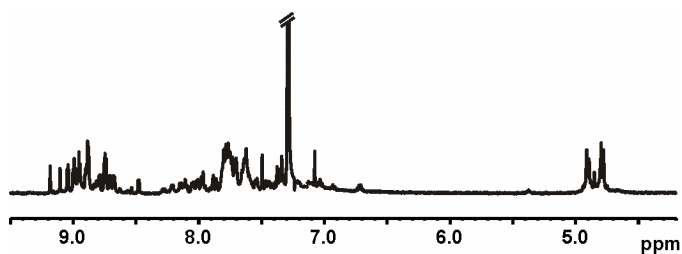


**Figure 8.** Downfield region of the  $^1\text{H}$  NMR spectrum in  $\text{CDCl}_3$  solution acquired for the first fraction separated by semi-preparative GPC (7.81 min).

When we acquired the  $^1\text{H}$  NMR spectrum of the second peak we realized that it corresponded to a pure product but it did not coincide with that of the solid used as starting material, putatively the *trans*-monoporphyrin **Zn-11** (Figure 9).

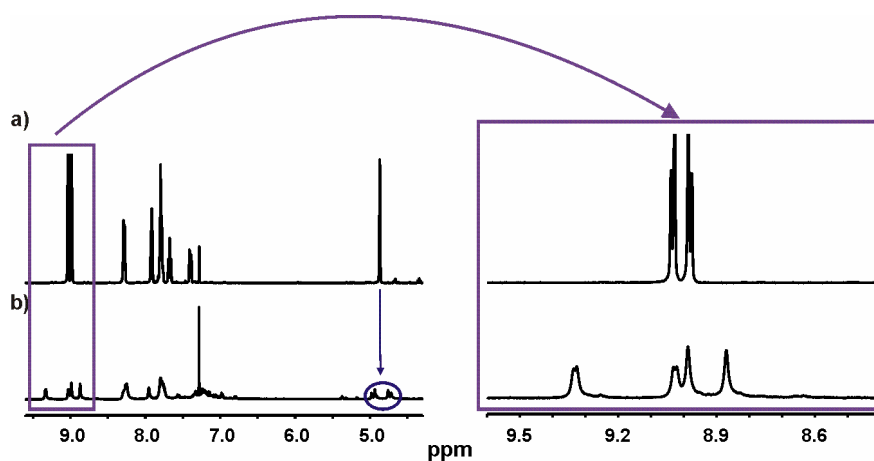


**Figure 9.** Selected region of the  $^1\text{H}$  NMR in  $\text{CDCl}_3$  of (a) the solid used as starting material, **Zn-11**, and (b) the second peak separated by semi-preparative GPC (rt 8.71 min).

We obtained a MALDI/MS exact mass spectrum of this compound showing a molecular ion with a  $m/z$  value of 782.1702 au. This  $m/z$  value represents a difference of two less units of mass with respect to **Zn-11**. Combining all the spectroscopic data (MS, 1D and 2D

NMR) we tentatively assigned the structure shown in figure 10 to the compound present in the second isolated peak.

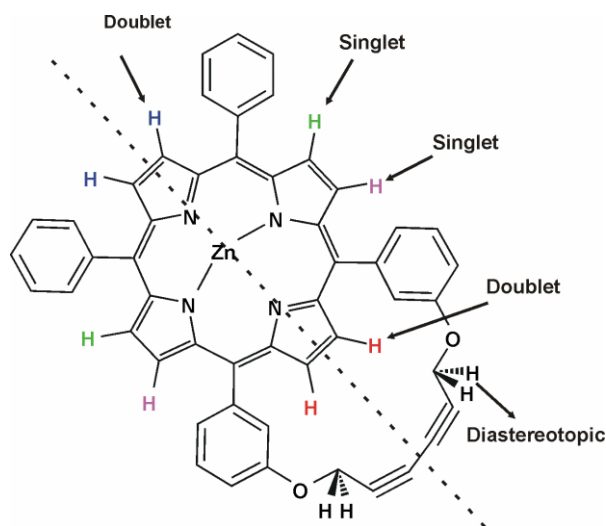


**Figure 10.** Structure assigned to the isolated product with *rt* 8.71 min, **Zn-12b**. Four types of  $\beta$ -pyrrolic protons and the methylene diastereotopic protons are marked.

The assigned structure, **Zn-12b**, was later confirmed through X-ray diffraction analysis of a single crystal grown from chloroform solution in the NMR tube (Figure 11).

Taken together, these results indicated that compound **Zn-12b** must be produced from an intramolecular Hay coupling reaction that takes place with the *cis*-**Zn-11** isomer. They also suggested that the solid used as starting material was composed by an undetermined mixture of the two isomer *cis* and *trans* of **H<sub>2</sub>-11** (Figure 12).

Repetitive purifications using flash column chromatography of the monoporphyrin **H<sub>2</sub>-11** as mixture of isomers gave consistently the same  $^1\text{H}$  NMR spectrum. This result is consistent with the impossibility of isomer separation using this technique. HPLC analysis of the mixture using normal phase (dichloromethane: hexane) gave an identical result. On the contrary, HPLC-MS analysis using reverse phase allowed the detection and separation of the two isomers that were present in a 1:1 ratio in the reaction mixture.

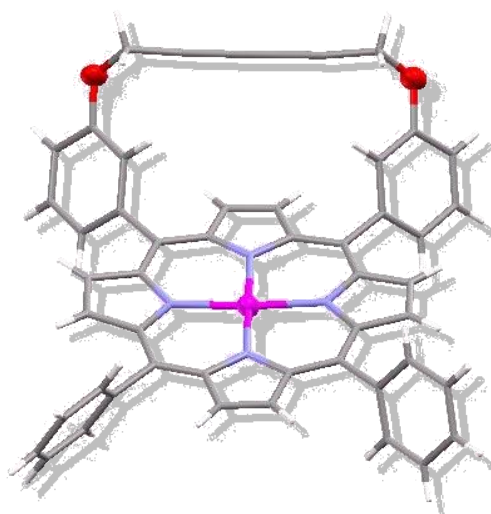


Figure 11. Solid state structure of Zn-12b.

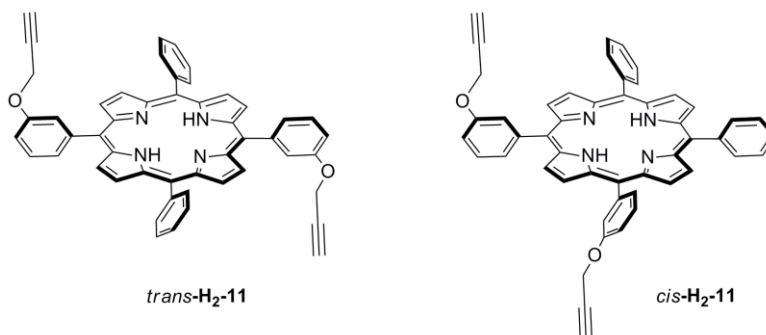
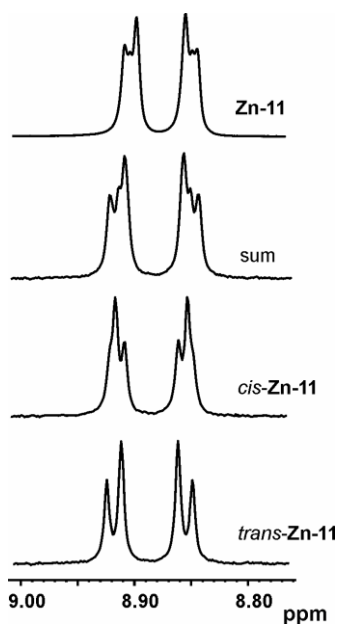


Figure 12. Line structures of the two isomeric porphyrins that must be present in the solid used as starting material: *trans*-H<sub>2</sub>-11 and *cis*-H<sub>2</sub>-11.

In order to understand why we had not realized that the solid used as starting material in the Hay Coupling reactions was a mixture of the two isomers of Zn-11 we acquired the <sup>1</sup>H NMR spectra of both of them separately. Different proton signals are observed for the β-pyrrolic protons (8.80-9.00 ppm) in each isomer. The *trans* isomer shows the typical coupling pattern for a first order AB system with the expected roof effect. For the *cis* isomer the signals of the β-pyrrolic protons arise from a superimposition of a regular AB system with two additional signals resulting from A<sub>2</sub> and B<sub>2</sub> spin systems. The <sup>1</sup>H NMR

spectra of the isolated isomers are very different. From them it is reasonably easy to assign their structures based on geometry considerations to explain the multiplicity and shape of the proton signals. However, when both isomers are mixed in solution the resulting  $^1\text{H}$  NMR spectra is misleading. One is tempted to simply assign the complexity of the observed spectrum as the result of a second order spin system of the type AA'BB' instead of the existence of an isomer mixture. A theoretical  $^1\text{H}$ -NMR spectrum of the  $\beta$ -pyrrolic region for a 1:1 mixture of the two isomers was obtained using the software TOPSPIN (Figure 13). There is a perfect agreement between the protons signals observed for the  $\beta$ -pyrrolic protons of the solid used as starting material and the ones obtaining by adding the spectra of the separated isomers. This result constitutes the final evidence of our misassignment of the composition of the solid used as starting material in the Hay Coupling reactions as being the single *trans*-Zn-11 isomer.

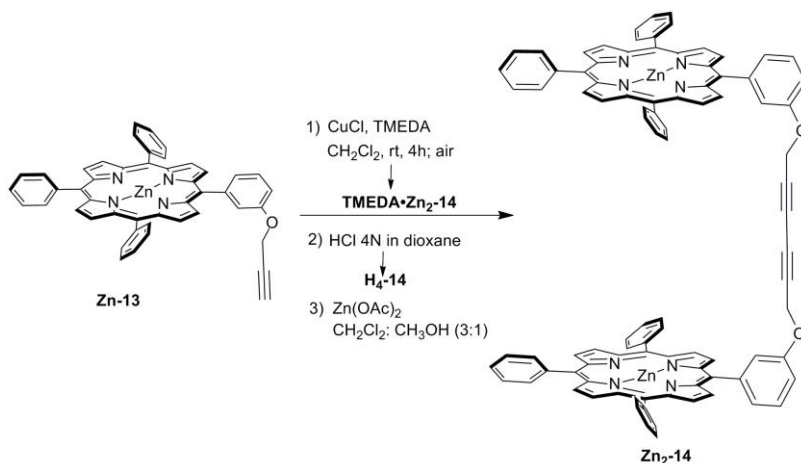


**Figure 13.**  $\beta$ -pyrrolic region of the  $^1\text{H}$  NMR spectra of the isomers, *trans*-Zn-11 and *cis*-Zn-11, together with the spectra obtained by adding both of them and that of the solid used as the starting material in the Hay Coupling reactions.

## 2.4 Synthesis of bis-porphyrin tweezers receptors using the Hay coupling reaction

It is well established that the Hay Coupling reaction proceeds quantitatively when applied in the synthesis of related linear and cyclic butadiyne-linked porphyrin oligomers.<sup>22</sup>

Before becoming aware of the presence of two isomers in the starting material used in the synthesis of **Zn<sub>2</sub>-12** discussed in the previous paragraph we were intrigued by the detection in all reaction crudes of a compound that we thought was starting material. In order to find out if there was something special in the structure of the monoporphyrin used as starting material that prevented the reaction to go to completion, we decided to test the Hay coupling conditions with a zinc porphyrin analog, **Zn-13**, featuring only one propargyl chain in the *meta* position of the *meso*-phenyl substituent. Porphyrin **H<sub>2</sub>-13** was obtained as a secondary product in the synthesis of disubstituted porphyrin **H<sub>2</sub>-11**. Oxidative coupling using the Hay conditions of **Zn-13** afforded the linear butadiyne linker dimer in 70 % yield (Scheme 4).



**Scheme 4.** The monopropargylated zinc porphyrin **Zn-13** dimerizes under the “Hay coupling conditions” to give the bis-porphyrin tweezer **Zn<sub>2</sub>-14** coordinated to TMEDA. Removal of the diamine by treatment with HCl 4N in dioxane and subsequent metallation with Zn(OAc)<sub>2</sub> affords the tweezers receptor **Zn<sub>2</sub>-14**.

<sup>22</sup> Anderson, S.; Anderson, H. L.; Sanders, J. K. M. *Acc. Chem. Res.* **1993**, *26*, 469-475.

The reaction crude,  $\text{TMEDA}\cdot\text{Zn}_2\text{-14}$ , was analyzed using GPC chromatography after purification through alumina column. The analysis showed a major peak in the chromatogram suggesting that the reaction has taken place almost quantitatively. The  $^1\text{H}$  NMR of the crude showed the protons signals expected for the tweezers  $\text{Zn}_2\text{-14}$  and indicated the partial complexation with TMEDA (Figure 14 and 15a). Free  $\text{Zn}_2\text{-14}$  was obtained using the demetallation-metallation procedure already described above.

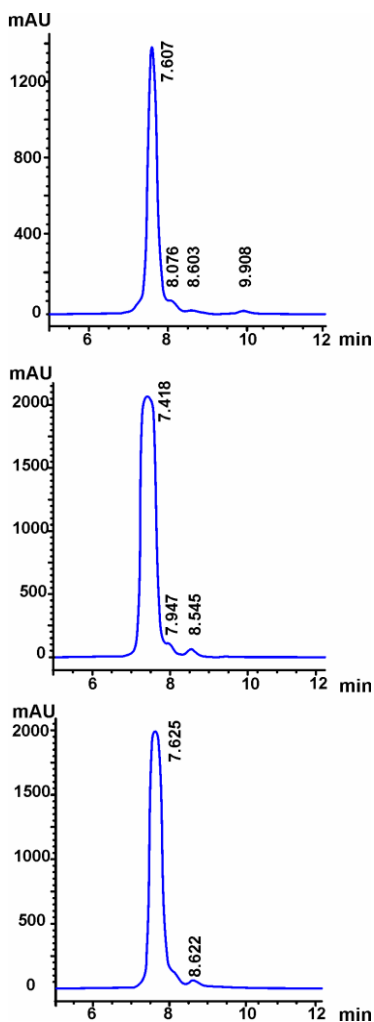


**Figure 14.** GPC chromatograms using toluene as eluent,  $\lambda=420$  nm. Top: reaction crude after alumina purification. Middle: crude after demetallation. Bottom: after metallation.

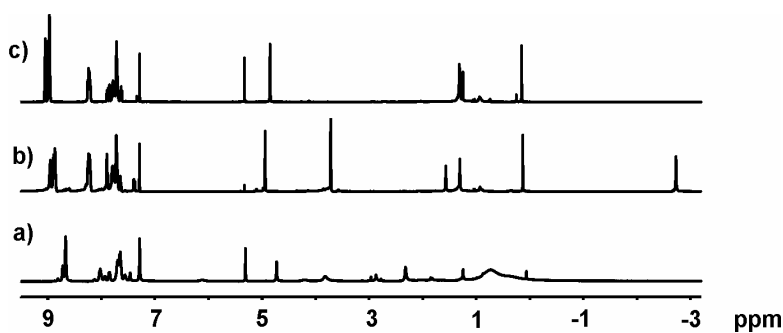


**Figure 15.** <sup>1</sup>H NMR spectra in CDCl<sub>3</sub> solution of a) reaction crude after purification through a neutral alumina; b) crude of the demetallation process (the signal of the -NH's- appears at -2.7 ppm); c) after crude obtained after metallation with Zn(OAc)<sub>2</sub>.

In order to obtain an analytically pure sample of tweezers **Zn<sub>2</sub>-14** the crude obtained after metalation with Zn(OAc)<sub>2</sub> was purified using semi-preparative GPC.

The obtained linear bis-porphyrin **Zn<sub>2</sub>-14** was characterized using <sup>1</sup>H NMR and mass spectrometry. The assignment of the proton signals is shown in figure 16.

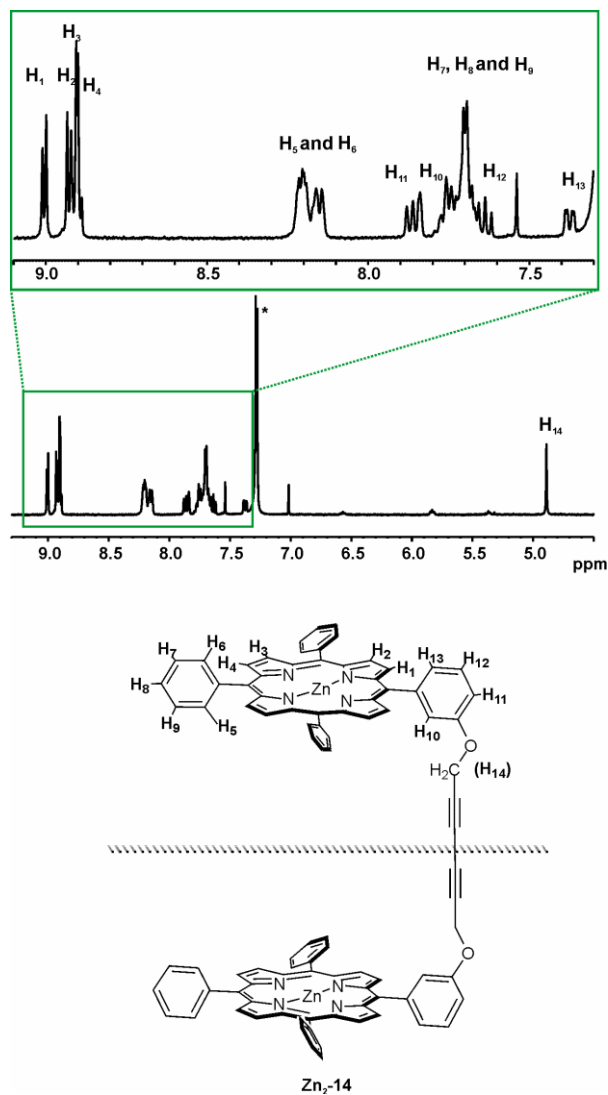
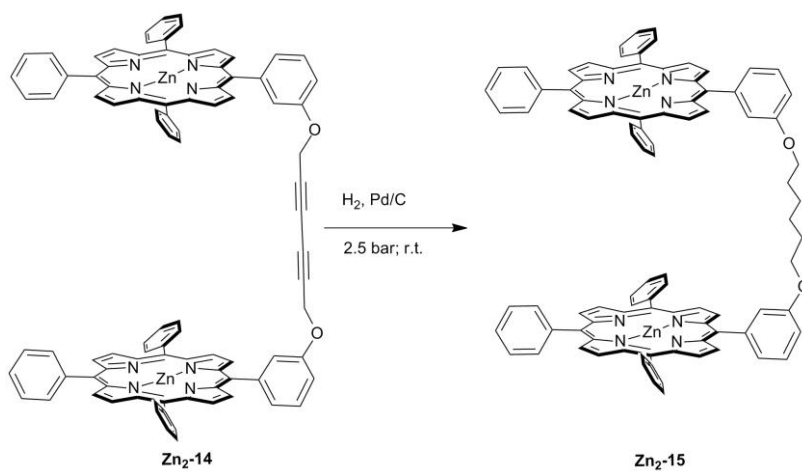


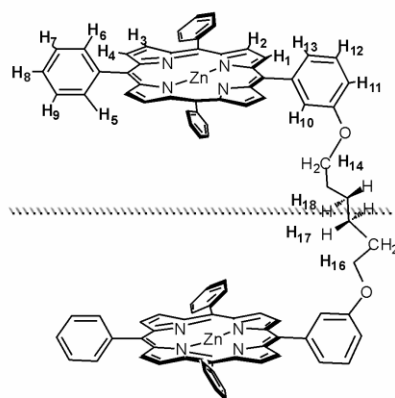
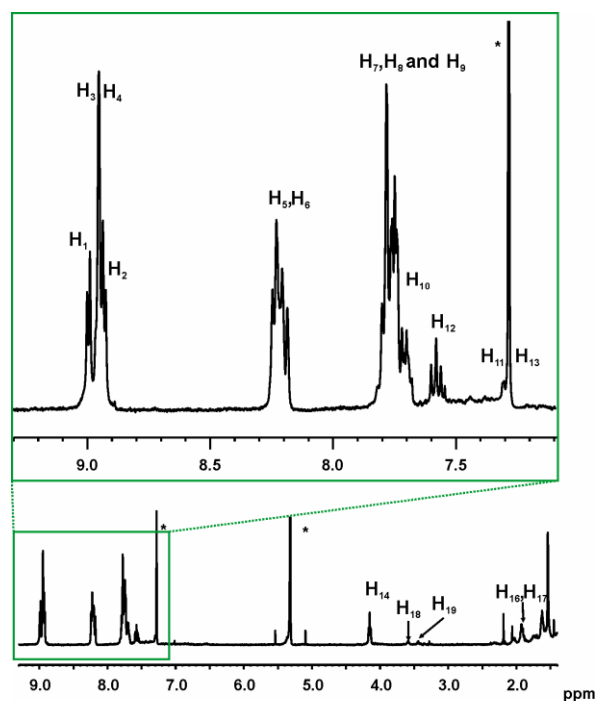
**Figure 16.**  $^1\text{H}$  NMR spectrum of the bis-porphyrin tweezer **Zn<sub>2</sub>-14** and its line structure indicating the proton assignment. The asterisk represents the solvent signal ( $\text{CDCl}_3$ ).

We were also interested in preparing a more flexible version of **Zn<sub>2</sub>-14**. Catalytic hydrogenation of the triple bonds in **Zn<sub>2</sub>-14** using Pd/C 10% yielded almost quantitatively tweezers **Zn<sub>2</sub>-15** having a fully saturated alkyl chain of six methylene units spanning the two porphyrin rings (see Scheme 5).



**Scheme 5.** Synthesis of **Zn<sub>2</sub>-15**.

The fully saturated linear bis-porphyrin **Zn<sub>2</sub>-15** was characterized using high resolution <sup>1</sup>H NMR spectroscopy and mass spectrometry. Figure 17 depicts the proton assignment.



Zn<sub>2</sub>-15

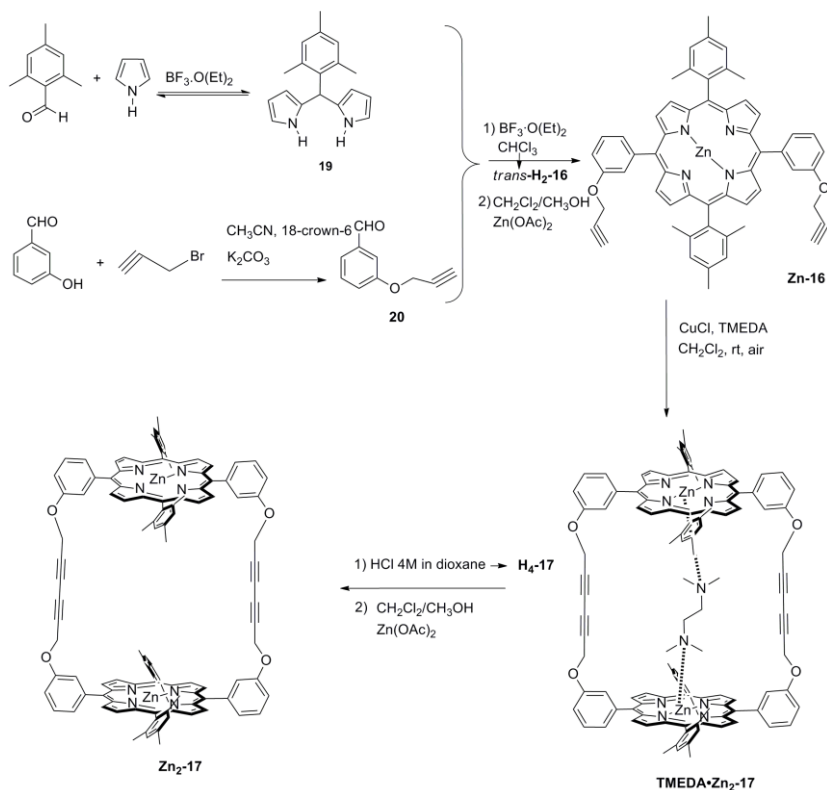
**Figure 17.** <sup>1</sup>H NMR spectrum of bis-porphyrin tweezer **Zn<sub>2</sub>-15**. There have been assigned the signals for the structure. The structure has symmetry, as it is possible to see in the drawing. The asterisk represents the solvent signals (CDCl<sub>3</sub> and CH<sub>2</sub>Cl<sub>2</sub>).

## 2.5 Synthesis of bis-porphyrin macrocycles using the Hay coupling reaction

For the construction of our cyclic dimers **Zn<sub>2</sub>-17** and **Zn<sub>2</sub>-18** we designed a monoporphyrin unit, *trans*-**Zn-16**, bearing four *meso*-aryl substituents: two of them containing a peripheral functional group (propargyloxy) and two other with facially encumbering groups (methyl).

*Trans*-substituted *meso*-tetraaryl porphyrins of the ABAB-type, like *trans*-**H<sub>2</sub>-16**, are readily prepared condensing a 5-arylsubstituted dipyrromethane with an aromatic aldehyde.<sup>20</sup> However, as shown in the first section of this chapter, 5-arylsubstituted dipyrromethane has a tendency to revert to their starting material under reaction condition producing the scrambling of the mixture and the formation of the *trans* and *cis* isomers in similar extends with the consequent problem of separation which in some cases can be very tedious. To reduce scrambling and increase the possibility of isomer separation using flash chromatography, we chose to condense 5-mesityldipyrromethane **19** with 3-propargyloxibenzaldehyde **20**. The use of sterically hindered 5-dipyrromethanes tends to reduce the scrambling in MacDonald-type 2+2 condensations due to destabilization of the intermediate carbocation formed from the dipyrromethane dissociation and thus minimize the formation of the unwanted *cis*-A<sub>2</sub>B<sub>2</sub>-type porphyrin.<sup>23</sup> Using the condensation conditions described by Lindsey et al.<sup>20</sup> for the reaction of **19** with **20** allowed the isolation of the *trans*-monoporphyrin **H<sub>2</sub>-16** in an overall yield of 26%. Next, the porphyrin site of *trans*-**H<sub>2</sub>-16** was metallated with zinc acetate yielding *trans*-**Zn-16** in almost quantitative yield. The *trans*-**Zn-16** monoporphyrin was stirred in a dichloromethane solution, under air, with the addition of a high molar excess of copper(I) chloride and *N,N,N',N'*-tertamethylenediamine (TMEDA) for 4 h giving a dark red solid after the usual work-up. An aliquot of the reaction crude was dissolved in CHCl<sub>3</sub>-*d* to make a <sup>1</sup>H-NMR analysis which indicated the presence of the expected proton signals for the diacetylenic dimer **Zn<sub>2</sub>-17** (Scheme 6).

<sup>23</sup> Littler, B. J.; Ciringh, Y.; Lindsey, J. S. *J. Org. Chem.* **1999**, *64*, 2864-2872.



**Scheme 6.** Synthesis of monoporphyrin **Zn-16** and bis-porphyrin **Zn<sub>2</sub>-17**.

Not unexpectedly, we also observed protons signals corresponding to ditopic coordinated  $\text{TMEDA}$  molecules included in the cavity of **Zn<sub>2</sub>-17** (Figure 18). The X-ray analysis of a crystal grown from the above  $\text{CHCl}_3$ -*d* solution confirmed the existence of the inclusion complex  $\text{TMEDA} \cdot \text{Zn}_2\text{-17}$  in the solid state (Figure 18).

In order to obtain uncomplexed **Zn<sub>2</sub>-17** the above reaction crude was dissolved in dichloromethane and treated with 4N  $\text{HCl}$  aqueous solution to promote the demetallation of the porphyrin units of  $\text{TMEDA} \cdot \text{Zn}_2\text{-17}$ . The crude thus obtained was purified by GPC affording the diacetylenic bis-porphyrin free base **H<sub>4</sub>-17** (Figure 19).

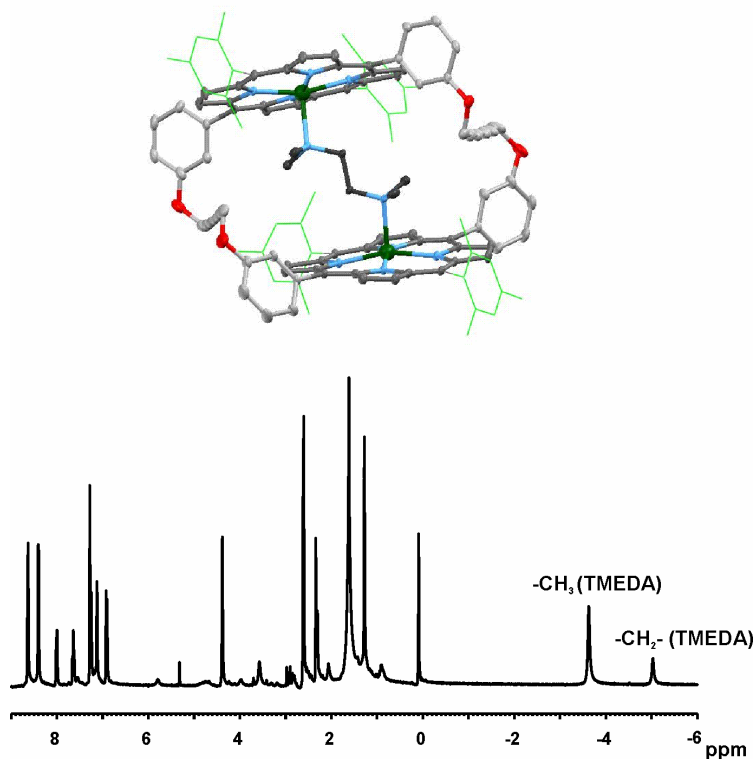


**Figure 18.** Bottom: <sup>1</sup>H NMR spectrum of the reaction crude obtained in the oxidative coupling of **Zn-16** under “Hay coupling conditions”. The two broad upfield signals correspond to the TMEDA bound protons. Top: X-ray structure of the TMEDA•Zn<sub>2</sub>-17 complex.

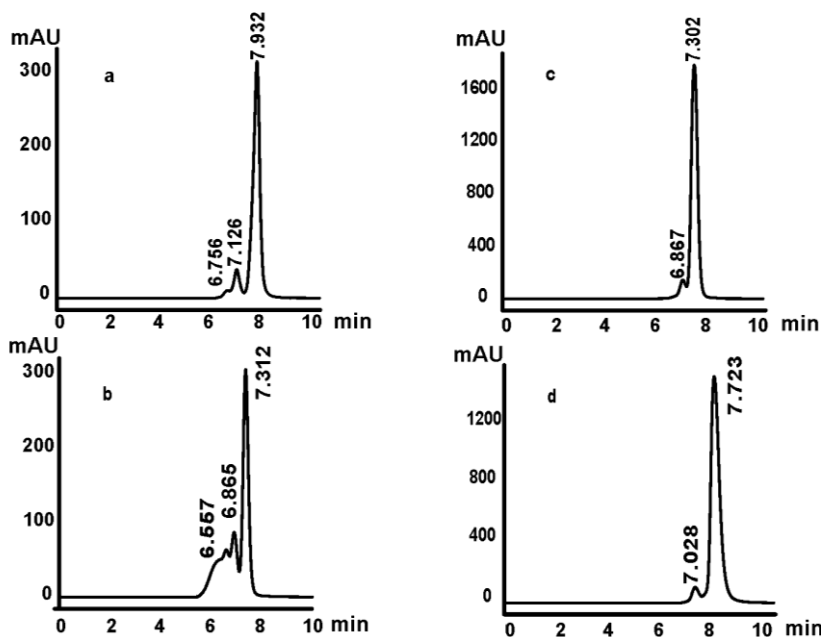
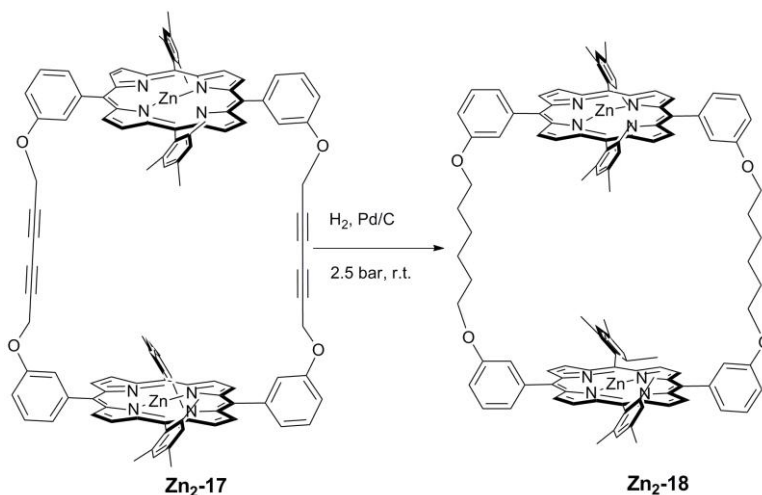


**Figure 19.** GPC chromatograms of a) the reaction crude; b) and c) two fractions obtained after purification with semi preparative GPC ; d) chromatogram of **Zn<sub>2</sub>-17**.

The purified free base was treated with zinc acetate followed by flash chromatography purification on neutral aluminium oxide to produce uncomplexed **Zn<sub>2</sub>-17** in an overall yield of 58% (Scheme 6).

The catalytic hydrogenation of **Zn<sub>2</sub>-17** was carried out using Pd/C 10% and 2.5 bar of hydrogen pressure. Cyclic dimer **Zn<sub>2</sub>-18**, with completely reduced linker chains, was isolated in 55 % after chromatography of the hydrogenated crude (Scheme 7).



**Scheme 7.** Line structures of the cyclic dimer, **Zn<sub>2</sub>-18**, obtained from the hydrogenation of the linker chains in bis-porphyrin **Zn<sub>2</sub>-17**.

The <sup>1</sup>H NMR spectra of cyclic bis-porphyrins, **Zn<sub>2</sub>-17** and **Zn<sub>2</sub>-18**, indicate that these compounds exist in solution as a mixture of two conformers that shows slow chemical exchange in the <sup>1</sup>H NMR timescale. Based on the chemical shift values and NOESY experiments, we assigned an expanded conformation to the major isomer and one a collapsed geometry for the minor one. They are in an 80:20 ratio for **Zn<sub>2</sub>-17** and in 75:25 ratio for **Zn<sub>2</sub>-18**. This behavior is a clear indication of the high conformation flexibility of the cyclic bis-porphyrin structures (Figures 20-27).

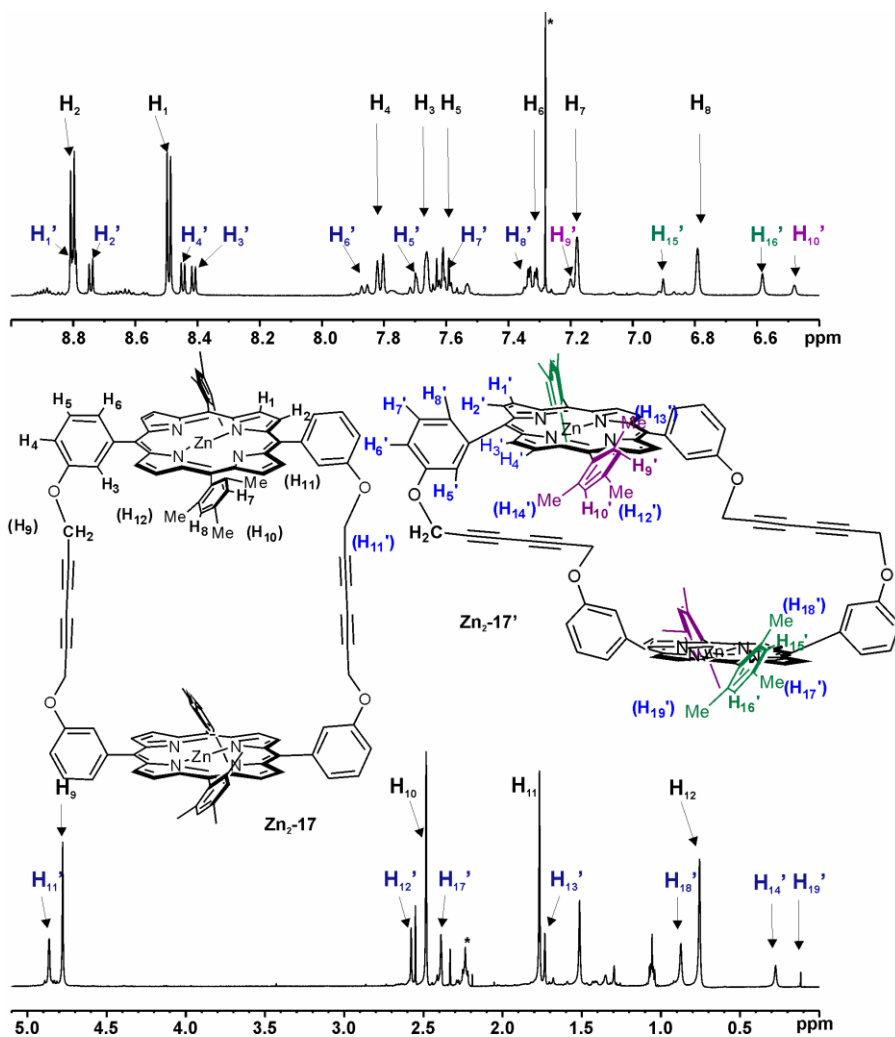


**Figure 20.**  $^1H$  NMR spectrum of diacetylenic bis-porphyrin macrocycle,  $Zn_2-17$ . The proton signals assigned to the two conformers,  $Zn_2-17$ , the expanded one, and  $Zn_2-17'$ , the collapsed one, which are in a relative mixture of approximately 80:20 are indicated.

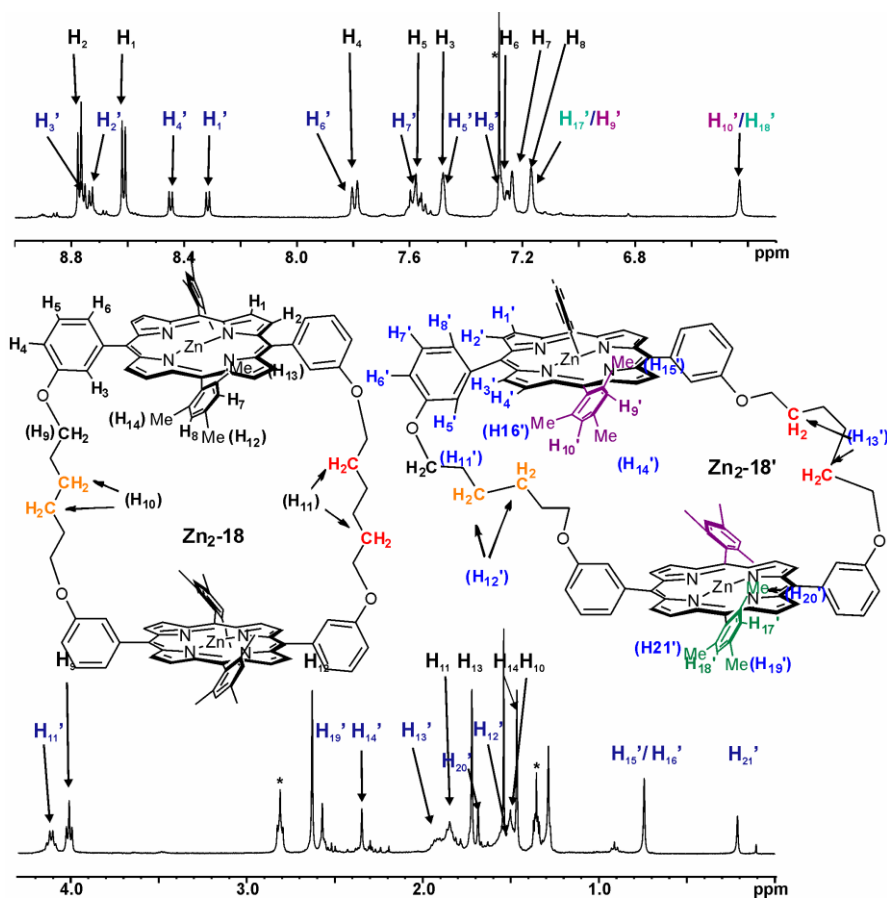


**Figure 21.**  $^1\text{H}$  NMR spectrum of bis-porphyrin cyclic dimer, **Zn<sub>2</sub>-18**. The proton signals of the two conformers, **Zn<sub>2</sub>-18**, the expanded one, and **Zn<sub>2</sub>-18'**, the collapsed one, which are in a relative mixture of approximately 75:25 are indicated.

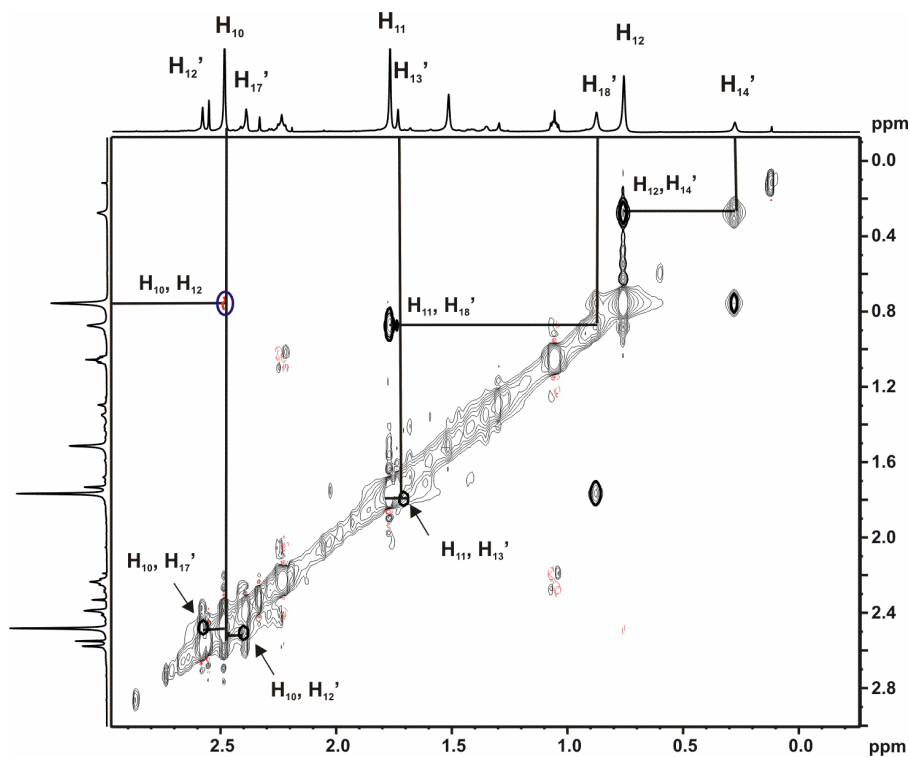


**Figure 22.** Upfield region of the <sup>1</sup>H, <sup>1</sup>H-2D ROESY (400 MHz, CDCl<sub>3</sub>, 25° C) spectrum of Zn<sub>2</sub>-17. Some cross peaks of interest have been marked (black colour), and also a coupling peak has been circled (blue colour).

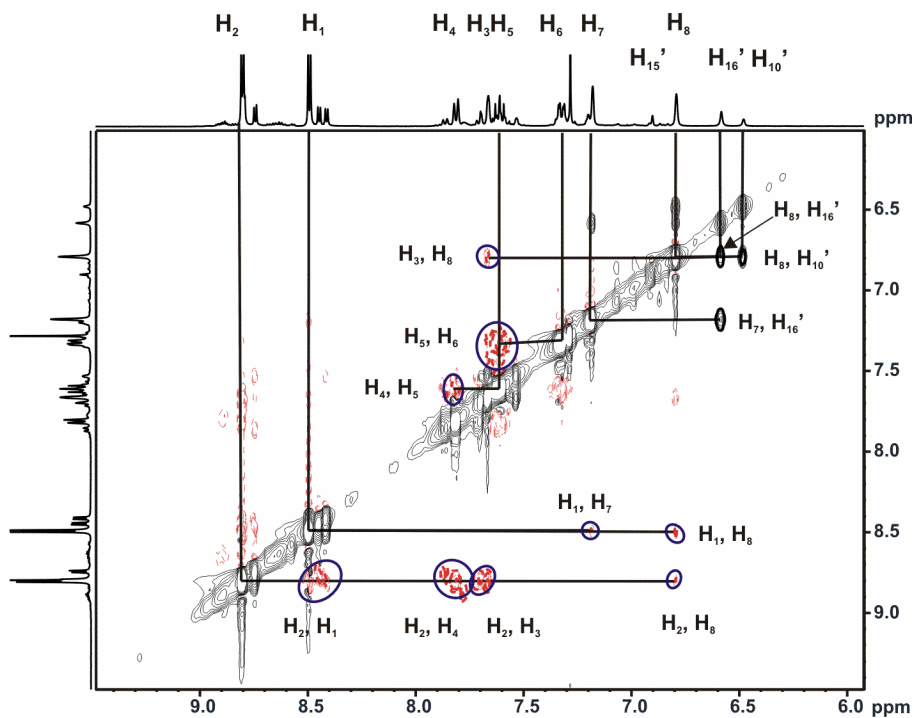


**Figure 23.** Downfield region of the  $^1\text{H}$ ,  $^1\text{H}$ -2D ROESY (400 MHz,  $\text{CDCl}_3$ ,  $25^\circ\text{C}$ ) spectrum of  $\text{Zn}_2\text{-17}$ . Some cross peaks of interest have been marked (black colour), and also coupling peaks have been circled (blue colour).

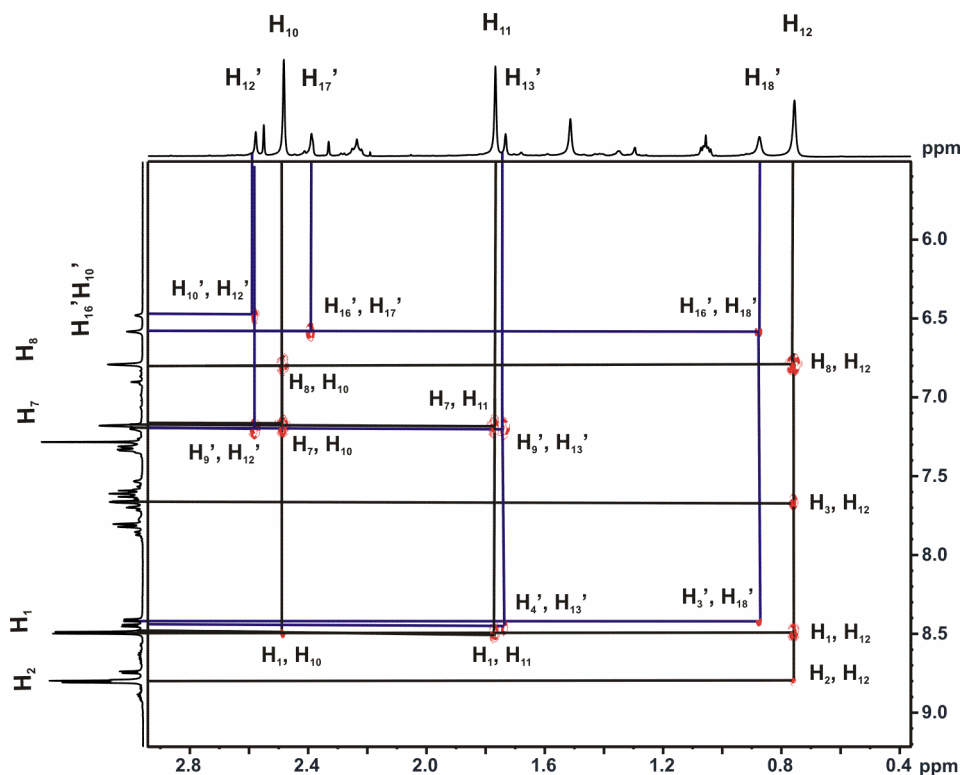


**Figure 24.**  $^1\text{H}$ ,  $^1\text{H}$ -2D ROESY (400 MHz,  $\text{CDCl}_3$ ,  $25^\circ\text{C}$ ) spectrum of **Zn<sub>2</sub>-17**. As here is represented the upfield region in one column and the downfield region in other column there are only marked the coupling peaks. The blue lines are referring to the **Zn<sub>2</sub>-17'** conformer.

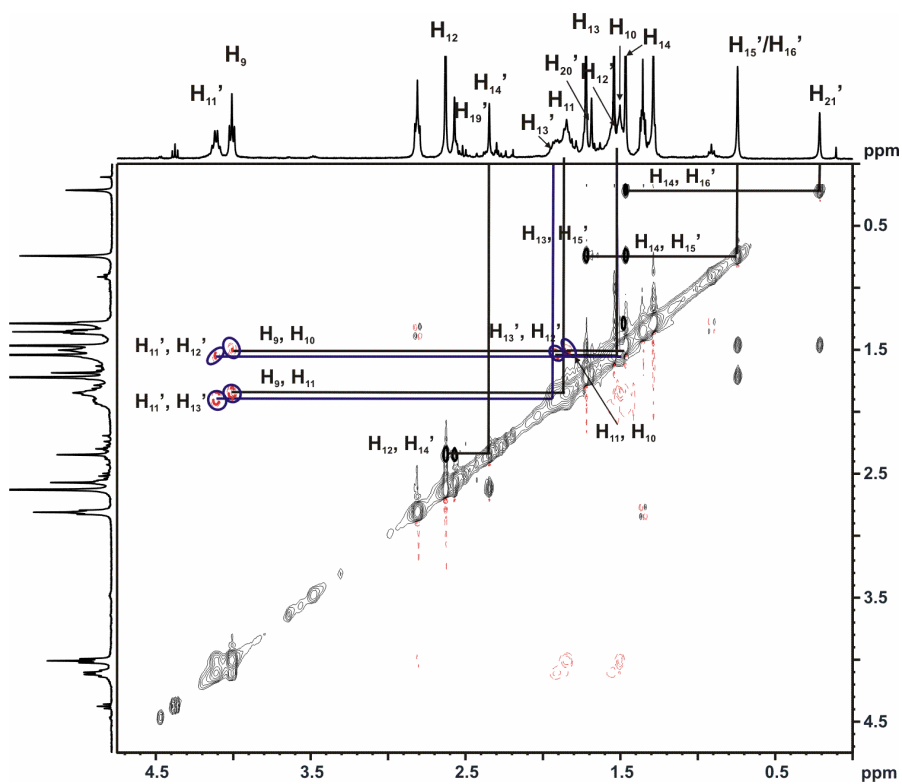


**Figure 25.** Upfield region of the  $^1\text{H}$ ,  $^1\text{H}$ -2D ROESY (400 MHz,  $\text{CDCl}_3$ ,  $25^\circ\text{C}$ ) spectrum of **Zn<sub>2</sub>-18**. Some cross peaks of interest have been marked (black colour), and also coupling peaks have been circled (blue colour). The blue lines are referring to the **Zn<sub>2</sub>-18'** conformer.

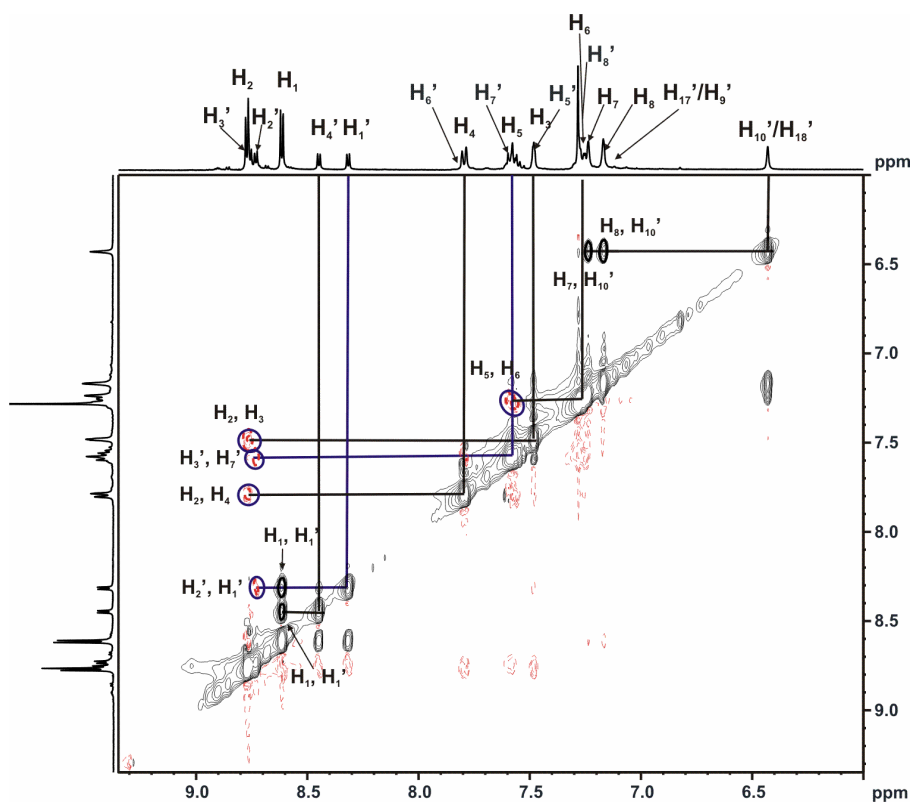


**Figure 26.** Downfield region of the  $^1\text{H}$ ,  $^1\text{H}$ -2D ROESY (400 MHz,  $\text{CDCl}_3$ ,  $25^\circ\text{C}$ ) spectrum of **Zn<sub>2</sub>-18**. Some cross peaks of interest have been marked (black colour), and also coupling peaks have been circled (blue colour). The blue lines are referring to the **Zn<sub>2</sub>-18'** conformer.

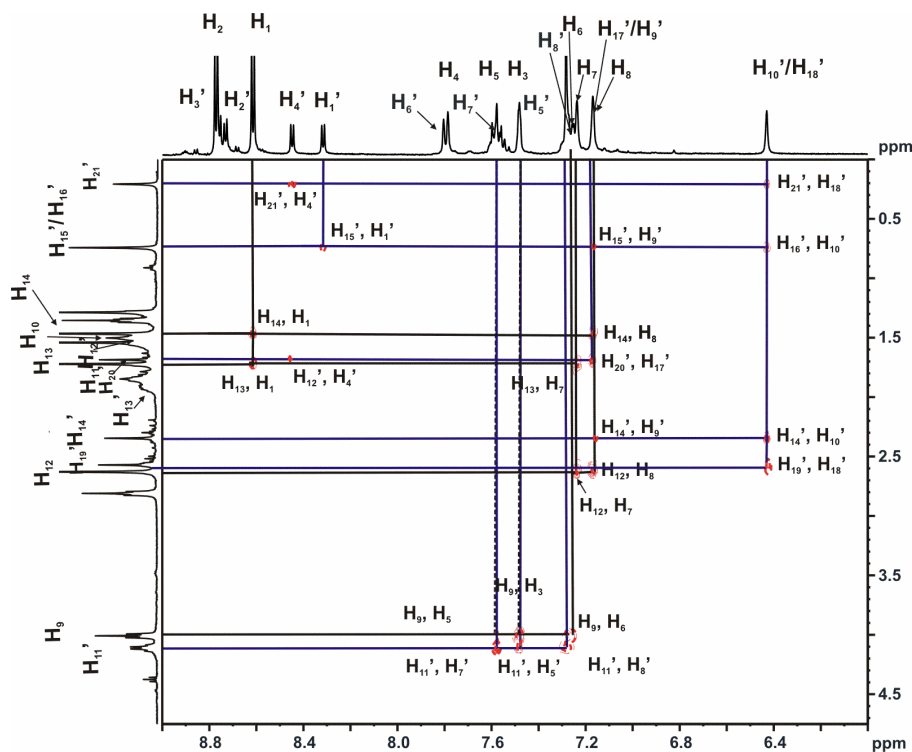


**Figure 27.**  $^1\text{H}$ ,  $^1\text{H}$ -2D ROESY (400 MHz,  $\text{CDCl}_3$ ,  $25^\circ\text{C}$ ) spectrum of **Zn<sub>2</sub>-18**. As here is represented the upfield region in one column and the downfield region in other column there are only circled the coupling peaks. The blue lines are referring to the **Zn<sub>2</sub>-18'** conformer.

### 3. Conclusions

The synthesis of the cyclic bis-porphyrin, **Zn<sub>2</sub>-12**, using Hay coupling was made but later on we realized that the starting material was a mixture of two isomers: *cis* and *trans*.

To avoid scrambling in the synthesis of the monoporphyrin we designed a dipyrromethane containing a mesityl substituent which disfavours the formation of a carbocation from the dipyrromethane and minimizes the formation of unwanted products.

We described the synthesis with very good yields of a pair of bis-porphyrin tweezers, **Zn<sub>2</sub>-14** and **Zn<sub>2</sub>-15**, and a pair of cyclic bis-porphyrins, **Zn<sub>2</sub>-17** and **Zn<sub>2</sub>-18**, differing on the saturation grade of the linking chains, starting from propargyl substituted monoporphyryns subjected to the Hay coupling conditions. It is worth to note the difference between the phenyl group in the *meso* positions of the porphyrin in the tweezers (simple phenyl group) and the macrocycles (mesitylphenyl group).

### 4. Experimental section

#### 4.1 General information and instrumentation

All commercial reagents, unless otherwise noted, were reagent grade and used without further purification. Solvents were of HPLC grade quality, obtained commercially and used without further purification. Anhydrous solvents were obtained from a solvent purification system SPS-400-6 from Innovative Technologies, Inc. Pyrrole was freshly distilled under vacuum just prior to use. <sup>1</sup>H NMR spectra were recorded on Bruker Avance 400 (400.1 MHz for <sup>1</sup>H NMR) and Bruker Avance 500 (500.1 MHz for <sup>1</sup>H NMR) NMR spectrometers. High resolution mass spectra were obtained using a Bruker Autoflex MALDI-TOF Mass Spectrometer. Analytical gel permeation chromatography (GPC) was carried out on Styragel® HR1 Toluene (7.8 x 300 mm) Waters column with 100% toluene. Flash column chromatography was performed with Silica gel Scharlab60. Crystal data set were collected

at Beam line BM16<sup>24</sup> at ESRF wavelength = 0.7380 Å; Si111 monochromator; absorption coefficient = 0.553 mm<sup>-1</sup>; ADSC Q210r CCD detector and cooled with an Oxford Cryostream low temperature device ( $T = 100(2)$  K). Full-sphere data collection was used with  $\varphi$  scans.

Programs used: Data collection MXCube, Indexing Apex2 V2009.11 (Bruker-Nonius 2008), data reduction Saint + Version 7.60A (Bruker AXS 2008) and absorption correction SADABS V. 2008/1 (2008). *Structure Solution*: SIR2007.<sup>25</sup> and SHELXTL Version 6.10 (Sheldrick, 2000) was used.<sup>26</sup> *Structure Refinement*: SHELXTL-97-UNIX VERSION.

## 4.2 Synthesis

### Synthesis of 3-(prop-2-ynyloxy)benzaldehyde, **20**:

3.40 g (1.5 equivalents, 24.57 mmol) of K<sub>2</sub>CO<sub>3</sub> and 0.216 g (0.05 equivalents, 0.819 mmol) of 18-crown-6 were added to a solution of 2 g (1 equivalent, 16.38 mmol) of *m*-hydroxybenzaldehyde and 2.92 g (1.5 equivalents, 24.57 mmol) of propargylbromide in dry CH<sub>3</sub>CN followed by refluxing (80-90°C) overnight under N<sub>2</sub>. The solid precipitated in the reaction mixture was filtered and washed with CH<sub>3</sub>CN. The product was filtered through a silica column eluting with CH<sub>3</sub>CN. The solvent was evaporated and we obtain the desired product (2.60 g, 99%).

<sup>1</sup>H NMR (400 MHz, CDCl<sub>3</sub>, 25 °C)  $\delta$  (ppm) 10.01 (s, 1H), 7.49 (m, 3H), 7.27 (m, 1H), 4.78 (d, 2H,  $J = 2.3$  Hz), 2.57 (t, 1H,  $J = 2.3$  Hz).

### Synthesis of 5,15-bis(3-propargyloxyphenyl)-10,20-bisphenyl-porphyrin, **H<sub>2</sub>-11**, and Zn-5,15-bis(3-propargyloxyphenyl)-10,20-bisphenyl-porphyrin, **Zn-11**:

A solution of 2.04 g of 5-phenyldipyromethane, **5b** (1 equivalent, 9.18 mmol), and 1.47 g of 3-(prop-2-ynyloxy)benzaldehyde, **20** (1 equivalent, 9.18 mmol), in 25 mL of propionic

<sup>24</sup> The macromolecular crystallography station at beamline BM16 at the ESRF Juanhuix, J.; Labrador, A.; Beltran, D.; Herranz, J. F.; Carpentier, P.; Bordas, J. *Rev. Sci. Instrum.* **2005**, *76*, -. 086103.

<sup>25</sup> Caliandro, R.; Carrozzini, B.; Cascarano, G. L.; De Caro, L.; Giacovazzo, C.; Siliqi, D. *J. Appl. Crystallogr.* **2007**, *40*, 883-890.

<sup>26</sup> Sheldrick, G. M. *SHELXTL Crystallographic System 6.14*, Bruker AXS Inc., Madison, Wisconsin, **2000**.

acid was refluxed in a flask (protected from light) under N<sub>2</sub> for 2 h. The propionic acid was distilled and the mixture was dissolved in CH<sub>2</sub>Cl<sub>2</sub>, washed with bicarbonate until the pH of the solution was basic, and the organic phase was extracted. The product was purified by flash chromatography using silica (big column) and eluting with dichloromethane. Then, another column was performed, using a mixture of DCM/Hex as eluent, being first 3:7, when the first fraction was eluted the relation is 4:6, until the last fraction was recovered; we only employed DCM. 0.391 g of the final product were isolated (15%). 0.180 g (1 equivalent, 0.249 mmol) of this **H<sub>2</sub>-11** purple solid was metallated with 0.453 g (10 equivalents, 2.49 mmol) of Zn(OAc)<sub>2</sub> in 48 ml of a CH<sub>2</sub>Cl<sub>2</sub>/CH<sub>3</sub>OH (3/1) solution covered with aluminum paper to protect it from the light, and the solution was stirred at room temperature overnight. Then, the solvent was evaporated and the final product, **Zn-11**, was purified by flash chromatography on neutral aluminum oxide using CH<sub>2</sub>Cl<sub>2</sub> and then CH<sub>2</sub>Cl<sub>2</sub>/THF (90:10) as eluent (0.167 g, 85%).

<sup>1</sup>H NMR **H<sub>2</sub>-11** (400.1 MHz, CDCl<sub>3</sub>, 25 °C) δ (ppm) 8.96 (d, 2H, *J* = 2.1 Hz), 8.95 (s, 2H), 8.91 (s, 2H), 8.90 (d, 2H, *J* = 2.1 Hz), 8.27 (dd, 4H, *J* = 6.9 Hz and 1.70 Hz), 7.93 (d, 2H, *J* = 1.9 Hz), 7.91 (s, 2H), 7.81 (m, 6H), 7.70 (t, 2H, *J* = 8.5 Hz), 7.45 (dd, 2H, *J* = 8.5 Hz and 2.6 Hz), 4.93 (d, 2H, *J* = 2.3 Hz), 2.62 (t, 2H, *J* = 2.3 Hz), -2.71 (s, 2H); HR-MS (MALDI) *m/z* calcd. for C<sub>50</sub>H<sub>34</sub>N<sub>4</sub>O<sub>2</sub> (M<sup>+</sup>) 722.2673, found: 722.2678 (0.24 ppm); Elemental analysis calcd (%) for C<sub>50</sub>H<sub>34</sub>N<sub>4</sub>O<sub>2</sub>: C 83.08 H 4.74 N 7.75 O 4.43; found: C 80.63 H 4.58 N 7.23 O 7.56.

### Synthesis of 5-(3-propargyloxyphenyl)-10,15,20-bisphenyl-porphyrin, **H<sub>2</sub>-13**, and Zn-5-(3-propargyloxyphenyl)-10,15,20-bisphenyl-porphyrin, **Zn-13**:

Porphyrin **H<sub>2</sub>-13** was obtained as a secondary product in the synthesis of disubstituted porphyrin **H<sub>2</sub>-11**, and in the purification of the latter, the former eluted as the second fraction in the flash chromatography. **H<sub>2</sub>-13** was metallated with Zn(OAc)<sub>2</sub> following the procedure already described for **H<sub>2</sub>-11** giving **Zn-13**.

<sup>1</sup>H NMR **H<sub>2</sub>-13** (400.1 MHz, CDCl<sub>3</sub>, 25 °C) δ (ppm) 8.97 (d, 2H, *J* = 4.8 Hz), 8.92 (d, 2H, *J* = 4.8 Hz), 8.91 (s, 4H), 8.28 (dd, 6H, *J* = 7.6 and 1.8 Hz), 7.94 (m, 1H), 7.91 (s, 1H), 7.82 (m, 9H), 7.71 (dd, 1H, *J* = 8.1 and 7.6 Hz), 7.46 (ddd, 1H, *J* = 8.1, 2.7 and 0.9 Hz), 4.93 (d, 2H, *J* = 2.3 Hz), 2.63 (t, 1H, *J* = 2.3 Hz), -2.70 (s, 2H).

### Synthesis of Zn<sub>2</sub>-14:

To a 150 ml CH<sub>2</sub>Cl<sub>2</sub> solution of 140 mg (1 equivalent, 0.191 mmol) of **Zn-13**, 1.32 g (70 equivalents, 13.384 mmol) of copper (I) chloride and 2.02 ml (70 equivalents, 13.384 mmol) of TMEDA were added. The mixture was stirred for 4h under air at room temperature. The reaction mixture changes its colour from fuchsia to green. Then, the reaction mixture was washed with water, dried over Na<sub>2</sub>SO<sub>4</sub>, and evaporated to dryness. The crude (0.325 g) was subjected to column chromatography on neutral alumina using CH<sub>2</sub>Cl<sub>2</sub> as eluent. The acetylenic bis-porphyrin tweezer, with TMEDA coordinated to the Zn units (as we could observe by <sup>1</sup>H-NMR, see synthesis of TMEDA•Zn<sub>2</sub>-17) was redissolved in the minimum amount of CH<sub>2</sub>Cl<sub>2</sub> and then HCl 4N in dioxane was added. The green solution was stirred for 30 minutes and then extracted with CH<sub>2</sub>Cl<sub>2</sub> in order to remove the TMEDA. The purified final product, **H<sub>4</sub>-14**, was obtained in a good yield (0.100g, 72%). To a solution of 98 mg (1equivalent, 0.061mmol) of **H<sub>4</sub>-14** in a 36 ml mixture of CH<sub>2</sub>Cl<sub>2</sub>/CH<sub>3</sub>OH (3:1), 0.40g (20 equivalents, 1.217 mmol) of Zn(OAc)<sub>2</sub> were added. The bottom flask was covered with aluminium paper to protect it from the light and the solution was stirred at room temperature overnight. The reaction can be followed by alumina TLC in CH<sub>2</sub>Cl<sub>2</sub>/hexane (1/1). Total conversion was observed. Then, the solvent was evaporated and the final product was purified by flash chromatography on neutral aluminum oxide using CH<sub>2</sub>Cl<sub>2</sub> and then CH<sub>2</sub>Cl<sub>2</sub>/THF (90:10) as eluent. **Zn<sub>2</sub>-14** was obtained in quantitative yield.

<sup>1</sup>H NMR (400.1 MHz, CDCl<sub>3</sub>, 25 °C) δ (ppm) 9.05 (d, 4H, *J* = 4.7 Hz), 8.99 (d, 4H, *J* = 4.7 Hz), 8.98 (d, 4H, *J* = 4.7 Hz), 8.96 (d, 4H, *J* = 4.7 Hz), 8.23 (m, 12H), 7.89 (dt, 2H, *J* = 7.7 and 1.2 Hz), 7.85 (dd, 2H, *J* = 2.8 and 1.5 Hz), 7.75 (m, 18H), 7.63 (dd, 2H, *J* = 8.3 and 7.5 Hz), 7.33 (ddd, 2H, *J* = 8.3, 2.6 and 0.9 Hz), 4.85 (s, 4H); HR-MS (MALDI) *m/z* calcd. for C<sub>94</sub>H<sub>58</sub>N<sub>8</sub>O<sub>2</sub>Zn<sub>2</sub> (M<sup>+</sup>) 1458.3260, found:1458.3131 (8.8 ppm); UV-visible (Toluene): λ<sub>max</sub> (ε, M<sup>-1</sup> cm<sup>-1</sup>) 420 (934285.71).

### Synthesis of Zn<sub>2</sub>-15:

To a 10 ml THF solution of 40 mg of **Zn<sub>2</sub>-14** (1 equivalent, 0.023 mmol) were added 15 mg of Pd/C dissolved in 4 ml of THF. This suspension was stirred under H<sub>2</sub> in a high pressure room, under 2.5 bar of pressure, during 15h, and using a 20 ml flask. The reaction can be followed by silica TLC in CH<sub>2</sub>Cl<sub>2</sub>/hexane (1/1). The crude was filtered through celita, and

purified using chromatography on neutral alumina (DCM and later THF as eluents). The fraction eluted was evaporated to leave **Zn<sub>2</sub>-15** as a purple solid (30 mg, 75%).

<sup>1</sup>H NMR (400.1 MHz, CDCl<sub>3</sub>, 25 °C) δ (ppm) 8.83 (d, 4H, *J* = 4.7 Hz), 8.81 (d, 4H, *J* = 4.7 Hz), 8.79 (d, 4H, *J* = 4.7 Hz), 8.77 (d, 4H, *J* = 4.7 Hz), 8.07 (m, 12H), 7.69 (m, 18H), 7.57 (t, 2H, *J* = 1.9 Hz), 7.56 (s, 2H), 7.30 (ddd, 2H, *J* = 8.3, 2.6 and 0.9 Hz), 4.11 (t, 4H, *J* = 6.3 Hz), 3.68 (d, 1H, *J* = 6.3 Hz), 3.65 (d, 1H, *J* = 6.3 Hz), 1.59 (t, 6H, *J* = 6.3 Hz); HR-MS (MALDI) *m/z* calcd. for C<sub>94</sub>H<sub>66</sub>N<sub>8</sub>O<sub>2</sub>Zn<sub>2</sub> (M<sup>+</sup>) 1466.3886, found: 1466.3804 (5.6 ppm); UV-visible (Toluene): λ<sub>max</sub> (ε, M<sup>-1</sup> cm<sup>-1</sup>) 420 (746715.33).

### Synthesis of 2,2'-(mesitylmethylene)bis(1H-pyrrole), **19**:

A solution of 1.417 g (1 equivalent, 9.56 mmol) of mesitaldehyde and 25.7 g (40 equivalents, 382 mmol) of pyrrole, previously distilled, was degassed with an Ar flow for 20min. Then, 0.136 g (0.1 equivalents, 0.956 mmol) of BF<sub>3</sub>·(OEt)<sub>2</sub> were added. The light brown mixture was stirred for 30 min. under Ar atmosphere. The solution was diluted with CH<sub>2</sub>Cl<sub>2</sub> (50ml) and immediately washed with 0.1N NaOH (200 mg, 50 ml) and water (50ml). Evaporation of the solvent under reduced pressure at 40°C resulted in brownish oil. The oil was triturated in cyclohexane (washing with EtOH if it is darkly) yielding a solid that was collected by filtration and then washed with cyclohexane and hexane. Finally a white solid was obtained (0.32 g, 12.7%).

<sup>1</sup>H NMR (400.1 MHz, CDCl<sub>3</sub>, 25 °C) δ (ppm) 7.96 (bs, 2H, NH), 6.89 (s, 2H), 6.68 (s, 2H), 6.17 (q, 2H, *J* = 2.9 Hz), 6.03 (s, 2H), 5.93 (s, 1H, *meso*-H), 2.29 (s, 3H), 2.08 (s, 6H).

### Synthesis of 5,15-bis(3-propargyloxyphenyl)-10,20-bis(1,3,5-trimethylphenyl)-porphyrin, **H<sub>2</sub>-16**, and Zn-5,15-bis(3-propargyloxyphenyl)-10,20-bis(1,3,5-trimethylphenyl)-porphyrin, **Zn-16** :

A solution of 0.499g (1 equivalent, 3.11 mmol) of 3-(prop-2-ynoxy)benzaldehyde, **20**, and 0.823 g (1 equivalent, 3.11 mmol) of 2,2'-(mesitylmethylene)bis(1H-pyrrole), **19**, in 100 ml of CHCl<sub>3</sub> was purged with Ar for 10 minutes. Then 0.146 g (0.33 equivalents, 1.027 mmol) of BF<sub>3</sub>·O(Et)<sub>2</sub> were added. The solution was stirred at room temperature for 1 hour and then DDQ was added. The mixture was stirred at room temperature for an additional hour. The solvent was removed in vacuum. The residual solid was purified by column chromatography on silica gel with hexane/dichloromethane/triethylamine (50/50/1) as

eluent. The third fraction was collected and evaporated to leave **H<sub>2</sub>-16** as a purple solid (0.290 mg, 26%). This fraction was also analyzed by HPLC (Zorbax Eclipse C18, CH<sub>3</sub>CN:H<sub>2</sub>O-0.1%TFA 1ml/min, 420 nm, sample dissolved in CH<sub>3</sub>CN) eluting at 21 min. 0.270 mg (1 equivalent, 0.335mmol) of this **H<sub>2</sub>-16** purple solid was metallated with 0.614g (10 equivalents, 3.35 mmol) of Zn(OAc)<sub>2</sub> in 40 ml of a CH<sub>2</sub>Cl<sub>2</sub>/CH<sub>3</sub>OH (3/1) solution covered with aluminum paper to protect it from the light, and the solution was stirred at room temperature overnight. Then, the solvent was evaporated and the final product, **Zn-16**, was purified by flash chromatography on neutral aluminum oxide using CH<sub>2</sub>Cl<sub>2</sub> and then CH<sub>2</sub>Cl<sub>2</sub>/THF (90:10) as eluent (0.230 g, 85%).

<sup>1</sup>H NMR (400.1 MHz, CDCl<sub>3</sub>, 25 °C) δ (ppm) 9.00 (d, 4H, *J* = 4.7 Hz), 8.85 (d, 4H, *J* = 5.1 Hz), 7.93 (m, 4H), 7.67 (t, 2H, *J* = 7.8 Hz), 7.38 (dd, 2H, *J* = 8.4 and 2.3 Hz), 7.34 (s, 4H), 4.83 (t, 4H, *J* = 1.8Hz), 2.69 (s, 6H), 2.58 (t, 2H, *J* = 2.4 Hz), 1.91 (s, 12H); HR-MS (MALDI) *m/z* calcd. for C<sub>56</sub>H<sub>44</sub>N<sub>4</sub>O<sub>2</sub>Zn (M<sup>+</sup>) 868.2750, found:868.2740 (1 ppm); UV-visible (Toluene): λ<sub>max</sub> (ε, M<sup>-1</sup> cm<sup>-1</sup>) 423 (586731.92).

#### Synthesis of TMEDA•Zn<sub>2</sub>-17:

To a 200 ml CH<sub>2</sub>Cl<sub>2</sub> solution of 137 mg (1 equivalent, 0.157 mmol) of **Zn-16**, 1.09 g (70 equivalents, 11.02 mmol) of copper (I) chloride and 1.3 ml (70 equivalents, 11.02 mmol) of TMEDA were added. The mixture was stirred for 4h under air at room temperature. The reaction mixture changes its colour from fuchsia to green. Then, the reaction mixture was washed with water, dried over Na<sub>2</sub>SO<sub>4</sub>, and evaporated to dryness. The crude (0.144 g, 98%) was analyzed by GPC (Styragel HR1 column in Toluene, 1ml/min; 420 nm; 1mg/ml; inject: 5uL): major peak at 7.45 min. and minor peak at 6.75 min. The former must be the diacetylenic bis-porphyrin with TMEDA inside and the latter must correspond to polymers formed in the reaction.

<sup>1</sup>H NMR (400.1 MHz, CDCl<sub>3</sub>, 25 °C) δ (ppm) 8.64 (d, 8H, *J* = 3.3 Hz), 8.40 (d, 8H, *J* = 3.3 Hz), 8.01 (d, 4H, *J* = 6.8 Hz), 7.64 (t, 4H, *J* = 7.8 Hz), 7.25 (s, 8H), 7.12 (s, 4H), 6.91 (d, 4H, *J* = 7.3 Hz), 4.38 (s, 8H), 2.62 (s, 12H), 2.61 (s, 12H), 1.28 (s, 12H), -3.62 (s, 12H, -CH<sub>3</sub>- of coordinated TMEDA), -5.03 (s, 4H, -CH<sub>2</sub>- of coordinated TMEDA).

### Synthesis of Zn<sub>2</sub>-17:

The acetylenic bis-porphyrin with TMEDA was redissolved in the minimum amount of CH<sub>2</sub>Cl<sub>2</sub> and then HCl 4N in dioxane was added. The green solution was stirred for 30 minutes and then extracted with CH<sub>2</sub>Cl<sub>2</sub> in order to remove the TMEDA. The reaction crude was purified by semi-preparative GPC (UltraStyragel toluene column, flow 6 ml/min, injections 20mg/ml) collecting the second peak at 7.31 min. which is the clean diacetylenic bis-porphyrin **H<sub>4</sub>-17** (0.100g, 69%). To a solution of 98 mg (1 equivalent, 0.061mmol) of **H<sub>4</sub>-17** in a 36 ml mixture of CH<sub>2</sub>Cl<sub>2</sub>/ CH<sub>3</sub>OH (3:1), 0.40g (20 equivalents, 1.217 mmol) of Zn(OAc)<sub>2</sub> were added. The bottom flask was covered with aluminium paper to protect it from the light and the solution was stirred at room temperature overnight. The reaction can be followed by alumina TLC in CH<sub>2</sub>Cl<sub>2</sub>/hexane (1/1). Total conversion was observed. Then, the solvent was evaporated and the final product was purified by flash chromatography on neutral aluminum oxide using CH<sub>2</sub>Cl<sub>2</sub> and then CH<sub>2</sub>Cl<sub>2</sub>/THF (90:10) as eluent. **Zn<sub>2</sub>-17** was obtained as a purple solid (70mg, 58%).

<sup>1</sup>H NMR (400.1 MHz, CDCl<sub>3</sub>, 25 °C) δ (ppm) 8.80 (d, 8H, *J* = 4.7 Hz, **H<sub>2</sub>**), 8.49 (d, 8H, *J* = 4.7 Hz, **H<sub>1</sub>**), 7.81 (d, 4H, *J* = 7.3 Hz, **H<sub>4</sub>**), 7.66 (s, 4H, **H<sub>3</sub>**), 7.61 (t, 4H, *J* = 7.3 Hz, **H<sub>5</sub>**), 7.33 (dd, 4H, *J* = 8.5 and 2.4 Hz, **H<sub>6</sub>**), 7.18 (s, 4H, **H<sub>7</sub>**), 6.79 (s, 4H, **H<sub>8</sub>**), 4.78 (s, 8H, **H<sub>9</sub>**), 2.48 (s, 12H, **H<sub>10</sub>**), 1.77 (s, 12H, **H<sub>11</sub>**), 0.76 (s, 12H, **H<sub>12</sub>**), see Figure 19; HR-MS (MALDI) *m/z* calcd. for C<sub>112</sub>H<sub>84</sub>N<sub>8</sub>O<sub>4</sub>Zn<sub>2</sub> (M<sup>+</sup>) 1732.5193, found:1732.5244 (3 ppm); UV-visible (Toluene): λ<sub>max</sub> (ε, , M<sup>-1</sup> cm<sup>-1</sup>) 418 (789190.67).

### Synthesis of Zn<sub>2</sub>-18:

To a 10 ml THF solution of 38 mg of **Zn<sub>2</sub>-17** (1 equivalent, 0.023 mmol) were added 14 mg of Pd/C dissolved in 4 ml of THF. This suspension was stirred under H<sub>2</sub> in a high pressure room, under 2.5 bar of pressure, during 15h, and using a 20 ml flask. The reaction can be followed by silica TLC in CH<sub>2</sub>Cl<sub>2</sub>/hexane (1/1). The crude was cleaned passing it through celita, eluting with THF, and then the product was passed through another column on neutral alumina, eluting with CH<sub>2</sub>Cl<sub>2</sub>, and finally few millilitres of THF. The fraction eluted was evaporated to leave **Zn<sub>2</sub>-18** as a purple solid (20 mg, 55%).

<sup>1</sup>H NMR (400.1 MHz, CDCl<sub>3</sub>, 25 °C) δ (ppm) 8.77 (d, 8H, *J* = 4.7 Hz, **H<sub>2</sub>**), 8.62 (d, 8H, *J* = 4.7 Hz, **H<sub>1</sub>**), 7.79 (d, 4H, *J* = 7.3 Hz, **H<sub>4</sub>**), 7.58 (t, 4H, *J* = 7.3 Hz, **H<sub>5</sub>**), 7.48 (s, 4H, **H<sub>3</sub>**), 7.26 (dd, 4H, *J* = 7.3 and 2.6 Hz, **H<sub>6</sub>**), 7.24 (s, 4H, **H<sub>7</sub>**), 7.17 (s, 4H, **H<sub>8</sub>**), 4.01 (t, 8H, *J*

= 6.2 Hz, **H<sub>9</sub>**), 2.63 (s, 12H, **H<sub>12</sub>**), 1.85 (m, 8H, **H<sub>11</sub>**), 1.72 (s, 12H, **H<sub>13</sub>**), 1.50 (m, 8H, **H<sub>10</sub>**), 1.47 (s, 12H, **H<sub>14</sub>**), see Figure 20; HR-MS (MALDI) *m/z* calcd. for C<sub>112</sub>H<sub>100</sub>N<sub>8</sub>O<sub>4</sub>Zn<sub>2</sub> (M<sup>+</sup>) 1748.6445, found: 1748.6248 (11 ppm); UV-visible (Toluene): λ<sub>max</sub> (ε, M<sup>-1</sup> cm<sup>-1</sup>) 419 (772176.67).

UNIVERSITAT ROVIRA I VIRGILI  
SUPRAMOLECULAR CHEMISTRY OF BIS-PORPHYRINS  
Laura Patricia Hernández Eguía  
ISBN:978-84-694-0308-2/DL:T-204-2011

## CHAPTER 3

***“Tweezers and macrocyclic bis-porphyrin receptors. Study of their binding interactions with monotopic and ditopic amines”***

UNIVERSITAT ROVIRA I VIRGILI  
SUPRAMOLECULAR CHEMISTRY OF BIS-PORPHYRINS  
Laura Patricia Hernández Eguía  
ISBN:978-84-694-0308-2/DL:T-204-2011

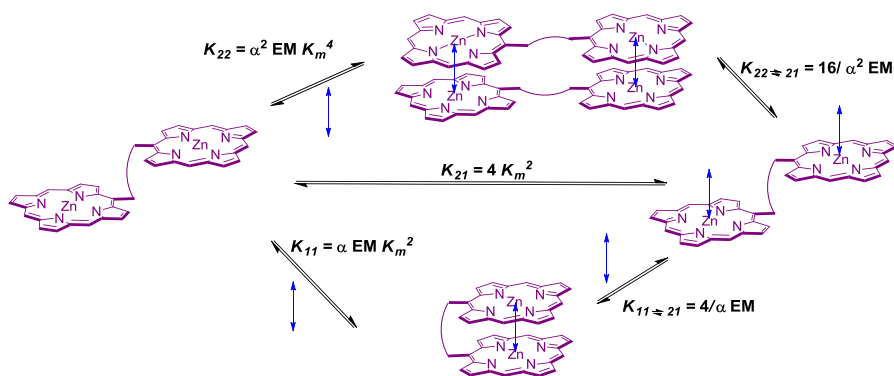
## 1. Introduction

In the previous chapter we have described the preparation of two zinc bis-porphyrin tweezers receptors, **Zn<sub>2</sub>-14** and **Zn<sub>2</sub>-15**, and two cyclic bis-porphyrin receptors, **Zn<sub>2</sub>-17** and **Zn<sub>2</sub>-18**, differing each pair on the saturation degree of the carbon chain used to span the porphyrin binding units (synthesis described in Chapter 2). In this chapter, our interest resides in the evaluation of their binding abilities towards mono- and ditopic amines such as quinuclidine and DABCO, or pyridine and 4,4'-bipyridyl (bipy). We are mainly interested in the evaluation of differences in the stability constants of the ditopic complexes they form and that can be related to the reduced conformational flexibility provided by the degree of saturation of the carbon chain used as spacer or to the macrocyclic nature. It is worth noting, that due to the geometrical features embedded in the structures of the two zinc bis-porphyrin tweezers receptors, **Zn<sub>2</sub>-14** and **Zn<sub>2</sub>-15** the formation with the two ditopic diamines, DABCO and bipy, of inter- and intramolecular complexes having 2:2 and 1:1 stoichiometry, respectively, is plausible. We will devote some of our efforts in trying to demonstrate the complexation binding model that is operative in those cases, in other words, the stoichiometry of the formed sandwich complex (Scheme 1).

Heteromeric complexes (amine-porphyrin) are formed when bidentate amine ligands are used to direct the self-assembly of metalloporphyrins. During our research program, aimed at the modular assembly of supramolecular receptors featuring an internal cavity, by means of the bis-porphyrin/amine sandwich motif<sup>1</sup> as intermolecular interaction, we became interested in studying if different ditopic nitrogen ligands would translate into differences in the tertiary structures (shape and number of components) of the complexes they form with acyclic zinc bis-porphyrin receptors. The construction of such structures constitutes the starting point for the understanding of the behavior of more elaborate assemblies with potential applications as molecular hosts.

---

<sup>1</sup> Ballester, P.; Oliva, A. I.; Costa, A.; Deya, P. M.; Frontera, A.; Gomila, R. M.; Hunter, C. A. *J. Am. Chem. Soc.* **2006**, *128*, 5560-5569.



**Scheme 1.** Schematic representations of the possible equilibria involved in the binding of a ditopic ligand (blue arrow) to an acyclic zinc bis-porphyrin. Overall ( $K_{11}$ ,  $K_{22}$  and  $K_{21}$ ) and stepwise equilibrium constants ( $K_{11 \rightleftharpoons 21}$  and  $K_{22 \rightleftharpoons 21}$ ) are shown and related to  $K_m$ ,  $EM$ ,  $\alpha$ , which is the cooperativity factor of the ligand, and statistical correction factors.

## 2. Results and discussion

### 2.1 Bis-porphyrin tweezers: mono- and ditopic amines

We describe the binding properties of the two zinc bis-porphyrin tweezers receptors, **Zn<sub>2</sub>-14** and **Zn<sub>2</sub>-15**, in the presence of four different ligands: two ditopic ligands, DABCO and 4,4'-bipyridyl (bipy), and two monodentate ligands, quinuclidine and pyridine (Figure 1).

We performed molecular modelling studies<sup>2</sup> in order to obtain some hints about what should be the most favorable stoichiometry for the sandwich complexes derived from the bis-porphyrin tweezers and the ditopic ligands, DABCO and bipy (Figures 2 and 3).

<sup>2</sup> *CAChe WorkSystem*, version 6.1.12.33; Fujitsu Limited (USA), 2004.

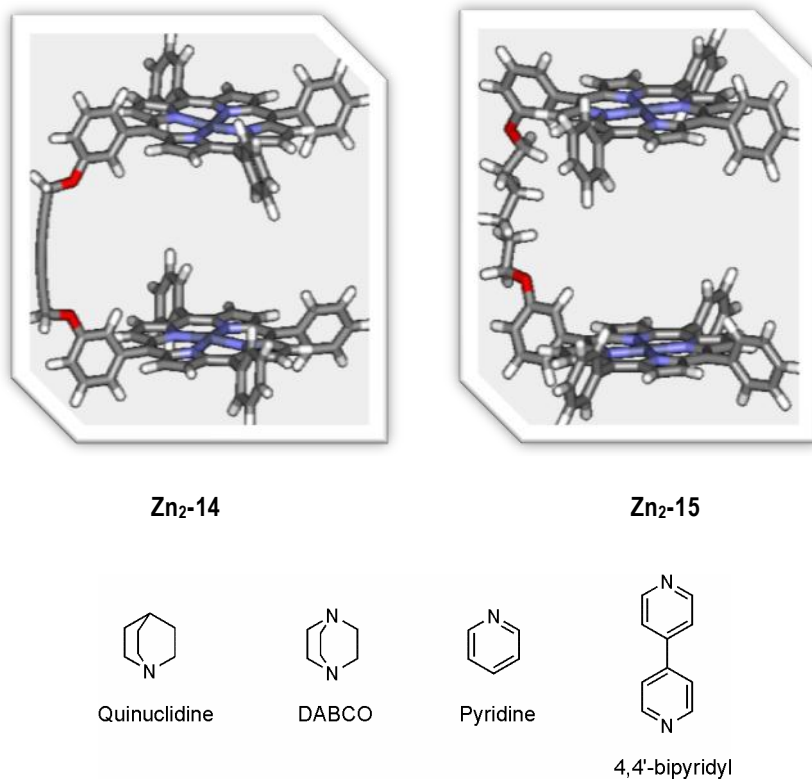


**Figure 1.** Molecular mechanics optimized structures (CACHe, MM3) of the 1,3-diyne-bridged bis-porphyrin, **Zn<sub>2</sub>-14**, and of the saturated alkyl-bridged bis-porphyrin, **Zn<sub>2</sub>-15**. Line structures of the four amines (quinuclidine, DABCO, pyridine and 4,4'-bipyridyl) used in the evaluation of the binding properties of the bis-porphyrin tweezers receptors.

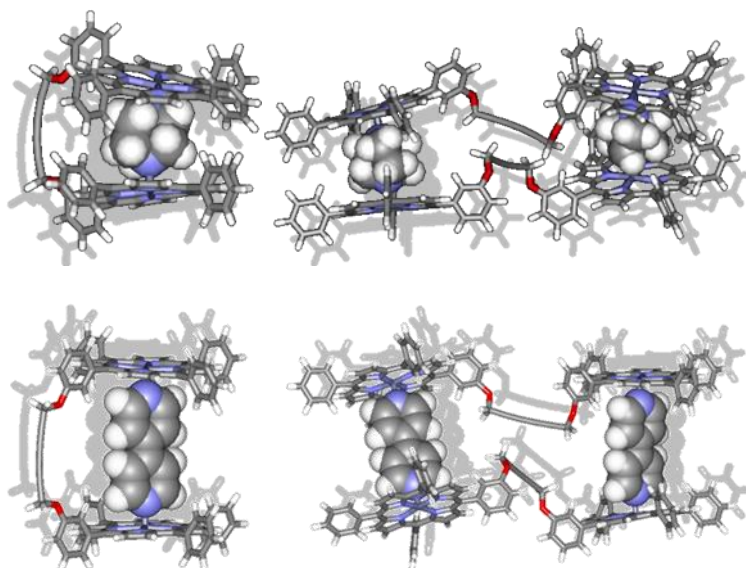


**Figure 2.** Side view of the CAChe minimized structures for the **Zn<sub>2</sub>-14** bis-porphyrin (stick representation) in 1:1 and 2:2 stoichiometries with DABCO and 4,4'-bipyridyl (CPK representation).

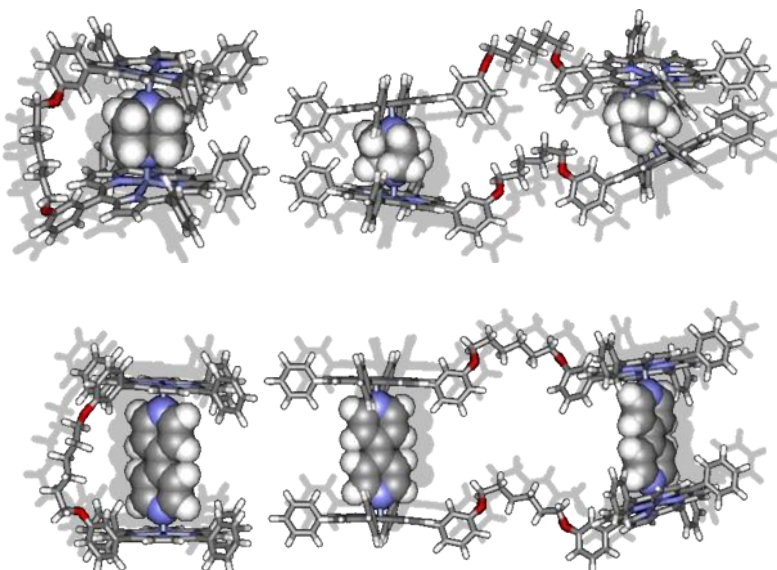


**Figure 3.** Side view of the CAChe minimized structures for the **Zn<sub>2</sub>-15** bis-porphyrin (stick representation) in 1:1 and 2:2 stoichiometries with DABCO and 4,4'-bipyridyl (CPK representation).

We can derive from the minimized structures that most probably is the intramolecular 1:1 stoichiometry for the largest ligand, 4,4'-bipyridyl, that shows a better complementarity between the two bis-porphyrins, **Zn<sub>2</sub>-14** and **Zn<sub>2</sub>-15**, and the diamine ligand. In the case of DABCO, we do not dare to put forward any prediction about the preferred stoichiometry for the sandwich complex. In all the sandwich complexes involving DABCO, the modelling studies suggest a poor cofacial arrangement of the porphyrin units. For the intramolecular 1:1 complexes, the size of the aromatic cavity between the two porphyrin units that is controlled by the flexible spacer seems to be too large to include a DABCO molecule in a ditopic interaction without requiring a non-cofacial arrangement of the binding units.

### a. UV-visible titrations

Titrations carried out using UV-visible spectroscopy are specially indicated when the free host, or the free guest absorb light at wavelengths having maxima that are different from one another and also from that of the complex they form. In addition, when working at micromolar concentrations, UV-visible spectroscopy is an ideal technique to probe the complexation processes.

The free metallated bis-porphyrin **Zn<sub>2</sub>-14** presents an absorption Soret band at 420 nm. On the one hand, the 10 nm red shift experienced by the Soret absorption band of a Zn-porphyrin during the titration with an amine is indicative of the formation of an axial 1:1 amine-porphyrin complex. On the other hand, the initial interaction of a bis-porphyrin receptor with a ditopic ligand like DABCO usually produces a red shift of only 5 nm being indicative of the formation of a 1:2 amine-porphyrin sandwich complex in which the two porphyrin units are excitonically coupled.<sup>3</sup>

---

<sup>3</sup> Hunter, C. A.; Sanders, J. K. M.; Stone, A. J. *Chem. Phys.* **1989**, *133*, 395-404.

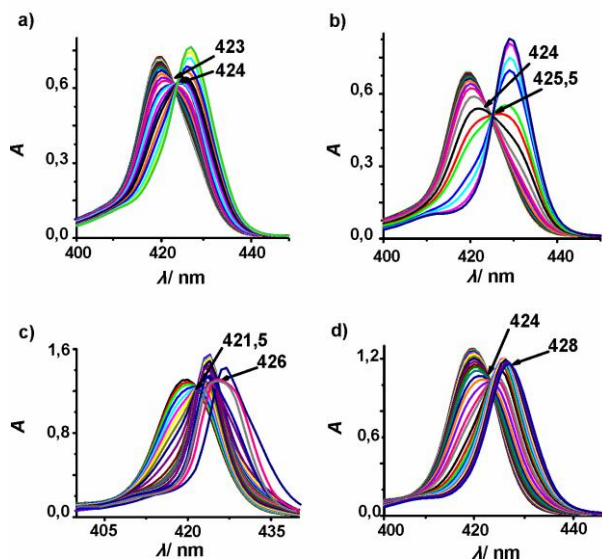


**Figure 4.** UV-visible titration spectra (Soret region) obtained in the titration of bis-porphyrin **Zn<sub>2</sub>-14** with the four nitrogenated ligands in chloroform. a) pyridine, from 0 to 1000 equivalents are added; b) quinuclidine, from 0 to 4200 equivalents are added; c) DABCO, from 0 to 1500 equivalents are added; d) bipy, from 0 to 4600 equivalents are added. The concentration of **Zn<sub>2</sub>-14** was maintained constant throughout the titration, a) and b)  $[\text{Zn}_2\text{-14}] = 7.60 \times 10^{-7}$  M; c) and d)  $[\text{Zn}_2\text{-14}] = 1.38 \times 10^{-6}$  M. The observed isosbestic points are indicated by an arrow.

Figures 4a and 4b corresponds to the titrations of **Zn<sub>2</sub>-14** with pyridine and quinuclidine respectively, simple monodentate amines. In both cases, the formation of sandwich structures is not possible due to the monotopic nature of the nitrogen ligand. The Soret band of **Zn<sub>2</sub>-14**, originally centered at 419 nm, shifts to 427 nm for the titration with pyridine and to 429 nm for quinuclidine in response to the addition of 2000 and 140 equivalents of the ligand respectively. During this titration we expect the formation of two different complexes with 1:1 and the 2:1 (amine:**Zn<sub>2</sub>-14**) stoichiometry.

The third titration shown in Figure 4c was performed using DABCO, a ditopic amine. In this case and as expected, we detect the formation of a sandwich complex which corresponds with the band that emerges at 425 nm during the first phase of the titration. The sandwich complex must be very stable thermodynamically because it does not break up until the addition of 1500 equivalents of diamine producing the

decrease of the band centered at 425 nm and the appearance of a new band at 430 nm that can be assigned to a 2:1 open complex.

The fourth titration depicted in Figure 4d corresponds to the data obtained with the other ditopic amine, 4,4'-bipyridyl. As shown before, this diamine also enables the formation of sandwich-like structures with **Zn<sub>2</sub>-14**. Due to the increase in the distance between the two nitrogen atoms in bipy compared to DABCO the exciton coupling of the porphyrin units is reduced and the red shift of the band for the sandwich complex increases. The thermodynamic stability of the sandwich complex formed by **Zn<sub>2</sub>-14** and bipy seems to be reduced with respect to the one assembled with DABCO, since only 1000 equivalents of bipy are required to induce the decrease of the band assigned to the sandwich and the appearance of a new Soret band for the 2:1 open complex.

In each one of the four UV-visible titration experiments we can detect two isosbestic points, indicative of two sequential two-state equilibria: the first between the free bis-porphyrin and the 1:1, intra- or intermolecular, and the second between the 1:1 sandwich and the 2:1 complexes (Figure 4).

Next we carried out a set of similar titrations with the second acyclic bis-porphyrin, **Zn<sub>2</sub>-15**, employing the same methodology (Figure 5). In general, the complexation systems behave analogously to what we have described for the unsaturated analog **Zn<sub>2</sub>-14**.

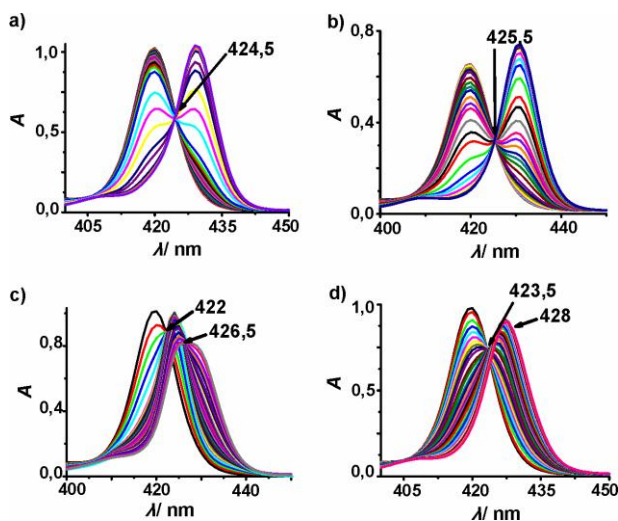


**Figure 5.** UV-visible titration spectra (Soret region) obtained in the titration of bis-porphyrin **Zn<sub>2</sub>-15** with the four nitrogen ligands in chloroform. a) pyridine, 0 to 4500 equivalents added; b) quinuclidine, 0 to 600 equivalents added; c) DABCO, 0 to 8500 equivalents added; d) bipy, 0 to 4500 equivalents added. The concentration of **Zn<sub>2</sub>-15** was maintained constant throughout the titration, a) and b) [**Zn<sub>2</sub>-15**] =  $1.14 \times 10^{-6}$  M ; c) and d) [**Zn<sub>2</sub>-15**] =  $1.30 \times 10^{-6}$  M. The observed isosbestic points are indicated by an arrow.

At this stage of the binding studies we are aware of the formation of a sandwich complex, but we cannot state its stoichiometry. As mentioned in the beginning of the chapter, 1:1 intramolecular sandwich complex or a 2:2 intermolecular sandwich assembly are geometrically feasible.

Typically, the Soret absorption band of Zn-bis-porphyrin tweezers is red-shifted around 5 nm implying the formation of a 1:1 sandwich complex with DABCO inside. The reason of that is due to the exciton coupling between the Zn-porphyrin transitions when they are cofacially arranged.<sup>4</sup> In the case of 4,4'-bipyridyl the exciton coupling is reduced because the distance between the two porphyrins which is imposed by the length of the diamine is increased. Therefore, the Soret band of the sandwich complex for bipy is expected to be red-shifted between 7 and 10 nm with respect to the free bis-porphyrin. It is also possible that coincides with the one corresponding to the open 2:1 complex introducing an additional difficulty to the analysis of the titration data.

<sup>4</sup> Anderson, H. L. *Inorg. Chem.* **1994**, *33*, 972-981.

We analyzed mathematically the data obtained for the four titrations of each bis-porphyrin, using the SPECFIT software which analyzes the whole series of spectra simultaneously.<sup>5</sup> The two systems with the monotopic ligands were fitted to a simple model considering three UV-active species, the free bis-porphyrin and two complexes with 1:1 and 2:1 stoichiometry (Figures 6 and 8). Likewise, the titrations with the ditopic ligands were fitted to same binding model. However, for the latter case and due to the unknown stoichiometry of the sandwich complex the data were also fitted to a binding model involving a 2:2 complex instead of a 1:1. Our expectations were to see a clear difference in the goodness of the fit of the data to the two binding models and from there to be able to infer which is the most probable stoichiometry of the sandwich.

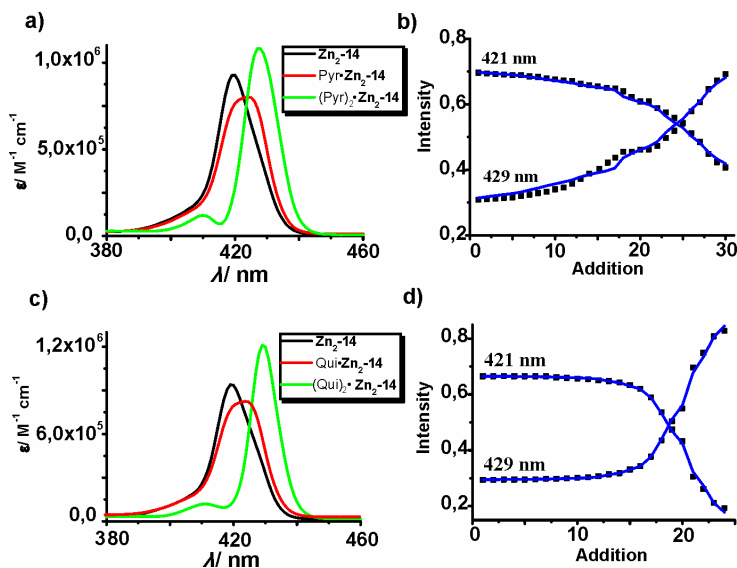


**Figure 6.** Left column, calculated UV-visible spectra of the intramolecular complexes formed between **Zn<sub>2</sub>-14** with a) pyridine and c) quinuclidine: free **Zn<sub>2</sub>-14** (black line), 1:1 complex (red line) and the 2:1 complex (green line). Right column: fit of the titration data to the experimental binding curves at two different wavelengths, 421 and 429 nm, b) for pyridine and d) for quinuclidine. The black squares represent the experimental titration data and the blue curves are the theoretical binding curves.

<sup>5</sup> SPECFIT, version 3.0; Spectra Software Associates, Marlborough, MA (USA), 2007 a) Gampp, H.; Maeder, M.; Meyer, C. J.; Zuberbuhler, A. D. *Talanta* **1985**, *32*, 95-101 Gampp, H.; Maeder, M.; Meyer, C. J.; Zuberbuhler, A. D. *Talanta* **1986**, *33*, 943-951.

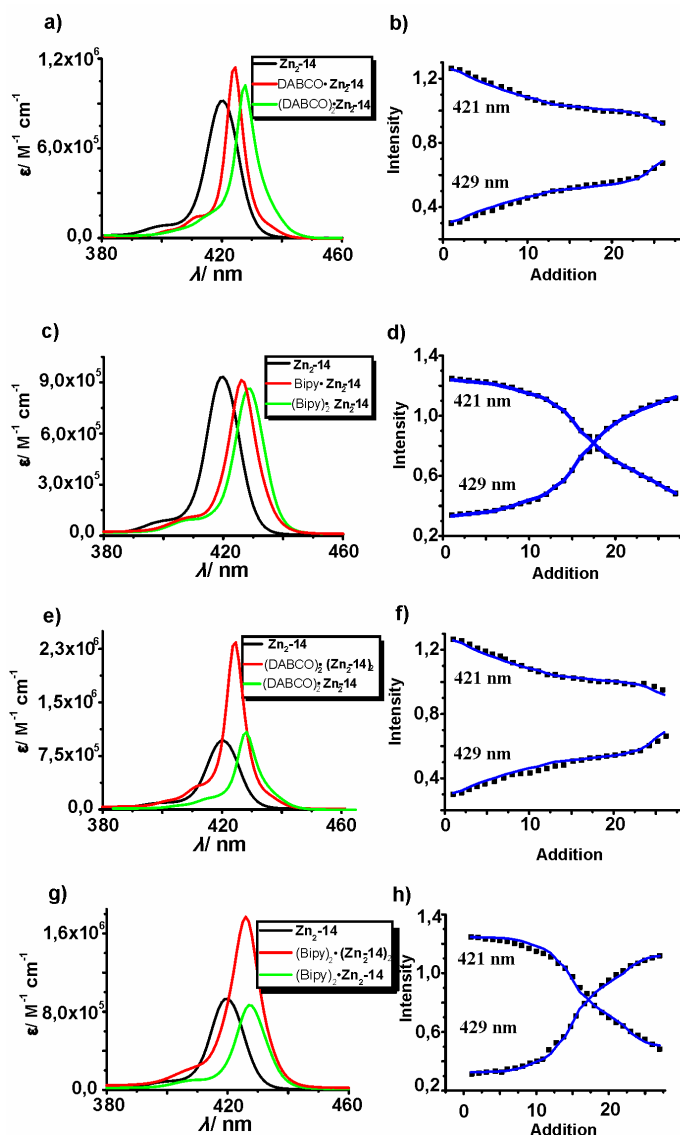


**Figure 7.** Left column, calculated UV-visible spectra of the intramolecular complexes formed between **Zn<sub>2</sub>-14** with a) DABCO and c) bipy: free **Zn<sub>2</sub>-14** (black line), 1:1 complex (red line) and the 2:1 complex (green line); e) DABCO and g) bipy: free **Zn<sub>2</sub>-14** (black line), 2:2 complex (red line) and the 2:1 complex (green line). Right column: fit of the titration data to the experimental binding curves at two different wavelengths, 421 and 429 nm, b) for DABCO and d) for bipy, when it is fitted to a 1:1 complex; f) for DABCO and h) for bipy, when it is fitted to a 2:2 complex. The black squares represent the experimental titration data and the blue curves are the theoretical binding curves.

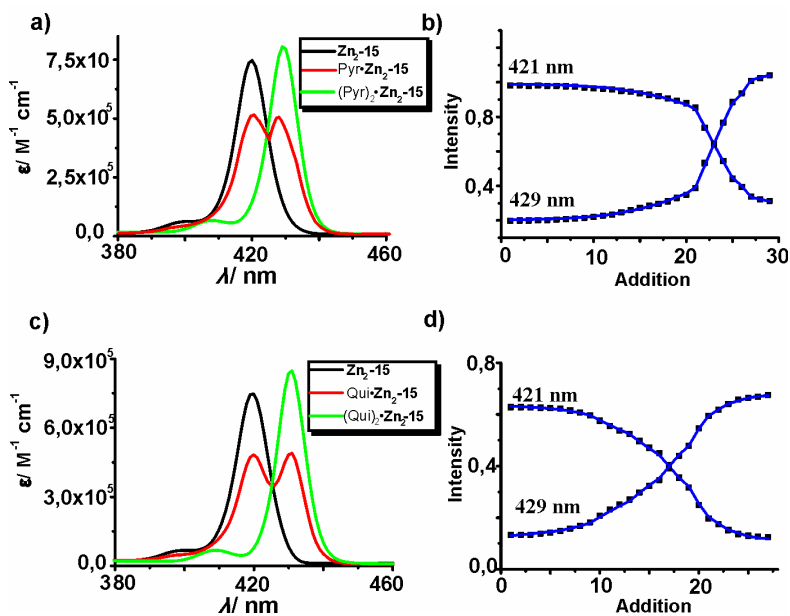


**Figure 8.** Left column, calculated UV–visible spectra of the intramolecular complexes formed between  $\text{Zn}_2\text{-14}$  with a) pyridine and c) quinuclidine: free  $\text{Zn}_2\text{-15}$  (black line), 1:1 complex (red line) and the 2:1 complex (green line). Right column: fit of the titration data to the experimental binding curves at two different wavelengths, 421 and 429 nm, b) for pyridine and d) for quinuclidine. The black squares represent the experimental titration data and the blue curves are the theoretical binding curves.

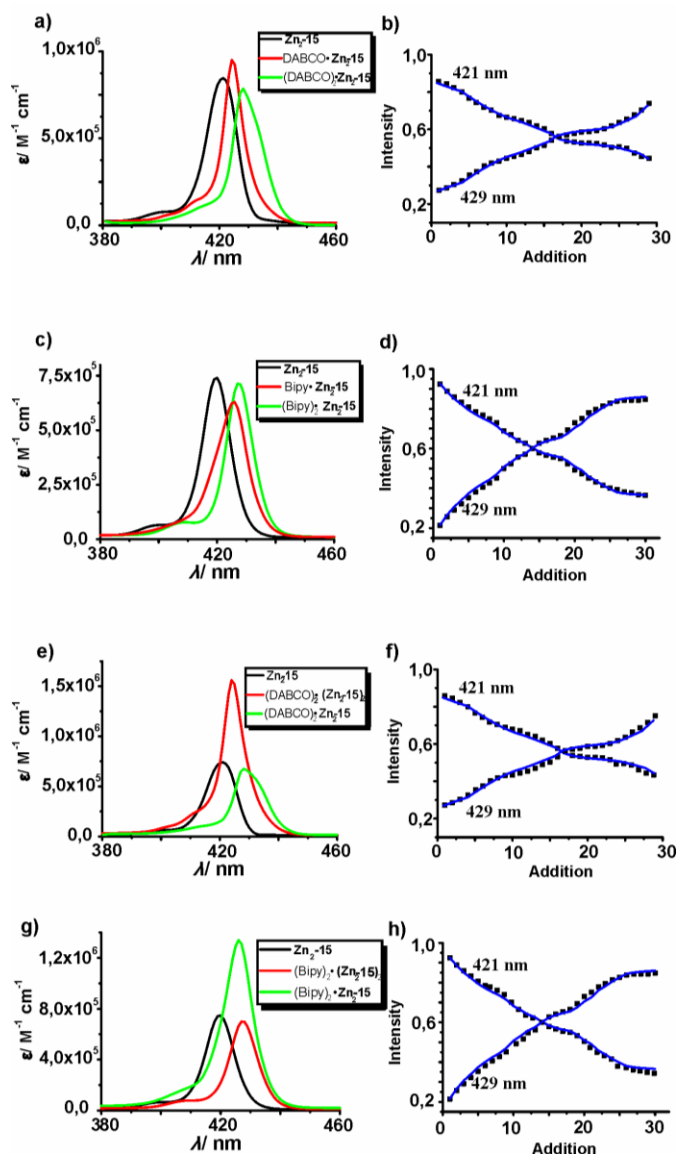


**Figure 9.** Left column, calculated UV-visible spectra of the intramolecular complexes formed between  $\text{Zn}_2\text{-14}$  with a) DABCO and c) bipy: free  $\text{Zn}_2\text{-15}$  (black line), 1:1 complex (red line) and the 2:1 complex (green line); e) DABCO and g) bipy: free  $\text{Zn}_2\text{-15}$  (black line), 2:2 complex (red line) and the 2:1 complex (green line). Right column: fit of the titration data to the experimental binding curves at two different wavelengths, 421 and 429 nm, b) for DABCO and d) for bipy, when it is fitted to a 1:1 complex; f) for DABCO and h) for bipy, when it is fitted to a 2:2 complex. The black squares represent the experimental titration data and the blue curves are the theoretical binding curves.

The calculated values for the stability constants of the different complexes are summarized in the next tables (table 1, for **Zn<sub>2</sub>-14**, and table 2, for **Zn<sub>2</sub>-15**). For the ditopic ligands, the experimental data were fitted to the two possible binding models and as shown in the figures 7 and 9 the goodness of the fit is similar and cannot be used to discard any of the models. During the fitting procedures the stability constant  $K_{21}$  was fixed to the statistical estimated value obtained with the equations  $K_{21} = K_m^2$  for a monotopic ligand (v.i., Scheme 2) and to  $K_{21} = 4K_m^2$  for a ditopic ligand (see above, Scheme 1). The  $K_m$  values for each type of N-Zn interaction were determined in previous studies on the topic.

**Table 1.** Thermodynamic or macroscopic stability constant values for complexes formed by the bis-porphyrin **Zn<sub>2</sub>-14** and the nitrogen ligands calculated using SPECFIT.  $K_{21}$  was fixed to the estimated statistical value.

| <b>Zn<sub>2</sub>-14</b>  |   |  |
|---|---|--|
| <b>N-ligands</b>  | <b>1:1 Complex</b>  | <b>2:2 Complex</b>   |
| <b>Pyridine</b> <sup>6</sup><br>$K_m = 3.75 \times 10^3 \text{ M}^{-1}$       | $K_{11} = 9.40 \times 10^3 \text{ M}^{-1}$<br>$K_{21} = 1.40 \times 10^7 \text{ M}^{-2}$    | -  |
| <b>Quinuclidine</b> <sup>7</sup><br>$K_m = 4.00 \times 10^4 \text{ M}^{-1}$   | $K_{11} = 9.55 \times 10^4 \text{ M}^{-1}$<br>$K_{21} = 1.60 \times 10^9 \text{ M}^{-2}$    | -  |
| <b>DABCO</b> <sup>7</sup><br>$K_m = 8.90 \times 10^4 \text{ M}^{-1}$          | $K_{11} = 8.71 \times 10^5 \text{ M}^{-1}$<br>$K_{21} = 3.17 \times 10^{10} \text{ M}^{-2}$ | $K_{22} = 7.59 \times 10^{17} \text{ M}^{-4}$<br>$K_{21} = 3.17 \times 10^{10} \text{ M}^{-2}$ |
| <b>4,4'-bipyridyl</b> <sup>8</sup><br>$K_m = 4.00 \times 10^3 \text{ M}^{-1}$ | $K_{11} = 4.89 \times 10^4 \text{ M}^{-1}$<br>$K_{21} = 6.40 \times 10^7 \text{ M}^{-2}$    | $K_{22} = 3.05 \times 10^{15} \text{ M}^{-4}$<br>$K_{21} = 6.40 \times 10^7 \text{ M}^{-2}$    |

<sup>6</sup> Satake, A.; Kobuke, Y. *Tetrahedron* **2005**, *61*, 13-41.

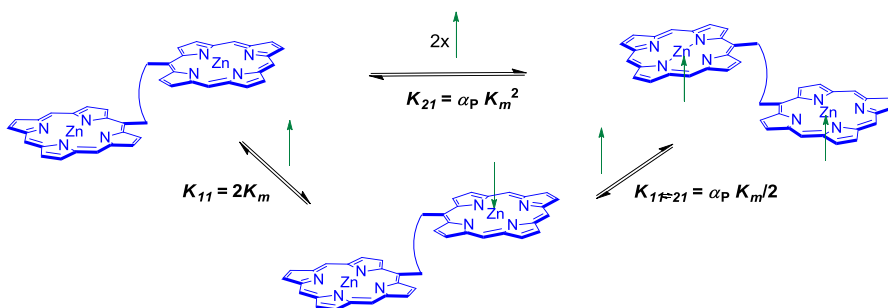
<sup>7</sup> Ballester, P.; Costa, A.; Castilla, A. M.; Deya, P. M.; Frontera, A.; Gomila, R. M.; Hunter, C. A. *Chem.--Eur. J.* **2005**, *11*, 2196-2206.

<sup>8</sup> Camara-Campos, A.; Hunter, C. A.; Tomas, S. *Proc. Natl. Acad. Sci. U. S. A.* **2006**, *103*, 3034-3038.

**Table 2.** Thermodynamic or macroscopic stability constant values for complexes formed by the bis-porphyrin **Zn<sub>2</sub>-15** and the nitrogen ligands calculated using SPECFIT.  $K_{21}$  was fixed to the estimated statistical value.

| <b>Zn<sub>2</sub>-15</b>  |   |  |
|---|---|--|
| <b>N-ligands</b>  | <b>1:1 Complex</b>  | <b>2:2 Complex</b>   |
| <b>Pyridine</b> <sup>6</sup><br>$K_m = 3.75 \times 10^3 \text{ M}^{-1}$       | $K_{11} = 5.25 \times 10^3 \text{ M}^{-1}$<br>$K_{21} = 1.40 \times 10^7 \text{ M}^{-2}$    | -  |
| <b>Quinuclidine</b> <sup>7</sup><br>$K_m = 4.00 \times 10^4 \text{ M}^{-1}$   | $K_{11} = 8.40 \times 10^4 \text{ M}^{-1}$<br>$K_{21} = 1.60 \times 10^9 \text{ M}^{-2}$    | -  |
| <b>DABCO</b> <sup>7</sup><br>$K_m = 8.90 \times 10^4 \text{ M}^{-1}$          | $K_{11} = 1.00 \times 10^6 \text{ M}^{-1}$<br>$K_{21} = 3.17 \times 10^{10} \text{ M}^{-2}$ | $K_{22} = 1.50 \times 10^{18} \text{ M}^{-4}$<br>$K_{21} = 3.17 \times 10^{10} \text{ M}^{-2}$ |
| <b>4,4'-bipyridyl</b> <sup>8</sup><br>$K_m = 4.00 \times 10^3 \text{ M}^{-1}$ | $K_{11} = 2.75 \times 10^5 \text{ M}^{-1}$<br>$K_{21} = 6.40 \times 10^7 \text{ M}^{-2}$    | $K_{22} = 2.09 \times 10^{16} \text{ M}^{-4}$<br>$K_{21} = 6.40 \times 10^7 \text{ M}^{-2}$    |

The stability constant values calculated from the titrations with the monotopic amines allowed us to derive the cooperativity factor of the bis-porphyrin,  $\alpha_P$ , in order to distinguish differences between the first and the second intermolecular interaction (N-Zn) of the ligand with the porphyrin and establishing the existence of negative or positive cooperativity in the system. The second intermolecular interaction between the nitrogen ligand and the zinc bis-porphyrin can be affected by the first binding event or both binding sites can act completely independent (this concept was explained in the general introduction of this thesis).



**Scheme 2.** Schematic representations of the possible binding equilibria involved in the complexation of a monotopic ligand (green arrow) with a zinc bis-porphyrin.

The cooperativity factors  $\alpha_P$  were calculated from the stepwise equilibrium binding constant  $K_{11\leftrightarrow 21}$  which is related to the overall calculated binding constants,  $K_{11}$  and  $K_{21}$  by following equation, equation 1:

$$K_{11\leftrightarrow 21} = \frac{K_{21}}{K_{11}}$$

(Equation 1)

Once the values of  $K_{11\leftrightarrow 21}$  are determined, the  $\alpha_P$  factor is directly calculated using equation 2, which relates  $K_{11\leftrightarrow 21}$  with  $K_m$ :

$$K_{11\leftrightarrow 21} = \alpha_P \frac{K_m}{2}$$

(Equation 2)

Table 3 summarizes the values for  $K_{11\leftrightarrow 21}$  and the cooperativity factors  $\alpha_P$  of the two acyclic Zn-bis-porphyrins **Zn2-14** and **Zn2-15** interacting with the monotopic nitrogen ligands pyridine and quinuclidine.

**Table 3.** Calculated values for the  $K_{11\leftrightarrow 21}$  equilibrium constant and the  $\alpha_P$  cooperativity factors in the binding of the two monotopic nitrogen ligands with **Zn<sub>2</sub>-14** and **Zn<sub>2</sub>-15**.

| <i>Bis-porphyrin</i><br><i>Ligand</i> | <b>Zn<sub>2</sub>-14</b>                      |            | <b>Zn<sub>2</sub>-15</b>                      |            |
|---------------------------------------|---|------------|---|------------|
|                                       | $K_{11\leftrightarrow 21}$ (M <sup>-1</sup> ) | $\alpha_P$ | $K_{11\leftrightarrow 21}$ (M <sup>-1</sup> ) | $\alpha_P$ |
| <b>Pyridine</b>                       | 1.49 x 10 <sup>3</sup>                        | 0.80       | 2.66 x 10 <sup>3</sup>                        | 1.42       |
| <b>Quinuclidine</b>                   | 1.68 x 10 <sup>4</sup>                        | 0.84       | 1.90 x 10 <sup>4</sup>                        | 0.95       |

The values determined for  $K_{11\leftrightarrow 21}$  with the two bis-porphyrins and the same amine are coincident within experimental error. As expected, the  $K_{11\leftrightarrow 21}$  values for quinuclidine are one order of magnitude larger than for pyridine. For the two bis-porphyrins and using any of the two monotopic amines, the value determined for  $\alpha_P$  is very close to one. This result indicates that the two porphyrin units in the bis-porphyrin receptors act as independent binding sites.<sup>4</sup>

Table 4 and 5 summarize the EM values that we have calculated from the stability constant values determined for the sandwich complexes with the UV-visible titrations. There are two different set of EM values depending on the binding model used to fit the titration data (Table 4 and Table 5 for 1:1 and 2:2 sandwich complexes respectively). The physical interpretation of the EM values corresponds to a sometimes hypothetical concentration necessary to induce the conversion of 50 % of the sandwich complex into open complex. It also quantifies the thermodynamic stabilization of the sandwich complex due to the intramolecular nature of one of the interactions involved in the structures of the sandwich architectures. The EM's were calculated using equation 3, for the 1:1 sandwich complexes and equation 4 for the 2:2 aggregates. The calculated values of EM shown in tables 4 and 5 fall within the previously reported range in the case of DABCO and do not help to distinguish between the two possible sandwich complexes.<sup>9</sup> For the largest ligand, 4,4'-bipyridyl, the EM values are more reasonable for the 1:1 complex, as we said before when the molecular modelling studies were made.

<sup>9</sup> Chi, X. L.; Guerin, A. J.; Haycock, R. A.; Hunter, C. A.; Sarson, L. D. *J. Chem. Soc., Chem. Commun.* **1995**, 2563-2565.

$$K_{11} = EM \cdot K_m^2$$

(Equation 3)

$$K_{22} = EM \cdot K_m^4$$

(Equation 4)

**Table 4.** Effective molarities for the 1:1 complexes formed between bis-porphyrins **Zn<sub>2</sub>-14** and **Zn<sub>2</sub>-15** with the two bidentate nitrogen ligands.

|                       | <b>Zn<sub>2</sub>-14</b> | <b>Zn<sub>2</sub>-15</b> |
|-----------------------|--------------------------|--------------------------|
|                       | <b>EM (M)</b>            |                          |
| <b>DABCO</b>          | 1.10 x 10 <sup>-4</sup>  | 1.26 x 10 <sup>-4</sup>  |
| <b>4,4'-bipyridyl</b> | 30.60 x 10 <sup>-4</sup> | 170 x 10 <sup>-4</sup>   |

**Table 5.** Effective molarities for the 2:2 complexes formed between bis-porphyrins **Zn<sub>2</sub>-14** and **Zn<sub>2</sub>-15** with the two bidentate nitrogen ligands.

|                       | <b>Zn<sub>2</sub>-14</b> | <b>Zn<sub>2</sub>-15</b> |
|-----------------------|--------------------------|--------------------------|
|                       | <b>EM (M)</b>            |                          |
| <b>DABCO</b>          | 0.012                    | 0.024                    |
| <b>4,4'-bipyridyl</b> | 11.91                    | 81.64                    |

## b. <sup>1</sup>H NMR titrations

We also probed the complexation process of the series of bis-porphyrin receptors with the different amine ligands using <sup>1</sup>H NMR spectroscopy in CDCl<sub>3</sub> solutions and at room temperature. For the sake of space, the experiments discussed in this section refer only to the results obtained in the complexation process with the ditopic amines. These studies were performed to gain further insight into the structure of the complexes. The concentration used in the <sup>1</sup>H NMR experiments (~ 1 mM) is too high for the accurate determination of association constants higher than 10<sup>4</sup> M<sup>-1</sup>.

We did not observe significant differences in the complexation processes involving the receptors **Zn<sub>2</sub>-14** or **Zn<sub>2</sub>-15** and the ditopic ligands when studied by <sup>1</sup>H NMR spectroscopy.

For both receptors, the addition of 0.5 equivalents of DABCO induced the appearance of a singlet resonating at  $\delta = -5$  ppm. This signal corresponds to the methylene protons of the DABCO sandwiched between two porphyrin units.<sup>10</sup> The signal remained sharp and did not experience any chemical shift change until the addition of 1 equivalent of DABCO. Moreover, the first additions of DABCO produced a broadening of the proton signals of the bis-porphyrin receptor and the emergence of a new set of signals corresponding to the protons of the receptor in the sandwich complex. The free and bound proton signals of the receptors are in slow exchange on the NMR time scale. The proton signals corresponding to the bound receptor increase to the expenses of the proton signals of free receptor with the incremental addition of DABCO. The upfield shift experienced by the  $\beta$ -pyrrolic protons is also a consequence of the mutual ring current effects of the porphyrins units involved in the sandwich.<sup>11</sup> When more than 1 equivalent of DABCO is added the proton signals of the bound bis-porphyrin start shifting downfield and the DABCO signal at -5 ppm broadens and even disappear. At this point, the titration enters in a fast chemical exchange regime on the <sup>1</sup>H NMR time scale. What is happening is that a new equilibrium between the 1:1 sandwich complex and the 2:1 open complex is established in the presence of more than 1 equivalent of DABCO. Figure 10 shows, as an example, a set of <sup>1</sup>H NMR spectra acquired in the titration of **Zn<sub>2</sub>-14** with DABCO and the **Zn<sub>2</sub>-15** bis-porphyrin behaves identically.

---

<sup>10</sup> Anderson, H. L.; Hunter, C. A.; Meah, M. N.; Sanders, J. K. M. *J. Am. Chem. Soc.* **1990**, *112*, 5780-5789.

<sup>11</sup> Taylor, P. N.; Anderson, H. L. *J. Am. Chem. Soc.* **1999**, *121*, 11538-11545.

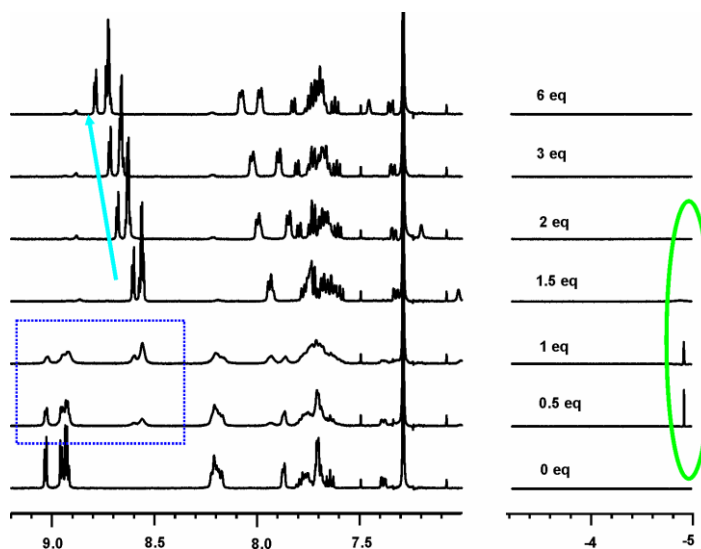


**Figure 10.** Selected regions for the  $^1\text{H}$  NMR spectra acquired in the titration of bis-porphyrin **Zn<sub>2</sub>-14** with the bidentate amine, DABCO, in  $\text{CDCl}_3$  at 298K. The bound DABCO signals are circled in green, a blue dashed square shows the region where the system is in slow exchange, and the blue arrow is marking when the porphyrin signals shifted downfield.

When 4,4'-bipyridyl is used as the ditopic ligand the addition of 0.5 equivalents of diamine to both receptors induces upfield shifts in their proton signals. The upfield shift of the signals continues until 1 equivalent of bipy has been added. The addition of more than 1 equivalent of bipy provokes the shifting of the receptors signals to the downfield region. The observation of such a biphasic behavior constitutes a clear indication of the existence of complexes with different stoichiometry in solution. In this case, the formation of the sandwich complex and its destruction to yield the open complex are processes that take place under fast chemical exchange. Two set of doublets for the protons of the sandwiched bipy appear, at  $\delta = 2.1$  and  $4.7$  ppm. This large upfield shift experienced by the proton signals of the bipy ( $\Delta\delta = -4.65$  and  $-3.3$  ppm respectively; the free bipy presents two doublets at  $8.75$  and  $8$  ppm) indicates the axial coordination of the ligand and inclusion between the two porphyrins. When more than 1 equivalent of bipy is added the bound ligand also participates in a fast exchange equilibrium in the NMR time scale with the free ligand which was almost absent up to this point. At this stage the signals of coordinated bipy broaden and finally disappear. When 20 equivalents of bipy are added, broad signals

corresponding with averaged chemical shift values for free and bound bipy are observable. Figure 11 shows a titration of **Zn<sub>2</sub>-15** with 4,4'-bipyridyl as an example. We observed a complete analogous behavior for **Zn<sub>2</sub>-14**. The most important difference is that the addition of only 4 equivalents of bipy to **Zn<sub>2</sub>-14** produced proton signals with chemical shift values close to those of the free ligand. This result indicates that the destruction of 1:1 sandwich complex, bipy•**Zn<sub>2</sub>-14**, occurs with the addition of lower equivalents of bipy, as it was demonstrated with the value of EM for **Zn<sub>2</sub>-15** with bipy.

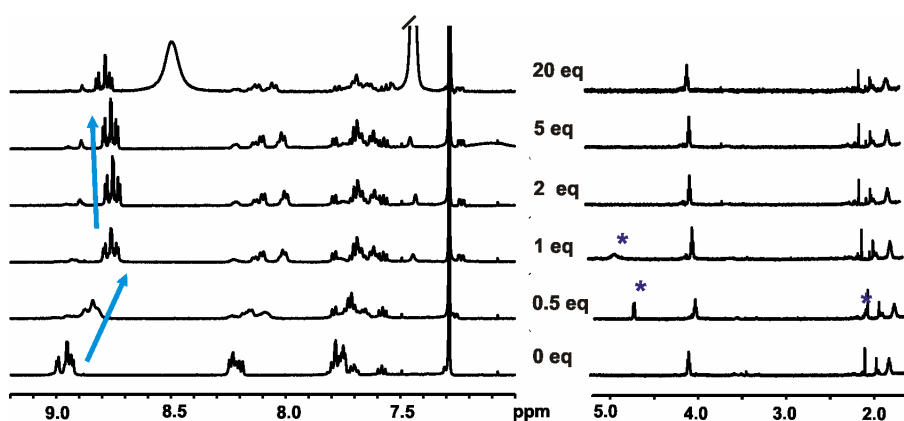


**Figure 11.** Selected regions of the <sup>1</sup>H NMR spectra acquired in the titration of bis-porphyrin **Zn<sub>2</sub>-15** with the bidentate amine, 4,4'-bipyridyl, in CDCl<sub>3</sub> at 298K. The bound bipy signals are marked with an asterisk, and the blue arrows are signaling when the porphyrin signals shifted upfield and then downfield.

We also performed a DOSY (Diffusion-Ordered SpectroscopY) experiment of **Zn<sub>2</sub>-14** in the presence of 1 equivalent of DABCO. The DOSY technique provides a big insight to know the size and hence, the stoichiometries of self-assembled structures.<sup>12</sup>

<sup>12</sup>Macchioni, A.; Ciancaleoni, G.; Zuccaccia, C.; Zuccaccia, D. *Chem. Soc. Rev.* **2008**, *37*, 479-489.

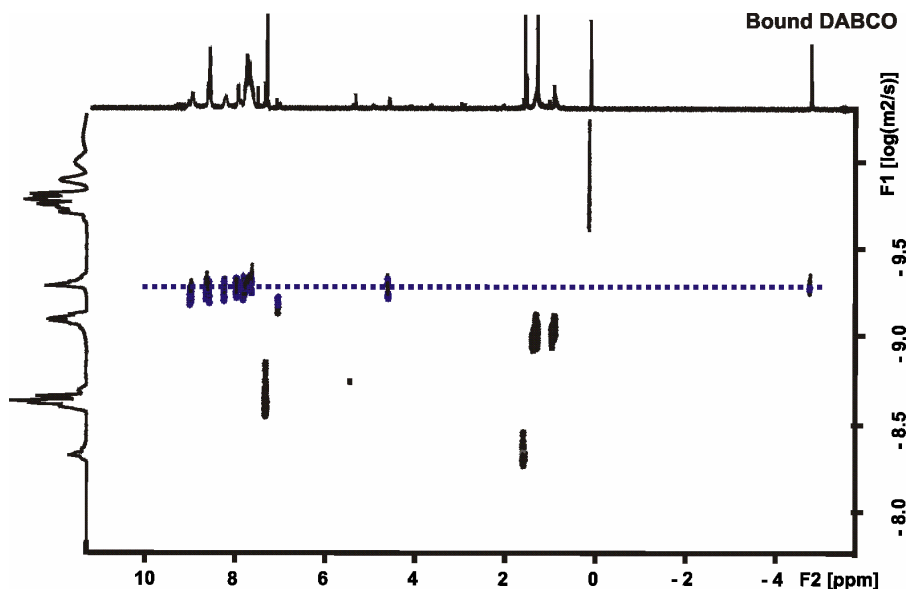


**Figure 12.** DOSY profile of bis-porphyrin **Zn<sub>2</sub>-14** in the presence of 1 equivalent of DABCO in CDCl<sub>3</sub> at 298 K and millimolar concentration.

From this DOSY experiment we were able to calculate an average diffusion coefficient,  $D$ , from the integration of different signals of the complex and applying a simple one-component exponential fit<sup>13</sup> using the T1/T2 module of the Bruker software Topspin 1.3. Figure 12 shows the DOSY experiment of the complex formed by DABCO and **Zn<sub>2</sub>-14** where it is easy to see that the protons of the receptor and DABCO have the same diffusion coefficient indicating that they belong to same supramolecular aggregate. We integrated the decay of five protons signals and fit the obtained values to the monoexponential equation for the decay of the intensity in a field gradient. The average value of the diffusion coefficient was  $D = 4.39 \times 10^{-10} \text{ m}^2 \text{ s}^{-1}$ . Using the calibration curve available in our group,<sup>13</sup> we estimated the molecular weight of the complex as 1690 g mol<sup>-1</sup>. The molecular weight of the 1:1 complex is 1574 g mol<sup>-1</sup>, so the calculated value only deviates 7.4% with respect to the real molecular weight of the 1:1 complex. The obtained result supports the hypothesis that the bis-porphyrins selectively include a DABCO molecule between two porphyrin units forming a 1:1 sandwich complex instead of the 2:2

<sup>13</sup> Oliva, A. I.; Gomez, K.; Gonzalez, G.; Ballester, P. *New J. Chem.* **2008**, *32*, 2159-2163.

complex. Figure 13 depicts the fit of the decay of one of the integrated proton signals of the DOSY experiment to the theoretical exponential curve decay.

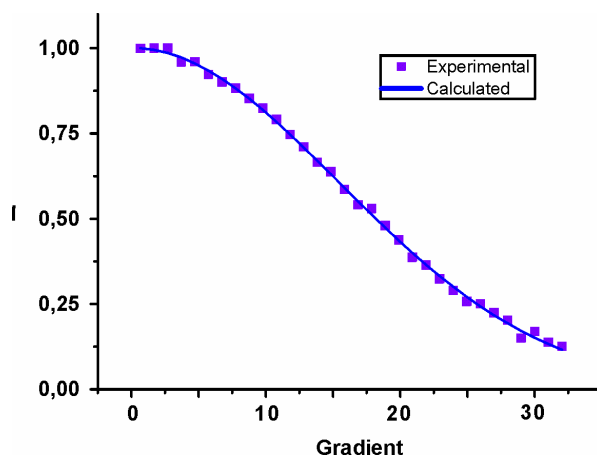


**Figure 13.** Data points for the decay of one of the signals of the complex with DABCO and **Zn<sub>2</sub>-14**, from the experimental data in figure 12, fitted to the monoexponential theoretical decay curve (solid line).

The analysis of the UV-visible titration data obtained for DABCO and the acyclic bis-porphyrin receptors did not produce convincing evidence for the stoichiometry of the sandwich complex. However, the results derived from the DOSY experiment unequivocally assigned a 1:1 stoichiometry the sandwich complex with DABCO. We expected a similar result from the DOSY experiment carried out with the sandwich complex derived from bipy. A DOSY experiment carried out on a chloroform solution of **Zn<sub>2</sub>-14** containing 1 equivalent of bipy and using the same procedure described above allowed the calculation of diffusion coefficient value of  $D = 4.37 \times 10^{-10} \text{ m}^2 \text{ s}^{-1}$  for the sandwich complex. Using the calibration curve, we calculated a molecular weight for such species of  $1712 \text{ g mol}^{-1}$ . This value represents a small deviation of only 5.7% with respect to the molecular weight of  $1618.53 \text{ g mol}^{-1}$  for the bipy•**Zn<sub>2</sub>-14** and certifies the formation of the sandwich with 1:1 stoichiometry.

## 2.2 Binding studies of bis-porphyrin macrocycles with ditopic amines

The binding studies of the two cyclic bis-porphyrin receptors, **Zn<sub>2</sub>-17** and **Zn<sub>2</sub>-18** (Figure 14), were carried out only using ditopic amines as guest. In addition to the complexation with DABCO and 4,4'-bipyridyl, we also studied in the complexation with TMEDA. TMEDA is also a ditopic amine which was used as the Cu(I) ligand and template in the Hay coupling reaction used in the synthesis of **Zn<sub>2</sub>-17**. Luckily, we were able to grow single crystals of the TMEDA•**Zn<sub>2</sub>-17** and solve its structure in the solid state by X-ray diffraction analysis (see chapter 2).

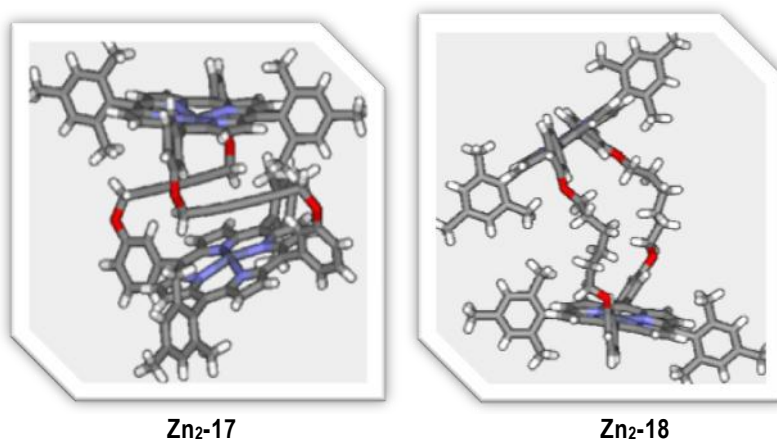


**Figure 14.** Molecular structures of the two macrocycles, **Zn<sub>2</sub>-17** and **Zn<sub>2</sub>-18**. The structures were obtained from an energy minimization using CAChe<sup>2</sup> and the solid state structures as input.

### a. UV-visible titrations

As we did before with the acyclic bis-porphyrins, the UV-visible titrations were carried out at micromolar concentrations. UV spectra of the three titrations of **Zn<sub>2</sub>-17** with the ditopic ligands are shown in figure 15. The behavior observed in the titrations is very similar to the one described previously for the acyclic receptors **Zn<sub>2</sub>-14** and **Zn<sub>2</sub>-15**. In the initial phase of the titration a 1:1 sandwich complex is formed. The 1:1 sandwich complex opens up in the presence of excess of the ditopic diamine ligand to afford open 2:1 complexes in a

second phase of the titrations. The existence of two different and consecutive binding equilibria can also be substantiated from the existence of two isosbestic point in most of the titrations. To simplify the discussion, we will only show the titration spectra obtained for **Zn<sub>2</sub>-17**, but we report the stability constant values calculated for the complexes formed by the series of ditopic diamines with the cyclic receptors **Zn<sub>2</sub>-17** and **Zn<sub>2</sub>-18**.

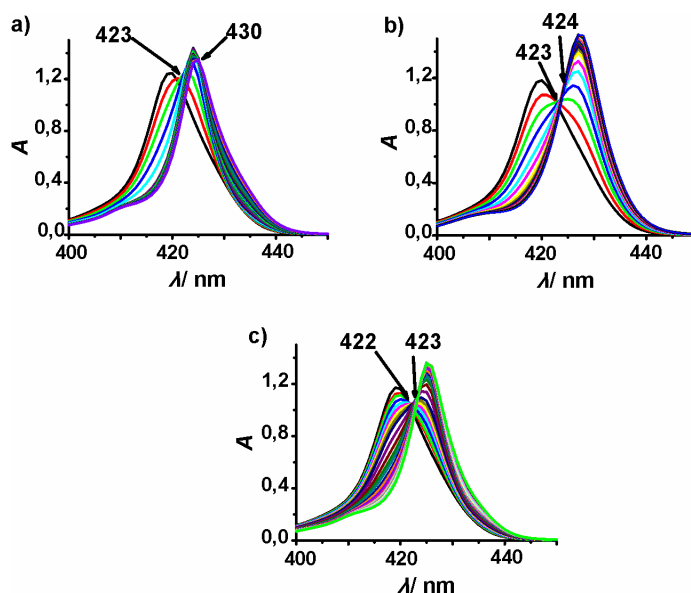
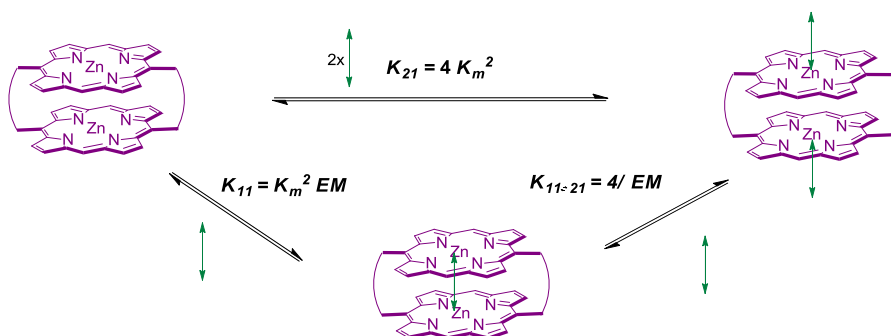


**Figure 15.** UV-visible titration spectra (Soret region) of cyclic bis-porphyrin **Zn<sub>2</sub>-17** with the three ditopic nitrogen ligands in chloroform. a) DABCO, 0 to 4000 equivalents added; b) bipy, 0 to 2000 equivalents added; c) TMEDA, 0 to 3000 equivalents added. The concentration of **Zn<sub>2</sub>-17** was maintained constant throughout the titration,  $[\text{Zn}_2\text{-17}] = 1.50 \times 10^{-6}$  M in the three cases. The observed isosbestic points, one for each phase of the titration, are indicated by an arrow.

The free metallated bis-porphyrin **Zn<sub>2</sub>-17** features an absorption Soret band centered at 419 nm. Figure 15a, depicts the UV-visible spectra obtained in the titration with DABCO. In this case, the initial formation of the 1:1 sandwich complex produces a shift in the Soret band to 424 nm. The sandwich complex is highly stable thermodynamically and requires the addition of 3200 equivalents of diamine to produce the subsequent decrease of intensity and red shift of the Soret band assignable to the formation of the 2:1 open complex.

Figure 15b corresponds to the titration with 4,4'-bipyridine. Based on molecular modelling studies the structure of this diamine also enables the formation of 1:1 sandwich complex. The initial phase of the titration shows the appearance of an isosbestic point and a red shift of the Soret band to 427 nm. We assign this shift to the formation of the 1:1 complex having a reduced exciton coupling between the porphyrin units due to the larger distance spanning them compared to the DABCO complex. However, the incremental addition of bipy provokes that the initially formed Soret band with maximum at 427 nm rapidly shifts further to the red to 430 nm with the appearance of a new isosbestic point. This phase of the titration corresponds to the opening of the 1:1 complex yielding the linear 2:1 assembly. The fact that only 1500 equivalents of bipy are required to induce the destruction of the 1:1 complex points out to a reduced thermodynamic stability compared to the one formed with DABCO. In each one of the three UV-visible titration experiments we detect two isosbestic points, indicative of two consecutive two-state equilibria corresponding to the free porphyrin being converted to the 1:1 complex and its destruction to afford the open 2:1 complex.

We performed the mathematical analysis of the titration data using the SPECFIT software and a binding model considering three UV-active species: free porphyrin, 1:1 and 2:1 complexes. During the data fitting the value of  $K_{21}$  was maintained fixed to the statistical value estimated using the formula  $K_{21} = 4K_m^2$  (v.i., Scheme 3). The corresponding  $K_m$  (microscopic stability constant of the N-Zn interaction) values for each diamine were derived from previous studies on the topic and from the titration of the Zn-monoporphyrin (Zn-TPP) with TMEDA performed in this study (Table 6).



**Scheme 3.** Schematic representations of the possible equilibria involved in the binding of a ditopic ligand (green arrow) to a cyclic zinc bis-porphyrin.

**Table 6.** Thermodynamic or macroscopic constants calculated for the complexes formed by the cyclic bis-porphyrin **Zn<sub>2</sub>-17** and **Zn<sub>2</sub>-18** and the diamine series using SPECFIT. The value of  $K_{21}$  was fixed to the statistical value.

| N-ligands   | Bis-porphyrins   | Zn <sub>2</sub> -17   | Zn <sub>2</sub> -18   |
|---|--|---|---|
|   | <b>DABCO</b> <sup>7</sup><br>$K_m = 8.90 \times 10^4 \text{ M}^{-1}$                     | $K_{11} = 2.88 \times 10^6 \text{ M}^{-1}$<br>$K_{21} = 3.17 \times 10^{10} \text{ M}^{-2}$ | $K_{11} = 1.71 \times 10^6 \text{ M}^{-1}$<br>$K_{21} = 3.17 \times 10^{10} \text{ M}^{-2}$ |
| <b>4,4'-bipyridyl</b> <sup>8</sup><br>$K_m = 4.00 \times 10^3 \text{ M}^{-1}$ | $K_{11} = 3.93 \times 10^5 \text{ M}^{-1}$<br>$K_{21} = 6.40 \times 10^7 \text{ M}^{-2}$ | $K_{11} = 3.70 \times 10^5 \text{ M}^{-1}$<br>$K_{21} = 6.40 \times 10^7 \text{ M}^{-2}$    |   |
| <b>TMEDA</b> <sup>a</sup><br>$K_m = 3.60 \times 10^2 \text{ M}^{-1}$          | $K_{11} = 4.79 \times 10^6 \text{ M}^{-1}$<br>$K_{21} = 1.27 \times 10^5 \text{ M}^{-2}$ | $K_{11} = 8.88 \times 10^5 \text{ M}^{-1}$<br>$K_{21} = 1.27 \times 10^5 \text{ M}^{-2}$    |   |

<sup>a</sup> Calculated from the titration of TMEDA with Zn-TPP.

Table 7 summarizes the calculated EM values which quantify the thermodynamic stabilization due to intramolecular interactions in the 1:1 sandwich complexes. The corresponding EM's were calculated from equation 3, as before, related to  $K_{11}$  and  $K_m$ :

$$K_{11} = EM \cdot K_m^2$$

(Equation 3)

**Table 7.** Effective molarities for the 1:1 complexes formed between bis-porphyrins **Zn<sub>2</sub>-17** and **Zn<sub>2</sub>-18** and the three bidentate nitrogen ligands.

|                       | <b>Zn<sub>2</sub>-17</b> | <b>Zn<sub>2</sub>-18</b> |  |
|-----------------------|--------------------------|--------------------------|--|
|                       | <b>EM (M)</b>            |                          | <b>EM(Zn<sub>2</sub>-17)/EM(Zn<sub>2</sub>-18)</b> |
| <b>DABCO</b>          | 0.0004                   | 0.0002                   | 2  |
| <b>4,4'-bipyridyl</b> | 0.025                    | 0.023                    | 1  |
| <b>TMEDA</b>          | 37                       | 7                        | 5.2  |

The first conclusion that can be drawn from the EM values summarised in table 7 is that cyclic bis-porphyrin **Zn<sub>2</sub>-17**, the one with the triple bonded chain, forms more stable complexes with the diamines than the cyclic dimer with the flexible linker chains, **Zn<sub>2</sub>-18**, for the shortest diamines DABCO and TMEDA. 4,4-bipyridyl is adapted equally well to both macrocycles. It is noticed that the flexible ligand, TMEDA, take profit of this feature and the 1:1 complexes increment their stability in one order of magnitude with respect to the complexes formed with the rigid diamines.

### b. <sup>1</sup>H NMR titrations

We also carried out titrations in CDCl<sub>3</sub> at millimolar concentrations using <sup>1</sup>H NMR spectroscopy at room temperature in order to gain additional information on the structure of the inclusion 1:1 complexes.

The behavior in the complexation process of **Zn<sub>2</sub>-17** and **Zn<sub>2</sub>-18** with each one of the ditopic diamines is very similar. The main differences we observed can be related to the relative thermodynamic stability between the 1:1 sandwich complex and the 2:1 open complex. The EM value is the physical parameter used to quantify the concentration of the ligand at which 50% of the bis-porphyrin is involved in the 1:1 sandwich complex and the

other 50% forms the 2:1 open complex. The higher the EM value a larger number of equivalents of ligands will be necessary to induce its destruction. The experiments discussed in this section are selected examples representative to the general behavior we observed.

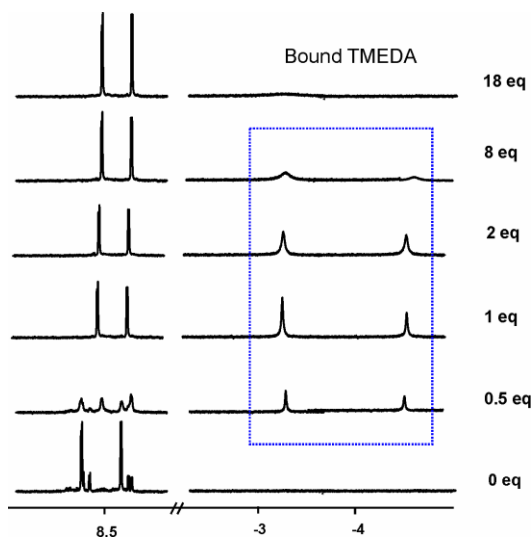


**Figure 16.** Selected regions of the  $^1\text{H}$  NMR titration of bis-porphyrin  $\text{Zn}_2\text{-17}$  with the bidentate amine, TMEDA, in  $\text{CDCl}_3$  at 298K. The bound TMEDA signals are in a blue dashed square.

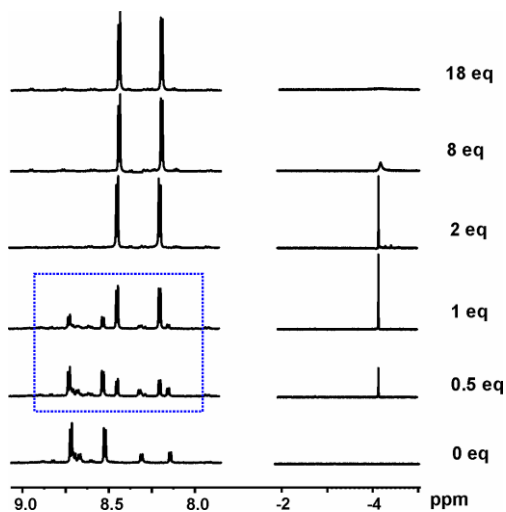


**Figure 17.** Selected regions of the  $^1\text{H}$  NMR titration of bis-porphyrin  $\text{Zn}_2\text{-18}$  with the DABCO, in  $\text{CDCl}_3$  at 298K. A blue dashed square shows the region where the system is in slow exchange.

The complexation behavior observed by  $^1\text{H}$  NMR during the titration of the two macrocyclic receptors with the diamine series is similar to the one described for the tweezers receptors. In all cases, the initial addition of the ditopic ligand induces the formation of a 1:1 inclusion or sandwich complex through a slow chemical exchange. Separate signals for the free and bound receptor can be observed. The remarks of the 1:1 complex are the high upfield signals detected for the protons of the included ligands. When 1 equivalent of ditopic ligand is added the 1:1 complex is the only species detected in the  $^1\text{H}$  NMR spectra. An increase in the concentration of the ditopic ligand causes the destruction of the 1:1 complex and the concomitant formation of the 2:1 open complex through a fast chemical exchange equilibrium not only for the proton signals of the receptor but also for those of the ditopic ligand. We were able to grow single crystals from the 1:1 complexes  $\text{TMEDA}\cdot\text{Zn}_2\mathbf{17}$  and  $\text{DABCO}\cdot\text{Zn}_2\mathbf{18}$ . The solid state structures of these complexes (Figure 18 and chapter 2) reveal the expected sandwich motif. The ditopic ligand is included in the cavity sandwiched between the two porphyrin units. This finding is in complete agreement with the results obtained in solution.

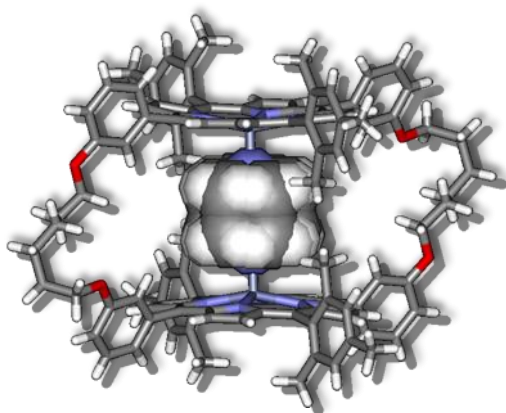


**Figure 18.** X-ray crystal structure of the  $\text{DABCO}\cdot\text{Zn}_2\mathbf{18}$  1:1 complex. The distance between the two Zn atoms of cofacial porphyrins is 6.975 Å. Both Zn atoms are pushed through the inner of the cavity, so the porphyrins lose the planarity.

### 3. Conclusions

Complexation studies with different mono and ditopic amines have been carried out using two series of zinc bis-porphyrins; one series consisted on two acyclic receptors with slightly different conformational flexibility due to the degree of saturation of the carbon chain used to span the porphyrin units, the other one included two macrocyclic analogs. The methods used for probing the interactions between the receptors and the amines were UV-visible and  $^1\text{H}$  NMR titrations. Both methods are complementary and require different experimental working conditions, specially the concentration of the host.

In the case of the acyclic or tweezer bis-porphyrin receptors, based on geometric requirements the sandwich complexes could be formed with 1:1 or 2:2 stoichiometry. The data from the UV-visible titration experiments fitted equally well to two theoretical binding models. However, DOSY experiments unequivocally assigned a 1:1 stoichiometry to the sandwich complexes being formed in solution. The acyclic bis-porphyrin receptors are highly flexible and can adopt conformations that are complementary for the ditopic binding of diamine ligands with very different shape and sizes like DABCO or bipy with high association constants. Surprisingly, not only the tweezers receptors are highly flexible, their macrocyclic counterparts, also display a similar conformational propensity. The macrocyclic receptors series also forms highly stable thermodynamic 1:1 complexes with three different diamines. The values of the stability constants determined for the 1:1 complexes of the cyclic receptors are larger than for the acyclic counterparts since the former benefit from the macrocyclic effects.

### 4. Experimental section

#### 4.1 General information and instrumentation

$^1\text{H}$  NMR spectra were recorded on Bruker Avance 400 (400.1 MHz for  $^1\text{H}$  NMR) and Bruker Avance 500 (500.1 MHz for  $^1\text{H}$  NMR) NMR spectrometers. UV-visible spectra were measured on a UV-Vis spectrophotometer Shimadzu UV-2401PC.

Diffusion experiments were carried out on a 500 MHz Avance NMR spectrometer using a 5 mm BBI probe-head equipped with a Z-gradient capable of generating 55 G cm<sup>-1</sup> field strengths. The temperature (298 K) was monitored using a BVT-3000 temperature unit and calibrated with a 4% methanol in methanol-d<sub>4</sub> sample. The gradient shape was sinusoidal, its duration was 1 ms and its strength (G) was varied automatically in the course of the experiment. The strength of the gradient shape was increased linearly, acquiring 32 gradient levels. The time between the mid-points of the gradients, D, was chosen as 150 ms. Low and high gradient strengths were set at 2% and 95% of maximum, respectively. The measurements were carried out with sample spinning and with external airflow. Thermal convection was minimized through rotation of the sample in all experiments.<sup>16</sup> All DOSY experiments were obtained with a longitudinal eddy-current delay (LED) bipolar gradient pulse pair and two spoil gradients pulse sequence (ledbpgp2s)<sup>17</sup> in the standard Bruker pulse sequence library. All experiments were processed with standard Bruker 1D and 2D DOSY software.

Crystal data set were collected at Beam line BM16<sup>14</sup> at ESRF wavelength = 0.7380 Å; Si111 monochromator; absorption coefficient = 0.553 mm<sup>-1</sup>; ADSC Q210r CCD detector and cooled with an Oxford Cryostream low temperature device ( $T = 100(2)$  K). Full-sphere data collection was used with  $\varphi$  scans.

Programs used: Data collection MXCube, Indexing Apex2 V2009.11 (Bruker-Nonius 2008), data reduction Saint + Version 7.60A (Bruker AXS 2008) and absorption correction SADABS V. 2008/1 (2008). *Structure Solution*: SIR2007.<sup>15</sup> and SHELXTL Version 6.10 (Sheldrick, 2000) was used.<sup>16</sup> *Structure Refinement*: SHELXTL-97-UNIX VERSION.

---

<sup>14</sup> The macromolecular crystallography station at beamline BM16 at the ESRF Juanhuix, J.; Labrador, A.; Beltran, D.; Herranz, J. F.; Carpentier, P.; Bordas, J. *Rev. Sci. Instrum.* **2005**, *76*, -. 086103.

<sup>15</sup> Caliendo, R.; Carrozzini, B.; Cascarano, G. L.; De Caro, L.; Giacobazzo, C.; Siliqi, D. *J. Appl. Crystallogr.* **2007**, *40*, 883-890.

<sup>16</sup> Sheldrick, G. M. *SHELXTL Crystallographic System 6.14*, Bruker AXS Inc., Madison, Wisconsin, **2000**.

## 4.2 Binding studies

### a. UV-visible titrations

The UV-visible titration was carried out at 25 °C by running a spectrum of the host solution of the bis-porphyrins in CHCl<sub>3</sub>, at 1 μM in a 1 cm path length quartz cuvette, and adding incremental aliquots of an amine solution. To avoid the dilution of the host solution the titrating guest solution was prepared using the solution of the host as the solvent. After each addition of guest a new UV-visible spectrum was obtained. The set of data obtained from the UV-visible spectrophotometric titration (25-35 points) were analyzed by fitting the whole series of spectra at 1 nm interval for the UV-visible titration using the software SPECFIT 3.0, which uses a global system with expanded factor analysis and Marquardt least-squares minimization to obtain globally optimized parameters.

### b. <sup>1</sup>H NMR titrations

Standard solutions of Zn-bis-porphyrins (1 mM) were prepared and using those solutions as solvent, an amine solution (10 mM) that will be used for the titration experiments was prepared. In this way the incremental addition of amine to the initial porphyrin solution will not dilute the porphyrin concentration; <sup>1</sup>H NMR titration was carried out by acquiring a spectrum of an aliquot (500 μL) of the porphyrin (host) stock solution in CDCl<sub>3</sub> at a concentration around 1mM, and adding increasing aliquots of the DABCO solution (guest), also in CDCl<sub>3</sub>, and at a concentration approximately 10 mM. After each addition, a new <sup>1</sup>H NMR spectrum was acquired.

## CHAPTER 4

***“Solution and solid state studies of two cyclic Zn-bis-porphyrins with fullerenes. Preliminary photophysical characterization”***

UNIVERSITAT ROVIRA I VIRGILI  
SUPRAMOLECULAR CHEMISTRY OF BIS-PORPHYRINS  
Laura Patricia Hernández Eguía  
ISBN:978-84-694-0308-2/DL:T-204-2011

## 1. Introduction

As discussed in previous chapters, metalloporphyrins are stunning compounds for the construction of supramolecular architectures. Fullerenes are valuable spherical molecules with low reduction potentials and strong electron acceptor properties, specifically they can accept up to six electrons.<sup>1,2,3,4</sup> They are recognized by porphyrins in a very unintentional way, which prompted the birth of a new supramolecular recognition element.<sup>5</sup> The combined use in supramolecular chemistry of porphyrins and fullerenes is appreciated not only for the affinity between the flat tetrapyrrole and the curved surface of the fullerene,<sup>6,7</sup> but also for the capability of photoinduce charge-separated species in their assemblies thus mimicking the natural photosynthesis processes.<sup>8,9</sup> Porphyrins are sensitizers and electron donors while fullerenes are electron acceptors.

Another significant reason that makes the construction of hosts for fullerenes an interesting endeavour is their reduced solubility in water and many organic solvents. The process of solubilising fullerenes in organic solvents using host guest chemistry has also evolved into extraction techniques that can be used for purification.<sup>10,11,12,13</sup> Fullerenes are being used in many research areas as chemistry, biology (i.e. photodynamic therapy)<sup>14</sup> or material science<sup>15</sup> and there is a constant need of pure material to further in their application.

---

<sup>1</sup> Martin, N.; Sanchez, L.; Illescas, B.; Perez, I. *Chem. Rev. (Washington, DC, U. S.)* **1998**, *98*, 2527-2547.

<sup>2</sup> Imahori, H.; Sakata, Y. *Eur. J. Org. Chem.* **1999**, 2445-2457.

<sup>3</sup> Guldi, D. M. *Chem. Commun.* **2000**, 321-327.

<sup>4</sup> Hirsch, A.; Editor *Fullerenes and Related Structures.* **1999**.

<sup>5</sup> Diederich, F.; Gomez-Lopez, M. *Chem. Soc. Rev.* **1999**, *28*, 263-277.

<sup>6</sup> Sun, D.; Tham, F. S.; Reed, C. A.; Boyd, P. D. W. *Proc. Natl. Acad. Sci. U. S. A.* **2002**, *99*, 5088-5092.

<sup>7</sup> Boyd, P. D. W.; Reed, C. A. *Acc. Chem. Res.* **2005**, *38*, 235-242.

<sup>8</sup> Gust, D.; Moore, T. A.; Moore, A. L. *Acc. Chem. Res.* **2001**, *34*, 40-48.

<sup>9</sup> Wasielewski, M. R. *J. Org. Chem.* **2006**, *71*, 5051-5066.

<sup>10</sup> Atwood, J. L.; Koutsantonis, G. A.; Raston, C. L. *Nature (London, United Kingdom)* **1994**, *368*, 229-31.

<sup>11</sup> Haino, T.; Yanase, M.; Fukazawa, Y. *Angew. Chem., Int. Ed.* **1998**, *37*, 997-998.

<sup>12</sup> Huerta, E.; Cequier, E.; de Mendoza, J. *Chem. Commun.* **2007**, 5016-5018.

<sup>13</sup> Huerta, E.; Metselaar, G. A.; Fragoso, A.; Santos, E.; Bo, C.; de Mendoza, J. *Angew Chem Int Edit* **2007**, *46*, 202-205.

<sup>14</sup> Bonnett, R. *Chemical Aspects of Photodynamic Therapy*, **2000**.

<sup>15</sup> de la Torre, G.; Claessens Christian, G.; Torres, T. *Chem. Commun.* **2007**, 2000-2015.

Cyclic metalloporphyrin dimers form thermodynamically stable inclusion complexes with fullerenes (**C**<sub>60</sub>, **C**<sub>70</sub>, **C**<sub>76</sub> and **C**<sub>120</sub>)<sup>16</sup> in organic solvents due to the macrocyclic<sup>17</sup> and multivalency effects.<sup>18</sup> Furthermore, the binding capability of these cyclic host molecules towards fullerenes can be easily tuned by the choice of the central metal, the nature of the β-pyrrolic substituents and the selection of the length and degree of unsaturation of the hydrocarbon linker chain used to connect the two porphyrin units.<sup>19</sup>

The use of porphyrin as binding sites for fullerenes was spurred after the first reports of the cocrystallization of **C**<sub>60</sub> or **C**<sub>70</sub> with porphyrins.<sup>20</sup> The fit of a supramolecular complex relies on the complementarity shape between the host and the guest. For this reason, it is supposed that spherical guests are appropriate to be recognized by macrocyclic receptors. The complex formation will also benefit from the preorganization of the cavity to the size of a specific guest<sup>21,22</sup> and that the van der Waals contacts between the two binding associates are highly increased in this type of inclusion complex.

Many examples in literature<sup>23,24</sup> are concerned with the use as binding unit for fullerenes substituted-pyrrole porphyrins with only two *meso*-phenyl substituents. The scrambling process is highly reduced during the syntheses of such structures. Furthermore, pyrrole-β-substituted porphyrins experience an increase in π-basicity compared to unsubstituted ones and tend to adopt a shallow concave conformation in avoiding steric clashes between *meso* and β-pyrrolic substituents. Both effects are important in the stabilization of the supramolecular aggregates they form with the fullerenes, as well as the observation that the β-pyrrolic substituents usually surround the fullerene. In our study, we selected a non β-pyrrolic substituted monoporphyrin unit bearing, however, four *meso*-aryl substituents. Two of the *meso* phenyl groups contain a peripheral functional group

<sup>16</sup> Zheng, J. Y.; Tashiro, K.; Hirabayashi, Y.; Kinbara, K.; Saigo, K.; Aida, T.; Sakamoto, S.; Yamaguchi, K. *Angew Chem Int Edit* **2001**, *40*, 1858-1861.

<sup>17</sup> Cram, D. J. *Angew. Chem., Int. Ed. Engl.* **1986**, *25*, 1039-1057.

<sup>18</sup> Mulder, A.; Huskens, J.; Reinhoudt, D. N. *Org. Biomol. Chem.* **2004**, *2*, 3409-3424.

<sup>19</sup> Yanagisawa, M.; Tashiro, K.; Yamasaki, M.; Aida, T. *J. Am. Chem. Soc.* **2007**, *129*, 11912-11913.

<sup>20</sup> Sun, Y.; Drovetskaya, T.; Bolskar, R. D.; Bau, R.; Boyd, P. D. W.; Reed, C. A. *J. Org. Chem.* **1997**, *62*, 3642-3649.

<sup>21</sup> Beer, P. D.; Gale, P. A. *Angew. Chem., Int. Ed.* **2001**, *40*, 486-516.

<sup>22</sup> Sessler, J. L.; Seidel, D. *Angew. Chem., Int. Ed.* **2003**, *42*, 5134-5175.

<sup>23</sup> Tashiro, K.; Aida, T.; Zheng, J.-Y.; Kinbara, K.; Saigo, K.; Sakamoto, S.; Yamaguchi, K. *J. Am. Chem. Soc.* **1999**, *121*, 9477-9478.

<sup>24</sup> Tashiro, K.; Aida, T. *J. Inclusion Phenom. Macrocyclic Chem.* **2001**, *41*, 215-217.

(propargyloxy) and the other two facially encumbering groups (methyl). The incorporation of the two *meso*-mesityl substituents was engineered as an alternative to  $\beta$ -pyrrolic substitution with the aim to maintain the  $\pi$ -basic properties of the porphyrin unit and induce a shallow concave cavity on their faces. The facially encumbering methyl groups will not only delimitate the cavity of the porphyrin faces but could also engage in additional CH- $\pi$  interactions increasing the van der Waals contacts with the bound fullerene as the  $\beta$ -pyrrolic substituents do.<sup>25</sup>

We report here the binding properties of the two cyclic zinc bis-porphyrins **Zn<sub>2</sub>-17** and **Zn<sub>2</sub>-18**, in the presence of fullerenes of different size: **C<sub>60</sub>**, **C<sub>70</sub>**, and the icosahedral (Ih) isomer of **C<sub>80</sub>** filled with scandium nitride, **Sc<sub>3</sub>N@C<sub>80</sub>** (Figure 1).<sup>26</sup> This work was undertaken to try to quantify the qualitative hypothesis previously stated by Boyd et al. in 2002 and based on results derived from MALDI mass spectrometry experiment indicating that porphyrin hosts bind stronger to bigger endohedral fullerenes than do smaller and empty fullerenes.<sup>27</sup> These results are also in agreement with the higher retention times measured for the endohedral fullerenes towards porphyrin-appended silica stationary phases for chromatographic purification.<sup>28</sup>

---

<sup>25</sup> Perez, E. M.; Capodilupo, A. L.; Fernandez, G.; Sanchez, L.; Viruela, P. M.; Viruela, R.; Ortí, E.; Bietti, M.; Martin, N. *Chem. Commun.* **2008**, 4567-4569.

<sup>26</sup> Elliott, B.; Yu, L.; Echegoyen, L. *J. Am. Chem. Soc.* **2005**, *127*, 10885-10888.

<sup>27</sup> Sun, D. Y.; Tham, F. S.; Reed, C. A.; Chaker, L.; Boyd, P. D. W. *J. Am. Chem. Soc.* **2002**, *124*, 6604-6612.

<sup>28</sup> Xiao, J.; Savina, M. R.; Martin, G. B.; Francis, A. H.; Meyerhoff, M. E. *J. Am. Chem. Soc.* **1994**, *116*, 9341-9342.

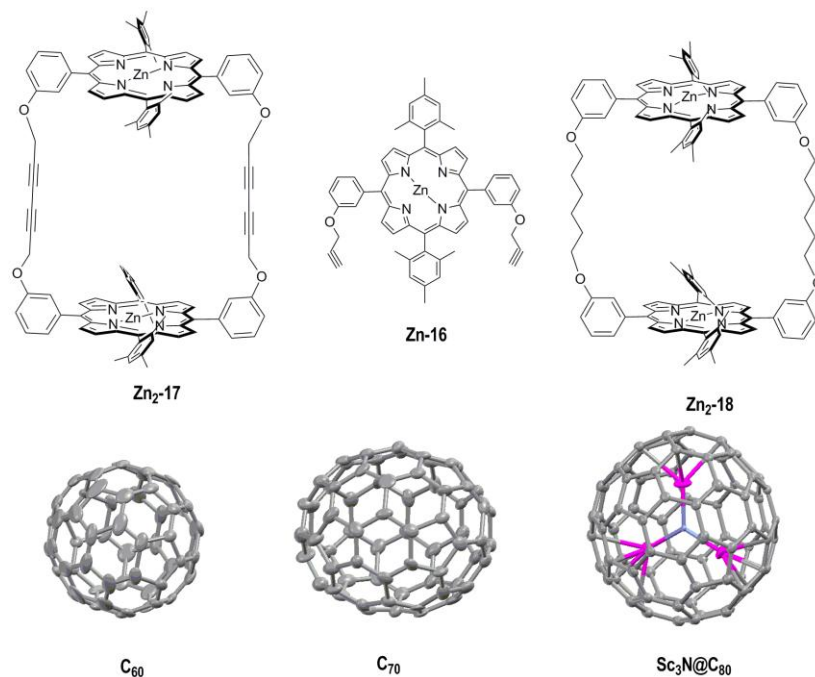


**Figure 1.** Line structures of the two bis-porphyrin macrocycles, **Zn<sub>2</sub>-17** and **Zn<sub>2</sub>-18**, and 3D molecular structures of the three fullerenes in ellipsoid display.

We also report preliminary results obtained during the photophysical characterization of the supramolecular complexes formed by the two cyclic receptors and the empty fullerenes.

To the best of our knowledge, there is only one example of the synthesis of related cyclic bis-metalloporphyrin hosts possessing aryl substituents in all *meso* positions.<sup>29</sup> Likewise, the binding properties of fully or partially *meso*-aryl substituted cyclic metalloporphyrin dimers towards endohedral **C<sub>80</sub>** fullerenes was not reported when we initiated our studies. During the course of this work, one article describing the complexation properties of a trisporphyrin receptor with the empty fullerenes and the endohedral fullerene **La@C<sub>82</sub>** has appeared.<sup>30</sup>

<sup>29</sup> Vaijayanthimala, G.; Krishnan, V.; Mandal, S. K. *J. Chem. Sci. (Bangalore, India)* **2008**, *120*, 115-129.

<sup>30</sup> Gil-Ramirez, G.; Karlen, S. D.; Shundo, A.; Porfyrakis, K.; Ito, Y.; Briggs, G. A. D.; Morton, J. J. L.; Anderson, H. L. *Org. Lett.* **2010**, *12*, 3544-3547.

## 2. Results and discussion

### 2.1 Binding studies of the cyclic bis-porphyrin receptors with C<sub>60</sub> and C<sub>70</sub>: Photophysical characterization of the solution assemblies.

We started measuring the spectroscopic properties of each cyclic Zn-bis-porphyrin receptor, **Zn<sub>2</sub>-17**, **Zn<sub>2</sub>-18**, as well as the monoporphyrin **Zn-16** used as starting material in their synthesis. Although the spectroscopic properties of the fullerenes **C<sub>60</sub>** and **C<sub>70</sub>** are well known, they were reevaluated in this study. All the data obtained in these preliminary studies will become highly valuable for the subsequent photophysical characterization of the formed supramolecular assemblies.

The steady-state absorption and emission spectra of all the species were measured in toluene and dichloromethane solution (Figure 2). In both solvents the absorption spectra obtained for the macrocyclic receptors are very similar but do not coincide with the spectrum in epsilon scale of monomer **Zn-16** multiplied by two. A significant decrease in the molar absorption coefficient of the Soret band of the cyclic receptors is observed when compared with the value corresponding to the monoporphyrin multiplied by two. This difference can be quantified in toluene and dichloromethane as 25% and 45% respectively.<sup>31</sup> Moreover, the Soret band of the two bis-porphyrin receptors **Zn<sub>2</sub>-18** and **Zn<sub>2</sub>-17** experience blue-shifts of 3nm and 4nm respectively compared with the absorption maximum of **Zn-16** (See text in figure 2).

---

<sup>31</sup> Flamigni, L.; Ventura, B.; Oliva, A. I.; Ballester, P. *Chem.--Eur. J.* **2008**, *14*, 4214-4224.

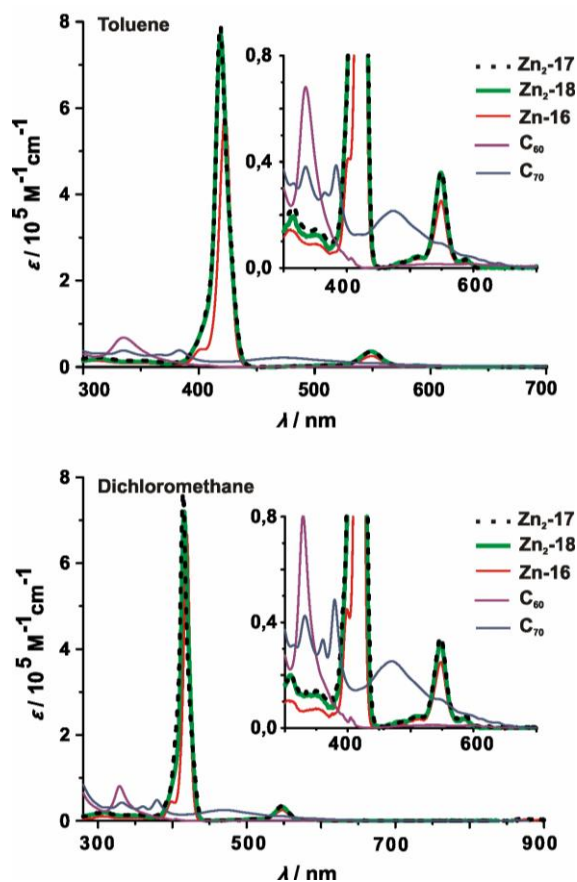


**Figure 2.** Absorption spectra of **Zn<sub>2</sub>-17**, **Zn<sub>2</sub>-18**, **Zn-16**, **C<sub>60</sub>** and **C<sub>70</sub>** in toluene (top) and dichloromethane (bottom). The maximum wavelength of the porphyrin compounds are, in toluene, **Zn-16**: 422nm, **Zn<sub>2</sub>-17**: 418nm, **Zn<sub>2</sub>-18**: 419nm; and in dichloromethane, **Zn-16**: 419nm, **Zn<sub>2</sub>-17**: 414nm and **Zn<sub>2</sub>-18**: 415nm.

The following tables summarize the luminescence properties of all the species investigated at 295K and 77K. (Fullerenes were only studied at room temperature).

**Table 1.** Luminescence properties of components **Zn-16**, **Zn<sub>2</sub>-17**, **Zn<sub>2</sub>-18**, **C<sub>60</sub>** and **C<sub>70</sub>** in toluene, at 295K and 77K.

| Compound                 | 295K                       |         |                    | 77K                        |                    |
|--------------------------|----------------------------|---------|--------------------|----------------------------|--------------------|
|                          | $\lambda_{\max}/\text{nm}$ | $\Phi$  | $\tau / \text{ns}$ | $\lambda_{\max}/\text{nm}$ | $\tau / \text{ns}$ |
| <b>Zn-16</b>             | 590; 640                   | 0.041   | 2.1                | 595; 650                   | 2.7                |
| <b>Zn<sub>2</sub>-17</b> | 592; 642                   | 0.034   | 2.1                | 596; 653                   | 2.7                |
| <b>Zn<sub>2</sub>-18</b> | 592; 640                   | 0.038   | 2.1                | 596; 652                   | 2.7                |
| <b>C<sub>60</sub></b>    | 720                        | 0.00092 | 1.2                | -                          | -                  |
| <b>C<sub>70</sub></b>    | 662; 686                   | 0.0022  | 0.56               | -                          | -                  |

In both solvents and at room temperature, **Zn-16**, **Zn<sub>2</sub>-17** and **Zn<sub>2</sub>-18** were excited at 424 nm whereas **C<sub>60</sub>** and **C<sub>70</sub>** were excited at 375 nm. Working at 77K the three porphyrin compounds were excited at 440 nm. The fluorescence quantum yields,  $\phi$ , were calculated by steady state comparative method using tetraphenylporphyrin (TPP) as a reference.<sup>32</sup>  $\phi$  is the ratio of photons absorbed to photons emitted through fluorescence, thus, giving the probability of the excited state to be deactivated by fluorescence.

<sup>32</sup> Fungo, F.; Otero, L. A.; Sereno, L.; Silber, J. J.; Durantini, E. N. *Dyes and Pigments* **2001**, *50*, 163-170.

**Table 2.** Luminescence properties of components **Zn-16**, **Zn-17**, **Zn-18**, **C<sub>60</sub>** and **C<sub>70</sub>** in dichloromethane, at 295K and 77K.

|                       | 295K                             |         |                  | 77K                              |                  |
|-----------------------|----------------------------------|---------|------------------|----------------------------------|------------------|
|                       | $\lambda_{\text{max}}/\text{nm}$ | $\Phi$  | $\tau/\text{ns}$ | $\lambda_{\text{max}}/\text{nm}$ | $\tau/\text{ns}$ |
| <b>Zn-16</b>          | 590; 642                         | 0.033   | 1.9              | 595; 650                         | 2.6              |
| <b>Zn-17</b>          | 590; 640                         | 0.030   | 1.9              | 596; 653                         | 2.6              |
| <b>Zn-18</b>          | 590; 640                         | 0.029   | 1.9              | 596; 652                         | 2.6              |
| <b>C<sub>60</sub></b> | 720                              | 0.00021 | 1.1              | -                                | -                |
| <b>C<sub>70</sub></b> | 660; 690                         | 0.00083 | 0.53             | -                                | -                |

When light is emitted from excited states of any substance we can talk of luminescence. These processes can be divided in two categories: fluorescence and phosphorescence, depending on the nature of the excited state. In excited singlet states, the electron in the excited orbital is paired to the second electron in the ground state, and return to the ground state is allowed and occurs rapidly (fluorescence). When the light is emitted from triplet excited states, in which the electron has the same spin orientation as the ground-state electron the phenomenon is called phosphorescence; the transitions are forbidden and the emission rates are slow (milliseconds-seconds). Porphyrins are typical fluorescence molecules.

The intensity of fluorescence can be decreased by a wide variety of processes, and such decreases in intensity are called “quenching”. Quenching mechanisms can be static, when it has to do with the complexation with another molecule that occurs in the ground state, or dynamic, due to collisions in the excited state.

## 2.2 Binding studies with $C_{60}$ and $C_{70}$

### a. UV-visible and fluorescence titrations

Before attempting the photophysical characterization of the complexes formed in solution by the cyclic bis-porphyrin receptors and the fullerenes we need to determine the stoichiometry and stability constants of the aggregates. However, the calculation of stoichiometry and accurate association constants values for supramolecular complexes involving photochemically “non innocent” guests is especially difficult when using spectrophotometric titrations. The incremental addition of the guest during the titration provokes the presence of a coloured species in great excess with respect to the others (i.e. free host and simple 1:1 complex). This is the case of fullerenes guests since they are UV-visible active and absorb light in the same range of energies that the porphyrin receptors.<sup>31</sup> An added difficulty to the systems under study arises from the minimal changes observed in the absorption spectra of the two interacting partners when involved in complex formation.

The stability constants of the assemblies were determined in two different solvents, toluene and dichloromethane, by means of titration experiments using UV-visible and fluorescence spectroscopies.

Table 3 summarizes the calculated association constant values for the different systems we studied. In all cases, the absorption titration data were analyzed using the SPECFIT software and a binding model that assumes the exclusive formation of a 1:1 complex and the existence of three coloured (UV-active) species in equilibrium, free host, free guest and 1:1 complex. The titration data derived from the emission experiments were analyzed in a similar manner but only two absorbing species were considered, the free receptor and the complex because the emission of the free guest is negligible compared to the species involving the porphyrins. As shown in the table, the association constant values calculated from the absorption and emission titration experiments are in good agreement. The stability constant values determined for the complexes of the empty fullerenes with the cyclic receptor **Zn2-18** are one order of magnitude higher in dichloromethane than in toluene. We also determined the solubility of  $C_{60}$  and  $C_{70}$  in toluene as 1.6 mg/mL and 1.8 mg/mL respectively, and 0.1 mg/mL and 0.05 mg/mL respectively in dichloromethane: these values quantify the ability of the solvent to solvate the fullerenes. As expected, the

highest binding constant is obtained in the worst solvent. Nevertheless, the observed variation of the stability constants reflects the strength of solvation of both the host and the guest. The macrocyclic receptor having diyne spacers, **Zn<sub>2</sub>-17**, did not show changes in the absorption spectra during the titration with **C<sub>60</sub>** and a minor alteration in fluorescence when **C<sub>60</sub>** was added.<sup>23</sup> However, we were able to derive a significant value for the binding constant of **Zn<sub>2</sub>-17** with **C<sub>70</sub>**, from fluorescence titrations.

**Table 3.** Binding constants ( $K$ ,  $M^{-1}$ ) values for the complexes formed by the cyclic receptors **Zn<sub>2</sub>-17** and **Zn<sub>2</sub>-18** with the empty fullerenes (**C<sub>60</sub>** and **C<sub>70</sub>**) in toluene (Tol) and dichloromethane (DCM). The values were derived from spectrophotometric and spectrofluorimetric titrations carried out at room temperature.

| Complex                                  | Absorption        |                   | Emission          |                   |
|--|-------------------|-------------------|-------------------|-------------------|
|  | $K/M^{-1}$        | $K/M^{-1}$        | $K/M^{-1}$        | $K/M^{-1}$        |
|  | Tol               | DCM               | Tol               | DCM               |
| <b>C<sub>70</sub>• Zn<sub>2</sub>-18</b> | $3.2 \times 10^4$ | $2.2 \times 10^5$ | $3.2 \times 10^4$ | $2.2 \times 10^5$ |
| <b>C<sub>60</sub>• Zn<sub>2</sub>-18</b> | $2.0 \times 10^4$ | $1.2 \times 10^5$ | $2.0 \times 10^4$ | $1.2 \times 10^5$ |
| <b>C<sub>70</sub>• Zn<sub>2</sub>-17</b> | -                 | -                 | $3.1 \times 10^4$ | $7.2 \times 10^4$ |
| <b>C<sub>60</sub>• Zn<sub>2</sub>-17</b> | -                 | -                 | -                 | -                 |

The spectrophotometric and the spectrofluorimetric titrations were carried out using solution of the macrocycles with concentration range in the order of  $2\text{-}3 \times 10^{-7}$  M and adding incremental amounts of the fullerene solutions. The fluorescence studies were performed by exciting at the isosbestic point of the Soret band, observed in the corresponding UV-visible titrations.<sup>33</sup> During the titration experiments the Soret band of **Zn<sub>2</sub>-18**, with six methylene linker chains, experiences a red shift of 1-5 nm with a decrease in intensity

<sup>33</sup> Solladie, N.; Walther, M. E.; Gross, M.; Figueira Duarte, T. M.; Bourgogne, C.; Nierengarten, J.-F. *Chem. Commun.* **2003**, 2412-2413.

indicating that the binding takes place through  $\pi$ -electronic interaction.<sup>34</sup> Most likely, the interaction geometry adopted by the complexes formed by the unsaturated cyclic receptor **Zn2-17** and the fullerenes (vide infra) are different to the ones exhibited by their counterparts involving the fully saturated receptor **Zn2-18**. Thus, the resulting  $\pi$ -electronic interactions produced minimum changes in the Soret band of **Zn2-18** (Figures 3-5).<sup>35</sup>

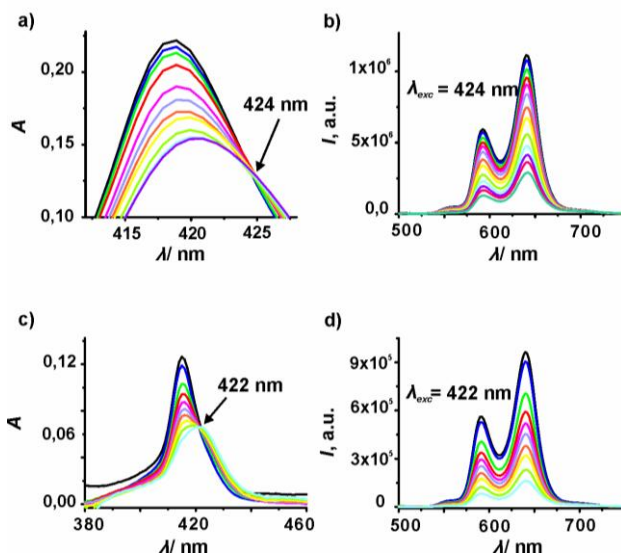


**Figure 3.** a) UV-visible titration of **Zn2-18** with **C70** in toluene.  $[\text{Zn2-18}] = 2.84 \times 10^{-7}$  M and additions of **C70** from 0-140 equivalents. Soret band was red-shifted from 419 to 421 nm. At 424 nm appeared an isosbestic point. b) Fluorescence titration of **Zn2-18** with **C70** in toluene.  $[\text{Zn2-18}] = 2.26 \times 10^{-7}$  M and additions of **C70** from 0-230 equivalents. The excitation wavelength was set at 424 nm (the isosbestic point in the UV-visible titration). A quenching of the 75% was observed. c) UV-visible titration of **Zn2-18** with **C70** in dichloromethane.  $[\text{Zn2-18}] = 1.76 \times 10^{-7}$  M and additions of **C70** from 0-100 equivalents. Soret band was red-shifted from 415 to 420 nm. At 422 nm appeared an isosbestic point. d) Fluorescence titration of **Zn2-18** with **C70** in dichloromethane.  $[\text{Zn2-18}] = 1.76 \times 10^{-7}$  M and additions of **C70** from 0-100 equivalents. The excitation wavelength was set at 422 nm (the isosbestic point in the UV-visible titration). A quenching of the 85% was observed.

<sup>34</sup> Ouchi, A.; Tashiro, K.; Yamaguchi, K.; Tsuchiya, T.; Akasaka, T.; Aida, T. *Angew Chem Int Edit* **2006**, *45*, 3542-3546.

<sup>35</sup> Konarev, D. V.; Neretin, I. S.; Slovokhotov, Y. L.; Yudanov, E. I.; Drichko, N. V.; Shul'ga, Y. M.; Tarasov, B. P.; Gumanov, L. L.; Batsanov, A. S.; Howard, J. A. K.; Lyubovskaya, R. N. *Chem.--Eur. J.* **2001**, *7*, 2605-2616.

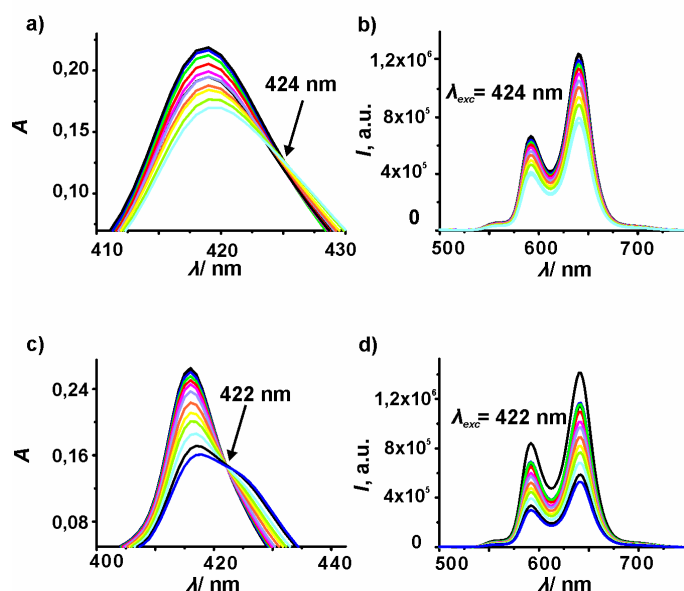


**Figure 4.** a) UV-visible titration of **Zn<sub>2</sub>-18** with **C<sub>60</sub>** in toluene. [**Zn<sub>2</sub>-18**]= $2.92 \times 10^{-7}$  M and additions of **C<sub>60</sub>** from 0-75 equivalents. Soret band was red-shifted from 419 to 420 nm. At 424 nm appeared an isosbestic point. b) Fluorescence titration of **Zn<sub>2</sub>-18** with **C<sub>60</sub>** in toluene. [**Zn<sub>2</sub>-18**]= $2.26 \times 10^{-7}$  M and additions of **C<sub>60</sub>** from 0-175 equivalents. The excitation wavelength was set at 424nm (the isosbestic point in the UV-visible titration). A quenching of the 45% was observed. c) UV-visible titration of **Zn<sub>2</sub>-18** with **C<sub>60</sub>** in dichloromethane. [**Zn<sub>2</sub>-18**]= $3.68 \times 10^{-7}$  M and additions of **C<sub>60</sub>** from 0-40 equivalents. Soret band was red-shifted from 415 to 418 nm. At 422 nm appeared an isosbestic point. d) Fluorescence titration of **Zn<sub>2</sub>-18** with **C<sub>60</sub>** in dichloromethane. [**Zn<sub>2</sub>-18**]= $3.54 \times 10^{-7}$  M and additions of **C<sub>60</sub>** from 0-43 equivalents. The excitation wavelength was set at 422nm (the isosbestic point in the UV-visible titration). A quenching of the 63% was observed.

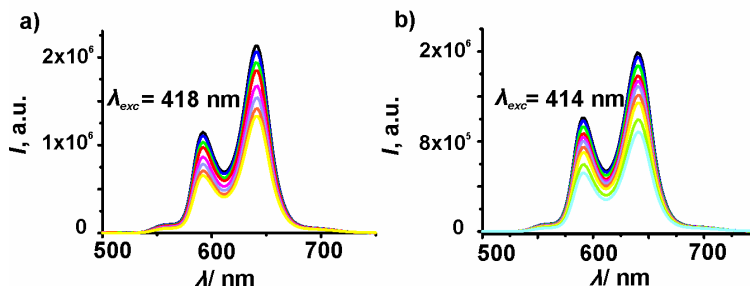


**Figure 5.** a) Fluorescence titration of **Zn<sub>2</sub>-17** with **C<sub>70</sub>** in toluene. [**Zn<sub>2</sub>-17**]= $3.3 \times 10^{-7}$  M and additions of **C<sub>70</sub>** from 0-122 equivalents. The excitation wavelength was set at 418 nm (Soret band does not change along a UV-visible titration). A quenching of the 38% was observed. b) Fluorescence titration of **Zn<sub>2</sub>-17** with **C<sub>70</sub>** in dichloromethane. [**Zn<sub>2</sub>-17**]= $2.2 \times 10^{-7}$  M and additions of **C<sub>70</sub>** from 0-75 equivalents. The excitation wavelength was set at 414nm (maximum in Soret band does not change along the titration).<sup>36</sup> A quenching of the 47% was observed.

## b. <sup>1</sup>H NMR titrations

In order to gain further insight in the characterization of the complexes formed between the cyclic porphyrins and the fullerenes we performed <sup>1</sup>H NMR titrations in deuterated toluene solutions. It was not possible to carry out a parallel study in dichloromethane solution due to low solubility of the fullerenes in this solvent (see above solubility data). Figure 6 depicts the selected downfield region of the <sup>1</sup>H NMR spectra acquired during the titration experiments of the two cyclic receptors with the empty fullerenes. The selected region is where the more significative spectral changes take place.

<sup>36</sup> D'Souza, F.; Chitta, R.; Gadde, S.; Zandler, M. E.; McCarty, A. L.; Sandanayaka, A. S. D.; Araki, Y.; Ito, O. *Chem.--Eur. J.* **2005**, *11*, 4416-4428.

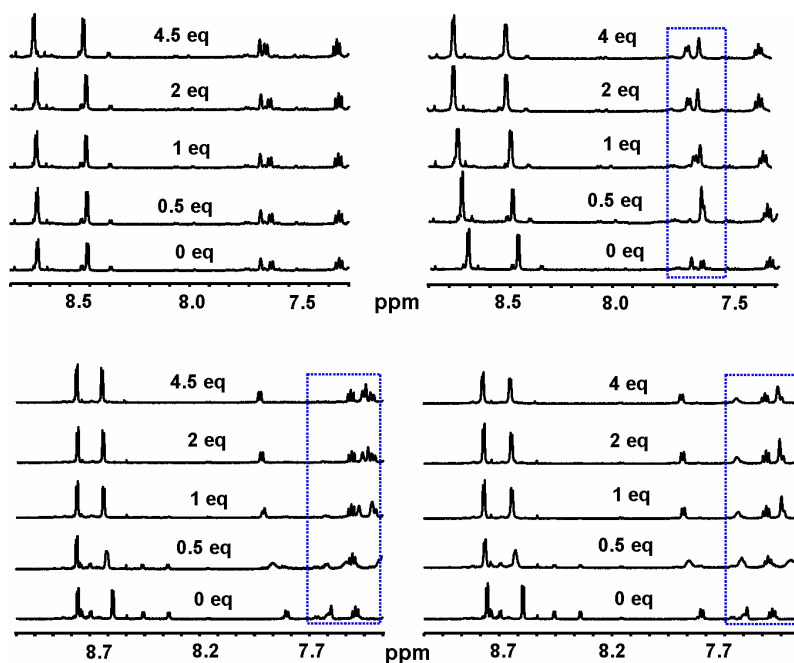


**Figure 6.** Downfield regions from the <sup>1</sup>H NMR titrations toluene-*d*<sub>8</sub>. Top left: **Zn<sub>2</sub>-17** with **C<sub>60</sub>**; top right: **Zn<sub>2</sub>-17** with **C<sub>70</sub>**; bottom left: **Zn<sub>2</sub>-18** with **C<sub>60</sub>**; bottom right: **Zn<sub>2</sub>-18** with **C<sub>70</sub>**.

As shown in figure 6, top left, the incremental addition of the empty fullerene **C<sub>60</sub>** to a 1 mM solution of **Zn<sub>2</sub>-17** did not produce significant changes in the proton signals of the receptor. This results indicates that the interaction of **C<sub>60</sub>** with the receptor **Zn<sub>2</sub>-17** having 1,3-butadiynyl spacers is too weak to be detected by <sup>1</sup>H NMR spectroscopy at 1 mM concentration. However, when the same receptor **Zn<sub>2</sub>-17** is titrated with the fullerene **C<sub>70</sub>** some proton signals experience chemical shift changes with the addition of an increasing amount of the guest. The complexation process shows fast exchange dynamics in the NMR time scale suggesting the formation of thermodynamically weak complexes. The β-pyrrolic protons assigned to the two conformers of the macrocycle **Zn<sub>2</sub>-17** (see chapter 2), shift downfield as a response to an increase in concentration of the fullerene guest. Both sets of protons are observed throughout the titration. The addition of more than 2 equiv of **C<sub>70</sub>** to the solution does not induced additional shifting to those proton signals. Some aromatic protons also experience downfield shifts during the titration and display the same shifting behavior described for the β-pyrrolic ones. Taken together, these observations indicate that both conformers are involved in the formation of different complexes with **C<sub>70</sub>**

and that the saturation of the formation of the complexes is reached with 2 equivalents of the fullerene. Clearly, the binding process is not selective for one of the conformers and does not alter the ratio of the conformers in the ground state. From the fact that the saturation is reached with 2 equivalents of guest at 1 mM concentration of host and assuming the formation of simple 1:1 complexes it is possible to estimate that the stability constant values should be in the range of  $10^3$ - $10^4$  M<sup>-1</sup>. This estimate is in complete agreement with the value previously derived from fluorescence titrations. On the contrary, the changes observed in the chemical shift values of the protons for the saturated cyclic bis-porphyrin, **Zn<sub>2</sub>-18**, during the titrations with the fullerenes are more dramatic. The addition of 0.5 equivalents of **C<sub>60</sub>** to a 1mM solution of **Zn<sub>2</sub>-18** produces a two fold change. On the one hand the signals of the β-pyrrolic protons assigned to the expanded conformer shift downfield and one of the resonating at  $\delta = 8.62$  ppm is significantly broaden. A similar behavior is observed for some of the aromatic protons of the receptor. Interestingly, the β-protons of the collapsed conformer do not show any variation in their chemical shifts but their intensity is considerably reduced. The addition of 1 equivalent of **C<sub>60</sub>** induces additional shifts in the protons signals mentioned above and has a narrowing effect in the signals that were broaden. Moreover, the proton signals corresponding to the collapsed conformer have completely disappeared to the expenses of the signals of the bound receptor. The addition of an extra equivalent of **C<sub>60</sub>** to the solution did not produce any change in the proton signals of the receptor spectrum. The <sup>1</sup>H NMR titration of **Zn<sub>2</sub>-18** with **C<sub>70</sub>** featured a completely analog behavior. The results presented above suggest that the expanded conformer of the **Zn<sub>2</sub>-18** binds the fullerenes forming an inclusion complex with a stability constant value much higher than for the collapsed one. Since the saturation of the chemical shift changes is obtained by the addition of 1 equivalent of the fullerene, it is possible to ascertain the presence of complexes with 1:1 stoichiometry at this molar ratio. The stability constant for these aggregates can be estimated as  $> 10^4$  M<sup>-1</sup> since they are formed quantitatively under stoichiometric control at 1mM concentration.

Luckily, several single crystals grew from the NMR tubes solutions containing excess of fullerene and were suitable for X-ray crystallography (figures 7-10). The analysis of the diffraction data allowed determining the solid state structure of the complexes formed between the **Zn<sub>2</sub>-17** and **C<sub>70</sub>** as well as **Zn<sub>2</sub>-18** and the two empty fullerenes, **C<sub>60</sub>** and **C<sub>70</sub>**.

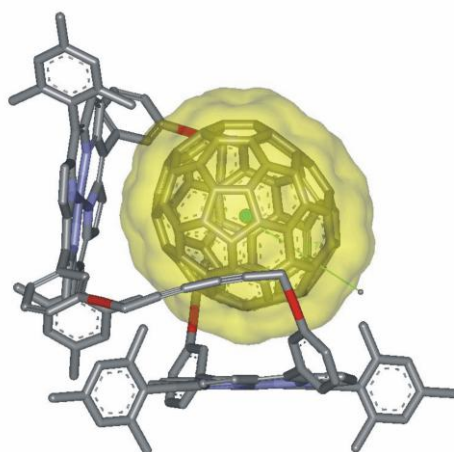


**Figure 7.** X-ray crystal structure of the 1:1 complex between bis-porphyrin **Zn<sub>2</sub>-17** and **C<sub>70</sub>**. Distances from the Zn atom to the closest C atom of the fullerene are around 3 Å.

In complete agreement with the conclusions reached from the <sup>1</sup>H NMR, all the solid state structures correspond to 1:1 stoichiometry complexes. In the solid state, the macrocyclic receptor **Zn<sub>2</sub>-17** adopts a scoop-shaped conformation in which the two porphyrin rings are located in an angle close to 90° and constitute the bottom and the back of the scoop while the 1,4-butadiynyl chains are the sides. The **C<sub>70</sub>** is included within the aromatic cavity of the two porphyrins and in order to maximize the  $\pi$ - $\pi$  interactions displays side-on contacts with one and end-on contacts with the other. The packing of crystals reveals that presence of a zig-zag motif of 1:1 complexes forming an infinite layer (Figure 8).

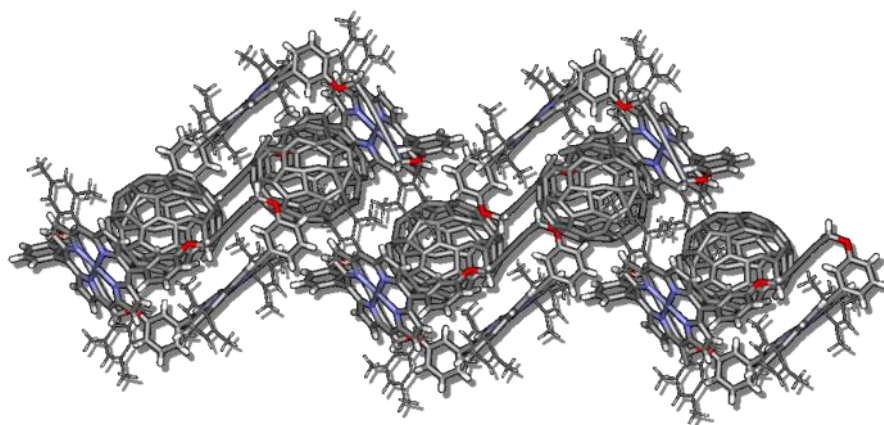


**Figure 8.** Bis-porphyrin **Zn<sub>2</sub>-17** forming a zig-zag channel with **C<sub>70</sub>**.

In the two following figures (Figures 9 and 10) are depicted the X-ray crystal structures of the 1:1 complexes formed by the cyclic bis-porphyrin **Zn<sub>2</sub>-18** with **C<sub>60</sub>** and **C<sub>70</sub>**. Aida has reported the solid state structure of the 1:1 complex of a related cyclic bis-porphyrin receptor having the same six methylene chain spacers. In Aida's structure the plane between the two porphyrin units is almost zero and the porphyrins are  $\beta$ -pyrrole substituted with only two meso-phenyl groups.<sup>16</sup> The two porphyrins are cofacially oriented and the fullerene is sandwiched between the two. The solid state structure even possesses a  $C_i$  symmetry element. Surprisingly and completely unexpected, the modification in the substitution of the porphyrin units carried-out in this study has a profound impact in the solid state structure of the complexes assembled with fullerenes. The clamshell-like conformation adopted by the receptor on including the two fullerenes is very similar and the two porphyrins ring are tilted with respect to each other. The angle formed by the two planes of the Zn-porphyrin unit is close to 60°; clearly the porphyrins are not cofacially oriented. In this conformation, the fullerene is sandwiched between two porphyrin planes in a way that has been proposed by Aida's in the case of bis-porphyrin cyclic receptor with alkyl chain spacer shorter than six methylene units. Most likely, the increase in the conformational flexibility of this receptor compared to the unsaturated counterpart is responsible for the observed change in its conformation on binding the fullerenes (**Zn<sub>2</sub>-17** scoop-like vs. **Zn<sub>2</sub>-18** clamshell-like). It is worthy to note, that in this conformation the interaction with **C<sub>70</sub>** benefits from a simultaneous side-on orientation. Additional CH- $\pi$  interactions between the methyl and methylene protons of the receptors and the aromatic system of the guest are present in the structure. The tilting of the porphyrin units away from the cofacial arrangement observed in the solid state can be due to a gain in the intramolecular forces resulting from the packing of the lattice. The high symmetry observed in the <sup>1</sup>H NMR titrations in solution and at room temperature suggests that the fullerene oscillates in the cavity much faster than the NMR timescale and/or would be sandwiched above the center of the porphyrin rings

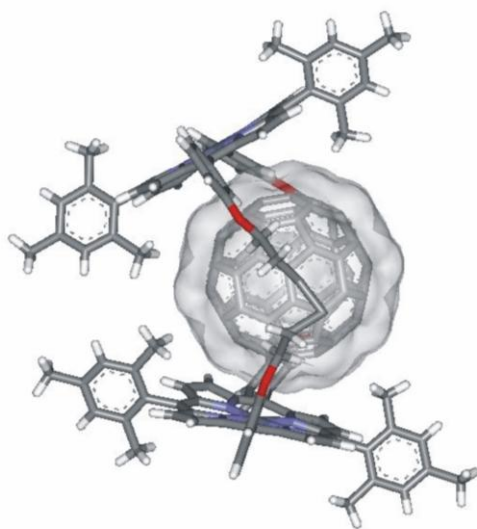


**Figure 9.** X-ray crystal structure of the 1:1 complex between bis-porphyrin **Zn<sub>2</sub>-18** and **C<sub>60</sub>**. Distances from the Zn atom to the closest C atom of the fullerene are 3.040 Å. The porphyrin planes are separated a distance of 11.982 Å from Zn to Zn.

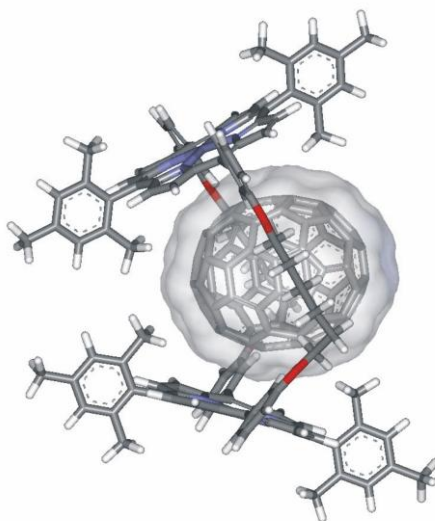


**Figure 10.** X-ray crystal structure of the 1:1 complex between bis-porphyrin **Zn<sub>2</sub>-18** and **C<sub>70</sub>**. Distances from the Zn atom to the closest C atom of the fullerene are around 3 Å. The porphyrin planes are separated a distance of 11.973 Å from Zn to Zn.

### **2.3 Preliminary photophysical studies of the systems cyclic bis-porphyrin/fullerene**

The value of the stability constants of the 1:1 complexes cyclic bis-porphyrin/fullerene is too small to allow its photophysical characterization in an equimolar solution under the typical concentration conditions used in these studies. For this reason and to maximize the concentration of the complex, preliminary photophysical experiments were carried out using solutions containing an excess of one of the two components to determine if the predominant excitation of one of them produce a luminescence quenching proportional to the percentage of complex present in the mixture. In the solution mixtures where the fullerenes were in excess of ten times we studied the quenching of the porphyrin emission (Figure 11), whereas in 1:1 mixtures we tried to detect changes in the fullerene emission. However, this experiment presents an added difficulty because not only the fullerene emission is weak but it is somewhat buried under the porphyrin emission bands (Figure 12).

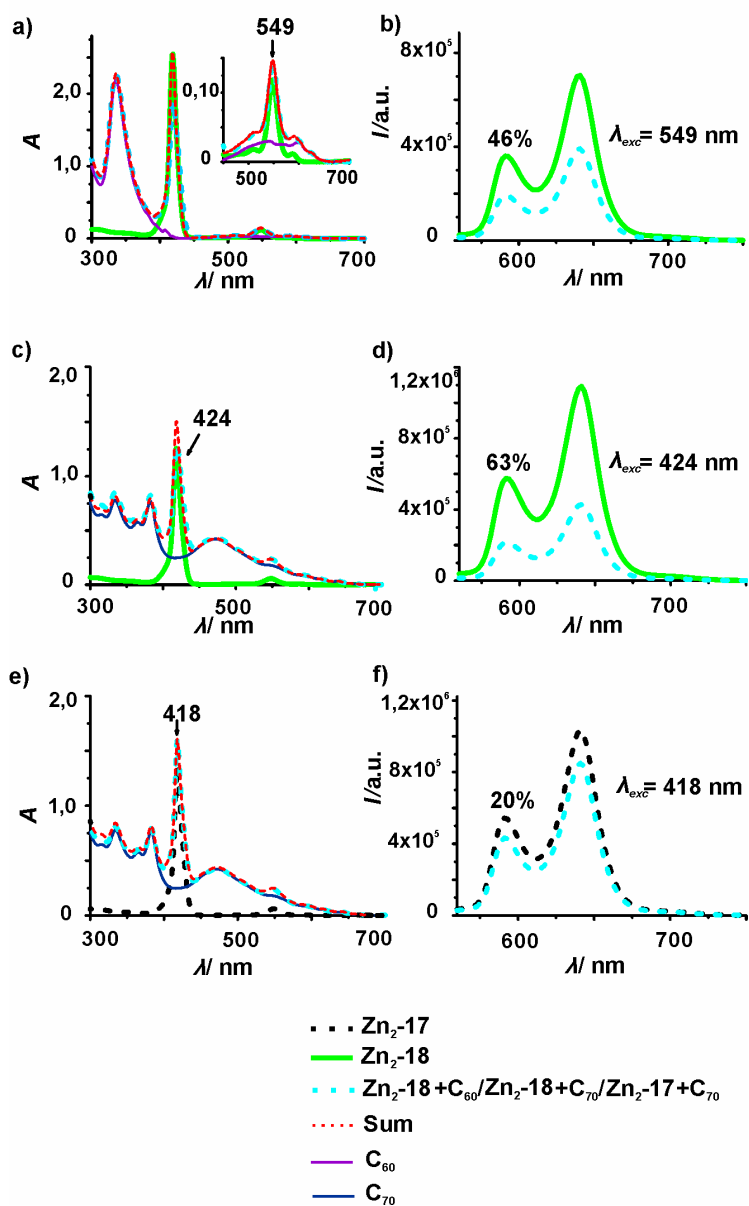


**Figure 11.** Absorption and emission spectra of  $\text{C}_{60}\cdot\text{Zn}_2\text{-18}$ ,  $\text{C}_{70}\cdot\text{Zn}_2\text{-18}$  and  $\text{C}_{70}\cdot\text{Zn}_2\text{-17}$  where fullerenes are in excess of 10 times over the porphyrin. It was excited prevalently the porphyrin at 549, 424 and 418 respectively, and the quenching was shown to be of 46%, 63% and 20%.

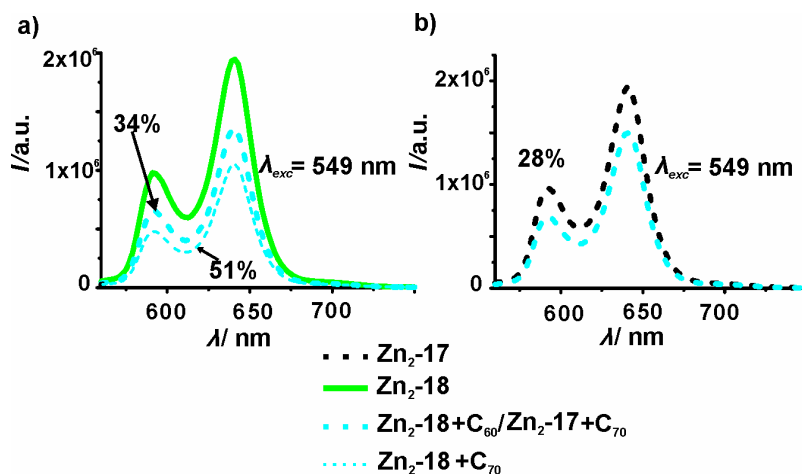


**Figure 12.** Emission spectra of 1:1 mixtures of  $C_{60} \cdot Zn_2-18$ ,  $C_{70} \cdot Zn_2-18$  and  $C_{70} \cdot Zn_2-17$ , exciting on porphyrin maxima (a:  $C_{60} \cdot Zn_2-18$ , 34% of quenching, and  $C_{70} \cdot Zn_2-18$ , 51% of quenching; b:  $C_{70} \cdot Zn_2-17$ , 28% of quenching).

Armaroli and coworkers<sup>37,38</sup> found out a direct relationship between a supramolecular face-to-face fullerene-porphyrin dyad and the presence of a broad absorption band in the near IR region of the spectrum. Later on, Aida and coworkers have observed the same phenomena.<sup>24</sup>

To find the band of our complexes in the region of the near-IR, first we performed simulations of the speciation profiles at different concentrations of  $Zn_2-18$  and  $Zn_2-17$  in order to find out the best concentration and equivalents ratio to perform these and the next photophysical studies. We proved the speciations at four different concentrations ( $1 \times 10^{-6}$  M,  $5 \times 10^{-6}$  M,  $1 \times 10^{-5}$  M and  $3 \times 10^{-5}$  M) and in the two solvents, using the HySS program.

We decided to carry on the experiment with a macrocycle concentration of  $3 \times 10^{-5}$  M in toluene, which provides a good solubility, and at two different concentrations of each fullerene providing mixtures with 2 and with 4 equivalents of fullerene, having a concentration of  $6 \times 10^{-5}$  M for the first and  $1.2 \times 10^{-4}$  M for the second case.

<sup>37</sup> Armaroli, N.; Marconi, G.; Echegoyen, L.; Bourgeois, J. P.; Diederich, F. *Chem.--Eur. J.* **2000**, *6*, 1629-1645.

<sup>38</sup> Hosseini, A.; Taylor, S.; Accorsi, G.; Armaroli, N.; Reed, C. A.; Boyd, P. D. W. *J. Am. Chem. Soc.* **2006**, *128*, 15903-15913.

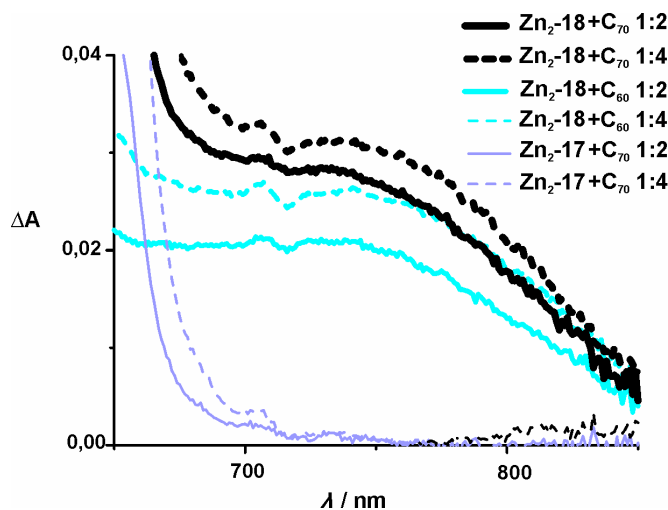


**Figure 13.** NIR-UV-visible spectra of  $C_{60} \cdot Zn_2-18$  (1:2),  $C_{60} \cdot Zn_2-18$  (1:4),  $C_{70} \cdot Zn_2-18$  (1:2),  $C_{70} \cdot Zn_2-18$  (1:4),  $C_{70} \cdot Zn_2-17$  (1:2) and  $C_{70} \cdot Zn_2-17$  (1:4) in toluene. In each spectrum the porphyrin contribution is subtracted.

The absorption band is good and reliable. In that region the absorption bands of each component are well separated. In these cases it appears centred at 740nm and it is more intense for  $C_{70} \cdot Zn_2-18$  (Figure 13). The non-existence of this band for  $C_{70} \cdot Zn_2-17$  is pointing to a different geometry of the assembly.

## 2.4 Binding with the endohedral fullerene $Sc_3N@C_{80}$ : solution and solid state

We were interested in evaluating the effects that the change in size and polarization of the endohedral fullerene  $Sc_3N@C_{80}$  with respect to the empty fullerenes would produce in the stoichiometry, geometry and the thermodynamic stabilization of the complexes assembled with  $Zn_2-18$ . Similarly to the studies described in the previous section, we have probed the binding with bis-porphyrin  $Zn_2-18$  by means of  $^1H$  NMR and spectrophotometric and spectrofluorimetric titrations. Our initial idea was to investigate the thermodynamic stability of the supramolecular complex in two different solvents: dichloromethane and toluene, as

we did with **C<sub>60</sub>** and **C<sub>70</sub>**. In dichloromethane solution the stability constant of the complex should be higher than due to the better solvation of fullerenes with the aromatic solvent.<sup>39</sup> However, due to the reduced solubility of **Sc<sub>3</sub>N@C<sub>80</sub>** in dichloromethane all the binding experiments were performed using toluene as the solvent. With the macrocycle linked by butadiyne spacers, **Zn<sub>2</sub>-17**, we probed the complexation process with **Sc<sub>3</sub>N@C<sub>80</sub>** by <sup>1</sup>H NMR in deuterated toluene.

The value of the complex stability constant was derived from spectrophotometric (Figure 14) and spectrofluorimetric (Figure 15) titrations carried out using a solution of the macrocycle **Zn<sub>2</sub>-18** at a concentration of  $9.13 \times 10^{-7}$  M. These high dilution conditions are necessary for keeping the porphyrin absorptivities in the sensibility scale of the spectrometer. The fluorescent studies were done in the same way as described above, exciting at the isosbestic point of the Soret band observed in the UV-visible titration. The UV-visible absorption spectral changes during the addition of **Sc<sub>3</sub>N@C<sub>80</sub>** are very similar to those described for the empty fullerenes. The shift of the maximum of the Soret band of the complex is 3nm to the red and the decrease in intensity are comparable with the changes observed for the empty fullerenes. However, the isosbestic point that is observed during the titration is slightly more shifted to the red with the endofullerene.<sup>35</sup>

On the basis of the titration data and using the same methodology described for the empty fullerenes we determined the stability constant for the 1:1 complex. The binding model used in the mathematical analysis of the titration data considers the exclusive formation of such a complex. The value obtained from the UV-visible titration is  $K_a = 2.3 \times 10^5$  M<sup>-1</sup>, which is in good agreement with the one from the luminescence data,  $K_a = 2.9 \times 10^5$  M<sup>-1</sup>. This value is nearly one order of magnitude higher than that of **C<sub>70</sub>**. Evidently, the greater size of the endohedral fullerene enables it to interact more strongly with the porphyrins units. Nonetheless, the electronic polarization in **Sc<sub>3</sub>N@C<sub>80</sub>** may also contribute towards the increased binding.

Due to the scarcity of the endohedral fullerene sample, we could only perform two additions, of 0.5 and 1.2 equivalents of **Sc<sub>3</sub>N@C<sub>80</sub>**, to two separated solutions in

---

<sup>39</sup> Ruoff, R. S.; Tse, D. S.; Malhotra, R.; Lorents, D. C. *J. Phys. Chem.* **1993**, *97*, 3379-3383.

deuterated toluene of the two macrocycles, **Zn<sub>2</sub>-17** and **Zn<sub>2</sub>-18** (Figure 16), in order to probe the complexation at millimolar concentrations by means of <sup>1</sup>H NMR.

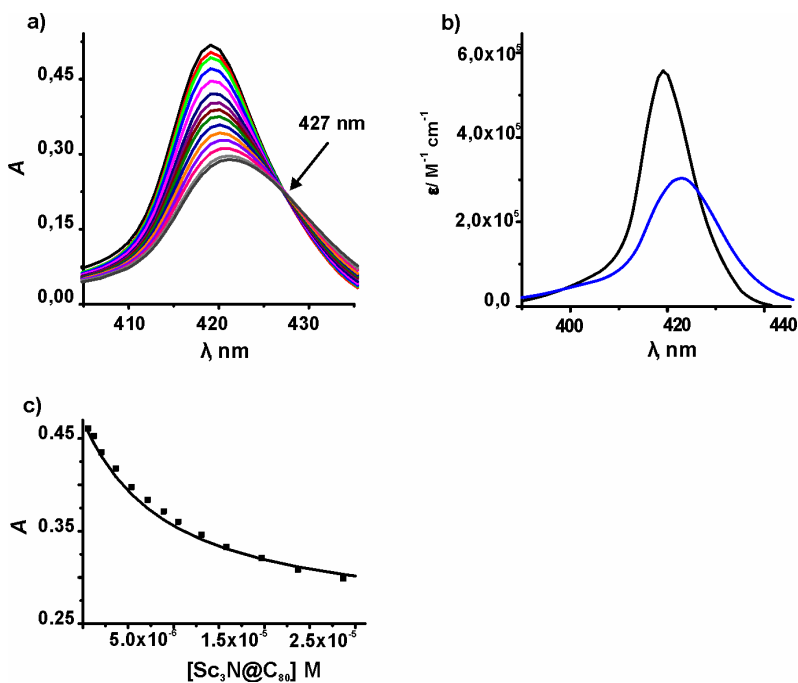


**Figure 14.** a) UV-visible titration of **Zn<sub>2</sub>-18** with **Sc<sub>3</sub>N@C<sub>80</sub>** in toluene.  $[\text{Zn}_2\text{-18}] = 9.13 \times 10^{-7}$  M and additions of **Sc<sub>3</sub>N@C<sub>80</sub>** from 0-36 equivalents. Soret band was red-shifted from 419 to 422 nm. At 427 nm appeared an isosbestic point. In this representation, we show the spectra subtracted by each contribution of **Sc<sub>3</sub>N@C<sub>80</sub>** to see better the changes in the macrocyclic receptor as well as to detect the isosbestic point; b) Calculated epsilons of **Zn<sub>2</sub>-18** (bold line), and of **Sc<sub>3</sub>N@C<sub>80</sub>·Zn<sub>2</sub>-18**, dashed line; c) Experimental data at a selected wavelength ( $\lambda = 421$  nm) in square dots fitted to the theoretical curve.

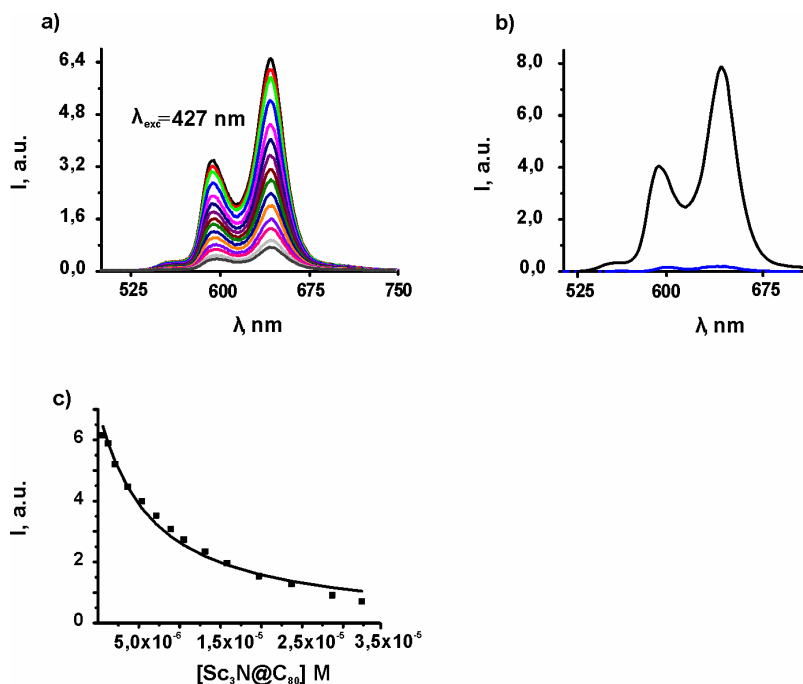


**Figure 15.** a) Fluorescence titration of  $Zn_2-18$  with  $Sc_3N@C_{80}$  in toluene.  $[Zn_2-18] = 9.13 \times 10^{-7}$  M and additions of  $Sc_3N@C_{80}$  from 0-36 equivalents. The excitation wavelength was set at 427 nm (the isosbestic point in the UV-visible titration). A quenching of the 90% was observed; b) Calculated fluorescence intensities of  $Zn_2-18$  (bold line), and of  $Sc_3N@C_{80} \cdot Zn_2-18$ , dashed line; c) Experimental data at a selected wavelength ( $\lambda = 642$  nm) in square dots fitted to the theoretical curve.

With respect to the  $^1H$  NMR titration experiments (Figure 16), for both receptors the addition of incremental amounts of  $Sc_3N@C_{80}$  produces downfield shifts, simplification and symmetrization of the  $\beta$ -pyrrole protons signals.

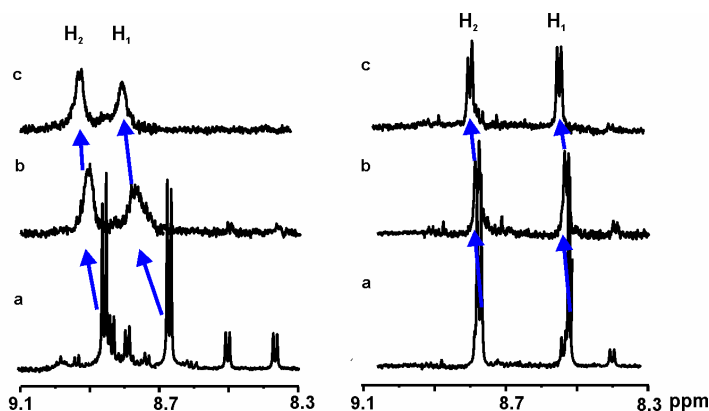


**Figure 16.** Top:  $^1\text{H}$  NMR titration of  $\text{Zn}_2\text{-18}$  with  $\text{Sc}_3\text{N@C}_{80}$  in toluene- $d_8$ .  $[\text{Zn}_2\text{-18}] = 9 \times 10^{-4}$  M and 2 additions of  $\text{Sc}_3\text{N@C}_{80}$  (0.5 and 1.2 equivalents); a) 0 eq; b) 0.5 eq; c) 1.2 eq. Bottom:  $^1\text{H}$  NMR titration of  $\text{Zn}_2\text{-17}$  with  $\text{Sc}_3\text{N@C}_{80}$  in toluene- $d_8$ .  $[\text{Zn}_2\text{-17}] = 9 \times 10^{-4}$  M and 2 additions of  $\text{Sc}_3\text{N@C}_{80}$  (0.5 and 1.2 equivalents); a) 0 eq; b) 0.5 eq; c) 1.2 eq.

As discussed above for the empty fullerenes, these results suggest at first glance the inclusion of the  $\text{Sc}_3\text{N@C}_{80}$  guest is selectively achieved by the expanded conformer of the receptor. In solution and at room temperature, the included guest must be either oscillating in the cavity at a rate that is fast in the NMR timescale or/and is sandwiched above the center of the two porphyrin rings. However, the dynamics of the two complexation processes are slightly different. Thus, the addition of approximately 0.5 equivalents of  $\text{Sc}_3\text{N@C}_{80}$  to a 1mM toluene- $d_8$  solution of any of the two dimers produced a noticeable upfield shift to the  $\beta$ -pyrrole proton signals but only to those assigned to the major isomer. On the contrary, the chemical shifts of the  $\beta$ -pyrrole protons of the minor isomer remained completely unaltered although their intensity was clearly diminished compared to the ratio found in the free state of the receptor. Taken together, these observations indicate that the endohedral fullerene  $\text{Sc}_3\text{N@C}_{80}$  is exclusively bound into the expanded isomer of the dimers reinforcing our previous assignment of the two conformational isomers. Clearly, the selective consumption of the expanded isomer drives the conformers' equilibrium towards the production of additional free expanded cyclic dimer at expenses of the collapsed isomer and explains the observed reduction of intensity for their proton signals. The chemical shift changes observed for the  $\beta$ -pyrrole protons of the

expanded isomer are more pronounced during the complexation process of **Sc<sub>3</sub>N@C<sub>80</sub>** with the hexyldioxo linker dimer **Zn<sub>2</sub>-18** than with the unsaturated parent compound **Zn<sub>2</sub>-17**. In striking contrast, only the complexation of **Sc<sub>3</sub>N@C<sub>80</sub>** with **Zn<sub>2</sub>-18** produced a significant broadening to the signals of the β-pyrrole protons that shift. This different behavior could be in principle assigned to the formation of a 1:1 complex with higher thermodynamic and kinetic stability for the interaction of **Sc<sub>3</sub>N@C<sub>80</sub>** with the hexyldioxo linker dimer **Zn<sub>2</sub>-18** than for **Zn<sub>2</sub>-17** as previously reported for the binding of **C<sub>60</sub>** and **C<sub>70</sub>**. However, the high association constant value determined for the 1:1 **Sc<sub>3</sub>N@C<sub>80</sub>•Zn<sub>2</sub>-18** complex together with the observation of a 1:2 complex in the solid state (*vide infra*) suggest the existence in solution of intermediate exchange equilibria between free receptor and complexes with different stoichiometry to be the ultimate responsible for the broadening of the signals. For both receptors, the addition of slightly more than 1 equivalent of **Sc<sub>3</sub>N@C<sub>80</sub>** induced additional downfield shifts of the β-pyrrole protons and in the case of **Zn<sub>2</sub>-18** the complete disappearance of the signals assigned to the collapsed isomer. For this receptor the β-pyrrole protons also became better defined at this point. Most likely, this is due to the predominance of the 1:1 complex in solution under these conditions. The statistically estimated stability constant for the 1:2 is in the order of  $4 \times 10^{10} \text{ M}^{-2}$  assuming a non-cooperative binding process.<sup>40</sup> Simulated speciation profiles of the full binding model demonstrate that the 1:2 complex is formed at negligible concentration values in the concentration range in which the UV-visible and fluorescence titrations have been performed. This result supports the simplification of the binding model used for the mathematical analysis of these titration data. On the contrary, at 0.9 mM concentration and with 0.5 equivalents of **Sc<sub>3</sub>N@C<sub>80</sub>**, the speciation profile shows that  $[\text{Zn}_2\text{-18}] = 8.5 \times 10^{-5} \text{ M}$ ,  $[1:1] = 1.0 \times 10^{-4} \text{ M}$  and  $[1:2] = 3.5 \times 10^{-4} \text{ M}$  and with 1 equivalent  $[\text{Zn}_2\text{-18}] = 1.0 \times 10^{-6} \text{ M}$ ,  $[1:1] = 4.8 \times 10^{-4} \text{ M}$  and  $[1:2] = 1.9 \times 10^{-4} \text{ M}$ .

We succeeded in growing single crystals of the complexes of both cyclic receptors with the endohedral fullerenes by slow evaporation of the toluene solutions prepared for the <sup>1</sup>H NMR studies and containing 1 equivalent of the endohedral fullerene.

---

<sup>40</sup> The value for the stability constant of the 1:2 complex can be statistically estimated as  $K_{12} = K_m^2 = 4 \times 10^{10} \text{ M}^{-2}$ .  $K_m$  was calculated from the UV-visible titration using a simple 1:1 binding model.

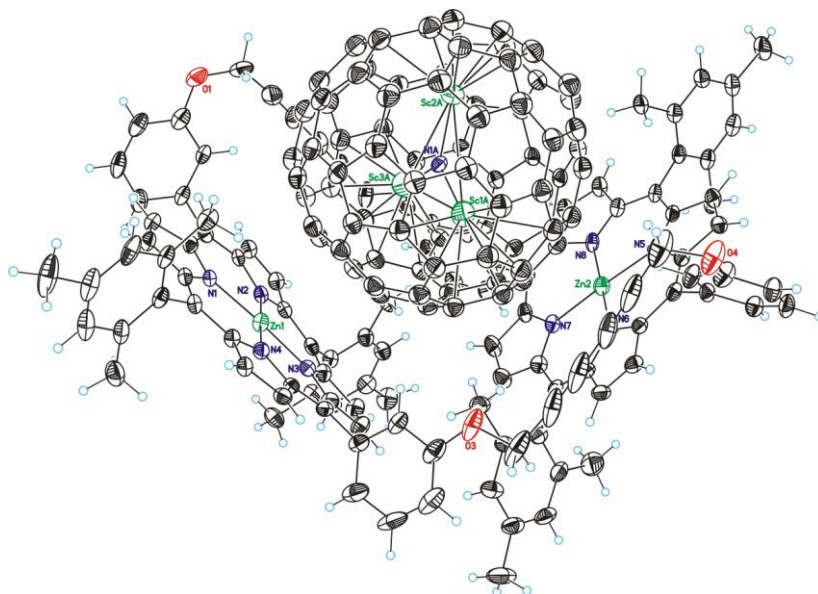


**Figure 17.** X-ray crystal structure of the 1:1 complex between bis-porphyrin **Zn<sub>2</sub>-17** and **Sc<sub>3</sub>N@C<sub>80</sub>**. Distances from the Zn atom to the closest C atom of the fullerene are 3.076 and 3.062 Å.

X-ray crystallography revealed the formation of a 1:1 complex of **Sc<sub>3</sub>N@C<sub>80</sub>** with the butadiyne linked receptor **Zn<sub>2</sub>-17**. In the solid state, the receptors adopts a scoop-like conformation very similar to the one described **C<sub>70</sub>•Zn<sub>2</sub>-17**. The crystal packing shows the formation of a zig-zag chain of **Sc<sub>3</sub>N@C<sub>80</sub>** also analogous to the one observed for **C<sub>70</sub>** when complexed with the same receptor (Figure 18).

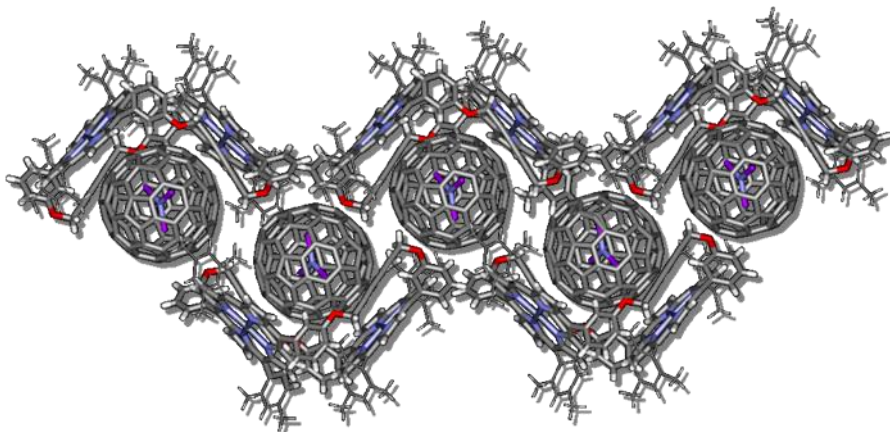


**Figure 18.** Bis-porphyrin **Zn<sub>2</sub>-17** forming a zig-zag channel with **Sc<sub>3</sub>N@C<sub>80</sub>**.

Surprisingly, the solid state structure of the single crystal grown from the solution of **Sc<sub>3</sub>N@C<sub>80</sub>** and **Zn<sub>2</sub>-18** revealed a 1:2 encapsulation complex. Two cyclic receptors self-assemble forming a supramolecular capsule that traps one molecule of **Sc<sub>3</sub>N@C<sub>80</sub>** in its interior (Figure 19). The complex possesses one C<sub>2</sub> symmetry plane and the asymmetric unit contains one cyclic receptor and only half of the atoms of the endohedral fullerene. The conformation adopted by the receptor in the 1:2 complex is in the middle of a scoop-shaped observed for the 1:1 complexes involving the receptor with butadiyne linkers and the clam-shaped described for the 1:1 complexes of **Zn<sub>2</sub>-18** with the empty fullerenes. Aida has reported the formation of related 1:2 complexes in the binding of **C<sub>70</sub>** by cyclic bis-porphyrin with -O(CH<sub>2</sub>)<sub>4</sub>-O linkers. The increase in size of the endohedral fullerene with respect to **C<sub>70</sub>** produces that the accessible π-surface not included in the aromatic cavity of the receptor is augmented allowing the establishment of attractive interactions with a second molecule of the receptor. The alkyl spacers of both receptors also interact with the encapsulated endohedral fullerene through CH-π interactions. In the light of this finding, it is possible to rationalize the results obtained in <sup>1</sup>H NMR titrations of **Zn<sub>2</sub>-18** with **Sc<sub>3</sub>N@C<sub>80</sub>**, assuming than in solution the 1:2 complex is the main species formed under strict stoichiometric control.

The scarcity of **Sc<sub>3</sub>N@C<sub>80</sub>** did not allow us to perform complete titrations and additional experiments at <sup>1</sup>H NMR concentration.

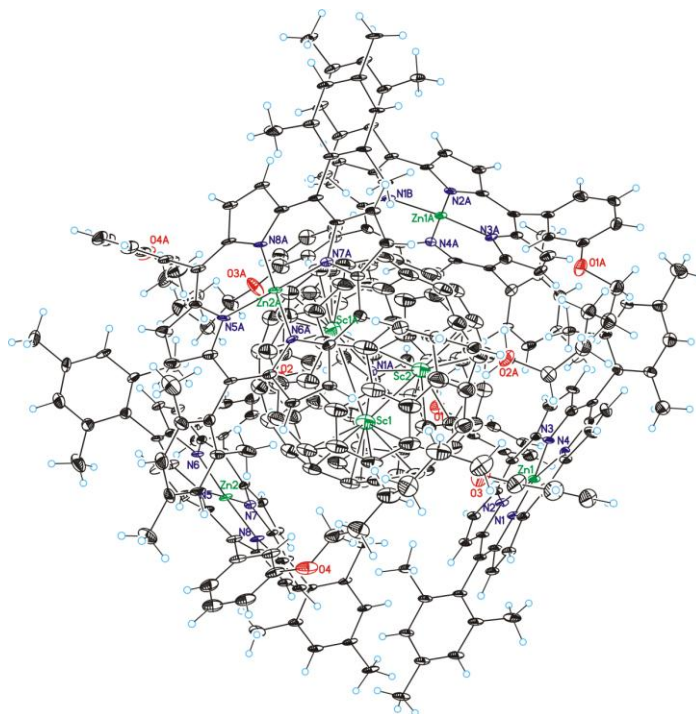


**Figure 19.** X-ray crystal structure of the 1:2 complex between bis-porphyrin **Zn<sub>2</sub>-18** and **Sc<sub>3</sub>N@C<sub>80</sub>**. Distances between Zn atoms of porphyrins belonging to different macrocycles and placed one in front of the other are 13.133 Å.

The trimetallic nitride unit inside the fullerene is oriented perpendicularly to one of the porphyrin planes, and it is aligned along one of the nitrogen-zinc-nitrogen axes of the porphyrin. The endohedral metallofullerene is entirely neutral, the **C<sub>80</sub>** cage bears a six negative charge but the nitride which has three negative charges is surrounded by three metals, Sc, with three positive charges each. The fullerene is positive inside and negative outside, providing a really fashionable structure to be used in electron or energy transfer devices. Figure 20 depicts the structure in order to see better the position of the bis-porphyrins.

All the crystal structures presented here were grown by slow evaporation of *p*-Xylol at 45°C for those which have the **Zn<sub>2</sub>-17** and at 60°C for those with **Zn<sub>2</sub>-18**.

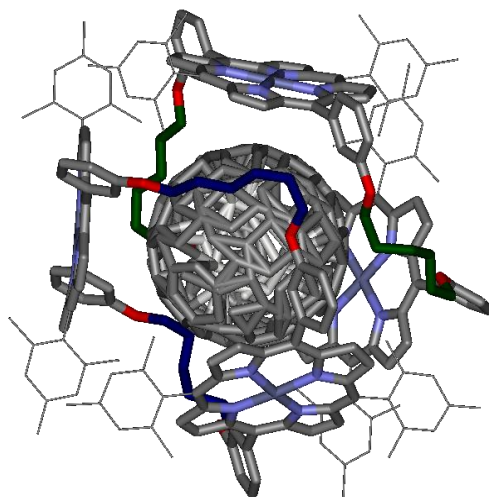


**Figure 20.** X-ray crystal structure of the 1:2 complex between bis-porphyrin **Zn<sub>2</sub>-18** and **Sc<sub>3</sub>N@C<sub>80</sub>**. The linker chains from both macrocycle are distinguish by the color of the linker chains, one in dark blue and the other in dark green. Hydrogens are removed for clarity.

### 3. Conclusions

We have studied and confirmed the formation, in solution and solid state, of inclusion complexes between two cyclic bis-porphyrins and three fullerenes of different size and properties. To the best of our knowledge, these are the first solid state structures of an endohedral fullerene bound to molecular bis-porphyrin. The more flexible hexyldioxo spaced host **Zn<sub>2</sub>-18** produced a capsule-type 1:2 complex in the solid state. This assembly can be considered as an evolved example of hetero “bucky onion” displaying two different levels of molecular encapsulation.

With the macrocycle with the triple bonds in the linker chains we didn't observe complexation with **C<sub>60</sub>** neither in solution nor in the solid state. The association is bigger with the macrocycle having the hydrogenated chains, due to the better flexibility and also to CH- $\pi$  interactions from the linkers and the fullerene, for the three types of fullerenes. We also proved that complexation is more favourable in dichloromethane than in toluene (until one order of magnitude for **C<sub>60</sub>** and **C<sub>70</sub>**).

In spite of we didn't have data from studies made in dichloromethane with the endohedral fullerene due to solubility problems, the association constant values derived from the studies in toluene are in the same order of the association constant values for **C<sub>60</sub>** and **C<sub>70</sub>** in dichloromethane.

All the studies, in solution: UV-visible, fluorescence and <sup>1</sup>H NMR, and the X-ray crystallographic data, are in perfect agreement between them.

Until now, the desired photophysical studies didn't give us reliable data, and we are waiting for these experiments in order to state the type of process that is taking place between the fullerenes and the porphyrins when the complexes are formed.

## 4. Experimental section

### 4.1 General information and instrumentation

All commercial reagents, unless otherwise noted, were reagent grade and used without further purification. Solvents were of HPLC grade quality, obtained commercially and used without further purification. Anhydrous solvents were obtained from a solvent purification system SPS-400-6 from Innovative Technologies, Inc. <sup>1</sup>H NMR spectra were recorded on Bruker Avance 400 (400.1 MHz for <sup>1</sup>H NMR) and Bruker Avance 500 (500.1 MHz for <sup>1</sup>H NMR) NMR spectrometers. UV-visible spectra were measured on a UV-Vis spectrophotometer Shimadzu UV-2401PC and the measurements of fluorescence were obtained on an Aminco Bowman Series 2 luminescence spectrometer. The NIR-UV-visible measurements were performed on a UV/vis/NIR spectrophotometer Perkin-Elmer Lambda 950. Lifetimes were measured with an IBH 5000F time-correlated single-photon counting device, using pulsed NanoLED excitation sources. Crystal data set were collected at Beam line BM16<sup>41</sup> at ESRF wavelength = 0.7380 Å; Si111 monochromator; absorption coefficient = 0.553 mm<sup>-1</sup>; ADSC Q210r CCD detector and cooled with an Oxford

---

<sup>41</sup> The macromolecular crystallography station at beamline BM16 at the ESRF Juanhuix, J.; Labrador, A.; Beltran, D.; Herranz, J. F.; Carpentier, P.; Bordas, J. *Rev. Sci. Instrum.* **2005**, *76*, -. 086103.

Cryostream low temperature device ( $T = 100(2)$  K). Full-sphere data collection was used with  $\varphi$  scans.

Programs used: Data collection MXCube, Indexing Apex2 V2009.11 (Bruker-Nonius 2008), data reduction Saint + Version 7.60A (Bruker AXS 2008) and absorption correction SADABS V. 2008/1 (2008). *Structure Solution*: SIR2007.<sup>42</sup> and SHELXTL Version 6.10 (Sheldrick, 2000) was used.<sup>43</sup> *Structure Refinement*: SHELXTL-97-UNIX VERSION.

## 2.1 Binding studies

### a. <sup>1</sup>H NMR titrations

We prepared a standard solution of **Zn<sub>2</sub>17** and **Zn<sub>2</sub>-18** (1 mM) and using this solution as solvent we prepared a fullerene (**C<sub>60</sub>**, **C<sub>70</sub>** or **Sc<sub>3</sub>N@C<sub>80</sub>**) solution (10 mM) that will be used for the titration experiments. In this way the incremental addition of fullerene to the initial porphyrin solution will not dilute the porphyrin concentration; <sup>1</sup>H NMR titration was carried out by acquiring a spectrum of an aliquot (500  $\mu$ L) of the porphyrin (host) stock solution in toluene-*d*<sub>8</sub> at a concentration around 1mM, and adding increasing aliquots of the fullerene solution (guest), also in toluene-*d*<sub>8</sub>, and at a concentration approximately 10 mM. After each addition, a new <sup>1</sup>H NMR spectrum was acquired.

### b. UV-visible and fluorescence titrations

The UV-visible and fluorescence titrations were carried out by running a spectrum of the host solution of **Zn<sub>2</sub>17** and **Zn<sub>2</sub>-18** in toluene or dichloromethane at  $\mu$ M concentration and adding to it incremental aliquots of the three different fullerene solutions **Sc<sub>3</sub>N@C<sub>80</sub>** solution also in the same solvent. To avoid the dilution of the host solution the titrating guest solution was prepared using the solution of the host as the solvent. After each addition of guest a new UV-visible and fluorescence spectrum was obtained. As in the luminescence experiment we want to excite the sample in the isosbestic point, we needed to run before a UV-visible titration experiment in order to find the wavelength of the

<sup>42</sup> Caliendo, R.; Carrozzini, B.; Cascarano, G. L.; De Caro, L.; Giacobuzzo, C.; Siliqi, D. *J. Appl. Crystallogr.* **2007**, *40*, 883-890.

<sup>43</sup> Sheldrick, G. M. *SHELXTL Crystallographic System 6.14*, Bruker AXS Inc., Madison, Wisconsin, **2000**.

isosbestic point that turned out to be 427 nm. The sets of data obtained from the UV-visible and fluorescence spectrophotometric titrations were analyzed by fitting the whole series of spectra at 1 nm interval for the UV-visible titration/using the software SPECFIT 3.0, which uses a global system with expanded factor analysis and Marquardt least-squares minimization to obtain globally optimized parameters.

## CHAPTER 5

### ***“Sandwich complexes mediated by DABCO coordination with porphyrins linked to cyclopeptides”***

The results written in this chapter have been accepted for publication in: Hernández-Eguía, Laura P.; Brea, R. J.; Castedo, L.; Ballester, P.; Granja, J. “Regioisomeric Control induced by DABCO Coordination to Rotatable Self-Assembled Bis- and Tetra-porphyrin  $\alpha,\gamma$ -Cyclic Octapeptide Dimers (DABCO = 1,4-Diazabicyclo[2.2.2]octane).” *Chem. Eur. J.* (2010), 0000-0000

UNIVERSITAT ROVIRA I VIRGILI  
SUPRAMOLECULAR CHEMISTRY OF BIS-PORPHYRINS  
Laura Patricia Hernández Eguía  
ISBN:978-84-694-0308-2/DL:T-204-2011

## 1. Introduction

With the aim of employing porphyrins as a significant part of more complex assemblies, that is, using their properties and functionality to achieve determined structural features, we started a collaboration project with Professor Juan R. Granja from the University of Santiago de Compostela. In his group they develop new synthetic strategies for the construction of peptide nanotubes focused on nanotechnological applications that could be involved in areas as catalysis, pharmacology, molecular recognition and also drawn in transport and optoelectronic devices.

The most widely known type of nanotube is the carbon nanotube,<sup>1</sup> which is also a member of the fullerene structural family, apart from others based on zeolites<sup>2</sup> or cyclodextrines.<sup>3</sup> However, it is not possible to guarantee the uniformity on its internal diameter, which together with the length, are crucial characteristics for the most relevant applications.

In the last few years highly efficient strategies have been worked out for obtaining tubular structures following the principles of supramolecular chemistry, such as the use of non-covalent bonds, affording more control in length and internal diameter. Among these alternatives is the stacking up of cyclic molecules,<sup>4</sup> where the control of the internal diameter resides on the macrocyclic unit. This is an example of a “bottom-up” approach to functional nanostructures. Others are sheet folding (proposed for the construction of carbon nanotubes from graphite),<sup>5</sup> construction of helicoidal structures<sup>6</sup> or assembling of rigid molecules as a barrel.<sup>7</sup>

Cyclopeptides are regarded as fashioned molecules to prepare nanotubes.<sup>8,9,10,11,12</sup> It is good to know that it is quite easy modify the value of the internal diameter of the nanotube

---

<sup>1</sup> Baughman, R. H.; Zakhidov, A. A.; de Heer, W. A. *Science* **2002**, *297*, 787-792.

<sup>2</sup> Langley, P. J.; Hulliger, J. *Chem. Soc. Rev.* **1999**, *28*, 279-291.

<sup>3</sup> Harada, A.; Li, J.; Kamachi, M. *Nature* **1993**, *364*, 516-518.

<sup>4</sup> Hartgerink, J. D.; Clark, T. D.; Ghadiri, M. R. *Chem.--Eur. J.* **1998**, *4*, 1367-1372.

<sup>5</sup> Iijima, S. *Nature* **1991**, *354*, 56-58.

<sup>6</sup> Prince, R. B.; Brunsveld, L.; Meijer, E. W.; Moore, J. S. *Angew. Chem., Int. Ed.* **2000**, *39*, 228-+.

<sup>7</sup> Sakai, N.; Mareda, J.; Matile, S. *Acc. Chem. Res.* **2005**, *38*, 79-87.

<sup>8</sup> Ghadiri, M. R.; Granja, J. R.; Milligan, R. A.; McRee, D. E.; Khazanovich, N. *Nature (London, United Kingdom)* **1993**, *366*, 324-7.

<sup>9</sup> Ghadiri, M. R.; Granja, J. R.; Buehler, L. K. *Nature (London, United Kingdom)* **1994**, *369*, 301-4.

only by changing the number of amino acids that form the cyclopeptide. In the last few years the self-assembly properties of cyclic oligopeptides that contain a  $\gamma$ -amino acid functionality installed in a cyclic backbone have been studied.<sup>13,14,15</sup> They are stacked up thanks to hydrogen bonds<sup>16</sup> between them, yielding a flat conformation in which all the aminoacids' lateral chains are looking outwards and the amide groups are oriented perpendicular to the plane of the ring. The C=O groups are oriented to one plane of the cyclopeptide and the N-H groups to the other, in a way that hydrogen bonds could be formed between them. Any cyclomonomer possesses a  $C_n$ -symmetry. Consequently, the self-assembly process of the cyclic monomer should produce a mixture of  $n$  nonequivalent regioisomeric dimers. Each dimer features a cross-strand pair-wise relationship between the amino acid components of the cyclic monomer (Scheme 1).<sup>17</sup>

The existence of more favorable cross-strand interactions between the side chains of monomers in one of the dimers should induce the prevalent formation of this system in the solution mixture. Previous studies directed at the search for pair-wise side-chain interactions that could control the selective formation of a single dimer met with limited success. Cyclic hexapeptides of the type *cyclo*[*L*-Ser-*D*-MeN- $\gamma$ -Ach-(*L*-Phe-*D*-MeN- $\gamma$ -Ach)<sub>2</sub>], in which the serine was introduced with the expectation that additional hydrogen bonding interactions between serine hydroxyl groups belonging to different cyclic monomers would favor the formation of one of the possible regioisomeric dimers, showed a reduced preference for the dimer in which the serines are in register.

---

<sup>10</sup> Leclair, S.; Baillargeon, P.; Skouta, R.; Gauthier, D.; Zhao, Y.; Dory, Y. L. *Angew. Chem., Int. Ed.* **2004**, *43*, 349-353.

<sup>11</sup> Ortiz-Acevedo, A.; Xie, H.; Zorbas, V.; Sampson, W. M.; Dalton, A. B.; Baughman, R. H.; Draper, R. K.; Musselman, I. H.; Dieckmann, G. R. *J. Am. Chem. Soc.* **2005**, *127*, 9512-9517.

<sup>12</sup> Ashkenasy, N.; Horne, W. S.; Ghadiri, M. R. *Small* **2006**, *2*, 99-102.

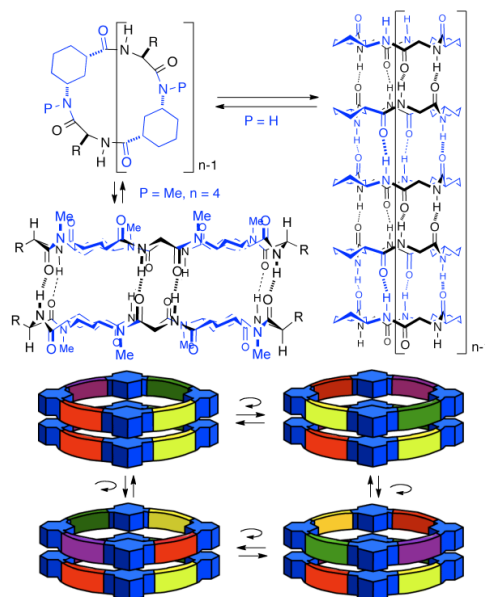
<sup>13</sup> Amarin, M.; Castedo, L.; Granja, J. R. *J. Am. Chem. Soc.* **2003**, *125*, 2844-2845.

<sup>14</sup> Brea, R. J.; Castedo, L.; Granja, J. R. *Chem. Commun. (Cambridge, U. K.)* **2007**, 3267-3269.

<sup>15</sup> Amarin, M.; Castedo, L.; Granja, J. R. *Chem.--Eur. J.* **2008**, *14*, 2100-2111.

<sup>16</sup> Brea, R. J.; Reiriz, C.; Granja, J. R. *Chem. Soc. Rev.* **2010**, *39*, 1448-1456.

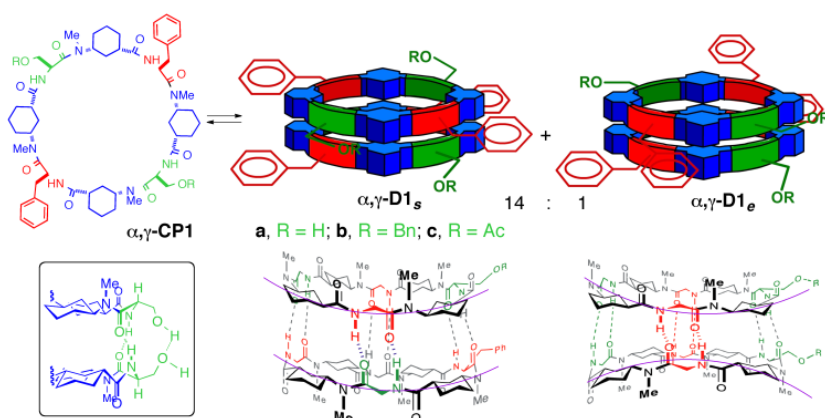
<sup>17</sup> Amarin, M.; Villaverde, V.; Castedo, L.; Granja, J. R. *J. Drug Delivery Sci. Technol.* **2005**, *15*, 87-92.



**Scheme 1.** Model representation of nanotube formation by the self-assembly of multiple copies of an  $\alpha,\gamma$ -cyclopeptide ( $\alpha,\gamma$ -CP) in which  $n = 2$  for the CP tetramer,  $n = 3$  for the CP hexamer and so on. The  $\gamma$ -amino acid is 3-aminocyclohexanecarboxylic acid ( $\gamma$ -Ach). Molecular representation of the dimer self-assembled from a substituted cyclooctapeptide ( $n = 4$ ) with  $c_4$  symmetry. At the bottom of the scheme is a cartoon representation of the four non-equivalent dimers that can be assembled from cyclooctapeptides that lack a symmetry axis.

Further studies on the cyclic octapeptide *cyclo*[(L-Ser-D-MeN- $\gamma$ -Ach-L-Phe-D-MeN- $\gamma$ -Ach)<sub>2</sub>] ( $\alpha,\gamma$ -CP1a), which in principle could form two hydrogen bonds between the four serine side chains of adjacent monomers in the  $\alpha,\gamma$ -D1a dimer, was also very disappointing (Scheme 2). In this case, the twofold-symmetric cyclic octapeptide, which contains two Ser and two Phe units in each monomer, led to the predominant formation of the regioisomeric dimer in which the chains of Phe and Ser are faced  $\alpha,\gamma$ -D1a<sub>s</sub> (Scheme 2), i.e. a “staggered” arrangement. The almost exclusive formation of the alternative “eclipsed” arrangement  $\alpha,\gamma$ -D1a<sub>e</sub> (Scheme 2) was expected, as this should be favoured by the formation of hydrogen bonds between the two Ser side chains of the monomers, which in this arrangement are in register. This unexpected behavior was attributed to a combination of conformational effects experienced by the CP scaffold when Ser are present and to the size mismatch. It is well known that Ser has a low tendency to be involved in  $\beta$ -sheets

compared to Phe.<sup>18</sup> It is likely that this sequence induces a slightly distortion of the optimum flat conformation of the cyclopeptide required to maximize the hydrogen bonding interactions in the  $\beta$ -sheet motif of the dimer. The staggered dimer in which the small Ser is confronted with the large Phe residue features additional complementarity between the shapes of the buckle conformation adopted by the monomers when compared to the alternative eclipsed regioisomer. The staggered arrangement allows for a better adjustment of the intermolecular hydrogen-bonding interactions. All of these effects translate into a lower energy for the staggered regioisomeric dimer compared to the eclipsed one. This interpretation is also supported by the fact that the ratio between staggered and eclipsed dimers is not modified by the introduction of protecting groups on the serine side chain, such as benzyl or acetate ( $\alpha,\gamma$ -CP1b and  $\alpha,\gamma$ -CP1c), as these must not change the buckled conformation adopted by the cyclic peptide.



**Scheme 2.** Solution equilibrium of octapeptides *cyclo*[(L-Ser-D-MeN- $\gamma$ -Ach-L-Phe-D-MeN- $\gamma$ -Ach)<sub>2</sub>] ( $\alpha,\gamma$ -CP1a, b or c) into the corresponding non-equivalent dimers. The staggered arrangement of the homologous residues provides the more favorable binding geometry for the dimer ( $\alpha,\gamma$ -D1<sub>s</sub>). The eclipsed arrangement of the monomers in the dimer  $\alpha,\gamma$ -D1<sub>e</sub> in which, in principle, it is possible to establish two hydrogen-bonding interactions between the hydroxyl groups of the serine side chains (model of this interaction is depicted in the inset) turns out to be energetically less favourable.

<sup>18</sup> Chou, P. Y.; Fasman, G. D. *Biochemistry* **1974**, *13*, 211-222.

We envisaged that an alternative approach for controlling the relative arrangement of the monomers in the dimer assembly could be based not on the direct interactions established between the side chains of the amino acid residues but on the use of an external component capable of forming a ditopic interaction with efficient binding sites covalently attached to the side chains. Based on previous experience,<sup>19</sup> we considered the use of Zn-porphyrins as potential binding units for the decoration of the dimeric aggregate. The 1:2 DABCO-porphyrin sandwich motif has been used in many cases to assemble zinc-porphyrin dimers that bear covalent spacers into cofacial intramolecular complexes (DABCO = 1,4-diazabicyclo[2.2.2]octane).<sup>20</sup> We planned the covalent functionalization of the cyclopeptide monomer with one or two Zn-porphyrin units. The hydrogen-bonding driven dimerization process of the monomer should induce the quantitative formation of bis- and tetraporphyrinic supramolecular aggregates, respectively. We expected to induce the cofacial orientation of the Zn-porphyrin units in the dimer by the ditopic coordination of one DABCO molecule. Needless to say, the formation of sandwich motifs in the supramolecular oligoporphyrinic systems requires that the appropriate geometrical features can be attained. Simple molecular modelling studies showed that sandwich complex formation was geometrically reasonable. Assuming that the staggered arrangement of porphyrin units is energetically more favourable in the free dimer, the addition of one equivalent of DABCO should induce the formation of the alternative cofacial arrangement of the monomers by ditopic coordination with two adjacent Zn-porphyrin units. In short, control of the relative arrangement of the monomers of the dimeric assembly could be achieved at will by means of an external molecular trigger.

To evaluate the feasibility of our proposal, we designed and synthesized two octacyclopeptides derived from  $\alpha,\gamma$ -CP1a. One peptide bears only one porphyrin unit ( $\alpha,\gamma$ -CP2) and the other one ( $\alpha,\gamma$ -CP3) contains two porphyrin units.

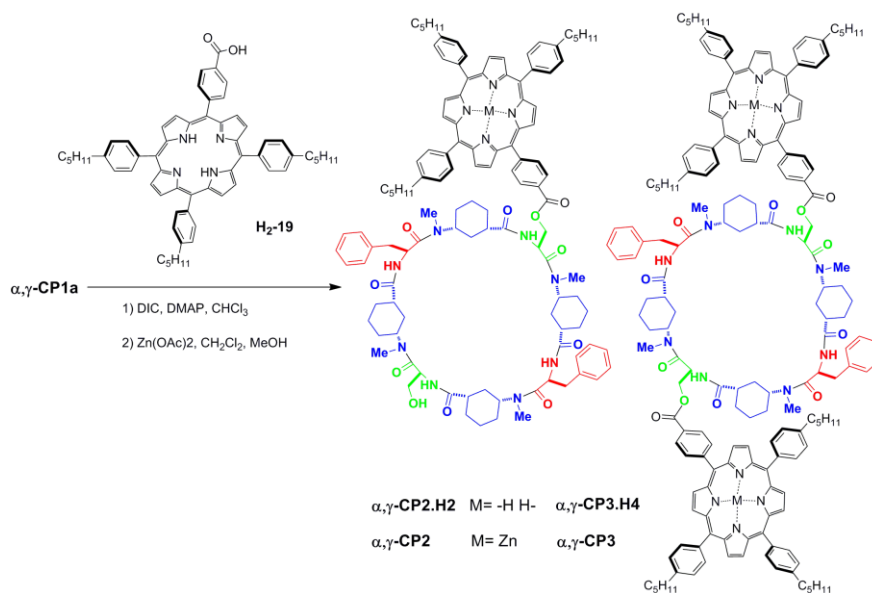
<sup>19</sup> Ballester, P.; Costa, A.; Castilla, A. M.; Deya, P. M.; Frontera, A.; Gomila, R. M.; Hunter, C. A. *Chem.--Eur. J.* **2005**, *11*, 2196-2206.

<sup>20</sup> Osswald, P.; You, C. C.; Stepanenko, V.; Würthner, F. *Chem.--Eur. J.* **2010**, *16*, 2386-2390.

## 2. Results and discussion

### 2.1 Synthesis and purification

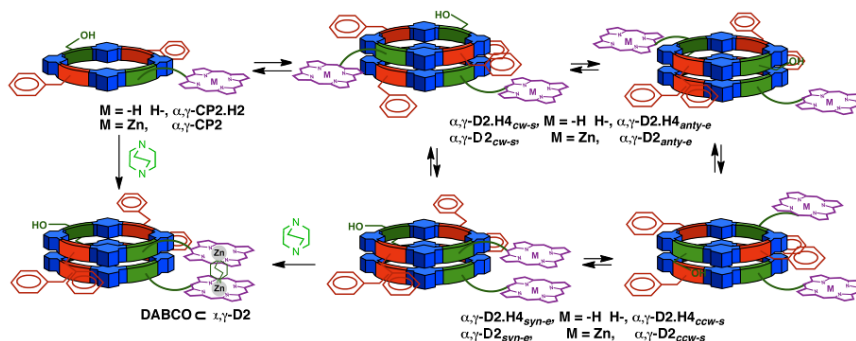
The synthesis of the CP precursor  $\alpha,\gamma$ -CP1a has been reported previously.<sup>21</sup> Treatment of  $\alpha,\gamma$ -CP1a with 1.5 equivalents of the porphyrin carboxylic acid **H<sub>2</sub>-19** in the presence of DIC provided a mixture of the porphyrin-CP conjugates  $\alpha,\gamma$ -CP2·H2 and  $\alpha,\gamma$ -CP3·H4 in a 2:3 ratio, which contain one and two porphyrin units, respectively (Scheme 3). The <sup>1</sup>H NMR spectra of both porphyrin-CP-derivatives in CDCl<sub>3</sub> are very complex. Nevertheless, the formation of dimeric supramolecular aggregates in solution can be inferred from the downfield shifts experienced by the N–H protons of the CP component, which resonate at  $\delta = 8.2$ – $9.0$  ppm, and by the spreading out of other proton signals.



**Scheme 3.** Preparation of  $\alpha,\gamma$ -CP2 and  $\alpha,\gamma$ -CP3 by esterification between  $\alpha,\gamma$ -CP1a and the porphyrin carboxylic acid **H<sub>2</sub>-19** followed by metallation with Zn(AcO)<sub>2</sub>.

<sup>21</sup> Amorin, M.; Castedo, L.; Granja, J. R. *Chem.--Eur. J.* **2005**, *11*, 6543-6551.

Based on previous results obtained with simpler substrates, we surmise the presence of four non-equivalent dimeric structures in solution in the case of the monoporphyrin cyclopeptide derivative  $\alpha,\gamma\text{-CP2}\cdot\text{H2}$  (Scheme 4).



**Scheme 4.** Dimer equilibrium of  $\alpha,\gamma\text{-CP2}\cdot\text{H2}$  and  $\alpha,\gamma\text{-CP2}$  to form the corresponding four non-equivalent dimers, two staggered ( $\alpha,\gamma\text{-D2.H4}_{ccw-s}/\alpha,\gamma\text{-D2}_{ccw-s}$  and  $\alpha,\gamma\text{-D2.H4}_{cw-s}/\alpha,\gamma\text{-D2}_{cw-s}$ ) and two eclipsed ( $\alpha,\gamma\text{-D2.H4}_{anti-e}/\alpha,\gamma\text{-D2}_{anti-e}$  and  $\alpha,\gamma\text{-D2.H4}_{syn-e}/\alpha,\gamma\text{-D2}_{syn-e}$ ), in which only the former Zn-metallated one can coordinate diamines such as DABCO to give the complex  $DABCO \subset \alpha,\gamma\text{-D2}$ .

Cyclic octapeptides like  $\alpha,\gamma\text{-CP2}\cdot\text{H2}$  have three differently sized residues [1 large (L = porphyrin), 2 medium (M = Phe) and 1 small (S = Ser)] and these are expected to form four regioisomeric structures upon dimerization (Figure 1). These four regioisomers can be classified into two main sets depending on the relative orientation of an imaginary diagonal line joining the two  $C_{\alpha}$  carbons of the Phe (M) residues of each monomer. We refer to the “staggered” isomer when the lines are perpendicular. In the “eclipsed” isomer the lines are parallel. Moreover, in each set there are two possible regioisomers as a function of the relative orientation of the porphyrin substituents (L) of each monomer. Thus, we named the regiodimer in the parallel arrangement as “syn” when the two porphyrins are in register or “anti” when each porphyrin unit faces a Ser residue. Finally, we refer to the two regioisomers with the perpendicular arrangement as “clockwise = cw” or “counterclockwise = ccw” depending on the sense of the shorter screw joining the two porphyrin units regardless of the face from which they are viewed.

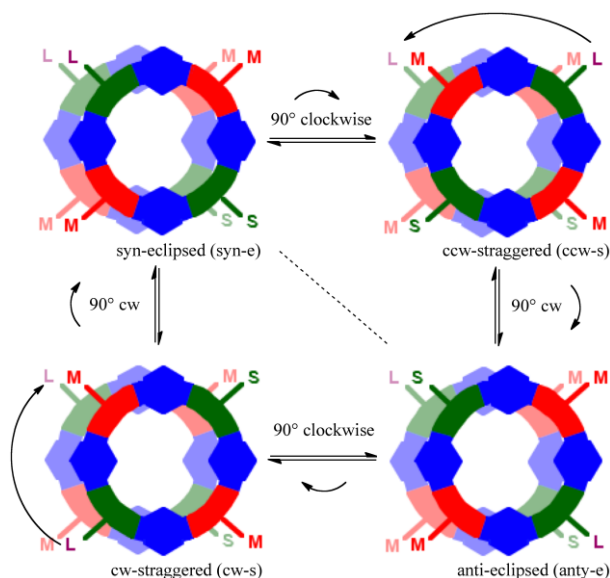


**Figure 1.** Top view of the schematic representation of the four non-equivalent dimers derived from  $\alpha,\gamma$ -CP2.H2 and  $\alpha,\gamma$ -CP2 and the nomenclature proposed for these systems.

Based on the previous results obtained with peptides  $\alpha,\gamma$ -CP1a,  $\alpha,\gamma$ -CP1b and  $\alpha,\gamma$ -CP1c, we propose that similar ratios of the regioisomeric dimers should be present in the solutions of  $\alpha,\gamma$ -D2 and  $\alpha,\gamma$ -D3. In the case at hand, we were not able to measure experimentally the ratio of the dimers in solution using  $^1\text{H}$  NMR experiments due to the complexity of the spectra. Consequently, we simply assume that the regioisomeric dimer that is found as the minor component of the mixture corresponds to the relative eclipsed-*syn* arrangement or  $\alpha,\gamma$ -D2.H4<sub>syn-e</sub>. By analogy to our observations with  $\alpha,\gamma$ -CP1a,  $\alpha,\gamma$ -CP1b and  $\alpha,\gamma$ -CP1c, this regioisomer should be found in an approximate ratio of 1:20 with respect to the other isomers. However, this is the regioisomeric dimer that features the appropriate arrangement of the porphyrin units (pre-organization) to be engaged in the formation of a sandwich complex with DABCO. On the other hand, the dimerization process of  $\alpha,\gamma$ -CP3-H4, which has only two differently sized residues – 2 porphyrins (L) and 2 Phe (M) – should produce only two regioisomeric dimers, i.e. “eclipsed” and “staggered” (Scheme 5). Once again, we tentatively assign the eclipsed arrangement or  $\alpha,\gamma$ -D3-H8<sub>e</sub> to the minor isomer present in the solution while the major isomer should correspond to the staggered arrangement or  $\alpha,\gamma$ -D3-H8<sub>s</sub>, in which potentially favorable  $\pi$ -

$\pi$  interactions between the large aromatic surfaces of the porphyrin substituents are excluded.

Metallation of the substituted porphyrin CPs was carried out by treatment of the corresponding free bases  $\alpha,\gamma$ -CP2·H2 and  $\alpha,\gamma$ -CP3·H4 with zinc(II) acetate (20 equiv) in a mixture of methylene chloride and methanol. The zinc-metallated porphyrin CPs  $\alpha,\gamma$ -CP2 and  $\alpha,\gamma$ -CP3 were isolated in almost quantitative yield after purification on a neutral alumina column (Scheme 3). The purity of the isolated metallated compounds was evaluated by gel permeation chromatography (GPC). A single chromatographic peak was observed for both compounds. In the case of  $\alpha,\gamma$ -CP3 the peak had a lower retention time than that for  $\alpha,\gamma$ -CP2. This finding is expected for a molecular species with a higher molecular weight. It is known that the CPs used as the scaffolds to attach the porphyrin substituents have a strong tendency to dimerize in organic solvents of low polarity ( $K_d \sim 10^8 \text{ M}^{-1}$ ). The chromatographic peaks obtained during the GPC analyses of the metallated compounds probably correspond to the mixture of dimeric regioisomers since toluene was used as the eluent.

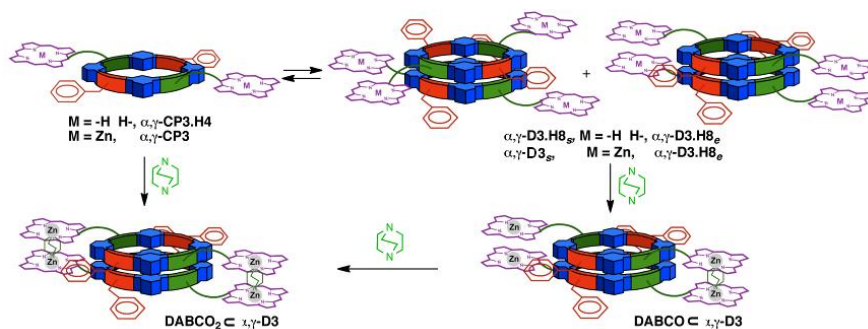
## 2.2 Coordination studies

The coordination of DABCO, see Schemes 4 and 5, to the two porphyrin cyclopeptide derivatives,  $\alpha,\gamma$ -CP2 and  $\alpha,\gamma$ -CP3, was first probed by carrying out UV-visible titrations in chloroform solution. The host concentration was kept constant at  $10^{-6} \text{ M}$  throughout the titration experiment. Due to the potential modification of the chirality induced from the CP scaffold to the Zn-bis-porphyrin units of the receptors upon DABCO binding, as well as the likely existence of exciton coupling between these units in the sandwich complexes, we also monitored the binding interactions by CD spectroscopy.<sup>22,23,24</sup> The binding process was also investigated by  $^1\text{H}$  NMR spectroscopy.

<sup>22</sup> Huang, X. F.; Nakanishi, K.; Berova, N. *Chirality* **2000**, *12*, 237-255.

<sup>23</sup> Borovkov, V. V.; Hembury, G. A.; Inoue, Y. *Acc. Chem. Res.* **2004**, *37*, 449-459.

<sup>24</sup> Etxebarria, J.; Vidal-Ferran, A.; Ballester, P. *Chem. Commun. (Cambridge, U. K.)* **2008**, 5939-5941.



**Scheme 5.** Dimer equilibrium of  $\alpha,\gamma$ -CP3.H4 and  $\alpha,\gamma$ -CP3 to form the corresponding two non-equivalent dimers, the staggered ( $\alpha,\gamma$ -D3.H8<sub>s</sub>/ $\alpha,\gamma$ -D3<sub>s</sub>) and the eclipsed ( $\alpha,\gamma$ -D3.H8<sub>e</sub>/ $\alpha,\gamma$ -D3<sub>e</sub>). Only the Zn-metallated eclipsed system can coordinate DABCO to give the complex  $DABCO_2 \subset \alpha,\gamma$ -D3 through the monocoordinated species  $DABCO \subset \alpha,\gamma$ -D3.

In order to simplify the analysis of the UV-visible titration data and due to the high tendency for dimerization exhibited in organic non-polar solvents such as chloroform by the cyclopeptide scaffold of the porphyrin monomers used in this study, we considered the self-assembled dimers  $\alpha,\gamma$ -D2 and  $\alpha,\gamma$ -D3 to be formed quantitatively in solution. Thus, the mathematical analyses of the experimental titration data were performed considering that the total concentration of the active receptor, i.e. the supramolecular tweezers  $\alpha,\gamma$ -D2 or  $\alpha,\gamma$ -D3, is half the concentration of cyclopeptides  $\alpha,\gamma$ -CP2 or  $\alpha,\gamma$ -CP3. Simple molecular modelling studies showed that both receptors can adopt conformations in which the two- or the four-porphyrin units are cofacially arranged. The calculated distances of the cofacial arrangements, as obtained from the minimized structures,<sup>25</sup> seem to be suitable for the ditopic coordination of DABCO (Figure 2). In the case of the dimer of receptor  $\alpha,\gamma$ -D2 the ditopic interaction with DABCO affords a 1:1 complex ( $DABCO \subset \alpha,\gamma$ -D2) in which one DABCO molecule is sandwiched between two porphyrin rings. Similarly, for receptor  $\alpha,\gamma$ -D3 the formation of a double sandwich complex ( $DABCO_2 \subset \alpha,\gamma$ -D3) is geometrically plausible.

<sup>25</sup> *CAChe WorkSystem*, version 6.1.12.33; Fujitsu Limited (USA), 2004.

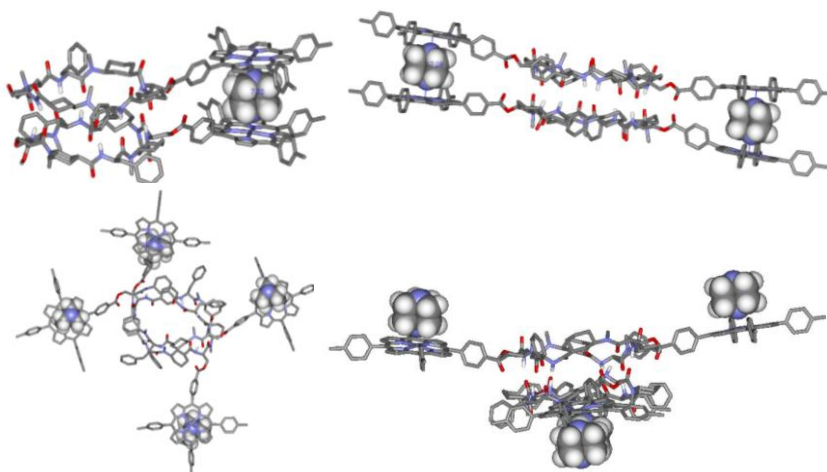


**Figure 2.** Top left: CAChe minimized structure of the 1:1 complex  $\text{DABCO} \subset \alpha, \gamma\text{-D2}_{e\text{-syn}}$ , in which one DABCO molecule is sandwiched between the two porphyrin rings of the homodimer resulted by self-assembly of peptide  $\alpha, \gamma\text{-CP2}$ . The calculated distance between the porphyrins is 7.23 Å. Top right: energy minimized structure of the 2:1 sandwich complex  $\text{DABCO}_2 \subset \alpha, \gamma\text{-D3}_e$ , revealing a calculated distance between the porphyrins of 7.23 Å. Bottom: Top (*left*) and side (*right*) view of the CAChe minimized structure of the higher stoichiometry specie for the homodimer obtained by self-assembly of peptide  $\alpha, \gamma\text{-CP3}$  ( $\text{DABCO}_4 \subset \alpha, \gamma\text{-D3}_s$ ). DABCO and CPs are shown as space-filled (CPK model) and capped-stick representations, respectively.

Our previous results<sup>19</sup> on Zn-bis-porphyrin receptors with covalent spacers evidenced the initial formation of cofacial 1:1 sandwich complexes with DABCO. Although these complexes are thermodynamically very stable, they open up in the presence of excess DABCO to yield monocoordinated DABCO species of higher stoichiometry. We expected similar complexation behavior for the supramolecularly assembled bis-porphyrin and tetraporphyrin tweezers  $\alpha, \gamma\text{-D2}$  and  $\alpha, \gamma\text{-D3}$  (Figure 3), affording open complexes of high stoichiometry and allowing the supramolecular system to equilibrate again through the inter-dimer conversion.

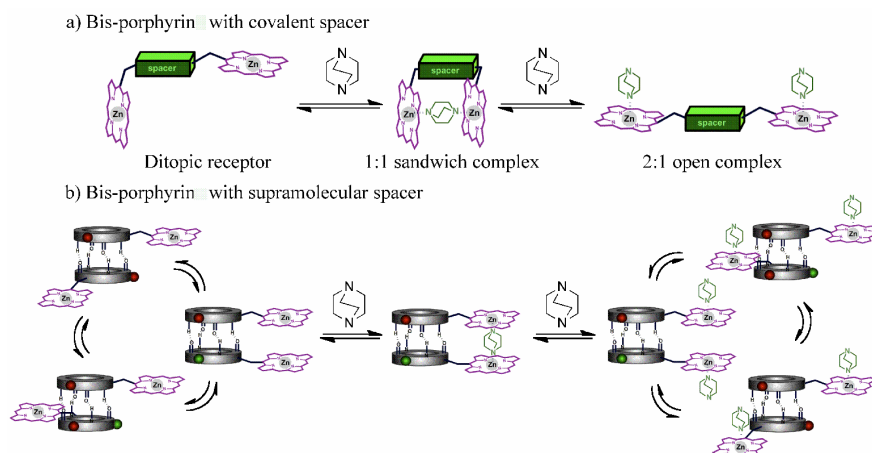


**Figure 3.** Schematic representation of the binding process for the coordination of DABCO with bis-porphyrins capable of adopting a cofacial arrangement: a) covalent spacer, b) supramolecular spacer using hydrogen bonding interactions. In the former receptor the addition of only one equivalent of DABCO causes locking of the inter-conversion of the components of the supramolecular receptor. The use of excess ligand liberates the inter-dimer conversion once again.

The UV-visible spectra obtained during the titration of the tweezers receptors  $\alpha,\gamma$ -D2 and  $\alpha,\gamma$ -D3 with DABCO are similar, which indicates that these two systems undergo related binding processes. In both cases, the initial addition of DABCO leads to a significant increase in the intensity of the Soret bands while the absorption maximum at 427 nm remains virtually unaltered (shifted by < 1 nm). The change in the intensity of the band is a direct consequence of the reduction of the half-bandwidths of the initial absorption bands centred at 426.0 and 426.1 for  $\alpha,\gamma$ -D2 and  $\alpha,\gamma$ -D3, respectively (half-bandwidth of 9 and 8 nm, respectively). The electronic absorption spectra provide interesting information about the relative orientation between the Zn-porphyrin chromophores in the free and bound states of multiporphyrin receptors. Typically, Zn-bisporphyrin tweezers receptors experience a 5 nm red shift that is characteristic of the formation of a DABCO sandwich complex. This 5 nm shift is due to the existence of exciton coupling between the Zn-porphyrin transitions of the cofacially arranged chromophores in the sandwich complex. In the case at hand, the minimal shift observed for the Soret band upon the initial binding of DABCO indicates that exciton coupling between the porphyrin transitions is already present in the free state of the receptors.

However, the observation of larger half-bandwidths for the free states of  $\alpha,\gamma$ -D2 or  $\alpha,\gamma$ -D3 than for the initially formed complexes hints at the existence of non-cofacially arranged conformations of the chromophores in the free states. The ditopic binding of DABCO should restrict the conformations of the receptors to those in which the porphyrin units are coplanar and excitonically coupled, thus producing a concomitant reduction of the half-bandwidths.

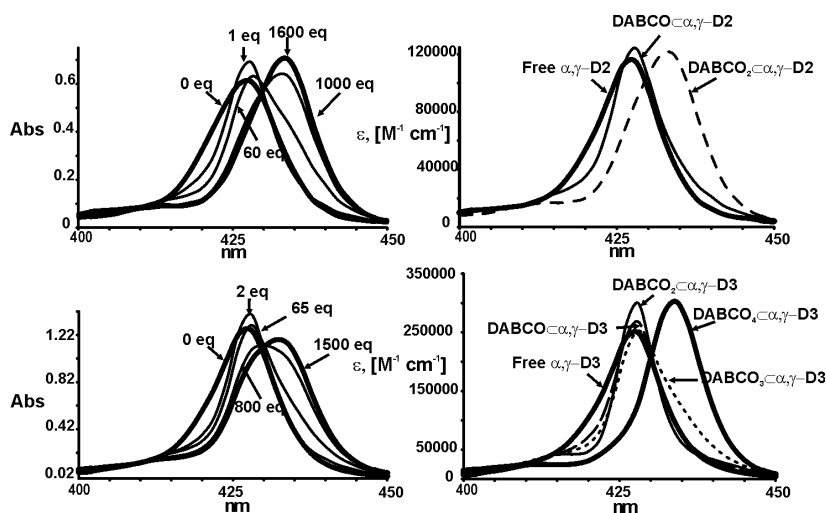


**Figure 4.** Selected spectra for the UV-visible titrations of  $\alpha,\gamma$ -D2 (top, left) and  $\alpha,\gamma$ -D3 (bottom, left) with DABCO showing the Soret band region. Number of equivalents added for  $\alpha,\gamma$ -D2: 0, 1, 60, 1000, and 1600. Number of equivalents added for  $\alpha,\gamma$ -D3: 0, 2, 65, 800, and 1500. Calculated UV-visible spectra of the complexes formed between  $\alpha,\gamma$ -D2 and DABCO: free  $\alpha,\gamma$ -D2, the 1:1 sandwich complex  $\text{DABCO} \llcorner \alpha,\gamma\text{-D2}$  and the 2:1 open complex  $\text{DABCO}_2 \llcorner \alpha,\gamma\text{-D2}$  (top, right), and of the free  $\alpha,\gamma$ -D3, a 1:1 sandwich complex  $\text{DABCO} \llcorner \alpha,\gamma\text{-D3}$ , a 2:1 sandwich  $\text{DABCO}_2 \llcorner \alpha,\gamma\text{-D3}$  and two complexes of higher stoichiometry partially and fully open,  $\text{DABCO}_3 \llcorner \alpha,\gamma\text{-D3}$  and  $\text{DABCO}_4 \llcorner \alpha,\gamma\text{-D3}$  (bottom, right).

On addition of more DABCO, the intensity of the absorption band centred at 427 nm decreased and its half-bandwidth increased. A new absorption band appeared at 432 nm at high DABCO concentrations. It is known that the monoporphyrin compound shows a Soret absorption at 431 nm when it is axially coordinated to DABCO. Taken together,

these results suggest that there are at least two consecutive state equilibria involved in the complexation of DABCO by the Zn-porphyrin tweezer receptors: the formation of a sandwich complex followed by its destruction in the presence of increasing amounts of DABCO to afford monocoordinated DABCO species. ESI/MS and DOSY experiments proved to be unsuccessful to study the formation of the different coordination complexes due to their reduced kinetic stability and to experimental limitations of the technique respectively.

We first analyzed the UV-visible titration data (Figure 4, top left) obtained for the complexation of DABCO with the Zn-bis-porphyrin cyclopeptide dimer,  $\alpha,\gamma$ -D2, using the SPECFIT<sup>26</sup> program and considering a binding model that involved three coloured stoichiometric states of the bis-porphyrin self-assembled tweezers: free  $\alpha,\gamma$ -D2, the 1:1 sandwich complex  $\text{DABCO} \subset \alpha,\gamma\text{-D2}$  and the 2:1 open complex  $\text{DABCO}_2 \subset \alpha,\gamma\text{-D2}$  (see Figure 3 for a schematic representation of the complexes).<sup>27</sup> The stability constant of the 2:1 open complex was estimated statistically to be  $K_{21} = 4K_m^2$  and this was kept fixed during the fitting procedure ( $\log K_{21} = 10.5$ ). The  $K_m$  value was derived from our previous studies on the coordination of DABCO to simple Zn-porphyrins.<sup>19</sup> The fit returned a calculated stability constant for the 1:1 sandwich complex of  $K_{11} = 2.2 \times 10^7 \text{ M}^{-1}$ . The UV-visible spectra (epsilon scale) of the complexes formed between  $\alpha,\gamma$ -D2 and DABCO are shown in Figure 4 (top right) along with that for the free receptor obtained from the fitting procedure. The fit of the titration data to the above mentioned theoretical binding model at one selected wavelength is represented in Figure 4 (top). The calculated spectra show the signatures expected for complexes with the geometries assigned to them: Soret band at 427 nm for DABCO sandwich complexes and at 432 nm for the open complex. The half-bandwidths are also consistent with our expectations. Indeed, a remarkably good fit of the titration data to the corresponding theoretical curves was obtained (Figure 5). The stability constant of the sandwich complex and the equation  $K_{11} = 2K_m^2 \text{EM}$  was used to estimate an effective molarity value of  $\text{EM} = 0.001 \text{ M}$ . This value falls within the expected range reported for related systems, although the magnitude obtained is a clear indication that the

<sup>26</sup> SPECFIT, version 3.0; Spectra Software Associates, Marlborough, MA (USA). a) Gampp, H.; Maeder, M.; Meyer, C. J.; Zuberbuhler, A. D. *Talanta* **1985**, 32, 95-101. b) Gampp, H.; Maeder, M.; Meyer, C. J.; Zuberbuhler, A. D. *Talanta* **1986**, 33, 943-951.

<sup>27</sup> The formation of interdimer sandwich complexes has not been taken into account due to thermodynamic considerations related with its estimated stability constant value ( $10^{10} \text{ M}^{-2}$ ) in relationship with the one determined for the intradimer sandwich complex ( $2 \times 10^7 \text{ M}^{-1}$ ).

complementarity between host and guest and the preorganization of the system is far from being optimal.<sup>28</sup>

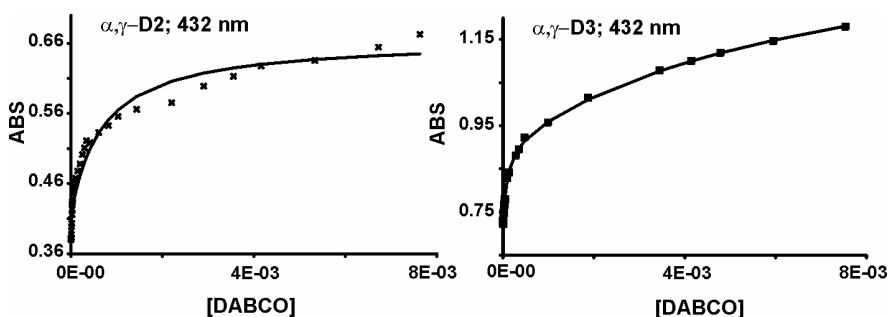


**Figure 5.** Fit of the UV-visible titration data (*points*) at selected wavelength (432 nm) to the theoretical curve (*straight line*) of the binding models discussed in the text,  $\alpha,\gamma$ -D2 at the left, and  $\alpha,\gamma$ -D3 at the right.

Before proceeding with the mathematical analysis of the experimental data obtained in the titration of the self-assembled Zn-tetraporphyrin  $\alpha,\gamma$ -D3 with DABCO, we performed a simulation of the expected speciation of the titration (Figure 6). A theoretical binding model was developed considering that the tetraporphyrin  $\alpha,\gamma$ -D3 can be involved in five different stoichiometric states: free  $\alpha,\gamma$ -D3, a 1:1 sandwich complex  $\text{DABCO} \subset \alpha,\gamma\text{-D3}$ , a 2:1 sandwich  $\text{DABCO}_2 \subset \alpha,\gamma\text{-D3}$  and two complexes that are partially and fully open,  $\text{DABCO}_3 \subset \alpha,\gamma\text{-D3}$  and  $\text{DABCO}_4 \subset \alpha,\gamma\text{-D3}$ , respectively. The stability constants for all the complexes were statistically estimated using the following equations:

$$K_{11} = 8Km^2EM \quad (1)$$

$$K_{21} = 8Km^4EM^2 \quad (2)$$

$$K_{31} = 32Km^4EM \quad (3)$$

$$K_{41} = 32Km^4 \quad (4)$$

<sup>28</sup> Anderson, H. L.; Anderson, S.; Sanders, J. K. M. *J. Chem. Soc., Perkin Trans. 1* **1995**, 2231-45.

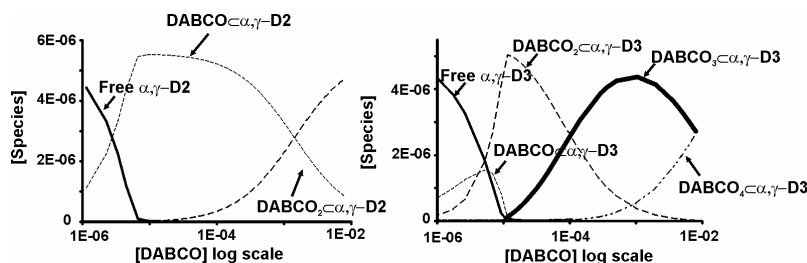
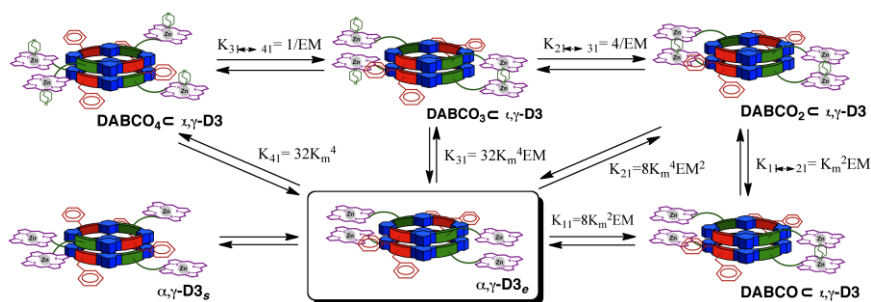


**Figure 6.** Speciation profiles derived from the UV titrations of  $\alpha,\gamma$ -D2 (left) and  $\alpha,\gamma$ -D3 (right). Each curve corresponds to one species.

We considered an EM =  $1 \times 10^{-3}$  M, the value calculated for  $\alpha,\gamma$ -D2, for all the sandwich complexes and a  $K_m = 8.9 \times 10^4$  M $^{-1}$  for the microscopic binding constant of DABCO with the Zn-porphyrins. Thus, the calculated log values for the stability constants are:  $\log K_{11} = 7.5$ ,  $\log K_{21} = 14.7$ ,  $\log K_{31} = 18.3$  and  $\log K_{41} = 21.3$ . The simulation revealed that all species should be considered in the theoretical binding model if their stability constants correspond to statistically estimated values. Next, we fitted the experimental titration data to the theoretical binding model considering that  $\alpha,\gamma$ -D3 is involved in the formation of the five species depicted in Scheme 6. In order to reduce the number of variables during the fitting procedure we fixed the values of the stability constants for the 1:1 and the 4:1 complexes to those estimated statistically. The fitting procedure gave the stability constants for the 2:1 and the 3:1 complexes ( $K_{21} = 1.26 \times 10^{15}$  M $^{-2}$  and  $K_{31} = 1.26 \times 10^{19}$  M $^{-3}$ ) and these are in good agreement with those estimated statistically. The UV-visible spectra calculated for the different species show the spectroscopic signatures expected for their geometries and stoichiometries (Figure 4). The stability constant calculated for the  $K_{21}$  complex can be translated to an  $EM^2 = 2.51 \times 10^{-6}$  M using eq (2) and yields an average value of EM = 0.0016 for each of the binding sites. The agreement obtained between the EM value calculated for the  $\alpha,\gamma$ -D2 bis-porphyrin tweezer and for the two binding sites of the Zn-tetraporphyrin  $\alpha,\gamma$ -D3 indicates that the formation of the 2:1 double sandwich complex does not show evidence of a highly positive cooperativity.<sup>29,30</sup> To better

<sup>29</sup> Ballester, P.; Oliva, A. I.; Costa, A.; Deya, P. M.; Frontera, A.; Gomila, R. M.; Hunter, C. A. *J. Am. Chem. Soc.* **2006**, *128*, 5560-5569.

evaluate the cooperativity factor of the two ditopic binding process of DABCO with  $\alpha,\gamma$ -D3 we determined the microscopic binding constant values of each event using the well known relationships  $K_{11} = 2K_{m1}$  and  $K_{11\rightleftharpoons 21} = K_{21}/K_{11} = K_{m2}/2$ . The relationship between microscopic binding constants and thermodynamic binding constant also known as statistical correction is simply dictated by the degeneracy of states when the reactants are transformed into products (entropic contribution). The ratio of microscopic binding constants affords a value of  $\alpha_P = K_{m2}/K_{m1} = 4.8$  for the cooperativity factor of the tetraporphyrin  $\alpha,\gamma$ -D3 indicating that this tetraporphyrin binds the second equivalent of DABCO with a fivefold increase over the first one and displays moderate cooperative binding.



**Scheme 6.** Schematic representation of the possible equilibria involved in the binding of DABCO to the zinc tetraporphyrin dimer  $\alpha,\gamma$ -D3. EMs are the effective molarities for the intramolecular interaction required for cyclization. Overall stability constants  $K_{21}$ ,  $K_{31}$ ,  $K_{41}$  and stepwise equilibrium constant  $K_{11}$ ,  $K_{11\rightleftharpoons 21}$ ,  $K_{21\rightleftharpoons 31}$ ,  $K_{31\rightleftharpoons 41}$  are shown and related to  $K_m$  (microscopic binding constant), EM, and statistical correction factors. The cooperativity factor of the ligand ( $\alpha_L$ ) and the cooperativity factor of the porphyrin ( $\alpha_P$ ) are supposed to be equal to 1.

In order to gain further insight into the structural features of the complexes formed through the interaction of DABCO with the cyclopeptide porphyrin tweezers  $\alpha,\gamma$ -D2 and  $\alpha,\gamma$ -D3, we studied their complexation processes using  $^1\text{H}$  NMR and CD spectroscopy. At millimolar concentration ( $^1\text{H}$  NMR) the addition of 0.3 equivalents of DABCO to a chloroform solution containing  $\alpha,\gamma$ -D2 led to the appearance of a singlet resonating at  $\delta =$

<sup>30</sup> Veling, N.; Thomassen, P. J.; Thordarson, P.; Elemans, J. A. A. W.; Nolte, R. J. M.; Rowan, A. E. *Tetrahedron* **2008**, *64*, 8535-8542.

-5.0 ppm (Figure 5). This signal is characteristic of the methylene protons of a DABCO molecule bound between two porphyrin units in a sandwich complex, as we expect is the case in the  $\text{DABCO} \subset \alpha, \gamma\text{-D2}$  complex. When more than 0.3 equivalents of DABCO were added, the signal at  $\delta = -5.0$  ppm broadened and finally disappeared when 1 equivalent of DABCO was present in solution. This signal broadening is due to chemical exchange with free DABCO molecules or DABCO molecules axially monocoordinated to the porphyrin in the open  $\text{DABCO}_2 \subset \alpha, \gamma\text{-D2}$  complex. The exchange rate is proportional to the concentration of free DABCO and  $\text{DABCO}_2 \subset \alpha, \gamma\text{-D2}$  complex, suggesting a bimolecular process in which one molecule of DABCO displaces another from the zinc atom in a concerted manner. The interaction of DABCO with Zn-tetraporphyrin  $\alpha, \gamma\text{-D3}$  was also investigated by  $^1\text{H}$  NMR spectroscopy. Again a singlet was observed at -5.0 ppm after the initial addition of the diamine ligand, which is indicative of the formation of sandwich complexes of the type  $\text{DABCO} \subset \alpha, \gamma\text{-D3}$  and  $\text{DABCO}_2 \subset \alpha, \gamma\text{-D3}$ . As expected, the proton signal showed analogous dynamic behavior to that described for  $\alpha, \gamma\text{-D2}$ . The incremental addition of DABCO led to broadening of the signal and this finally disappeared in the presence of close to 2 equivalents of DABCO (Figure 7). Further addition of DABCO until 1 equiv did not produce any noteworthy change in the  $^1\text{H}$ -NMR spectrum. Taken together, these observations suggest that the proton signals of the 1:1 ( $\text{DABCO} \subset \alpha, \gamma\text{-D3}$ ) and 2:1 ( $\text{DABCO}_2 \subset \alpha, \gamma\text{-D3}$ ) complexes formed by DABCO with  $\alpha, \gamma\text{-D3}$  must be very similar. Not surprisingly both species possess an eclipsed arrangement of the porphyrin units. They also suggest that the concentration of free  $\alpha, \gamma\text{-D3}$  in the presence of 0.5 equivalents of DABCO is close to the detection limit of the spectrometer. In this sense, a simulated speciation profile when 0.5 equivalents of DABCO are added assigns a concentration of free  $\alpha, \gamma\text{-D3}$  lower than  $3 \times 10^{-4}$  M in complete agreement with the observations (Figure 6).

Finally, the interaction of DABCO with the two tweezer receptors was also monitored by CD spectroscopy. Free receptors  $\alpha, \gamma\text{-D2}$  and  $\alpha, \gamma\text{-D3}$  feature silent CDs at micromolar concentrations. The incremental addition of DABCO to a chloroform solution of the self-assembled tweezers  $\alpha, \gamma\text{-D2}$  did not produce any significant changes in the CD spectrum of the free receptor.

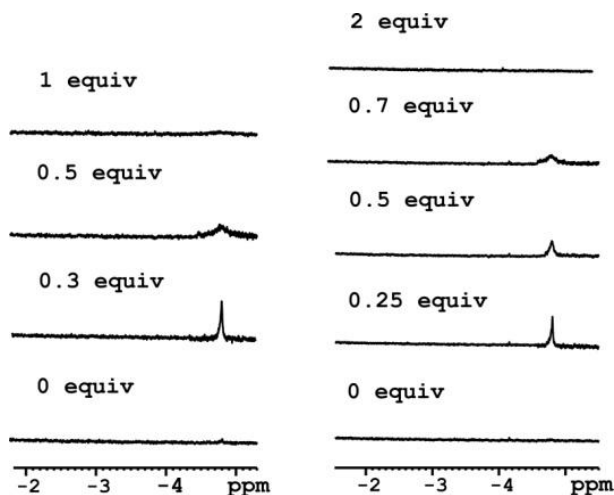


**Figure 7.** Selected region of the  $^1\text{H}$  NMR spectra obtained in the titrations of  $\alpha,\gamma\text{-D2}$  (left) and  $\alpha,\gamma\text{-D3}$  (right) with DABCO at r.t.

These observations suggest that the induction of chirality from the chiral CP scaffold to the porphyrin chromophores is almost negligible both in the free state of the receptors and in the  $\text{DABCO}\subset\alpha,\gamma\text{-D2}$  sandwich complex. In contrast, the initial addition of DABCO to the chloroform solution of  $\alpha,\gamma\text{-D3}$  led to the appearance and stepwise enhancement of a positive bisignate Cotton effect in the porphyrin Soret band. However, upon increasing the concentration of DABCO the absorbance values of the sample started to decrease. This result implies the existence of exciton coupling in the sandwich complexes formed initially by the interaction of  $\alpha,\gamma\text{-D3}$  and DABCO. The appearance of the positive CD couplet should probably be ascribed to the formation of the  $\text{DABCO}_2\subset\alpha,\gamma\text{-D3}$  complex, in which the conformational restrictions introduced by the two porphyrin sandwiches are able to transmit the backbone chirality to the chromophores, while the decrease in the intensity of the absorbance can be associated with the destruction of the double sandwich complex and the formation of the open  $\text{DABCO}_3\subset\alpha,\gamma\text{-D3}$  and/or  $\text{DABCO}_4\subset\alpha,\gamma\text{-D3}$  complexes for which we anticipated a silent CD similar to the free receptors (Figure 8). It is expected that in the  $\text{DABCO}_2\subset\alpha,\gamma\text{-D3}$  complex, the cofacial arrangement and short distance between the centres of the interacting electric dipoles of the porphyrins results in two energy exciton states, higher energy homocouplings [ $B_{\perp}(+)$  and  $B_{\parallel}(+)$ ] and lower energy homocouplings [ $B_{\perp}(-)$  and  $B_{\parallel}(-)$ ], which are well separated in the CD spectra.

Furthermore, in accordance with the CD exciton chirality method, the positive chirality observed for the first Cotton effect of the putative  $\text{DABCO}_2\text{C}\alpha,\gamma\text{-D3}$  complex should be produced by the clockwise coupling of the  $B_{\parallel}(-)$  transitions, which in turn corresponds to a right-handed chiral twist of the porphyrin units.

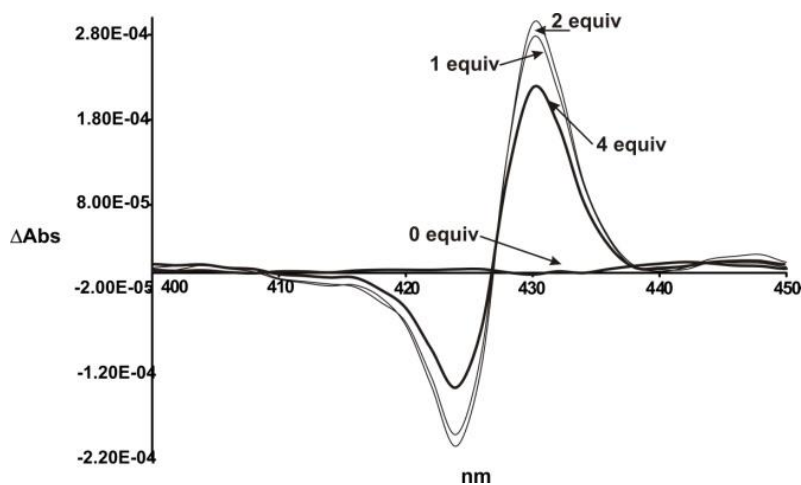


**Figure 8.** Selected spectra for the CD titration of  $\alpha,\gamma\text{-D3}$  with DABCO. Number of equivalents added: 0, 1, 2 and 4.

### 3. Conclusions

In summary, we have studied the complexation of the self-assembled bis- and tetraporphyrin tweezer receptors  $\alpha,\gamma\text{-D2}$  and  $\alpha,\gamma\text{-D3}$  with the ditopic ligand DABCO using UV-visible,  $^1\text{H}$  NMR and CD titration experiments. We have shown that both receptors are capable of forming sandwich complexes with DABCO. Under strict stoichiometric control, bis-porphyrin  $\alpha,\gamma\text{-D2}$  forms a simple 1:1  $\text{DABCO}\text{C}\alpha,\gamma\text{-D2}$  intramolecular complex, while the tetraporphyrin  $\alpha,\gamma\text{-D3}$  produces the corresponding  $\text{DABCO}_2\text{C}\alpha,\gamma\text{-D3}$  intramolecular sandwich complex with total regioisomeric control.

The formation of the  $\text{DABCO}_2\text{C}\alpha,\gamma\text{-D3}$  intramolecular sandwich complex shows evidence of moderate cooperative binding for the two ditopic binding sites. The intramolecular sandwich complexes open up in the presence of excess ligand to form open complexes ( $\text{DABCO}_2\text{C}\alpha,\gamma\text{-D2}$  and  $\text{DABCO}_4\text{C}\alpha,\gamma\text{-D3}$ ) in which DABCO molecules are axially monocoordinated to the porphyrin units. The destruction of the  $\text{DABCO}_2\text{C}\alpha,\gamma\text{-D3}$  intramolecular sandwich complex must occur through the intermediate species  $\text{DABCO}_3\text{C}\alpha,\gamma\text{-D3}$ , in which one binding site forms a sandwich complex with DABCO and the other is already open with two DABCO molecules axially monocoordinated to the porphyrin units.

In short, the coordination of DABCO to the CP oligoporphyrin tweezers allows the regioisomeric control of the dimeric assemblies formed in solution. These assemblies have potential applications as light-induced energy and electron-transfer switches regulated by DABCO coordination in the design of molecular machines or sensors. Nevertheless, such systems would require the introduction of additional chromophores in the cyclopeptide scaffold.

## 4. Experimental section

### 4.1 General information and instrumentation

Commercially available N-Boc amino acids, O-(7-azabenzotriazol-1-yl)-1,1,3,3-tetramethyluronium hexafluorophosphate (HATU) and O-Benzotriazol-1-yl-*N,N,N'*-tetramethyluronium tetrafluoroborate (TBTU) were all used as obtained from Novabiochem, Applied Biosystems or Bachem. *N,N'*-diisopropylcarbodiimide (DIC) and 4-dimethylaminopyridine (DMAP) were obtained from Aldrich. All other reagents obtained from commercial suppliers were used without further purification unless otherwise noted. 1,4-diazabicyclo [2.2.2]octane (DABCO) and 1-azabicyclo[2.2.2]octane (Quinuclidine) were sublimed prior to use. Deuterated chloroform ( $\text{CDCl}_3$ ) and  $\text{CHCl}_3$  were deacidified by passing through a short column of aluminium oxide 60, basic (Merck). Dichloromethane (DCM) and piperidine were dried and distilled over calcium hydride. DIEA was dried and distilled over calcium hydride, and then redistilled over nynhidrin. Analytical thin-layer chromatography was performed on E. Merck silica gel 60 F<sub>254</sub> plates. Compounds, which

were not UV active, were visualized by dipping the plates in a ninydrin solution and heating. Silica gel flash chromatography was performed using E. Merck silica gel (type 60SDS, 230-400 mesh). Preparative thin-layer chromatography was performed on E. Merck silica gel 60 F<sub>254</sub> plates (1 mm). Size exclusion chromatography was performed using a lipophilic Sephadex® LH20 resin. Solvent mixtures for chromatography are reported as v/v ratios. HPLC purification was carried out on Phenomenex Maxsil-10 silica column with CH<sub>2</sub>Cl<sub>2</sub>/MeOH gradients between 100 and 85:15. Analytical gel permeation chromatography (GPC) was used in order to ascertain the purity of the isolated free base and metallated porphyrins. It was carried out on Styragel® HR1 Toluene (7.8 x 300 mm) Waters column with 100% toluene. GPC purification was carried out on Ultrastyrigel® (19 x 300 mm) Waters column with 100% toluene. The wavelength selected for the chromatographic analyses was 420 nm, which corresponds with the maximum absorbance of the Soret band of the porphyrin ring. Toluene CHROMASOLV® for HPLC was used as solvent. Proton nuclear magnetic resonance (<sup>1</sup>H NMR) spectra were recorded on Varian-Inova 750 Mhz, Bruker AMX-500 MHz or Bruker WM-250 MHz spectrometers. Chemical shifts were reported in parts per million (ppm, δ) relative to tetramethylsilane (δ 0.00). <sup>1</sup>H NMR splitting patterns are designated as singlet (s), doublet (d), triplet (t), quartet (q) or pentuplet (p). All first-order splitting patterns were assigned on the basis of the appearance of the multiplet. Splitting patterns that could not be easily interpreted are designated as multiplet (m) or broad (br). Carbon nuclear magnetic resonance (<sup>13</sup>C NMR) spectra were recorded on Bruker AMX-500 MHz, Bruker AMX-400 MHz or Bruker WM-250 MHz spectrometers. Carbon resonances were assigned using distortionless enhancement by polarization transfer (DEPT) spectra obtained with phase angles of 135. Electrospray (ESI) mass spectra were recorded on a Bruker BIOTOF II mass spectrometer. Fast Atom Bombardement (FAB) mass spectra were recorded on a Micromass Autospec mass spectrometer. Mass Spectrometry of Laser Desorption/Ionization-Time of Flight (MALDI-TOF) was obtained on a Bruker Autoflex mass spectrometer. UV/Vis measurements were made on a Cary 100 Bio UV/Visible spectrophotometer, using NaCl solution UV cells. FTIR measurements were made on a JASCO FT/IR-400 spectrophotometer using 5-10 mM in CHCl<sub>3</sub> and placed in a NaCl solution IR cell. Circular dichroism (CD) spectra were recorded on a Chirascan instrument HP Compaq PC.

## 4.2 Binding studies

### a. $^1\text{H}$ NMR titrations

$^1\text{H}$ -NMR titrations were carried out by running a spectrum of the host ( $\alpha,\gamma$ -CP2 or  $\alpha,\gamma$ -CP3) solution in previously deacidified  $\text{CDCl}_3$  at a concentration around 1 mM and adding to it incremental aliquots of guest (DABCO) solution (using the host as solvent) also in deacidified  $\text{CDCl}_3$  at a concentration approximately 1 mM. After each addition, a new NMR spectrum was acquired.

### b. UV-visible titrations

The UV-visible titrations were carried out in previously deacidified  $\text{CHCl}_3$  through a similar methodology as described above. In this case, the host ( $\alpha,\gamma$ -CP2 or  $\alpha,\gamma$ -CP3) concentration was maintained constant at  $1\ \mu\text{M}$  all along the titration experiment. To avoid the dilution of the host solution, the titrating guest (DABCO) solutions were prepared using the solution of the host as the solvent. A new UV-visible spectrum was obtained after each addition of guest. To cover a wide range of guest concentrations it was necessary to prepare several solutions with different concentrations. The data obtained from the UV-visible spectrophotometric titrations were analyzed by fitting the whole series of spectra at 1 nm interval using the software SPECFIT 3.0 from Spectrum Software Associates, PMB 361, 197M Boston Post Road West, Marlborough, MA 01752, U.S.A. (E-mail: [SpecSoft@compuserve.com](mailto:SpecSoft@compuserve.com)), which uses a global system with expanded factor analysis and Marquardt least-squares minimization to obtain globally optimized parameters.<sup>26</sup>

### c. Circular dichroism titrations

CD titrations were performed in previously deacidified  $\text{CHCl}_3$  by adding solutions containing the guest (DABCO) to a solution of the host (peptide-based zinc porphyrins  $\alpha,\gamma$ -CP2 or  $\alpha,\gamma$ -CP3) in either a 1mm or 1cm path cuvette by using microliter syringes. In

all cases the zinc porphyrin derivatives were present in the guest solution at the same concentration as that in the cuvette to avoid dilution effects. A new CD spectrum was obtained after each addition of guest. The same as with the UV-visible data, the data obtained from the CD spectrophotometric titrations were analyzed by fitting the whole series of spectra at 1 nm interval using the software SPECFIT 3.0

### 4.3 Synthesis

#### Synthesis of 5-(4-carboxyphenyl)-10,15,20-tris(4-pentylphenyl)porphyrin, H<sub>2</sub>-19:

Mono-carboxymethylporphyrin, H<sub>2</sub>-20 (90.00 mg, 0.10 mmol), was added to a mixture of 8 mL of THF and 2 mL of 2 M aqueous KOH. The reaction was stirred for 14 h at 90 °C. Then, the THF was removed under vacuum and 80 mL of water were added to the resulting concentrate. The pH of the solution was adjusted to pH 4.0–5.0 using a solution of HCl (2 M), followed by the addition of 100 mL of CHCl<sub>3</sub>. The organic layer was separated, washed with water, dried over Na<sub>2</sub>SO<sub>4</sub> and filtered. The organic solvent was removed under vacuum, giving the corresponding pure free base monocarboxylic acid porphyrin, which was dried overnight before being used in the construction of the CP-based devices, obtaining the desired porphyrin **1** as purple solid in 95% yield.

<sup>1</sup>H NMR (CDCl<sub>3</sub>, 400.00 MHz, δ): 8.92 (d, *J* = 4.8 Hz, 2H), 8.89 (s, 4H), 8.80 (d, *J* = 4.8 Hz, 2H), 8.51 (d, *J* = 8.0 Hz, 2H), 8.36 (d, *J* = 8.0 Hz, 2H), 8.13 (d, *J* = 8.0 Hz, 6H), 7.59 (d, *J* = 8.0 Hz, 6H), 2.98 (t, *J* = 8.0 Hz, 6H), 1.95 (m, 6H), 1.56 (m, 12H), 1.08 (t, *J* = 6.8 Hz, 9H), -2.73 (br s, 2H). MS (MALDI-TOF) [*m/z* (%): 867 ([M -H]<sup>-</sup>), 100]. HRMS (MALDI-TOF) calculated for C<sub>60</sub>H<sub>59</sub>N<sub>4</sub>O<sub>2</sub> ([M -H]<sup>-</sup>) 867.4638, found 867.4623.

#### Synthesis of 5-(4-carboxymethylphenyl)-10,15,20-tris(4-pentylphenyl)porphyrin, H<sub>2</sub>-20:

Methyl 5-formylbenzoate (1.00 g, 6.10 mmol), 4-pentylbenzaldehyde (1.45 g, 9.10 mmol) and freshly distilled pyrrole (0.95 mL, 15.20 mmol) were added to a solution consisting of 530 mL of CH<sub>2</sub>Cl<sub>2</sub> and 4 mL of EtOH. The resulting solution was stirred under argon for 10 min. Then, the reaction mixture was protected from light and BF<sub>3</sub>·Et<sub>2</sub>O (0.69 mL, 6.10 mmol) was added. The solution was stirred for 1 h. Subsequently, DDQ (3.11 g, 15.20

mmol) was added and the reaction was stirred for another 1.5 h. Finally, the reaction was quenched by the addition of 3 mL of Et<sub>3</sub>N. The solvent was removed under vacuum and the residue was purified by flash column chromatography (50% CH<sub>2</sub>Cl<sub>2</sub>/hexanes), isolating the corresponding mono-carboxymethylporphyrin **3** as purple solid in 7.5% yield.

MS (MALDI-TOF) [m/z (%): 881 ([M -H]<sup>-</sup>, 100). HRMS (MALDI-TOF) calculated for C<sub>61</sub>H<sub>61</sub>N<sub>4</sub>O<sub>2</sub> ([M -H]<sup>-</sup>) 881.4795, found 881.4792.

### Synthesis of *cyclo*[D-Phe-L-MeN-γ-Ach-D-Ser-L-MeN-γ-Ach]<sub>2</sub> (α,γ-CP1):

A solution of *cyclo*[D-Phe-L-MeN-γ-Ach-D-Ser(Bn)-L-MeN-γ-Ach]<sub>2</sub> (α,γ-CP0, 50.0 mg, 41.5 μmol) in EtOH (500 μL) was treated with 10% Pd/C (8.8 mg, 8.3 μmol), and stirred at rt under hydrogen overnight. The resulting mixture was filtered through a celite pad, the residue was washed with ethanol, and the pooled filtrate and washings were concentrated under reduced pressure, affording 40.1 mg of α,γ-CP1 as a white solid (94%).

<sup>1</sup>H NMR (CDCl<sub>3</sub>, 750.00 MHz, δ): 8.96 (s, 2H, NH<sub>Ser</sub> α,γ-D1<sub>s</sub>), 8.65 (br s, 0.14H, NH<sub>Phe</sub> α,γ-D1<sub>e</sub>), 8.49 (d, *J* = 9.8 Hz, 2H, NH<sub>Phe</sub> α,γ-D1<sub>s</sub>), 8.14 (br s, 0.14H, NH<sub>Ser</sub> α,γ-D1<sub>e</sub>), 7.24-7.08 (m, 10.7H, Ar-H<sub>Phe</sub>), 5.31-5.24 (m, 2.14H, H<sub>αSer</sub>), 5.22-5.16 (m, 2.14H, H<sub>αPhe</sub>), 4.52-4.45 (m, 4.28H, H<sub>γAch</sub>), 3.89-3.81 (m, 2.14H, CH<sub>2βSer</sub>), 3.76-3.69 (m, 2.14H, CH<sub>2βSer</sub>), 3.32-3.25 (m, 4.28H, H<sub>αAch</sub>), 3.09-3.01 (m, 8.56H, NCH<sub>3</sub> + CH<sub>2βPhe</sub>), 2.97-2.90 (m, 2.14H, CH<sub>2βPhe</sub>), 2.80 (s, 6.42H, NCH<sub>3</sub>), 2.45-2.39 (m, 4.28H, CH<sub>2Ach</sub>), 1.92-1.03 (m, 32.10H, CH<sub>2Ach</sub> + OH<sub>Ser</sub>). <sup>13</sup>C RMN (CDCl<sub>3</sub>, 75.40 MHz, δ): 177.9 (CO), 174.2 (CO), 171.8 and 171.6 (CO), 168.6 and 168.6 (CO), 136.8 and 136.8 (C), 129.8 (CH), 128.2 (CH), 126.7 (CH), 67.0 (CH<sub>2</sub>), 53.3 (CH), 52.2 (CH), 51.2 (CH), 50.0 (CH), 44.4 (CH), 42.5 (CH), 39.3 (CH<sub>2</sub>), 32.2 and 32.1 (CH<sub>2</sub>), 30.8 (CH<sub>2</sub>), 29.9 and 29.8 (CH<sub>3</sub>), 29.1, 28.7 and 28.6 (CH<sub>2</sub>), 24.7 (CH<sub>2</sub>). FTIR (293 K, CHCl<sub>3</sub>): 3317 (amide A), 2935, 2863, 1660, 1620 (amide I), 1524 cm<sup>-1</sup> (amide II). MS (FAB<sup>+</sup>) [m/z (%): 1025 ([MH]<sup>+</sup>, 100). HRMS (FAB<sup>+</sup>) calculated for C<sub>56</sub>H<sub>81</sub>N<sub>8</sub>O<sub>10</sub> ([MH]<sup>+</sup>) 1025.60757, found 1025.60908.

**Cyclic peptide derivatization.** Mono- and bis-porphyrin derivatives α,γ-CP2 and α,γ-CP3 were prepared in only one step by coupling between porphyrin H<sub>2</sub>-19 and peptide α,γ-CP1.

**Synthesis of *cyclo*[D-Phe-L-MeN- $\gamma$ -Ach-D-Ser(Por)-L-MeN- $\gamma$ -Ach-D-Phe-L-MeN- $\gamma$ -Ach-D-Ser-L-MeN- $\gamma$ -Ach] ( $\alpha,\gamma$ -CP2·H2) and *cyclo*[D-Phe-L-MeN- $\gamma$ -Ach-D-Ser(Por)-L-MeN- $\gamma$ -Ach]<sub>2</sub> ( $\alpha,\gamma$ -CP3·H4):**

A solution of porphyrin **H2-19** (33.9 mg, 39.1  $\mu$ mol) in CDCl<sub>3</sub> (2 mL) was stirred and sonicated at rt for 10 min, and then DIC (9.2  $\mu$ L, 58.6  $\mu$ mol), *cyclo*[D-Phe-L-MeN- $\gamma$ -Ach-D-Ser-L-MeN- $\gamma$ -Ach]<sub>2</sub> ( $\alpha,\gamma$ -CP1, 20.0 mg, 19.5  $\mu$ mol) and DMAP (7.2 mg, 58.6  $\mu$ mol) were successively added. After 2 h stirring at rt, the solution was washed with HCl (5%) and NaHCO<sub>3</sub> (sat.), dried over Na<sub>2</sub>SO<sub>4</sub>, and concentrated under reduced pressure. The residue was purified by preparative thin-layer chromatography (5% MeOH in CH<sub>2</sub>Cl<sub>2</sub>) and size exclusion chromatography (CHCl<sub>3</sub>), giving 8.3 mg of  $\alpha,\gamma$ -CP2·H2 [23%, R<sub>t</sub> = 8.248 min (Styragel® HR1 Toluene, 7.8 x 300 mm, Waters column, 100% Toluene), R<sub>f</sub> = 0.46 (5% MeOH in CH<sub>2</sub>Cl<sub>2</sub>), garnet solid] and 16.2 mg of  $\alpha,\gamma$ -CP3·H4 [30%, R<sub>t</sub> = 6.228 min (Styragel® HR1 Toluene, 7.8 x 300 mm, Waters column, 100% Toluene), R<sub>f</sub> = 0.51 (5% MeOH in CH<sub>2</sub>Cl<sub>2</sub>), garnet solid].

**$\alpha,\gamma$ -CP2·H2:** <sup>1</sup>H NMR (CDCl<sub>3</sub>, 750.00 MHz,  $\delta$ ): 8.80-8.10 (m, 8.56H, NH<sub>Ser</sub> + NH<sub>Phe</sub>), 8.80 (br s, 12.84H, Ar-H<sub>Por</sub>), 8.63 (d, *J* = 4.3 Hz, 4.28H, Ar-H<sub>Por</sub>), 8.24 (d, *J* = 7.0 Hz, 4.28H, Ar-H<sub>Por</sub>), 8.15 (d, *J* = 6.8 Hz, 4.28H, Ar-H<sub>Por</sub>), 8.04 (d, *J* = 7.9 Hz, 12.84H, Ar-H<sub>Por</sub>), 7.49 (d, *J* = 6.9 Hz, 12.84H, Ar-H<sub>Por</sub>), 7.15-7.03 (m, 21.4H, Ar-H<sub>Phe</sub>), 5.78-5.08 (m, 8.56H, Ha<sub>Ser</sub> + Ha<sub>Phe</sub>), 4.77-4.28 (m, 8.56H, H $\gamma$ <sub>Ach</sub>), 3.86-3.49 (m, 8.56H, CH<sub>2</sub> $\beta$ <sub>Ser</sub>), 3.35-2.34 (m, 64.2H, H $\alpha$ <sub>Ach</sub> + NCH<sub>3</sub> + CH<sub>2</sub> $\beta$ <sub>Phe</sub> + CH<sub>2</sub><sub>Por</sub> + CH<sub>2</sub><sub>Ach</sub>), 2.05-0.71 (m, 119.84H, CH<sub>2</sub><sub>Ach</sub> + CH<sub>2</sub><sub>Por</sub> + CH<sub>3</sub><sub>Por</sub> + OH<sub>Ser</sub>), -2.84 (br s, 4.28H, NH<sub>Por</sub>). MS (MALDI-TOF) [*m/z* (%): 1898 ([M + Na]<sup>+</sup>, 10), 1876 ([MH]<sup>+</sup>, 100). HRMS (MALDI-TOF) calculated for C<sub>116</sub>H<sub>139</sub>N<sub>12</sub>O<sub>11</sub> ([MH]<sup>+</sup>) 1876.07, found 1876.28.

**( $\alpha,\gamma$ -CP3·H4):** <sup>1</sup>H NMR (CDCl<sub>3</sub>, 500.13 MHz,  $\delta$ ): 8.80-8.10 (m, 4.28H, NH<sub>Ser</sub> + NH<sub>Phe</sub>), 8.80 (br s, 12.84H, Ar-H<sub>Por</sub>), 8.63 (d, *J* = 9.8 Hz, 4.28H, Ar-H<sub>Por</sub>), 8.24 (d, *J* = 7.9 Hz, 4.28H, Ar-H<sub>Por</sub>), 8.14 (d, *J* = 7.4 Hz, 4.28H, Ar-H<sub>Por</sub>), 8.04 (d, *J* = 7.6 Hz, 12.84H, Ar-H<sub>Por</sub>), 7.49 (d, *J* = 7.2 Hz, 12.84H, Ar-H<sub>Por</sub>), 7.14-7.03 (m, 10.7H, Ar-H<sub>Phe</sub>), 5.83-5.08 (m, 4.28H, Ha<sub>Ser</sub> + Ha<sub>Phe</sub>), 4.71-4.26 (m, 4.28H, H $\gamma$ <sub>Ach</sub>), 3.61-3.52 (m, 4.28H, CH<sub>2</sub> $\beta$ <sub>Ser</sub>), 3.31-2.33 (m, 38.52H, H $\alpha$ <sub>Ach</sub> + NCH<sub>3</sub> + CH<sub>2</sub> $\beta$ <sub>Phe</sub> + CH<sub>2</sub><sub>Por</sub> + CH<sub>2</sub><sub>Ach</sub>), 2.01-0.71 (m, 87.74H, CH<sub>2</sub><sub>Ach</sub> + CH<sub>2</sub><sub>Por</sub> + CH<sub>3</sub><sub>Por</sub>), -2.84 (br s, 4.28H, NH<sub>Por</sub>). MS (MALDI-TOF) [*m/z* (%): 2726 ([MH]<sup>+</sup>, 100). HRMS (MALDI-TOF) calculated for C<sub>176</sub>H<sub>197</sub>N<sub>16</sub>O<sub>12</sub> ([MH]<sup>+</sup>) 2726.53, found 2726.57.

**Synthesis of *cyclo*[D-Phe-L-MeN-γ-Ach-D-Ser(Por-Zn)-L-MeN-γ-Ach-D-Phe-L-MeN-γ-Ach-D-Ser-L-MeN-γ-Ach] (α,γ-CP2):**

The free-base monoporphyrin CP derivative **α,γ-CP2·H2** (10.0 mg, 5.3 μmol) was dissolved in 8 mL of CH<sub>2</sub>Cl<sub>2</sub>/CH<sub>3</sub>OH (3:1) and Zn(OAc)<sub>2</sub> (9.8 mg, 53.3 μmol) was added. The reaction mixture was protected from light and stirred at room temperature overnight. After removal of the solvents under reduced pressure, the residue was purified by flash chromatography on neutral alumina oxide using CH<sub>2</sub>Cl<sub>2</sub> and then CH<sub>2</sub>Cl<sub>2</sub>/THF (90:10) as eluent, giving 5.9 mg of **α,γ-CP2** [57%, R<sub>t</sub> = 9.264 min (Styragel® HR1 Toluene, 7.8 x 300 mm, Waters column, 100% Toluene), R<sub>f</sub> = 0.04 (50% CH<sub>2</sub>Cl<sub>2</sub> in hexanes), purple solid].

<sup>1</sup>H NMR (CDCl<sub>3</sub>, 500.13 MHz, δ): 8.85-8.10 (m, 8.56H, NH<sub>Ser</sub> + NH<sub>Phe</sub>), 8.82 (br s, 12.84H, Ar-H<sub>Por</sub>), 8.73-8.10 (m, 12.84H, Ar-H<sub>Por</sub>), 8.02 (d, J = 6.6 Hz, 12.84H, Ar-H<sub>Por</sub>), 7.46 (m, 12.84H, Ar-H<sub>Por</sub>), 7.15-7.03 (m, 21.4H, Ar-H<sub>Phe</sub>), 5.87-5.12 (m, 8.56H, H<sub>αSer</sub> + H<sub>αPhe</sub>), 4.56-4.27 (m, 8.56H, H<sub>γAch</sub>), 3.61-3.53 (m, 8.56H, CH<sub>2βSer</sub>), 3.17-2.36 (m, 64.2H, H<sub>αAch</sub> + NCH<sub>3</sub> + CH<sub>2βPhe</sub> + CH<sub>2Por</sub> + CH<sub>2Ach</sub>), 2.04-0.72 (m, 119.84H, CH<sub>2Ach</sub> + CH<sub>2Por</sub> + CH<sub>3Por</sub> + OH<sub>Ser</sub>). MS (MALDI-TOF) [m/z (%): 1959 ([M + Na]<sup>+</sup>, 12), 1937 ([MH]<sup>+</sup>, 100). HRMS (MALDI-TOF) calculated for C<sub>116</sub>H<sub>137</sub>N<sub>12</sub>O<sub>11</sub>Zn ([MH]<sup>+</sup>) 1937.98, found 1937.69.

**Synthesis of *cyclo*[D-Phe-L-MeN-γ-Ach-D-Ser(Por-Zn)-L-MeN-γ-Ach]<sub>2</sub> (α,γ-CP3):**

The free-base bis-porphyrin CP derivative **α,γ-CP3·H4** (4.0 mg, 1.5 μmol) was dissolved in 4 mL of CH<sub>2</sub>Cl<sub>2</sub>/CH<sub>3</sub>OH (3:1) and Zn(OAc)<sub>2</sub> (5.4 mg, 30.0 μmol) was added. The reaction mixture was protected from light and stirred at room temperature overnight. After removal of the solvents under reduced pressure, the residue was purified by flash chromatography on neutral alumina oxide using CH<sub>2</sub>Cl<sub>2</sub> and then CH<sub>2</sub>Cl<sub>2</sub>/THF (90:10) as eluent, giving 4.0 mg of **α,γ-CP3** [96%, R<sub>t</sub> = 6.948 min (Styragel® HR1 Toluene, 7.8 x 300 mm, Waters column, 100% Toluene), R<sub>f</sub> = 0.06 (50% CH<sub>2</sub>Cl<sub>2</sub> in hexanes), purple solid].

<sup>1</sup>H NMR (CDCl<sub>3</sub>, 500.13 MHz, δ): 8.90-8.10 (m, 4.28H, NH<sub>Ser</sub> + NH<sub>Phe</sub>), 8.88 (br s, 12.84H, Ar-H<sub>Por</sub>), 8.71 (d, J = 9.8 Hz, 4.28H, Ar-H<sub>Por</sub>), 8.23 (d, J = 7.9 Hz, 4.28H, Ar-H<sub>Por</sub>), 8.16 (d, J = 7.4 Hz, 4.28H, Ar-H<sub>Por</sub>), 8.04 (d, J = 6.7 Hz, 12.84H, Ar-H<sub>Por</sub>), 7.48 (d, J = 7.6 Hz, 12.84H, Ar-H<sub>Por</sub>), 7.16-7.05 (m, 10.7H, Ar-H<sub>Phe</sub>), 5.81-5.13 (m, 4.28H, H<sub>αSer</sub> + H<sub>αPhe</sub>), 4.70-4.25 (m, 4.28H, H<sub>γAch</sub>), 3.83-3.71 (m, 4.28H, CH<sub>2βSer</sub>), 3.33-2.34 (m, 38.52H, H<sub>αAch</sub> + NCH<sub>3</sub> + CH<sub>2βPhe</sub> + CH<sub>2Por</sub> + CH<sub>2Ach</sub>), 2.05-0.72 (m, 87.74H, CH<sub>2Ach</sub> + CH<sub>2Por</sub> + CH<sub>3Por</sub>). MS

(MALDI-TOF) [m/z (%): 2872 ([M + Na]<sup>+</sup>, 81), 2850 ([MH]<sup>+</sup>, 100). HRMS (MALDI-TOF)  
calculated for C<sub>176</sub>H<sub>193</sub>N<sub>16</sub>O<sub>12</sub>Zn<sub>2</sub> ([MH]<sup>+</sup>) 2850.36, found 2850.56.

UNIVERSITAT ROVIRA I VIRGILI  
SUPRAMOLECULAR CHEMISTRY OF BIS-PORPHYRINS  
Laura Patricia Hernández Eguía  
ISBN:978-84-694-0308-2/DL:T-204-2011

UNIVERSITAT ROVIRA I VIRGILI  
SUPRAMOLECULAR CHEMISTRY OF BIS-PORPHYRINS  
Laura Patricia Hernández Eguía  
ISBN:978-84-694-0308-2/DL:T-204-2011